Ecological monitoring of semi-natural grasslands : statistical analysis of dense satellite image time series with high spatial resolution

Maïlys Lopes

THÈSE

En vue de l'obtention du

DOCTORAT DE L'UNIVERSITÉ DE TOULOUSE

Délivré par :

Institut National Polytechnique de Toulouse (INP Toulouse)

Discipline ou spécialité :

Agrosystèmes, Écosystèmes et Environnement

Présentée et soutenue par :

Mme MAÏLYS LOPES

le vendredi 24 novembre 2017

Titre :

Ecological monitoring of semi-natural grasslands: statistical analysis of dense satellite image time series with high spatial resolution

---

Ecole doctorale :

Sciences Ecologiques, Vétérinaires, Agronomiques et Bioingénieries (SEVAB)

Unité de recherche :

Dynamique et écologie des paysages agriforestiers (Dynafor)

Directeur(s) de Thèse :

M. MATHIEU FAUVEL

M. STEPHANE GIRARD

Rapporteurs :

Mme AGNÈS BEGUE, CIRAD MONTPELLIER

Mme LAURENCE HUBERT-MOY, UNIVERSITE RENNES 2

Membre(s) du jury :

M. DENIS ALLARD, INRA AVIGNON, Président

M. JEAN-BAPTISTE FERET, IRSTEA, Membre

M. MICHEL DURU, INRA TOULOUSE, Membre

Remerciements

Je tiens à exprimer toute ma gratitude envers mes deux directeurs de thèse, Mathieu Fauvel et Stéphane Girard, qui m'ont encadrée pendant ces trois années de thèse et qui m'ont fait bénéficier de leurs connaissances pointues en télédétection et en statistiques. A leurs côtés, j'ai appris ce qu'était le métier de chercheur. Merci Mathieu pour tous les conseils précieux que tu m'as donnés, qui ont permis d'améliorer mon travail tout au long de cette thèse. Merci de t'être rendu disponible lorsque j'en avais besoin. Merci Stéphane de m'avoir fait partager ton expertise, malgré l'encadrement à distance, rien ne pouvait t'échapper. J'ai aussi apprécié mes deux séjours dans ton équipe à Grenoble, au cours desquels j'ai beaucoup progressé grâce à tes talents de pédagogue.

Je remercie chaleureusement Marc Deconchat pour m'avoir accueillie au sein de Dynafor. Merci pour ta bienveillance, tes conseils, et ton soutien dans les moments difficiles. Je tiens aussi à te remercier pour ton aide précieuse lors de la construction de mon projet de post-doc.

Je souhaite remercier les membres de mon comité de thèse, Jordi Inglada, Jérôme Saracco et Olivier Thérond, qui ont suivi ma thèse et m'ont donné d'excellentes pistes de réflexion.

Je remercie aussi les membres du jury, Agnès Bégué, Laurence Hubert-Moy, Denis Allard, Michel Duru et Jean-Baptiste Féret pour avoir accepté de juger ma thèse. Merci pour votre intérêt dans mon travail, ainsi que pour vos commentaires et suggestions très constructifs.

Je remercie les deux stagiaires qui ont effectué leur projet de fin d'étude dans le cadre de ma thèse, Marc Lang et Donatien Dallery. Ils ont contribué significativement à l'avancement de mes travaux. Merci Donatien pour ton rôle clé sur le terrain, tu as assuré !

Je tiens à remercier les techniciens du laboratoire, et tout particulièrement Jérôme Molina, pour m'avoir aidé à préparer la campagne terrain et avoir participé aux relevés sur le terrain. Leur connaissance du terrain a permis de réaliser cette campagne sans encombres, alors que ce n'était pas gagné d'avance !

Je souhaite aussi remercier David Sheeren, qui même s'il n'était pas mon encadrant, a contribué sérieusement à mon travail de thèse, grâce à ses avis et retours constructifs.

Je remercie les écologues et agronomes de Dynafor et d'ailleurs, grâce à qui j'ai appris beaucoup de concepts sur les prairies et en écologie, et qui m'ont aidée à l'interprétation des résultats : Annie Ouin, Aude Vialatte, Clélia Sirami, Jean-Philippe Choisis, Gérard Balent, Emilie Andrieu, Michel Duru, Georges Bertoni, Nicolas Gross,

Rémi Duflot, Romain Carrié, Martin Vigan...

Je remercie aussi tous les doctorants et autres non-permanents du labo, stagiaires ou post-doctorants, auprès de qui j'ai pu recueillir du soutien, échanger des conseils, et passer de bons moments tout simplement : Martin, Romain, Nicolas S., Johanna, Clémence, Floriane, Nicolas K., Nirina, Yousra, Alexis, Audrey, Rémi, Julien, Eugénie, Hugo, Pierre-Alexis, Sylvain, Thibault, Justine... et tous les autres. Les réu pâté et autres verres avec vous vont me manquer !

Enfin, je remercie l'ensemble du laboratoire Dynafor, je ne peux citer tout le monde, mais je vous dis à tous un grand merci ! Vous tous contribuez à la bonne ambiance qui règne à Dynafor. On s'y sent comme dans une famille, ce qui permet de réaliser sa thèse dans des conditions très agréables. Merci pour votre bonne humeur, vos rires communicatifs et vos sourires ! Je n'oublierai pas les bons moments passés lors des AG, des CUMR, mais aussi des BBQ, des repas de Noël, des pauses café et déjeuner.

Mention spéciale à mes gestionnaires préférés, Valérie et Jérôme, qui méritent la palme d'or de l'efficacité et qui pensent à tout, toujours à tout, merci ! Merci aussi à Richard pour toute l'aide technique et matérielle informatique, et à Sylvie pour tout le reste, notamment pour la préparation de la soutenance :)

Je n'oublie pas de remercier Florence Forbes de m'avoir accueillie durant deux séjours à Mistis. Cela a été une expérience enrichissante, et rendue agréable grâce à une équipe accueillante et chaleureuse. Clément, Aina, Alexis, Brice, Emeline, Pablo, Nourou, Thibaud, Thomas : j'ai passé des séjours sympa à Grenoble grâce à vous !

Enfin, je remercie ma famille et tout particulièrement mes parents pour leur soutien et leurs conseils avisés, ce n'est sans doute pas par hasard que j'ai fait une thèse. J'ai une pensée pour ma grand-mère, qui nous a quittés au début de ma thèse.

Merci aussi à tous mes amis pour leurs encouragements et leur soutien, jusque dans les derniers moments, et surtout à Marina qui a toujours répondu présente lorsque j'en avais besoin.

Et pour finir, merci à toi qui te reconnaitras, qui m'a encouragée et m'a donné la confiance qui me manquait pour passer ce concours. Tu as été d'un soutien sans faille et c'est toi qui m'a procuré la force et l'inspiration dans cette dure épreuve qu'est la thèse, rendue encore plus difficile par ton départ dans la capitale. Merci de m'avoir supportée, malgré la distance, je te dois tout. Sans toi je ne serais pas arrivée là, merci pour tout.

Financements

Cette thèse a été réalisée dans le cadre d'un Contrat Jeune Scientifique (CJS) INRA-Inria. Elle a également reçu d'autres soutiens financiers qui ont permis de financer les sorties sur le terrain, les participations aux conférences et deux stages de Master :

- Fonds propres de l'UMR 1201 DYNAFOR,
- Fonds propres de l'équipe Mistis, Inria Grenoble Rhône-Alpes,
- Projet SEBIOREF (région Occitanie, INRA, IRSTEA),
- Projet OSO (TOSCA, CNES),
- Projet MUESLI (IDEX Université de Toulouse),
- Projet CLOHE (Bourse Défi Mastodons, CNRS).

Contents

General Introduction

Context

An era of global changes

Climate change is one of the biggest concerns of our century. Indeed, over the last decades, the Earth has been undergoing many global changes. These changes are responsible for the increase of pollution and greenhouse gases emissions and have caused a great rise of global warming [Tilman et al., 2001, Millennium Ecosystems Assessment, 2005]. Population growth is probably the most significant global change because it induced other global changes through the increase of human activities, such as urbanization, industrialization and agriculture expansion.

In particular, the growing demand for food led to the "Green Revolution" which involved changes and intensification of agricultural practices — mineral fertilizing, use of chemicals (such as herbicides and pesticides), deep ploughing, intensive animal farming — to become more productive [Tilman et al., 2001, Robinson and Sutherland, 2002]. In addition to contributing to climate change, these agricultural changes have implied modifications of the landscapes with the mechanization and the increase of the size of the crop fields. They have caused the destruction or the fragmentation of semi-natural elements such as hedgerows, permanent grasslands or woodlands, which are important sources of biodiversity [Tscharntke et al., 2005]. Hence, the last decades have been synonymous with global warming but also reduction of landscape diversity, both implying worldwide decline in biodiversity [Wilcox and Murphy, 1985, Tilman, 1999, Robinson and Sutherland, 2002, Millennium Ecosystems Assessment, 2005]. Today, agriculture intensification is considered as one of the major drivers of biodiversity loss [Tilman et al., 2001].

To cope with this alarming state, policies have been adopted in Europe to protect biodiversity in natural habitats with the European Union Habitats Directive (92/43/EEC). The Convention on Biological Diversity (CBD) was adopted during the 1992 Rio Earth Summit. In the frame of this international agreement for biological conservation, measures have been undertaken to reduce the rate of biodiversity loss [Butchart et al., 2010]. In Europe, agri-environmental policies have been set up for a more sustainable agriculture [Tscharntke et al., 2005], with among them, the Greening of the Common Agriculture Policy in 2013 that is an incentive for farmers to use their farmland more sustainably and to care for natural resources. The notion of ecosystem services, *i.e.*, the benefits that the humans obtain from the ecosystems, has arisen with the 2005 Millennium Ecosystem Assessment [Millennium Ecosystems Assessment, 2005]. Among the habitats referred by these policies, grasslands are considered as environmentally valuable habitats that provide a large number and variety of ecosystem services.

The importance of grasslands

Indeed, grasslands are species-rich habitats [WallisDeVries et al., 2002, Plantureux et al., 2005]. They are among the largest ecosystems in the world representing 40.5% of the terrestrial area (excluding Greenland and Antarctica) [Suttie et al., 2005] and covering 18% of France territory [Eurostat, 2010].

By definition, grasslands are lands covered with herbaceous plants with less than 10% tree and shrub cover [White et al., 2000]. These open habitats are prevented from woody plant encroachment by natural conditions — climatic (fire, drought, freeze), soil and topographic conditions — or agricultural activities (mowing, grazing). The heterogeneity of this habitat, composed of an association of spontaneous grasses and legume plants, is favorable to insects and micro-organisms [Fahrig et al., 2011, Gardi et al., 2002, Cole et al., 2006]. This diversity supports many ecosystem services such as carbon storage, erosion regulation, protection of water quality, food production, crop pollination, pest regulation (Table 1) [Sala and Paruelo, 1997, Peeters, 2009, Tilman et al., 2001, Millennium Ecosystems Assessment, 2005, Hönigová et al., 2012, Werling et al., 2014].

Table 1.: Essential ecosystem services provided by grasslands and classified into four categories according to the Millennium Ecosystem Assessment [Millennium Ecosystems Assessment, 2005].

Supporting	**Provisioning**
Nutrient cycle (carbon, nitrogen...)	Food production
Water cycle	(meat, milk, honey)
Wildlife habitat	Bioenergy
Genetic library	
Regulating	**Cultural**
Carbon storage	Biodiversity
Climate regulation	Aesthetic beauty
Erosion regulation	Tourism and Recreation
Protection of water quality	
Pollination	
Pest regulation	

In Europe, the Common Agriculture Policy (CAP) distinguishes between two types of grasslands based on their age: permanent or temporary. Permanent grasslands are grasslands that have not been ploughed for at least six years, whereas temporary grasslands are part of a 5-year crop rotation. The Greening of the 2013 CAP reform incites farmers to maintain their permanent grasslands.

However, from an ecological viewpoint, this typology is not very relevant. Indeed,

permanent grasslands can be improved to increase the biomass production, mainly through fertilizing and reseeding, that tend to select the most productive species to the detriment of species diversity [Socher et al., 2012, Allan et al., 2015]. But ecologists are more interested in the potential for biodiversity of grasslands. Although agricultural management of grasslands — mowing and/or grazing — is essential to maintain their biodiversity, an intensive use constitutes a threat for this biodiversity [Hansson and Fogelfors, 2000, Moog et al., 2002, Muller, 2002, Zechmeister et al., 2003, Plantureux et al., 2005, Allan et al., 2015]. Hence, a grassland categorized as "permanent" in the regulation may be intensively-used and thus may not necessarily hold a high biodiversity level. Extensively-used (few anthropogenic perturbations) grasslands with natural plant communities are more commonly referred to as "semi-natural grasslands" [Sullivan et al., 2010, Fahrig et al., 2011], even if for some ecologists, the term "permanent grassland" refers to this definition of grasslands (and not to the CAP definition). To illustrate this, Figure 1 shows pictures of three types of grasslands: (a) intensively-used grassland poor in diversity and where the seeding lines are visible (that can be classified as "permanent" in the regulation but not from the ecological viewpoint), (b) extensively-used ("semi-natural" or "permanent" from the ecological viewpoint) grassland rich in plant species, and (c) unused/abandoned grassland with woody plant encroachment that is turning into a fallow.

(a) (b) (c)

Figure 1.: Pictures of (a) an intensively used grassland, (b) an extensively used grassland, (c) an abandoned grassland.

Despite the regulations in favor of grasslands in Europe, semi-natural grasslands are degrading because of their intensified use or their abandonment, and their surface is continuously decreasing (Figure 2), leading to a loss of biodiversity and associated services [Eriksson et al., 1995, Millennium Ecosystems Assessment, 2005, Carboni et al., 2015]. Grassland species are also affected by global warming, which causes shifts in their phenology [Cleland et al., 2006, Richardson et al., 2013, CaraDonna et al., 2014]. A recent study [Butchart et al., 2010] revealed that most indicators of the state of

biodiversity show worldwide declines while indicators of pressures on biodiversity (resource consumption, nitrogen pollution, overexploitation, invasive alien species and climate change impacts) show worldwide increases.

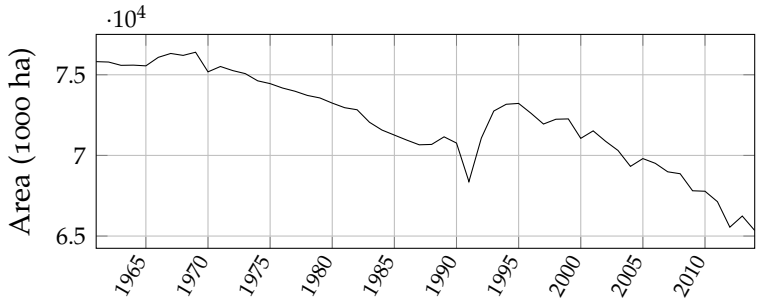

Figure 2.: Evolution of the "permanent meadows and pastures" surface area in the European Union. Source: FAO stat (http://www.fao.org/faostat/).

Hence, there is an important need to monitor biodiversity over large extents (national to international scales) in grasslands from a conservation perspective in order to assess the effectiveness of the environmental policies on grasslands' biodiversity [Sullivan et al., 2010, Pettorelli et al., 2014]. This monitoring should use similar methodologies to enable the comparison between countries.

Usually, ecologists monitor grasslands through field surveys. However, these surveys require important human and material resources, the knowledge of the assessor and a sampling strategy, which make them expensive and time consuming [Magurran, 2004, Rocchini et al., 2016]. Moreover, different methodologies can be employed and they tend to be influenced by the assessor [Rocchini et al., 2016]. Hence field surveys differ in their type and reliability, which can make difficult the comparison between study areas. Ecological surveys are thus limited in spatial extent and in temporal frequency, limiting grassland monitoring to a local scale and over a short period of time. Therefore, field surveys alone cannot address the needs to monitor biodiversity over large extents and other techniques should be considered.

Remote sensing, a useful tool to monitor grasslands

Remote sensing of vegetation

Remote sensing is a unique tool that can address the aforementioned needs. Indeed, thanks to their broad spatial coverage and their regular revisit frequency, satellite sensors acquire regular and repeatable observations over large extents, providing continuous information about vegetated areas [Duro et al., 2007, Pettorelli et al., 2014, Cord

et al., 2017]. Passive sensors measure the electromagnetic radiation reflected by terrestrial surfaces in a wide range of the electromagnetic spectrum (from visible to mid-infrared). The way vegetation reflects the light depends on its nature, state and configuration. For instance, healthy vegetation that is photosynthetically active absorbs the light in the blue and red wavelengths domain while it reflects in the green and near infrared wavelengths [Tucker, 1979] (Figure 3, green line). A dry/senescent/stressed vegetation will have a different spectral signature (Figure 3, red line). Hence, remotely sensed data give access to properties of the vegetation that cannot be seen by the human eye.

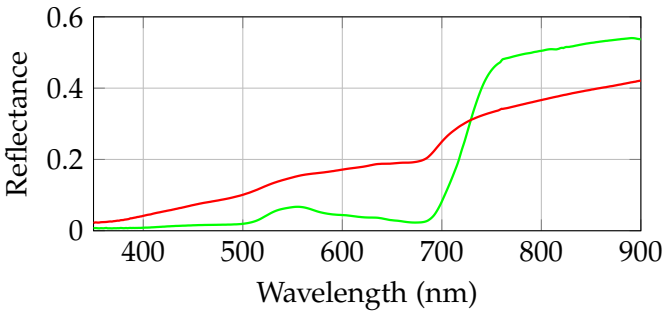

Figure 3.: Spectral signature of healthy vegetation (green) and of dry vegetation (red). The spectra were acquired with an ASD FieldSpec (ASD Inc.) in the same grassland at two different phenological periods (details are provided in Chapter 1).

Remote sensing has been used in ecology to detect land use change, monitor and map natural habitats, assess habitat structure and heterogeneity, estimate the species diversity, map primary productivity of a wide panel of land covers [Nagendra, 2001, Turner et al., 2003, Kerr and Ostrovsky, 2003, Groom et al., 2006, Duro et al., 2007, Nagendra et al., 2013, Pettorelli et al., 2014, Corbane et al., 2015].

Remote sensing of grasslands

However, grasslands have relatively not been studied much in the remote sensing literature compared to other land covers like crops or forest [Newton et al., 2009]. Most of the studies focusing on grasslands have agronomic applications, such as estimating biomass productivity and growth rate [Gu et al., 2013, Li et al., 2013, Gu and Wylie, 2015] or derivating biophysical parameters like the Leaf Ara Index (LAI), the Fraction of Photosynthetically Active Radiation (fPAR), the fraction of Vegetation Cover (fCOVER) and the chlorophyll content [Friedl et al., 1994, Wylie et al., 2002, Darvishzadeh et al., 2008, He et al., 2009, Asam et al., 2013].

Regarding ecological applications, works are relatively new and were applied to the mapping of grasslands types in Natura 2000 zones [Corbane et al., 2013, Buck et al., 2015], the identification of high nature value grasslands [Stenzel et al., 2017], the study of phenological response to climate change [Whittington et al., 2015], the assessment of species richness [Oldeland et al., 2010, Hall et al., 2012, Möckel et al., 2016], the mapping of groups/patterns of species [Schmidtlein and Sassin, 2004, Ishii et al., 2009, Feilhauer et al., 2011, Feilhauer et al., 2013, Schuster et al., 2015], of flowers [Chen et al., 2009, Shen et al., 2010, Carvalho et al., 2013, Landmann et al., 2015] and of pollination types [Feilhauer et al., 2016].

However, most of the works having ecological schemes were conducted at the scale of the grassland using hyperspectral data issued from a field spectroradiometer or an airborne sensor or satellite data with a very high spatial resolution ($\leq$ 5 meters/pixel) such as RapidEye. But these types of acquisitions are limited in time because they are expensive. Thus the works are constrained by the low temporal resolution and the small spatial cover of these sensors and they do not allow for a continuous monitoring of grasslands over the years and over large spatial extents.

Hence, grasslands have been mostly studied at regional to national scales with medium to low spatial resolution sensors that provide freely images with a high temporal resolution but where the Minimum Mapping Unit (MMU) is at least of hundreds of meters (i.e., MODIS: 250 m/pixel, SPOT-VEGETATION and NOAA AVHRR: 1 km/pixel) [Reed et al., 1994, Fontana et al., 2008, Verbesselt et al., 2010, Poças et al., 2012, Li et al., 2013, Hilker et al., 2014, Cao et al., 2015, Halabuk et al., 2015]. Although these sensors provide information over large spatial extents, this scale is only suitable for large, extensive, homogeneous and contiguous regions like steppes [Cao et al., 2015], but not for fragmented landscapes which are usually found in Europe and in France particularly [Eriksson et al., 2002, Zillmann et al., 2014]. These fragmented landscapes are made of a patchwork of different land covers that have a small area [Zillmann et al., 2014]. For these types of landscapes, grasslands can be smaller (less than 10,000 m²) than the pixel resolution [Ali et al., 2016]. As a consequence, pixels containing grasslands are usually a mixture of other contributions, which can limit the analysis [Nagendra, 2001, Nagendra et al., 2013, Blaschke et al., 2014]. For instance, Poças *et al.* [Poças et al., 2012] had to select manually large contiguous areas of semi-natural grasslands in a mountain region of Portugal to be able to use SPOT-VEGETATION data. Halabuk *et al.* [Halabuk et al., 2015] also had to select only one MODIS pixel per homogeneous sample site in Slovakia to classify mown grasslands. A 30-m pixel resolution, provided by Landsat sensor, might be still not sufficient for grassland characterization. Indeed, Lucas *et al.* [Lucas et al., 2007] and Toivonen and Luoto [Toivonen and Luoto, 2003] showed that it was more difficult to classify fragmented and complex elements, like semi-natural grasslands, than homogeneous habi-

tats, using Landsat imagery. Therefore, high spatial resolution images are required to detect small grasslands in fragmented landscapes [Gamon et al., 1993, Corbane et al., 2015, Ali et al., 2016].

Regarding high and very high spatial resolution sensors (about 10 m/pixel or less), as stated earlier, few intra-annual images are usually available for a given location because they are usually expensive [Wulder et al., 2004]. However, the monitoring of grassland phenology requires time series of remotely sensed images. Moreover, many studies involving grasslands type classification using RapidEye imagery (5 m) concluded that three inter-annual images were not enough and they increased the classification accuracy by increasing the number of observations [Franke et al., 2012, Schmidt et al., 2014, Buck et al., 2015, Schuster et al., 2015]. Hence, high temporal resolution data is recommendable for the study of grasslands.

Additionally, for the assessment of grasslands' plant species diversity, high spectral resolution is preferable [Rocchini et al., 2010, Wang et al., 2010, Oldeland et al., 2010, Feilhauer et al., 2013]. But hyperspectral data is also usually limited by its temporal resolution, because there are very few hyperspectral satellite sensors and their acquisitions are costly. Hence, very high spectral resolution data are usually acquired with airborne sensors or field spectroradiometers.

Finally, some studies using active data (radar, Lidar) to characterize grasslands can be reported [Bork and Su, 2007, Schuster et al., 2011, Voormansik et al., 2013, Ali et al., 2016], but the use of this type of data has not been addressed a lot in ecological applications compared to optical data

Therefore, given the heterogeneity of grasslands in fragmented landscapes, their phenological cycle and the punctuality of the anthropogenic events (e.g., mowing), dense high spatial and spectral resolutions time series are required for the monitoring of grassland biodiversity [Psomas et al., 2011, Hill, 2013, Schuster et al., 2015, Ali et al., 2016].

The new generation satellites

Until recently, satellite missions offering high revisit frequency (1–16 days) had coarse spatial resolution (*i.e.*, NOAA AVHRR, 1 km; MODIS, 250/500 m; PROBA-V, 100 m) (Figure 4). Conversely, high spatial resolution missions did not provide dense time series and/or were costly (*i.e.*, QuickBird, RapidEye, WorldView, Pléiades). Hence, the study of semi-natural grasslands in Europe has been limited by the resolutions of sensors or the cost of the images.

However, new missions like Sentinel-2 [Drusch et al., 2012] — launched in 2015 but fully operational in 2018 —, with a very high revisit frequency (five days) and high spatial resolution (10 m in four spectral channels, 20 m in six channels) provide new opportunities for grasslands' monitoring over the years in fragmented landscapes [Hill,

2013] at no cost, thanks to the European Space Agency (ESA) free data access policy.

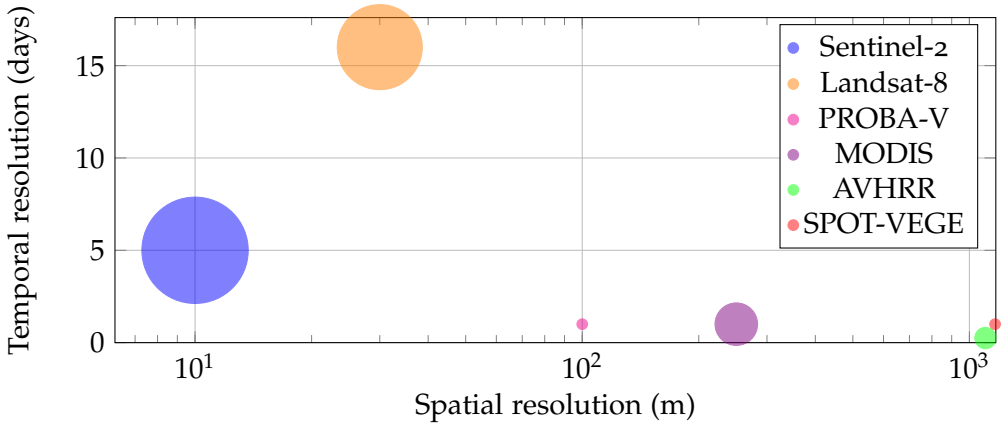

Figure 4.: Spatial and temporal resolutions of optical sensors providing free data. The radius of the circle is proportional to the number of spectral bands of the sensor.

New opportunities...

The properties of this type of sensor enable the acquisition of data with a high precision at national scales. First of all, the high spatial resolution allows for the detection of more details, such as intrafield variations [Ali et al., 2016]. For grasslands, it makes possible the identification of pure grassland pixels that are not mixed with other types of land cover. Moreover, several pixels can belong to the same grassland, and several pixels representing a smaller area in the grassland are more likely to capture the heterogeneity in a grassland (Figure 5).

Secondly, the high temporal resolution enables a finer monitoring of grasslands' phenology, with the possibility to detect with more precision (five days) the phenological events and the management practices during the vegetation cycle. In Figure 6, with a temporal resolution of one month (b) it is not possible to detect short phenological events, for instance the vegetation regrowth in the end of June that is visible with a temporal resolution of 5 days (a).

Finally, the high spectral resolution with spectral bands in the red edge (Figure 7) allows for a more complete characterization of the vegetation. Additionally, it has been shown that classification accuracies of vegetation are better when the spectral resolution is higher [Feilhauer et al., 2013, Zillmann et al., 2014, Sheeren et al., 2016].

Therefore, the new generation satellites make possible a finer and more precise analysis and monitoring of grasslands over wider areas.

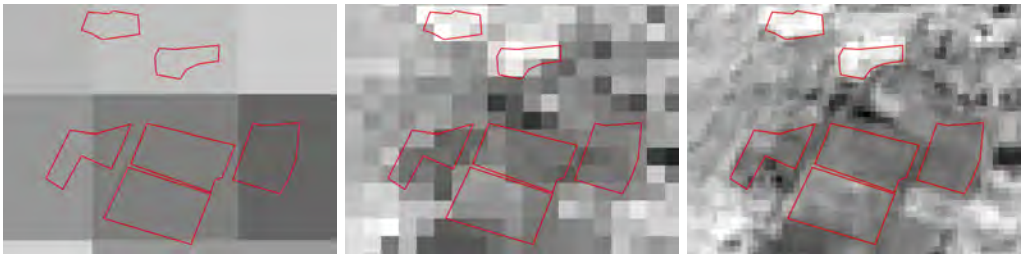

(a) 250 meters (b) 30 meters (c) 10 meters

Figure 5.: (a) Simulated MODIS, (b) simulated Landsat 8, and (c) Sentinel-2 images in the NIR band of the same area (southwest France). The red lines correspond to real grasslands spatial limits.

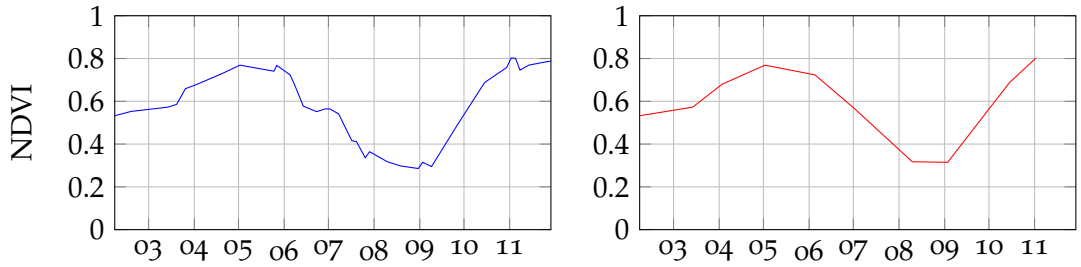

Figure 6.: Normalized Difference Vegetation Index (NDVI) temporal profile of a grassland's pixel with (a) acquired with a very high temporal resolution (Formosat-2, around 5 days) and (b) a medium temporal resolution (1 month). The x-axis represents the months of the year 2006.

... But also new challenges

However, the use of both the spectral and the temporal information in dense multi-spectral time series with a high spatial resolution involves high dimensional and big data issues. Indeed, we have to deal with a high number of spectro-temporal variables but with a small number of samples, because grasslands are relatively small objects in the landscape. Even with high spatial resolution sensors (around 10 meters), on average only a hundred of pixels compose these grasslands while there is about the same number of spectro-temporal variables during a year of acquisitions.

Moreover, decreasing the pixel size implies increasing the number of pixels to process for the same ground surface area. Hence, processing an entire regional area with high spatial resolution data implies dealing with a very large number of pixels. For

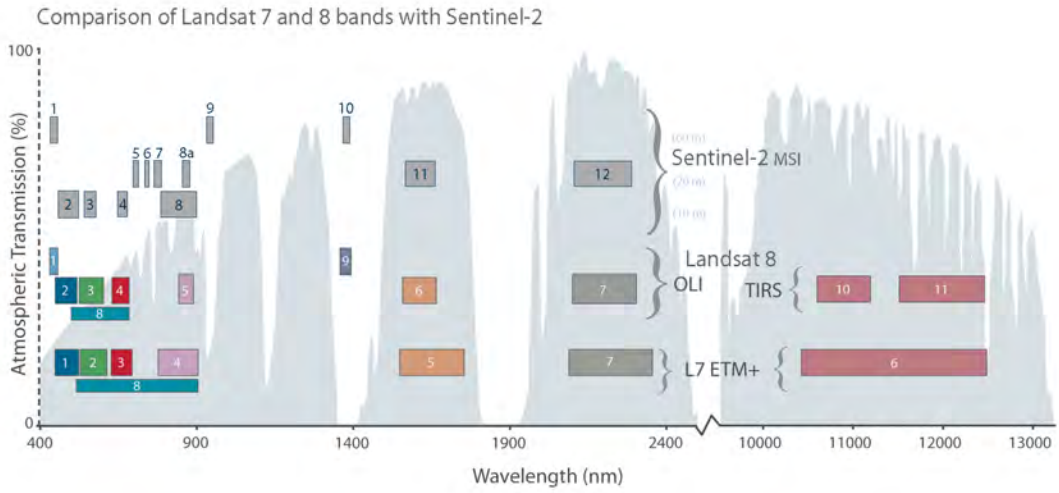

Figure 7.: Comparison of Sentinel-2 spectral bands with Landsat 8 and Landsat 7 (30 meters spatial resolution). Source: Landsat Science, NASA (https://landsat.gsfc.nasa.gov/.

instance, processing the French department "Haute-Garonne" (this administrative division is below the regional administrative level), that covers an area of 6,309 km², means processing more than 63 millions Sentinel-2 pixels. But the complexity of classification algorithms such as Support Vector Machine (SVM) [Cortes and Vapnik, 1995] increases proportionally (between n^2 and n^3) with the number n of pixels to process [Bottou and Lin, 2007].

In contrast, such a high spatial resolution makes possible the work at the object level, by considering several pixels in the grassland. Object-oriented approaches are more likely to characterize grasslands ecologically [Wang et al., 2010, Brenner et al., 2012, Stenzel et al., 2017] because landscape ecologists usually study grasslands at the parcel scale [Laliberte et al., 2007]. At the object level, objects are commonly modeled by their mean spectral value [Duro et al., 2012, Li et al., 2013, Dusseux et al., 2014b, Gómez Giménez et al., 2017]. However, such a representation might be too coarse for a grassland since it does not capture its heterogeneity. Semi-natural grasslands with a high biodiversity level are characterized by their heterogeneity [Öster et al., 2007] that should be accounted for. Hence, a spectral modeling of the grasslands at the object level is needed to account for the distribution of their pixels.

For statistical analysis, a similarity measure between each pair of grasslands is usually required. When a grassland is represented by the mean value of its set of pixels, or by its set of pixels itself, conventional measures used in supervised learning

models such as the Euclidean distance or the standard inner product between feature vectors, can be used. However, many similarity measures used to compare two objects represented by a distribution (Jeffries-Matusita distance, Bhattacharyya distance, Kullback-Leibler divergence) [Cha, 2007] are not numerically stable in a high dimensional space [Donoho, 2000, Fauvel et al., 2013]. Hence, when working with objects issued from SITS, specific derivations are required.

To deal with the high spatio-spectro-temporal resolutions new satellite sensors are now offering, dimension reduction is usually performed through the use of a vegetation index [Ding et al., 2014, Pan et al., 2015, Schmidt et al., 2014, Schuster et al., 2015], Principal Component Analysis [Cingolani et al., 2004] or seasonal metrics [Zillmann et al., 2014, Müller et al., 2015]. However, a large amount of spectro-temporal information is lost with these solutions. Hence, the high spatio-spectro-temporal resolutions have not really been addressed in the literature of remote sensing of vegetation.

As a conclusion of this introduction, the type of data provided by new generation satellites provides new opportunities for grassland monitoring but also new methodological and statistical challenges given the high dimension of data (*i.e.*, number of spectral and temporal measurements) and the large number of pixels to process. Suitable models are lacking with such high resolution data. Hence, new stakes have appeared with the new generation of satellites.

Objectives of this thesis

The objectives of this thesis are to:

1. Provide statistical tools suitable for the analysis and the monitoring of semi-natural grasslands using satellite image time series with a high spatial and a high temporal resolutions.
2. Define ecological variables issued from this type of data, that characterize grasslands and that can be used as inputs of ecological models.
3. Assess the potential of Sentinel-2 to characterize and to monitor semi-natural grasslands in fragmented landscapes.

These objectives imply:

- Analyzing the spectro-temporal response of semi-natural grasslands.
- Developing fast and robust methods and statistical models able to cope with the high dimensionality of the data for the classification of semi-natural grasslands.
- Working at the grassland level (one index/response variable per grassland) to be consistent with ecological studies.

- Finding an effective representation of the grasslands, through their pixels distribution, that accounts for their heterogeneity and their diversity.

The scope of this thesis is the semi-natural grasslands or "permanent grasslands" extensively-used, with a high biodiversity potential, providing ecosystem services related to pollination and pest regulation. Therefore, contrarily to many studies, we are not focused on the biomass production or the vegetation cover of the grasslands, but in their potential for biodiversity. We are interested in the characterization of factors that influence biodiversity in grasslands: species diversity, heterogeneity, age, type and intensity of management practices.

Hence the originality of this thesis lies in its thematic viewpoint since the work is performed with an ecological perspective. The research conducted in this thesis is exploratory and is aimed at giving research tracks for the analysis of semi-natural grasslands using satellite image time series with a high spatial and a high temporal resolutions.

The frame of this work is the new generation satellites providing time series of multispectral images such as Sentinel-2. Thus, no radar data are used in this work. Moreover, it does not deal with the pre-processing of the images (orthorectification, correction of atmospheric effects) since it is assumed that Sentinel-2 images are delivered at a level 1C (orthorectified, reflectance in top of atmosphere) by ESA and at a level 2A (ground reflectance, with a cloud mask) by THEIA land data center for several regions of the world including France.

Thesis organization

This thesis is divided into three parts, each of them comprising one to three chapters in the form of scientific articles. Introduction and conclusions are given for each part.

The first part is dedicated to the analysis of the spectro-temporal response of semi-natural grasslands under management practices. The aim is to describe and analyze the response according to the natural phenology and to the practices, in order to be able to interpret the spectro-temporal profile of grasslands. In Chapter 1, a field campaign was conducted with a spectroradiometer to collect spectral data in a set of grasslands during the growing season. We simulated the Sentinel-2 spectral bands to assess the potential of this sensor to monitor managed semi-natural grasslands. The analysis led us to make hypothesis about the mowing effect on the grassland's spectro-temporal signal through the proposition of an NDVI evolution model of mown semi-natural grasslands.

The second part deals with the development of methods for the supervised classification of grasslands using dense satellite image time series with a high spatial

resolution, suitable to the high dimensionality of the data. We proposed to model the distribution of grassland's pixels while accounting for their heterogeneity by a Gaussian distribution. First, in Chapter 2 we assess the efficiency of several smoothing algorithms to reconstruct missing data in time series due to the occurrence of clouds and their shadows. Then in Chapter 3 we introduce a similarity measure for the supervised classification of grasslands modeled by a Gaussian distribution, that is fast to compute. It was applied to classify the management practices using an intra-annual NDVI time series. Finally in Chapter 4 we present a similarity measure based on a flexible kernel that encompasses several similarity measures for the supervised classification of grasslands. It was applied using an intra-annual multispectral time series for the classification of management practices, and using an inter-annual NDVI time series for the discrimination between young and old grasslands.

While the second part was focused on the methodology with an application to the age and the management practices in grasslands, the third part is focused on the assessment of the species diversity and the definition of ecological indicators of the grasslands issued from remote sensing data. Hence this part is more thematic. In Chapter 5, we assess the potential of satellite image time series with a high spatial and a high temporal resolutions to predict the biodiversity indices of grasslands using a regression model based on kernels. In Chapter 6 we propose to use spectro-temporal heterogeneity measures, derived from the unsupervised clustering of the grasslands using a robust clustering algorithm, as a proxy for the species diversity.

Finally, all the results are discussed and outlooks of this work are provided in the general discussion.

Part I.

Analysis of grasslands spectro-temporal response

Introduction of Part I

Grasslands are semi-natural elements in farmed landscapes. They hold a significant biodiversity resource and are of major interest for ecologists. Grasslands have a natural phenology which depends on their plant composition, the soil properties and the weather conditions. This natural phenology is disturbed by the practices conducted in the grassland, which are necessary to prevent it from turning into a fallow and from woody plant encroachment. The management of the grasslands vary from a region to another, and practices also depend on the climate, the topography and the farming systems. In this work, we focus on grasslands in Europe that are used for feeding the livestock by grazing and/or producing hay or silage. They may receive fertilizing inputs but they are not irrigated.

Hence, many factors have an influence on the spectro-temporal response of this type of grasslands. These factors need to be accounted for when interpreting the signal and the classifications resulting from this signal.

The purpose of Part I is to analyze the spectro-temporal response of grasslands under different management practices, with a particular attention on the mowing practice. We only focus on the growing season of grasslands, which usually starts in the end of winter (February) and ends in the end of fall season (November).

Chapter 1 consists in a description of the spectro-temporal signal of managed grasslands measured on the field with a spectroradiometer resampled at Sentinel-2 spectral resolution.

1. Analysis of semi-natural grasslands' spectro-temporal response from field spectral data

1.1. Introduction

Semi-natural grasslands are an important source of biodiversity in farmed landscapes [Eriksson et al., 1995, Gardi et al., 2002, Sullivan et al., 2010]. They are open habitats with an association of grasses and legume plants which are favorable to insects and micro-organisms [Cole et al., 2006]. This diversity is maintained by an extensive agricultural management (mowing and/or grazing) that prevent the woody plant encroachment [Hansson and Fogelfors, 2000, Moog et al., 2002, Plantureux et al., 2005]. Thanks to their plant and animal composition, semi-natural grasslands provide many ecosystem services such as carbon storage, erosion regulation, food production, crop pollination, pest regulation [Sala and Paruelo, 1997, Werling et al., 2014]. However, the number and the area of these grasslands is in decline because of agriculture intensification, abandonment and urbanization [Peeters, 2009]. Hence, semi-natural grasslands are elements of substantial ecological interest that need to be monitored through the years. Usually, ecologists monitor grasslands with field surveys. But these field surveys require a lot of human and material resources, making them time-consuming and limited to local spatial and temporal scales [Skidmore et al., 2015].

Remote sensing constitutes a unique tool for monitoring grasslands because it provides repeatable spectral measurements of vegetated areas over large spatial extents [Pettorelli et al., 2014]. However, to properly analyze and monitor grasslands using remotely sensed data, it is important to be able to interpret their spectro-temporal signal [Asrar et al., 1986] which is related to their phenology. But contrarily to crops for which spectral signatures are well known [Odenweller and Johnson, 1984, Foerster et al., 2012] because their phenology is controlled by anthropogenic events, the spectro-temporal response of grasslands is not well defined. Indeed, in semi-natural grasslands, the effects of management practices (mowing, grazing...) are added to the natural phenology of grasslands [Ansquer et al., 2009]. The natural phenology depends among others on the type of grasslands (composition, structure, age) and the soil and weather conditions [Losvik, 1991]. The practices depend on the region, the

climate and on the farmers themselves. Hence, there is no unique spectral trend for semi-natural grasslands.

To give some examples, the spectral response of grasslands has been mostly studied according to their biophysical variables such as the aboveground biomass, the Leaf Area Index (LAI), the chlorophyll content [Wylie et al., 2002, Lu, 2006, Clevers et al., 2007, Darvishzadeh et al., 2008, Ullah et al., 2012], but not according to their phenology. Some works described the grasslands inter-annual phenology using long-term temporal data [Verbesselt et al., 2010, Sha et al., 2016] and detected natural events of the phenology such as the start and the end of the growing season [Fontana et al., 2008, White et al., 2009, Cao et al., 2015, Sha et al., 2016]. Most of these works were estimations at regional or national scales using low spatial resolution satellite data (from 250 meters to 1 km/pixel).

Only a few remote sensing works focused on the description of managed grassland's phenology at the grassland's scale. Among them, Turner *et al.* [Turner et al., 1992] studied the effect of management on the radiometric response of a tallgrass prairie with a field spectroradiometer. They provided a detailed description of the mowing and grazing effects with one to three measurements per month, but the study of mowing effect was conducted on experimental plots in a controlled environment. Maskova *et al.* [Mašková et al., 2008] also described the Normalized Difference Vegetation Index (NDVI) evolution (one measurement per month) of experimental grasslands under different treatments (mowing, mulching and unmanaged). But an experimental plot does not represent the diversity and heterogeneity within and among grasslands that can be found in a landscape.

Regarding works conducted in non-experimental grasslands, Pocas *et al.* [Poças et al., 2012] studied the impacts of management practices on the vegetation dynamics of irrigated semi-natural grasslands in Portugal using inter-annual SPOT-VEGETATION imagery (36 images per year). Nitze *et al.* [Nitze et al., 2015] described the EVI and NDVI curves of improved and semi-improved grasslands in Ireland using inter-annual MODIS imagery (23 images per year), but the definition of these two categories of grasslands was not provided. Dusseux *et al.* [Dusseux et al., 2014c] described the effect of management practices on the intra-annual variability of intensively used grasslands' LAI derived from satellite data (one acquisition per month), in Brittany, France. However, although the LAI is consistent to estimate the biomass production, it is not related to the diversity in species of a grassland. Hence, the study of the spectro-temporal response of semi-natural grasslands, extensively managed and with a high biodiversity potential has never been addressed yet.

In terms of Earth observations data used, the aforementioned works relied on medium to low spatial resolution satellite data such as MODIS (250 meters per pixel), SPOT-VEGETATION or AVHRR (1 km) with high temporal resolution, or (very) high spatial

resolution data (a few meters: field spectrometer, Quickbird) but with a low temporal resolution (one acquisition per month). For semi-natural grasslands in fragmented landscapes such as found in Europe, high spatial resolution data are required [Corbane et al., 2015] because they are small elements with an area of around 1 hectare (*i.e.*, 10,000 m²). Moreover, high temporal resolution data are necessary to monitor the phenology and the management practices. Until recently, satellite missions with a high temporal resolution (1 day) had low to medium spatial resolution (MODIS, AVHRR) and satellite data with high spatial resolution were costly and hence, a time series with a high temporal resolution was difficult to obtain. Landsat mission constituted a trade-off between spatial and temporal resolution (16 days, 30 meters), but these resolutions are not fine enough for grassland's monitoring. Now, new generation satellites such as Sentinel-2 [Drusch et al., 2012] provide freely images with a high temporal resolution (5 days) jointly with a high spatial resolution (10 m) in 13 spectral bands. Moreover, the THEIA land data centre provides pre-processed Sentinel-2 images of Europe. The unique properties of Sentinel-2 offer new opportunities for grasslands monitoring.

The scope of this work is to investigate the effects of the natural phenology of extensively managed semi-natural grasslands combined with their management practices on their spectro-temporal response using high spatial and high temporal resolution data, which has never been done before. The aim is to assess the potential of Sentinel-2 time series to monitor grasslands with a high potential in biodiversity, with a particular focus on mown grasslands. However, in 2016, Sentinel-2 was not fully operational and had a temporal resolution of 10 days. If an acquisition occurred on a cloudy day — which is frequent in the spring —, it would result in 20 days, or more, without spectral information. Hence, to ensure spectral acquisitions around the mowing season, a field campaign was conducted to simulate Sentinel-2 data with a spectroradiometer. The stakes were to monitor a set of selected grasslands with as much acquisitions as possible to simulate Sentinel-2 data. Five grasslands in southwest France managed differently (mowing, mixed — mowing and grazing —, two mowings) were monitored during the growing season, from March to September 2016. One or more acquisitions per month and per grassland were collected. The hyperspectral spectra were resampled to simulate the Sentinel-2 spectral bands and they were described according to the grassland's state.

In the next section, the materials and methods used in this study are presented. Then, the results are presented and discussed, before giving conclusions.

1.2. Materials and method

1.2.1. Study area

The study area is situated in the Long-Term Ecological Research site "Coteaux et Vallées de Gascogne" (LTER_EU_FR_003), located in Gascony, in southwest France near the city of Toulouse (43°17′N, 0°54′E, Figure 1.1). This hilly area is characterized by a mosaic of crops, small woods and grasslands. It is dominated by mixed crop-livestock farming. Grasslands provide food for cattle by grazing and/or producing hay or silage. Most of the grasslands are under mixed management — used for mowing and grazing. Grasslands are mainly located on steep slopes whereas annual crops are in the valleys on the most productive lands. The climate is sub-Atlantic with sub-Mediterranean and mountain influences (mean annual temperature, 12.5°C; mean annual precipitation, 750 mm) [Ryschawy et al., 2012, Carrié et al., 2017]. The weekly cumulated rainfalls and the daily average temperatures recorded in the study area during the field campaign can be seen in Figure 1.2.

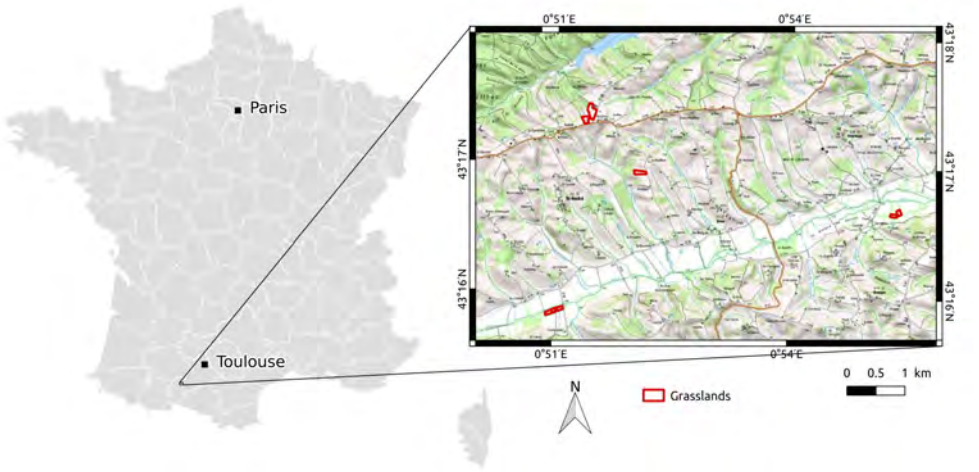

Figure 1.1.: Location of the sampled grasslands within the Long-Term Ecological Research site "Coteaux et Vallées de Gascogne", southwest France. The background layer is a topographic map from the French national database "BD Topo Scan25", ©IGN.

1.2.2. Grasslands' sampling design

Grasslands composing the dataset have been selected on different criteria. The grassland's area should correspond to at least one hundred Sentinel-2 pixels, *i.e.*, at least 100×100 m^2 = 1 hectare. The slope should be limited (lower than 20°) for grasslands

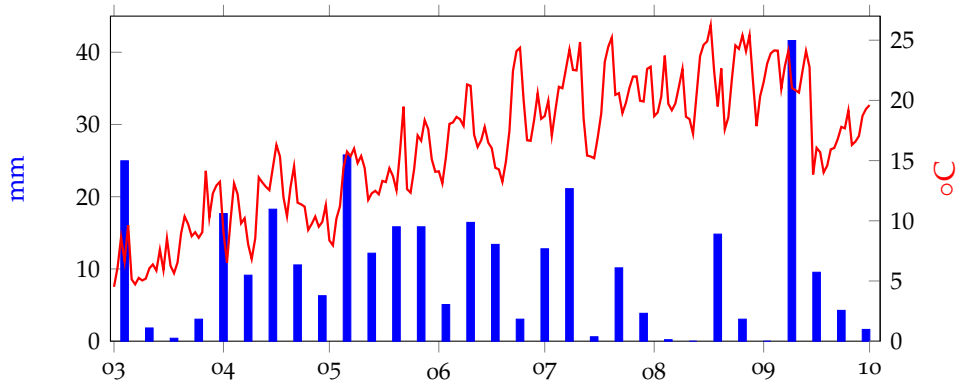

Figure 1.2.: Weekly cumulated rainfall (mm) in blue and daily average temperature (°C) in red in the study area. The x-axis corresponds to the months of year 2016. Data acquired at the weather station of St André, France (43°15′25″N, 0°51′35″E).

located in hills. All the grasslands should be mown, but no grazing before the mowing was allowed for the selection, in order to study the effect of the mowing on the spectral response. Among these fixed criteria, grasslands were selected on a gradient of use intensity, from annual and improved grassland mown twice to semi-natural grasslands extensively used. 18 grasslands were selected based on these criteria, after interviewing the farmers in January 2016. However, only 12 grasslands could actually be monitored since the start of the growing season in March, and only four grasslands have more than five measurement dates. These four grasslands are presented in this work as well as the only grassland being mown twice (Tables 1.1 and B.1 and Figure 1.1).

The grasslands are under mowing or mixed managements. For mixed management, grazing is normally conducted at least a few weeks after the mowing, in order to let the grassland regrow. Most of the selected grasslands receive fertilizing inputs as organic (manure) or mineral (Nitrogen, Potassium) fertilization in low quantities except for grassland 406 (Table 1.1). This grassland is annual and was sown with ryegrass (*Lolium perenne*) the year before the field campaign (ID 406) (Table B.1). It is used for producing silage and it is mown twice and grazed. Three grasslands are semi-natural grasslands that have not been ploughed and sown for at least a hundred years, composed of spontaneous species and having a high potential in biodiversity (IDs 131, 405 and 500, Table B.1). They are extensively-used. One grassland is "temporary", part of a rotation and more intensively-used than the semi-natural grasslands (ID 36). It is dominated by clover (*Trifolium repens*, Table B.1), characteristic of grazed grasslands.

Three grasslands are located on the top of a hill, with limited slope, and two semi-

Table 1.1.: Characteristics of the five monitored grasslands. ID is the grassland's number. Age refers to the number of years since last sowing. "Old" signifies the grassland has been there and never ploughed since the establishment of the current farmer's family. The grazing dates are approximate. The topography corresponds to the location in the area: top of a "hill" or bottom of a "valley".

ID	Age	Management	Input	Mowing date	Grazing	Area (ha)	Topography
36	8	Mixed	Minerals	May 27	July 6-15 and August 4-15	1.1	Hill
131	Old	Mixed	Organic	June 9	September 1-15	1.2	Valley
405	Old	Mixed	None	July 5	Not during the campaign	1.2	Hill
406	1	Mixed	Organic	April 29 and June 20	July 19 - August 15	2.6	Hill
500	Old	Mowing	Organic	June 20	None	1.7	Valley

natural grasslands are at the bottom of a valley (Table 1.1), where the soil is more humid.

The spectra were collected throughout the growing season, between March and September 2016 (Figure 1.3). Due to the weather conditions in the beginning of the growing season, the first acquisition dates were March 14, 15 or 23, although earlier dates would have been preferred. There is about one acquisition per month per grassland — sometimes two acquisitions per month, sometimes no acquisition in one month — which is fewer than intended. Ideally, the field campaign should have lasted until the end of October, but due to lending constraints, the last acquisition date was September 27 for two grasslands, and July 29 or August 25 for the other grasslands.

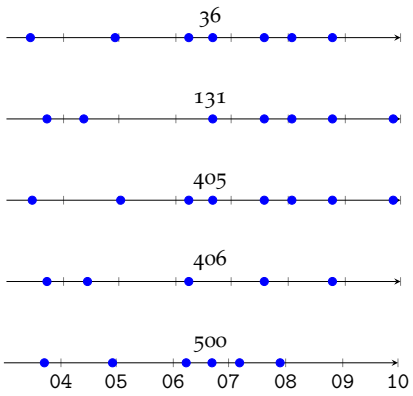

Figure 1.3.: Synthesis of spectra acquisition dates for each grassland (the corresponding ID is above the axis). The axis represents the months of year 2016.

1.2.3. Field spectral data acquisitions

An ASD FieldSpec (ASD Inc., Boulder, CO, USA) was used to collect the spectral data. Its full spectral range is between 350 and 2500 nm, with a 3 nm spectral resolution in the VNIR (Very Near Infrared) wavelengths (350 - 1000 nm) and 10 nm spectral resolution in the MIR (Mid-Infrared) wavelengths (1001 - 2500 nm).

The spectroradiometer was calibrated over a Spectralon reflectance panel (Labsphere Inc., North Sutton, NH, USA) to obtain the spectra in reflectance. The device was calibrated every 10 measurement plots and every time the light and atmospheric conditions changed. Spectra were collected under sunny and cloud-free conditions, between 10 a.m. and 4 p.m. local time, when the sun provides good lightning conditions.

In each grassland, between 40 and 60 sampling plots (depending on the grassland area) were measured on a random S-shaped pattern covering the whole extent of the grassland. Each plot had to be at least 10 meters (one Sentinel-2 pixel size) from the field boundaries to avoid edge effects [McCoy, 2004] (Figure 1.4.a). At each sampling plot, five measurements, each of them comprising 25 internal averaged spectrum collections, were recorded. The spectra were acquired with a field-of-view of 25° at a height of approximatively one meter above ground, which results in a ground surface area of around 45 cm of diameter per plot (Figure 1.4.b). The ground composition had to be homogeneous within the plot, *i.e.*, not a boundary between two very different soil occupations, in order to facilitate the interpretation of the collected spectra.

1.2.4. Signal processing

For each sampling plot, the average of the five measurements was computed to get a unique spectrum per plot. If an aberrant measure was present, it was removed from the average. It resulted in between 40 and 60 mean spectral measurements per grassland and date of acquisition.

There are three sensors in the spectroradiometer, corresponding to wavelengths 350-1000 nm, 1001-1830 nm and 1831-2500 nm. A break-point exists between the sensors which causes a jump in reflectance that requires correction. Jump correction was performed using a method based on tangents calculation that is used in the software *Spectral Analysis and Management System* (SAMS 2.0, developed at the Center for Spatial Technologies and Remote Sensing (CSTARS), University of California, Davis, USA, `https://github.com/carueda/sams`). The wavelengths corresponding to water absorption, *i.e.*, 1350-1410 nm, 1810-1970 nm and 2400-2500 m were removed.

In this study, we only focus on the visible and near infrared (NIR) spectral domain useful for vegetation characterization, *i.e.*, between 350 and 1100 nm [Peñuelas and Filella, 1998]. The hyperspectral data were resampled to simulate Sentinel-2 spectral bands [Feilhauer et al., 2013] corresponding to the 10-m and 20-m spatial resolutions

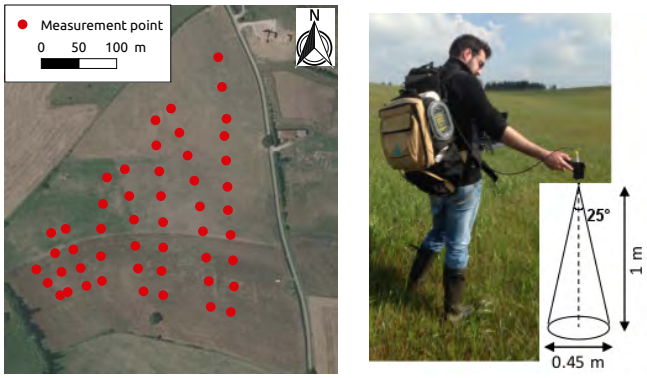

(a) (b)

Figure 1.4.: (a) Example of S-shaped pattern within the grassland. The red dots correspond to the sampling plots. The plots are at least 10 meters from the boundaries. The plot positions were acquired with a GPS device with a precision of around 2-3 meters. The background is an aerial photograph from the French orthophoto database "BD Ortho" ©IGN. (b) Schematic of the measure acquired with a sensor with a field-of-view of 25° at a height of one meter above ground.

Table 1.2.: Characteristics of Sentinel-2 spectral bands simulated in this study [Drusch et al., 2012].

Band	Central wavelength (nm)	Band width (nm)	Spatial resolution (m)
B2 (Blue)	490	65	10
B3 (Green)	560	35	10
B4 (Red)	665	30	10
B5 (Red edge 1)	705	15	20
B6 (Red edge 2)	740	15	20
B7 (Red edge 3)	783	20	20
B8 (NIR)	842	115	10
B8A (Narrow NIR)	865	20	20

bands of the visible and near infrared domain: B2, B3, B4, B5, B6, B7, B8, B8A (Table 1.2). The resampling is based on a simple weighted average of the wavelengths comprised in each spectral channel. The weights were attributed following the spectral responses of Sentinel-2 given in the document downloadable at: https://earth.esa.int/documents/247904/685211/Sentinel-2+MSI+Spectral+Responses. Hence,

only the spectral resolution of Sentinel-2 is taken into account in this study, not the spatial resolution.

Several vegetation indices were computed using the Sentinel-2 simulated spectral bands (Table 1.2):

- Normalized Difference Vegetation Index (NDVI) [Rouse et al., 1973] which reflects the photosynthetic activity of the vegetation:

$$\mathrm{NDVI} = \frac{\mathrm{B8} - \mathrm{B4}}{\mathrm{B8} + \mathrm{B4}},$$

- Modified Soil-Adjusted Vegetation Index 2 (MSAVI2) [Qi et al., 1994] which is equivalent to the NDVI but eliminates the soil contribution:

$$\mathrm{MSAVI2} = \frac{2 \times \mathrm{B8} + 1 - \sqrt{(2 \times \mathrm{B8} + 1)^2 - 8(\mathrm{B8} - \mathrm{B4})}}{2},$$

- Sentinel-2 Red Edge Point (S2REP) [Frampton et al., 2013] which estimates the red edge (RE) point (point of maximum slope along the RE) for Sentinel-2 that is used to estimate the chlorophyll content:

$$\mathrm{S2REP} = 705 + 35 \times \frac{\frac{\mathrm{B7}+\mathrm{B4}}{2} - \mathrm{B5}}{\mathrm{B6} - \mathrm{B5}}.$$

1.2.5. Spectral signatures of vegetation and soil

Prerequisites for the signal interpretation of grasslands can be found in Appendix A, where the typical spectral signature of vegetation and soil measured during this field campaign can be seen in Figures A.1 and A.2. The chlorophyll present in the leaves absorbs the electromagnetic signal in the blue and red wavelengths and reflects the light in the green wavelengths during the photosynthesis process [Tucker, 1979]. The spongy mesophyll tissue reflects the light in the near infrared (NIR) wavelengths. A dense vegetation with a high photosynthetic activity has a sharp increase in the NIR bands, making higher the red edge jump. The vegetation index values, such as NDVI, are usually high [Tucker, 1979, Jackson and Huete, 1991, Myneni et al., 1995]. Senescent vegetation has a lower photosynthetic activity, decreasing the reflectance in the NIR and decreasing the absorption in the blue and red wavelengths [Colwell, 1974, Asrar et al., 1986]. Therefore, the NDVI value is lower than for green vegetation [Jackson and Huete, 1991]. The soil reflectance increases slightly along the wavelengths axis from the visible to the NIR bands. The soil reflects more in the visible wavelengths — especially in the red — and less in the NIR bands than the vegetation. The NDVI

value of soil is close to zero [Jackson and Huete, 1991]. The reflectance depends on the soil type, its roughness, color and humidity [Huete et al., 1985, Asrar et al., 1986].

Dense vegetation and bare ground are two "extreme" land covers that can be found in a grassland. Usually, a mix of green vegetation, senescent vegetation and soil is measured in a grassland [Asrar et al., 1986], with proportions depending on the grassland state.

1.3. Results: Description of the signal depending on management practices

The spectral response of the monitored grasslands is described according to their management practice: one mowing, two mowings, mowing and grazing (mixed). We limit the analysis to the aforementioned Sentinel-2 spectral bands and vegetation indices. Full range of the spectral acquisitions as well as digital photographs of the measurement plots can be seen in Appendix B (Figures B.1 to B.5) for each grassland and each acquisition date.

1.3.1. One mowing

Two grasslands were mown once and not grazed during the growing season: grasslands 500 and 405 (Table 1.1). Grassland 500 was mown on June 20 while grassland 405 was mown later in the season, on July 7. These grasslands are both semi-natural grasslands extensively used, but grassland 500 is at the bottom of a valley while grassland 405 is on top of a hill.

We can see from Figure 1.5 that from the start of the growing season until the growth peak in mid-May, the reflectance in the green and NIR bands increases while the reflectance in the red band decreases. It results in a sharper red edge jump. Then, in June, the reflectance in the NIR for grassland 405 starts to decrease, while it remains stable for grassland 500. The mowing occurring on June 20 in grassland 500 makes the spectral response increase in the visible bands, while it decreases in the NIR band, reducing drastically the red edge jump. Moreover, just after the mowing, the standard deviation of the reflectances is higher in most bands but particularly in the visible and the red edge. Then, the vegetation starts regrowing but slower than the spring growth. The reflectance in the NIR bands slightly increases while it decreases in the visible bands. The spectral response of grassland 405 is different since it was mown later in July. By the end of June, the NIR reflectance has already started decreasing. However, this decrease is much more pronounced in July after the mowing. The reflectance in the visible bands also increases after the mowing and their standard deviation is higher after this event. Then, the vegetation starts regrowing again, the reflectance in

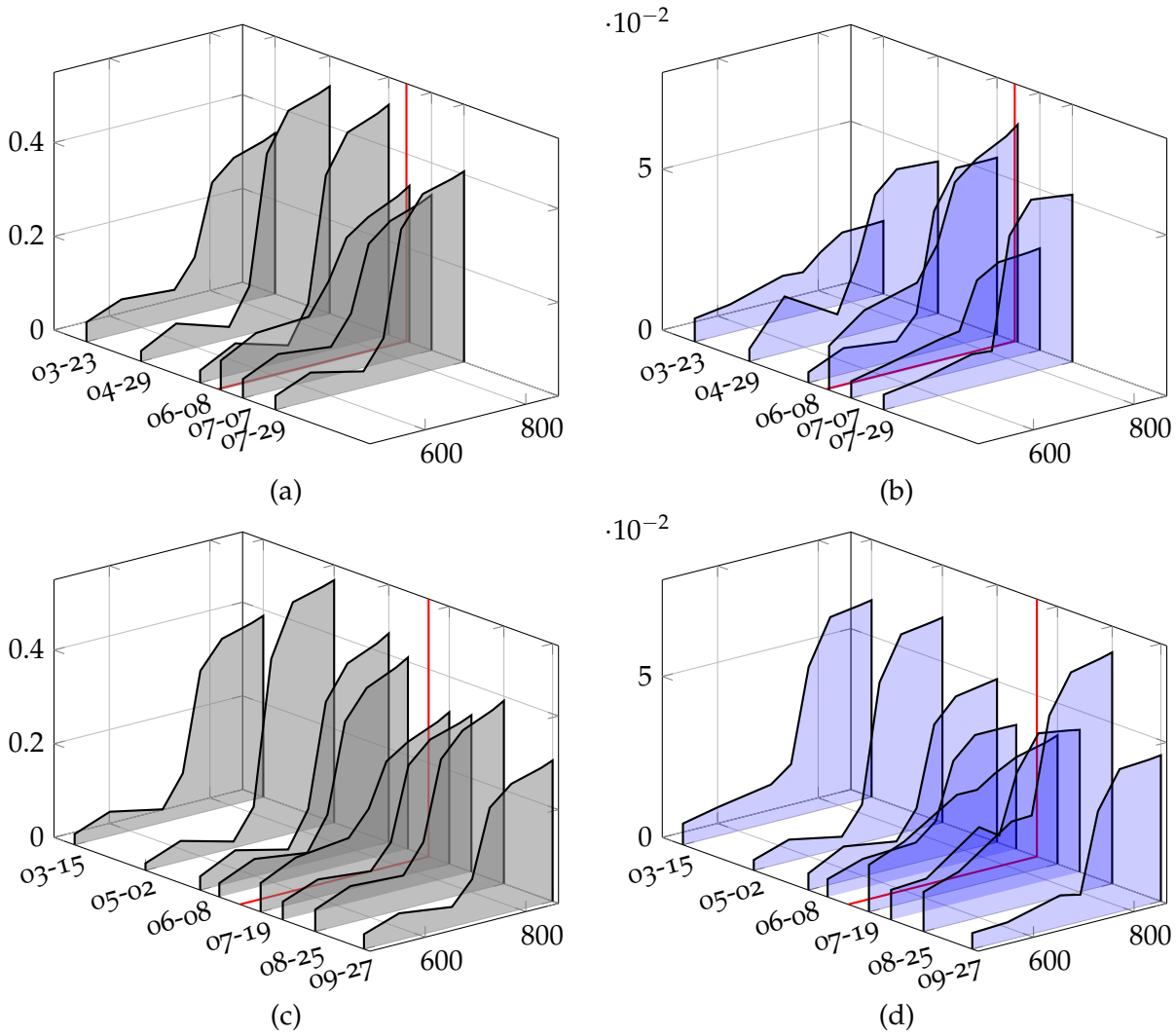

Figure 1.5.: Temporal dynamics of the (a) mean and (b) standard deviation of the measurements resampled at Sentinel-2 spectral resolution acquired in a semi-natural grassland mown on June 20 (red line) (ID 500), and of the (c) mean and (d) standard deviation of the measurements acquired in a semi-natural grassland mown on July 5 (red line) (ID 405). The x-axis is the wavelength (nm) and the y-axis is (a, c) the reflectance, (b, d) the standard deviation of the reflectance.

the visible bands decreases and increases gradually in the NIR bands. The standard deviation of NIR bands remains large in the summer. At the end of the summer on September 27, the reflectance in the visible bands and in the NIR bands is globally lower.

In terms of vegetation indices (VI), the NDVI has higher values than the MSAVI2, but it does not seem less sensitive to grassland's phenology (Figure 1.6). The S2REP shows similar trends to the other indices. Until the growth peak, the average VI values increase while their variances decrease, except for S2REP. The mowing in grassland 500 makes the VI values drastically decrease and their variances increase, particularly the NDVI variance. Then, the VI averages increase again to values almost equivalent to values before the mowing. NDVI variance is larger than before the mowing, contrarily to S2REP variance. Grassland 405 was mown later in the season. Therefore, before the mowing, the VI values start to decrease smoothly (approximatively from 0.9 to 0.8 for NDVI) with a slight increase of the variance. However, the mowing still has a significant impact on the NDVI, reducing its value to 0.5 and increasing its standard deviation. These effects are less visible with the other indices. Then, after this late mowing, the VI values rise again but with a high variance, especially for NDVI and MSAVI2, and at values lower than before the mowing. At the end of the summer, the values remain more or less stable.

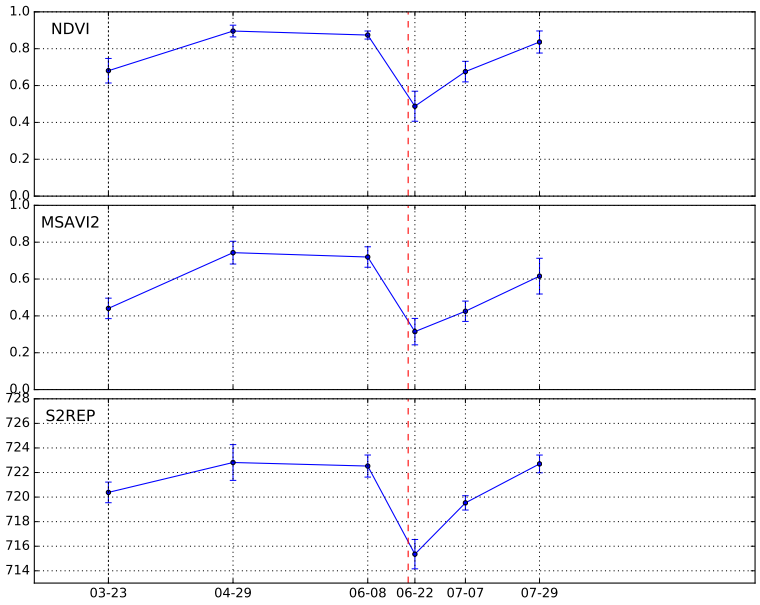

(a)

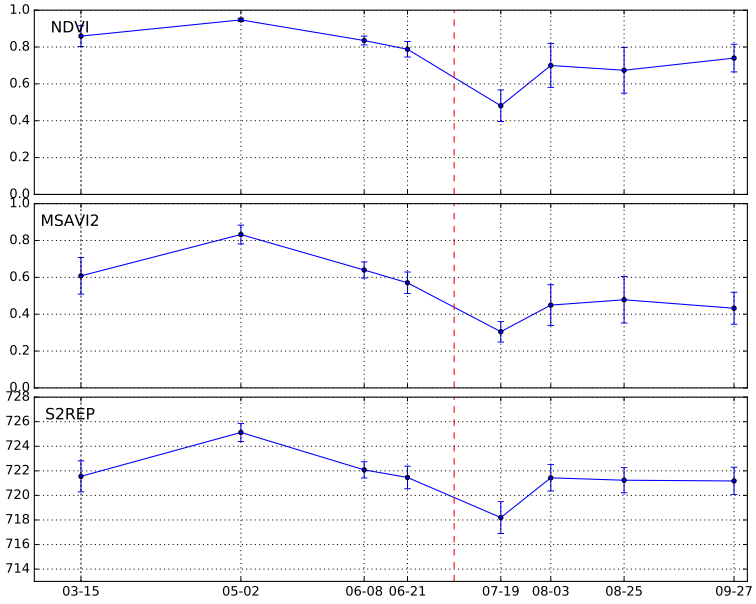

(b)

Figure 1.6.: Evolution of the mean ± standard deviation of the distribution of vegetation indices computed from Sentinel-2 spectral bands in (a) a semi-natural grassland mown on June 20 (dotted red line) (ID 500) and (b) a semi-natural grassland mown on July 5 (dotted red line) (ID 405). The x-axis is the acquisition date and the the y-axis is the vegetation index value.

1.3.2. Two mowings

Only one grassland was mown twice. It is a monospecific grassland of ryegrass that is used for producing silage (ID 406). It receives a high amount of fertilizer and it is grazed after the second mowing. Unfortunately, there were no measurement dates close to the two mowing dates (April 29 and June 20). After the first mowing occurring in spring, the regrowth is high and the NIR reflectances reach as high values as before the mowing (Figure 1.7). Indeed, the grassland received fertilization inputs during this period. However, after the second mowing occurring in the grassland on August 15, its spectral response becomes close to bare ground's spectral signature because of an important soil exposure (Figure B.3 in Appendix B). The standard deviation becomes equivalent and relatively low in all bands. Later in August, the grassland was grazed, preventing the grass from regrowing. The spectral response thus does not change a lot but its standard deviation is increases in all bands.

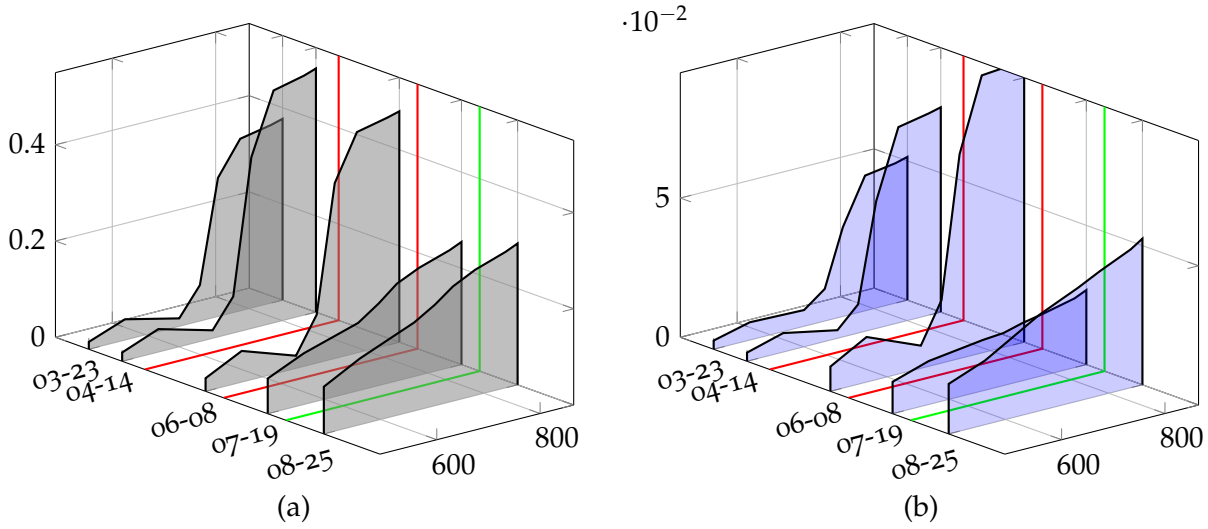

Figure 1.7.: Temporal dynamics of the (a) mean and (b) standard deviation of the measurements resampled at Sentinel-2 spectral resolution acquired in a sown grassland mown twice: April 29 and June 20 (red lines) and grazed between July 19 and August 15 (green line) (ID 406). The x-axis is the wavelength (nm) and the y-axis is (a) the reflectance, (b) the standard deviation of the reflectance.

The NDVI was close to saturation (NDVI $\approx$ 1) before the mowing, with a low standard deviation, and it reached this same level one month after the mowing in June (Figure 1.8). The MSAVI2 and the S2REP show generally higher standard deviations than NDVI, and their values are lower after the first mowing. However, after the second mowing, the values decrease for all VI. NDVI decreases to values close to 0.2,

which is lower than for the semi-natural grasslands. The standard deviation of the NDVI increases after the mowing, unlikely to the other indices that had a higher standard deviation before the mowing. After the grazing period, the NDVI and MSAVI2 decrease while the S2REP increases.

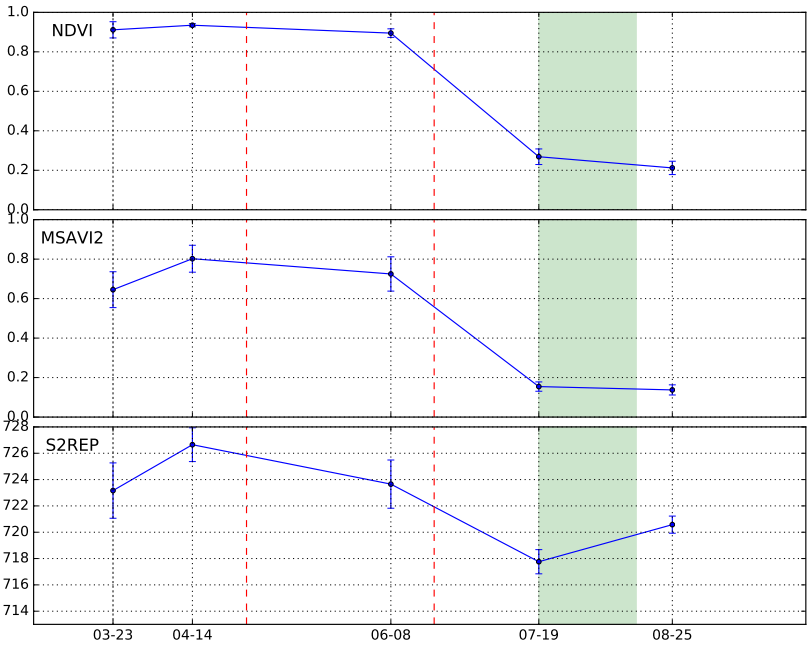

Figure 1.8.: Evolution of the mean $\pm$ standard deviation of the distribution of vegetation indices computed from Sentinel-2 spectral bands in a sown grassland mown twice: April 29 and June 20 (dotted red lines) and grazed between July 19 and August 15 (green filled zone) (ID 406). The x-axis is the acquisition date and the the y-axis is the vegetation index value.

1.3.3. Mowing and grazing

Two grasslands were mown and grazed during the field survey (Table 1.1): grassland 131 which is a semi-natural grassland extensively grazed at the bottom of a valley and grassland 36 which is a temporary grassland more intensively grazed on the top of a hill.

In this subsection, only the grazing part is presented because the mowing occurred before the grazing and has similar effects to those described for grasslands 500 and 405. Grassland 131 was grazed in the end of the summer, during the first half of September. The grazing makes the NIR reflectances decrease and the visible and red edge reflectances increase (Figure 1.9.a.). In terms of VI (Figure 1.10.a), their average value decreases while the variance of NDVI and S2REP increases.

Grassland 36 was grazed during two periods: July 6-15 and August 4-15. The grazing impact in grassland 36 seems stronger than for grassland 131 (Figure 1.9.b). The second period of grazing makes the spectral signature of the grassland close to dry grass' spectral signature (Figure B.5). The VI values (Figure 1.10.b) are also decreased after the grazing periods (except for the S2REP after the first grazing period). The standard deviation of NDVI increases a lot after the first period, unlikely to MSAVI2 and S2REP standard deviation. After the second period, all the VI standard deviations are lower. The VI values are globally lower than for grassland 131 after the grazing period.

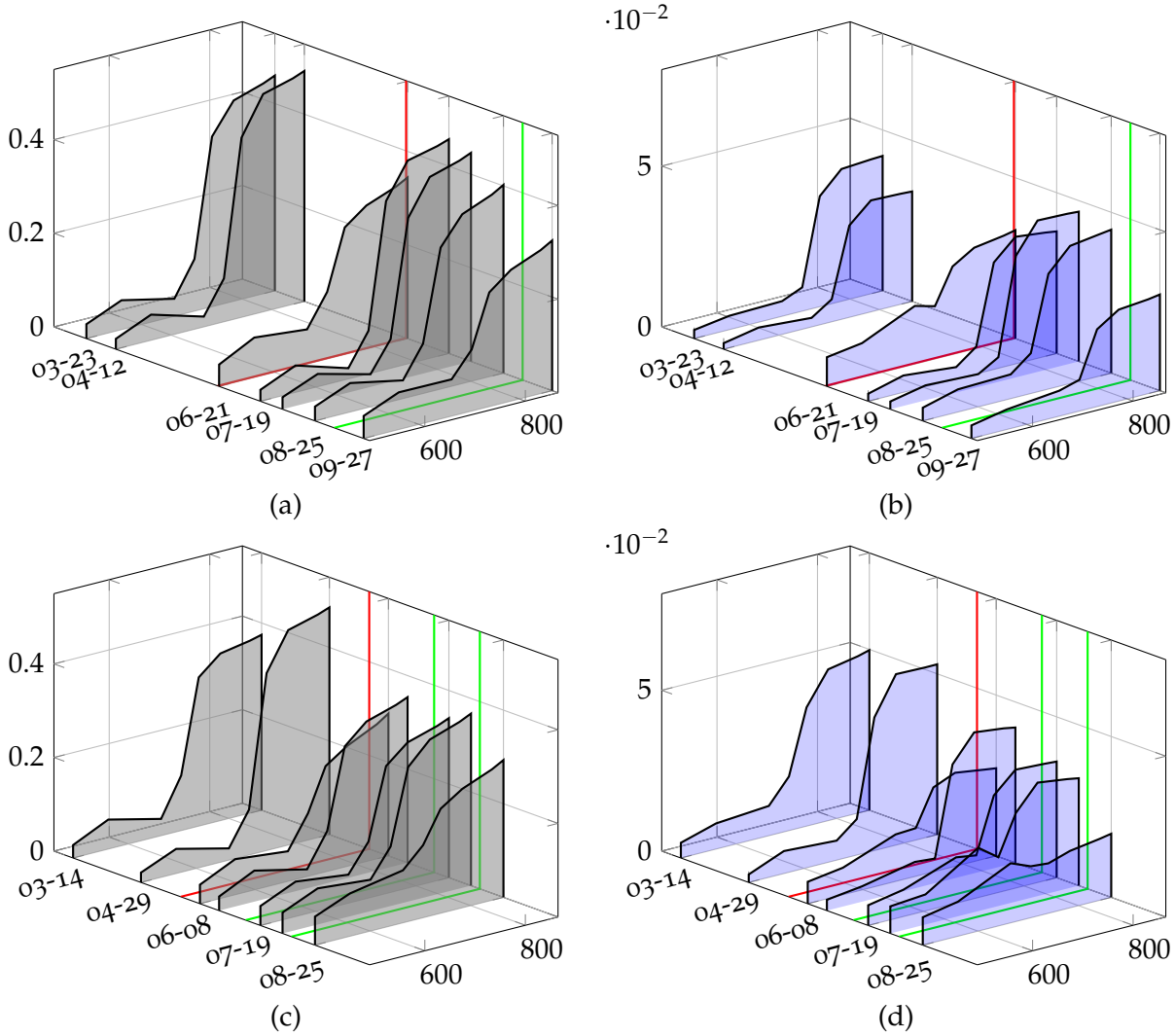

Figure 1.9.: Temporal dynamics of the (a) mean and (b) standard deviation of the measurements resampled at Sentinel-2 spectral resolution acquired in a semi-natural grassland mown on June 9 (red line) and grazed between September 1-15 (green line) (ID 131) and of the (c) mean and (d) standard deviation of the measurements acquired in a temporary grassland mown on May 27 (red line) and grazed between July 6-15 and August 4-15 (green lines) (ID 36). The x-axis is the wavelength (nm) and the y-axis is (a, c) the reflectance, (b, d) the standard deviation of the reflectance.

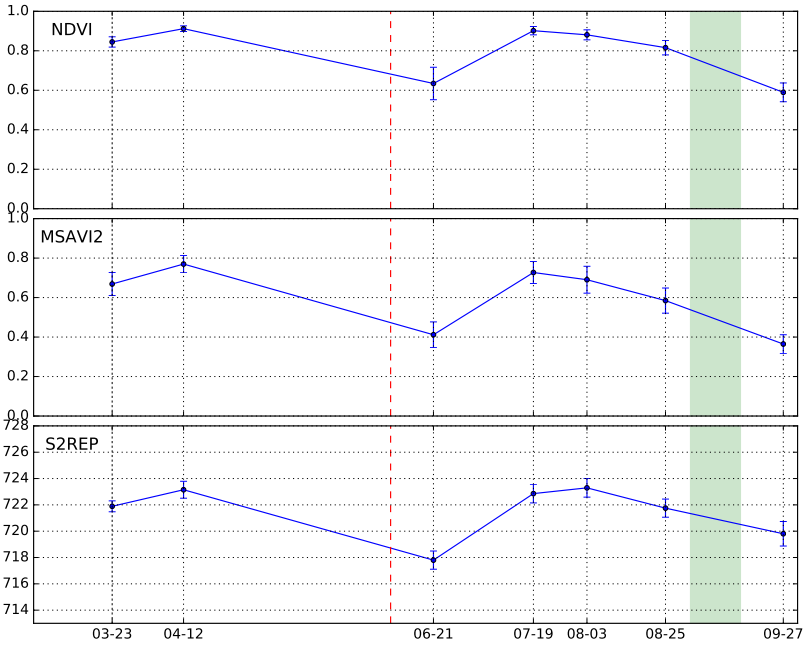

(a)

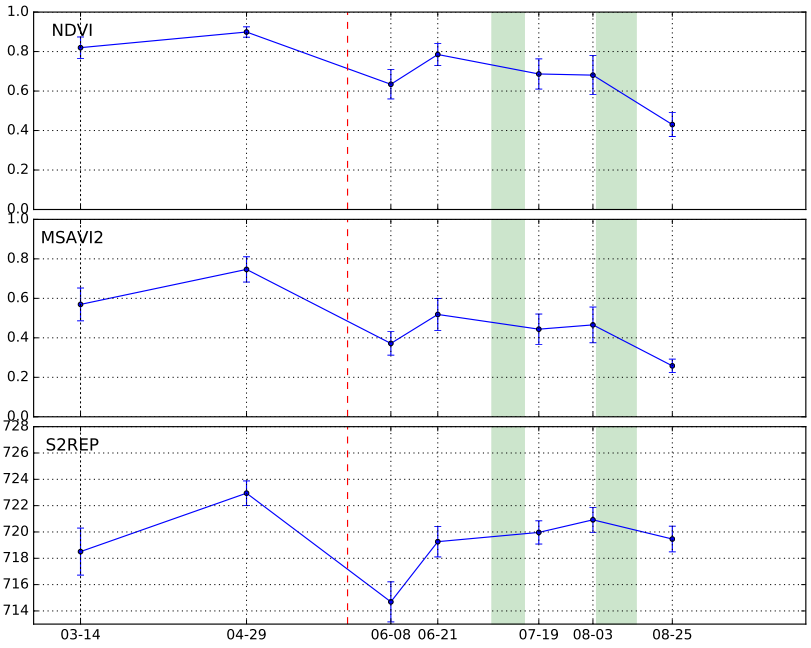

(b)

Figure 1.10.: Evolution of the mean $\pm$ standard deviation of the distribution of vegetation indices computed from Sentinel-2 spectral bands in (a) a semi-natural grassland mown on June 9 (dotted red line) and grazed between September 1-15 (blue filled zone) (ID 131) and (b) in a temporary grassland mown on May 27 (dotted red line) and grazed between July 6-15 and August 4-15 (blue filled zone) (ID 36). The x-axis is the acquisition date and the the y-axis is the vegetation index value.

1.4. Discussion

1.4.1. Semi-natural grasslands' spectro-temporal response

1.4.1.1. Mowing effect

From the start of the growing season to the growth peak, the green biomass develops and the reflectance in the red wavelengths decreases while the reflectance in the green and NIR wavelengths increases, making higher the red edge peak. Following the growth peak, the vegetation becomes little by little senescent and its photosynthetic activity reduces [Reed et al., 1994, Merzlyak et al., 1999], especially if the grassland is on top of a hill. Hence, the trend is reversed: visible reflectance increases while NIR reflectance decreases [Asrar et al., 1986, Gitelson and Merzlyak, 1994, Sims and Gamon, 2002]. In terms of vegetation indices (VI), their value increases until the growth peak and then it decreases. Therefore, if the grassland is mown late in the growing season, the VI already start decreasing before the mowing event because of senescent material accumulation [Turner et al., 1992] (Figure 1.11.b). Hence, contrarily to several studies that based the mowing detection on a unique NDVI decrease [Peterson and Aunap, 1998, Courault et al., 2010, Halabuk et al., 2015, Gómez Giménez et al., 2017], we showed that this is not the case in non-irrigated grasslands. These results are more in line with the study on unmown grasslands in the work of Turner *et al.* [Turner et al., 1992].

However, the results showed that the mowing still implies a sharp decrease of the NIR reflectance and of the VI values. The decrease is sudden whereas it is slower for natural senescence. More importantly, the mowing also implies an increase of the variance of the VI accounting for the soil effect (such as NDVI) within the grassland. Indeed, before the mowing, the vegetation is dense and it covers all the ground (Figure 1.11.a). Therefore the signal measured by the sensor is homogeneous and it only comes from vegetation. Hence, the NDVI can saturate around the growth peak with values close to 1. After the mowing, the soil is exposed (bare soil) in some areas of the grassland, the vegetation is sparse and composed both of senescent and green materials [Louault et al., 2005] (Figure 1.11.c). Therefore, the spectral response of the grassland is heterogeneous. The increase of variance for MSAVI2 and S2REP is less visible than for NDVI because they are less affected by soil effect. The VI values are globally lower than before the mowing. We could suppose that the increase of NDVI variance after the mowing is related to its saturation before the mowing. However, red and NIR reflectance variances increase after the mowing, confirming the NDVI variance increase.

The regrowth after the mowing is heterogeneous and sparse within the grassland. Some areas of the grassland grow faster than others, depending on the plant species, the soil properties, the topography and the water availability. Its explains why the

variance of VI, and of NDVI particularly, is higher than during the first part of the growing season.

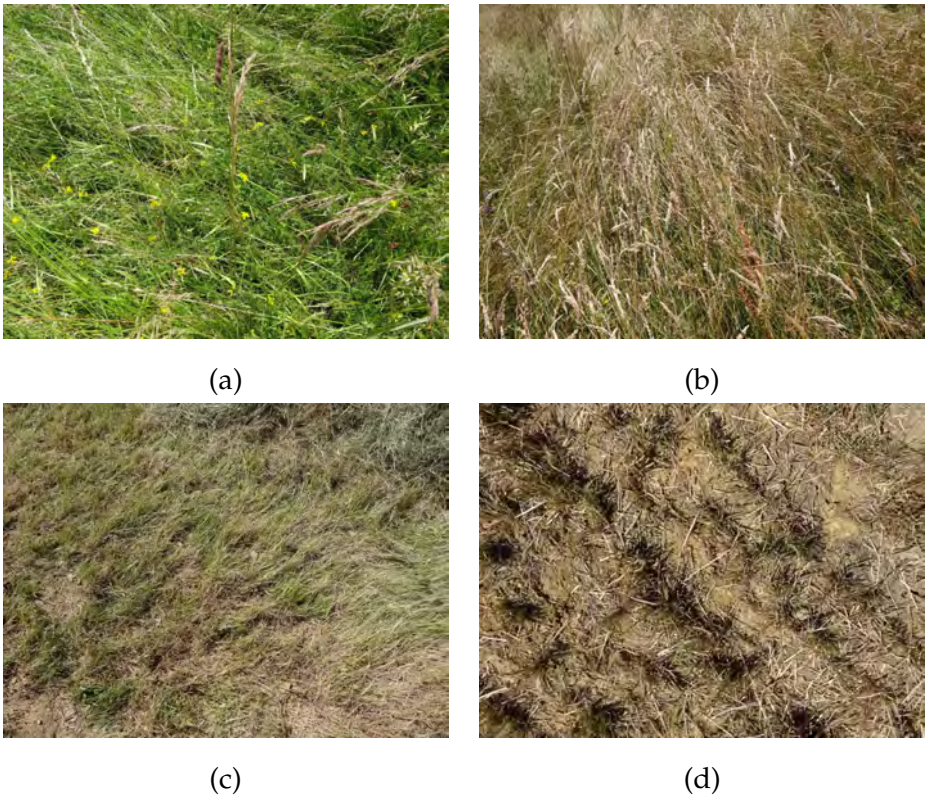

(a) (b)

(c) (d)

Figure 1.11.: Photographs of (a) dense vegetation after growth peak, (b) senescent vegetation before mowing, (c) ground cover after the mowing of a semi-natural grassland. (d) Photograph of the ground cover after the second mowing of an annual grassland.

The regrowth thus behaves differently between grasslands mown early and late. Indeed, plant regrowth is dependent on weather conditions and on rainfalls in non-irrigated environments. When the grassland is mown early in the season (spring), the plant regrowth is usually fast [Turner et al., 1992], because it benefits from the spring rainfalls and temperatures not too high (Figure 1.2). If the grassland is mown late (summer), there was more senescent biomass accumulation [Turner et al., 1992, Mašková et al., 2008]. The regrowth suffers from the scarcity of water combined with high temperatures (Figure 1.2). It is less dynamic because the plants are under stress. From Figure 1.2, we can notice that August was particularly dry and there were few rainy days until mid-September, combined with high temperatures. It explains why the spectral response did not vary a lot between the measures acquired in August and

September (grasslands 405 and 131).

In this study area, we also noticed a difference between grasslands located at the bottom of a valley (grasslands 500 and 131) and on the top of a hill (grassland 405). At the bottom of a valley, the soil is deeper and more humid, resulting in increased biomass compared to the top of a hill [Schimel et al., 1991]. Hence, grasslands tend to stay green longer than grasslands on the hills, which start to become senescent earlier. Grasslands on top of a hill are more exposed to the sun and have a drier and thiner soil [Schimel et al., 1991]. It results in higher VI values for grasslands in the valleys, while grasslands on hills have VI decreasing earlier. Moreover after the mowing, the regrowth is faster and greener for grasslands at the bottom of a valley, while it is slower for grasslands on top of a hill. Hence, the VI values increase rapidly for grasslands in the valleys and tend to be as high as before the mowing, while for grassland on hills, the VI values increase slower and do not reach values as high as before the mowing.

The high values of the VI after the second growth for grasslands located at the bottom of a valley (Figures 1.6.a and 1.10.a) confirm that these indices can saturate with a dense biomass. Indeed, if there was the same biomass production after the mowing than before the mowing, then a second mowing would be possible and necessary. However, after the second growth, the vegetation is not as green and as dense as before the first growth peak (Figure B.1 and B.4). Moreover, the NIR reflectance is always lower after the regrowth than after the first growth, regardless of the grassland (Figures 1.5.a and 1.9.a).

1.4.1.2. Mowings in annual grasslands

In our study area, grasslands mown twice are usually fertilized to speed up and enhance the growth. Our example was an annual ryegrass grassland which is closer to a crop than a grassland in terms of practices and phenology. The first mowing occurs usually very early in the growing season (April) and the regrowth rate is also high, thanks to the rainfalls and the inputs. Therefore, if there is no acquisition right after the first mowing (*i.e.*, a few days), one can miss the event. After the second mowing in June, the grassland has a spectral signal very close to bare soil's spectral signature with low NDVI (Figure A.2). Indeed, since it is an annual grassland sown with one species, the herbaceous stratum is almost nonexistent [Ovalle et al., 2006], the vegetation follows only the rows of seeding and its cover is not dense. Therefore, after the mowing in summer, the regrowth is very slow and there are large areas of bare soil because of the absence of herbaceous stratum, *i.e.*, of other species than the sown one (Figure 1.11.d). This does not occur in semi-natural grasslands, because there is a thick herbaceous layer composed of diverse diverse plant communities with an understorey below the tall herbaceous grasses. Hence there is a greater biomass accumulation and a dense vegetation cover [Chiarucci et al., 1999,Grytnes, 2000,Ovalle

et al., 2006]. Therefore, the spectro-temporal response of sown grasslands cannot be assimilated to the one of semi-natural grasslands.

1.4.1.3. Grazing effect

During grazing activity, biomass is removed from the grassland like for mowing. Hence, grazing increases the reflectance in the visible wavelengths, decreases the reflectance in the NIR wavelengths, making the NDVI decrease. However, in the case of mowing, the defoliation is usually homogeneous at the grassland scale, while in the case of grazing, it is heterogeneous with areas refused by the animals [Cid and Brizuela, 1998, Kohler et al., 2006]. Therefore, the variance of NDVI within the grassland is much higher for grazed grasslands than for mown grasslands.

The reflectance also depends on the grazing intensity. If the stocking rate is higher, the grazing amount will be higher, intensifying the soil degradation because of trampling [Sala and Paruelo, 1997, Louault et al., 2005, Klumpp et al., 2011]. Hence, the NDVI will be lower and with a higher standard deviation than for a grassland being extensively grazed. This effect was shown with grassland 36 that was more intensively grazed than grassland 131.

However, our study of grazing effect on the spectral-response is limited to grazing after mowing and for a short period of time. No grassland continuously grazed or grazed before the mowing were present in our dataset. For these types of management, the grazing effect is likely to differ from what we described.

Compared to other works, the NDVI averages found in this study are in agreement with those found by Dusseux *et al.* [Dusseux et al., 2014b] who separated grasslands on vegetation height statuses. The NDVI and the visible and NIR reflectances trends are in line with the results found by Turner *et al.* [Turner et al., 1992] on defoliation — mowing and grazing — and senescent accumulation effects.

1.4.1.4. Early and late mowing

The studied year had a particularly rainy spring (Figure 1.2) for the study area, resulting in shifting forward the usual timing for mowings and for the start of the senescence. Despite this time shift, we found that the effect of the mowing on the spectral response is very different if the mowing occurs early or late in the growing season. Contrarily to what has been found in irrigated-environments [Courault et al., 2010], the decrease of the NDVI does not mean a mowing occurred. It can be due to natural senescence of the vegetation [Reed et al., 1994] and this has not been often accounted for prior to the present work.

Hence, parametric models such as TIMESAT [Jönsson and Eklundh, 2004] that model the seasonal variations of the vegetation based on uni- or bi-modal seasonality

should be used carefully for semi-natural grasslands monitoring.

1.4.1.5. Assessment of the three vegetation indices for detecting the practices

Among the three vegetation indices computed in this study, the NDVI seemed to be better at detecting the mowing. Indeed, its variance increases after the mowing, because of heterogeneous plant regrowth, but also soil exposure. MSAVI2 was designed to not account for the soil influence. S2REP assesses the red edge point of vegetation. Hence, these two indices do not account for the soil exposure, while it seems to be an indicator of the mowing. Hence, MSAVI2 and S2REP have less variance and have higher values than NDVI after the mowing and grazing periods that expose the soil. Thus, we recommend to use the NDVI to detect the mowing.

Some studies report that the Enhanced Vegetation Index (EVI) is more sensitive to grasslands phenology and to the mowing than the NDVI [Nitze et al., 2015, Halabuk et al., 2015]. Indeed, around the growth peak, the NDVI can saturate [Huete et al., 2002]. We did not use EVI in our study because its computation requires several coefficients that are not known yet in our conditions, while NDVI is a band ratio with no parameters.

Finally, the NIR band seems interesting to describe the grassland phenology because it does not saturate. However, it can be more sensitive to the atmospheric effects than the VI.

1.4.2. Proposition of a NDVI trend model of mown semi-natural grasslands

Based on the observations made in this study, we propose a NDVI trend model for semi-natural grasslands (Figure 1.12):

1. The NDVI increases from the start of the growing season until the peak, then it stabilizes (solid line, a and b). Its standard deviation is low because of the dense vegetation cover (c).

2. If the grassland is not mown, the NDVI smoothly decreases as vegetation becomes senescent (solid line, a and b). The decrease will occur earlier in the season if the grassland is on top of a hill (solid line, b).

3. If the grassland is mown, it induces a sharp NDVI decrease (dotted and dash-dotted lines, a and b) combined with an increase of its standard deviation because of soil exposure (c).

4. After the mowing, the vegetation starts regrowing. The NDVI increase is fast if the grassland is in a valley (dotted and dash-dotted lines, a) and if the mowing occurred early in the season for a grassland on a hill (dotted line, a). The

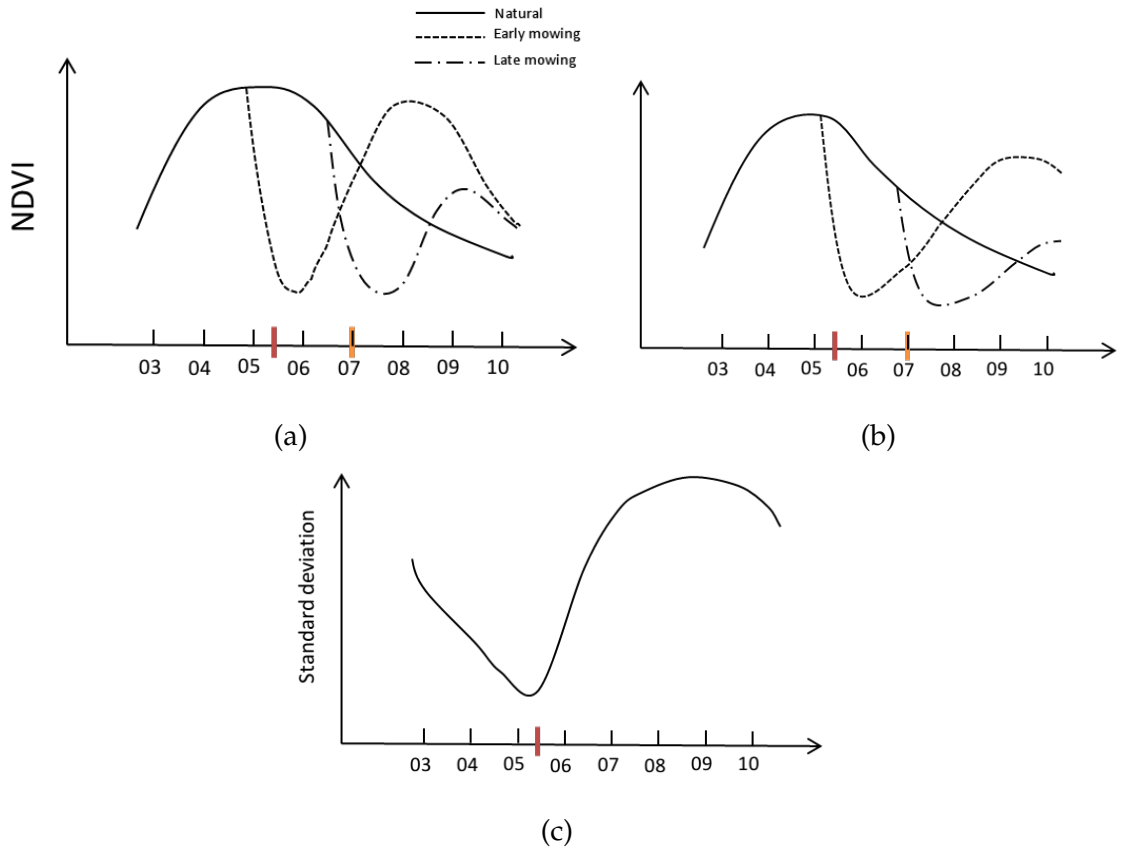

Figure 1.12.: NDVI trend model of a mown semi-natural grassland. (a) Grassland located at the bottom of a valley. (b) Grassland located at the top of a hill. The solid line corresponds to the natural trend of a grassland with no practice, but that was managed the season before (mowing or grazing). The dotted line corresponds to a grassland mown early (before June, red stick). The dash-dotted line corresponds to a grassland mown late (June and after, orange stick). (c) Trend of the standard deviation of NDVI before and after the mowing. The x-axis correspond to the months of year.

regrowth is slower than before the mowing if the mowing occurred late and the grassland is on top of a hill, implying a slower NDVI increase (dash-dotted line, b). For all cases, the NDVI has a higher standard deviation than before the mowing (c).

5. The NDVI values are almost as high as before the mowing for grasslands at the bottom of a valley mown early (dotted line, a). They are lower than before the mowing if the grassland is on top of a hill and mown early (dotted line, b). The

regrowth reach low values for grasslands at the bottom of a valley and mown late (dash-dotted line, a) and even lower for grasslands on top of hill and mown late (dash-dotted line, b).

This model gives approximate trends of NDVI between grasslands located on more or less fertile lands (valleys and hills) and mown early or late. Its depends on weather conditions that are different from a year to another.

The phenology of semi-natural grasslands and the management practices calendar depend on the regions and the climatic regions. Therefore, there could be differences in the spectral response of grasslands depending on the geographic area and the topography — such as the timing of the growth peak, the start of the senescence, the regrowth speed — and we suggest more investigations relating to this subject.

1.4.3. Potential of Sentinel-2 time series to monitor semi-natural grasslands

1.4.3.1. Spectral resolution

The spectral bands and the vegetation indices were all simulated using Sentinel-2 radiometric response. The NIR and red bands seemed to be good indicators of the grassland's phenology (greenup, senescence, mowing, regrowth). The red edge bands were also sensitive to the phenology but these bands have a spatial resolution of 20 meters with Sentinel-2 sensor. Hence, they may be less sensitive to the heterogeneity within grasslands than 10 meters bands.

From the results, the NDVI computed from Sentinel-2 red and NIR bands is potentially appropriate to monitor the phenology and the management practices in semi-natural grasslands. Since NDVI is a band ratio, it has the advantage of canceling out signal variations due to calibration, noise and changing irradiance conditions caused by changing sun angles, topography, clouds and atmospheric conditions [Tucker, 1979, Huete et al., 1999], facilitating the comparison between grasslands and study sites. Its main drawback is its saturation around the growth peak, when the biomass is the densest and the photosynthetic activity is the strongest.

More details about the analysis of spectral bands can be found (in French) in [Dallery, 2016].

1.4.3.2. Temporal resolution

The results showed the importance of a high revisit frequency, especially during the growing season. During this period, phenological events occur more rapidly because of great growth rate and the effects of management practices are quite local. Moreover, spring is usually rainy, which increases the occurrence of clouds in the time series.

This issue is illustrated with a time series acquired with Landsat 8 in Figure 1.13. It shows the NDVI temporal profile of grassland 36 (Figure 1.10). Landsat 8 has a medium temporal resolution (16 days) and a medium spatial resolution (30 meters). We removed the acquisitions contaminated by clouds. We can see that our model would be validated: the mean NDVI decreases and its standard deviation increases after the mowing. However, due to the coarse spatial resolution of this sensor, the mean and standard deviation are computed from only three pixels (see next subsection for explanations). Moreover, there is one month and a half between the two acquisitions before and after the mowing. Hence, the increase of NDVI standard deviation is slight. In addition, the detection of the mowing would be imprecise.

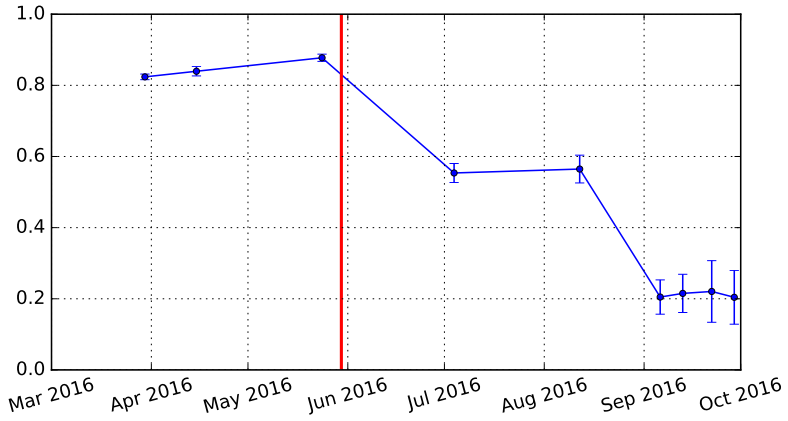

Figure 1.13.: Mean ± standard deviation of NDVI temporal profile of grassland 36 acquired with Landsat 8. The red line corresponds to the mowing date.

For grassland 406 with Landsat 8 acquisitions (Figure 1.14), our model would not be validated for the first mowing. Indeed, the acquisition after the mowing is too late and the vegetation has already regrown. Even if we can see a decrease of NDVI with an increase of the standard deviation, the decrease of NDVI is not steep.

Hence if one wants to detect the mowing, one should use hypertemporal data during the period of mowings. The same conclusions were drawn in [Nitze et al., 2015, Halabuk et al., 2015]. Sentinel-2 temporal resolution (5 days) should be suitable for managed grasslands monitoring. However, in 2016, Sentinel-2 was not fully operational. There were not enough clear images acquired during the growing season (only five images) to conduct an analysis with this sensor and to benchmark the simulated Sentinel-2 measurements against the actual acquisitions.

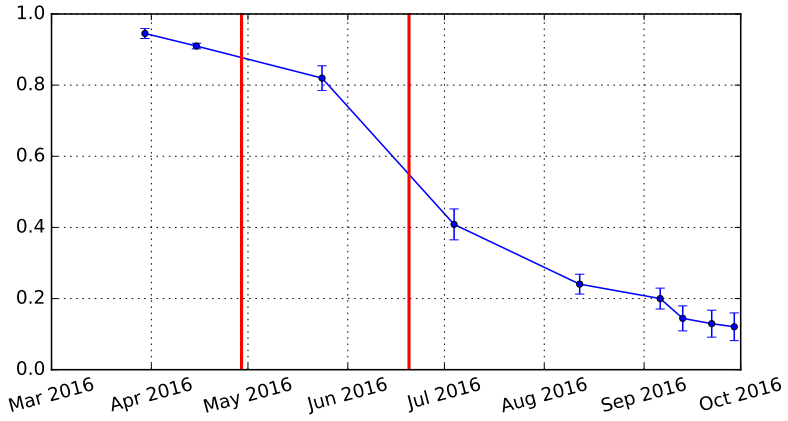

Figure 1.14.: Mean ± standard deviation of NDVI temporal profile of grassland 406 acquired with Landsat 8. The red line corresponds to the mowing dates.

1.4.3.3. Spatial resolution

The spatial resolution was not assessed in this study. However, we know that the average grassland size in the study area is around 1 hectare, which is equivalent to 100 Sentinel-2 pixels or 11 Landsat 8 pixels. Moreover, mixed pixels at the boundaries are usually removed to avoid the edge effects, by applying an inner buffer equivalent to the size of one pixel. Depending on the shape of the grassland, it could contain no more pixels after the buffer application (Table 1.3). With a buffer of 30 m, grassland 405 boundaries are so narrow (Figure 1.15.a, red lines) that they do not contain any Landsat 8 pixel after rasterization (Table 1.3). However with a buffer of 10 m (Figure 1.15.b, red lines), the grassland's boundaries still contain a certain number of Sentinel-2 pixels after rasterization (Table 1.3).

Table 1.3.: Number of pixels in the grasslands after applying an inner buffer and rasterizing the polygons.

ID	Area (ha)	Nb of Landsat 8 pixels	Nb of Sentinel-2 pixels
36	1.1	3	92
131	1.2	0	92
405	1.2	0	93
406	2.6	12	234
500	1.7	0	132

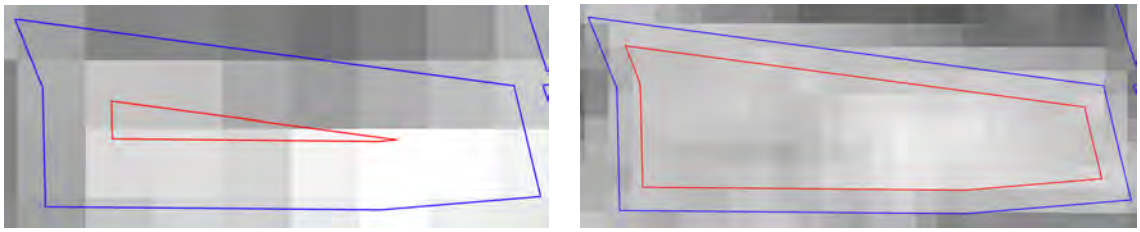

(a) (b)

Figure 1.15.: Boundaries of grassland 405 (blue lines). (a) Inner buffer of 30 m from the grassland's boundary (red lines) with a Landsat 8 image in the background. (b) Inner buffer of 10 m from the grassland's boundary (red lines) with a Sentinel-2 image in the background.

Hence, even a spatial resolution of 30 meters is too coarse for the study of grasslands in fragmented grasslands. Sentinel-2 spatial resolution should be fine enough to ensure a minimum number of pixels per grassland.

1.5. Conclusion

This study investigated the effect of the phenology and of the management practices on the spectro-temporal response of semi-natural grasslands. To do so, a set of five grasslands on a gradient of use intensity was monitored during the growing season using a field spectroradiometer and Sentinel-2 spectral bands were simulated from these measurements. Our results showed that the spectro-temporal response does not only depend on the practice itself but also on the phenological stage when the practice occurs, the weather conditions and the topography. We pointed out differences in the spectro-temporal profile of grasslands mown early and late, particularly because the vegetation starts to become senescent before the mowing for grasslands mown late, inducing a decrease of the vegetation indices. We also showed that vegetation indices sensitive to soil effect could be used to detect the management practices (mowing or grazing) because of the soil exposure and the sparse vegetation regrowth and their effect on the signal after these events.

We highlight the need of hypertemporal data to detect the management practices. A temporal resolution of more than 15 days is not sufficient to detect the mowing. Indeed, the natural phenology of grasslands can mask the effect of the practices. Sentinel-2 time series, with their spatial, spectral and temporal properties, should enable the monitoring of grasslands' phenology and the detection of the management practices. A model of NDVI evolution for extensively managed grasslands — mown early or late, and located at the bottom of a valley or on top of a hill — was proposed

and could be used with Sentinel-2 time series to monitor semi-natural grasslands. This model requires additional investigations to validate it in other regions because grasslands' phenology is subject to local climate.

This work was based on ground hyperspectral data and thus, with a very high spatial resolution. The results and conclusions may differ using satellite data with coarser spatial resolution because the soil effect on the signal might be less important. Therefore, the proposed spectro-temporal response must be compared with Sentinel-2 data when the sensor is fully operational.

Acknowledgements

We are grateful to Donatien Dallery for participating in the field work, for performing the processing of the spectra and the simulation of Sentinel-2 bands and for designing the database containing all the spectra collected during the field campaign. We would like to thank Jérôme Molina, Jérôme Willm and Bruno Dumora for helping collecting the spectral measurements. We are thankful to Bernard Mougenot, Jean-Baptiste Féret, Emmanuelle Vaudour and Eric Bécourt for the spectroradiometer lending. We thank Sylvie Duthoit for advising on the practical use of the device. We are grateful to all the farmers who let us collect measurements in their fields and provided us with information about their management practices.

Conclusion of Part I

This first part was aimed at analyzing the spectro-temporal response of grasslands according to their natural phenology and to the management practices. The practices conducted in the grasslands should be known prior to any signal interpretation because they have a non-negligible influence on the signal. Their impact on the spectro-temporal response will depend on their intensity, their date of occurrence, the weather conditions and the topography. A grassland mown early during the season will not have the same spectro-temporal profile than a grassland mown late because the weather conditions differ and the vegetation is not at the same stage. We proposed an NDVI evolution for mown semi-natural grasslands that are located in a valley or on a hill, and that are mown early or late (*i.e.*, after the vegetation starts to become senescent naturally).

The importance of the signal variability within the grassland was underlined in this work. Indeed, grasslands are heterogeneous because of differences of soil, topography and species composition. This heterogeneity have an influence on the signal measured by the sensor. For instance, we showed the high standard deviation of the signal after the mowing and the grazing, and during the regrowth.

In addition, the results presented in this first part highlighted the need of hyper-temporal resolution data to analyze grasslands with satellite imagery. A temporal resolution of 15 days or more is not sufficient to capture grasslands' phenology which is particularly dynamic in the growing season when most of the management practices occur. When fully operational, Sentinel-2 should be able to monitor semi-natural grasslands.

In the next part, methodological developments will be conducted to address the requirements for grassland's analysing using satellite image time series with a high spatial and temporal resolutions.

Part II.

Methodological developments for the supervised classification of grasslands using satellite image time series

Introduction of Part II

The previous part emphasized the need of hypertemporal data for the analysis of grasslands. The use of satellite image time series requires some smoothing, because of the presence of noise in the time series due to clouds and their shadows. An accurate smoothing is essential for analysis based on phenology. It should smooth the local extrema caused by noise but it should not underestimate the extrema that correspond to important phenological events such as the growing peak and the mowing. Moreover, it should be able to reconstruct the time series based on regular time samples to enable the comparison of geographic areas that were monitored on different and irregular temporal grids.

Furthermore, the use of dense time series issued from new generation satellites such as Sentinel-2 (*i.e.*, associated with high spatial resolution and multispectral data) implies big data issues. Indeed, because grasslands are small elements in the landscape, we have to deal with a large number of spectro-temporal variables with a number of samples of the same range. Reducing the data dimension by considering the mean value in grasslands is not appropriate because it leads to a loss of information that is important for the grassland characterization. Indeed, grassland heterogeneity must be accounted for their analysis. Moreover, an analysis at the grassland level is needed to be consistent with ecological studies which work at the parcel scale. Hence, how to account for the pixels distribution in a grassland while working with high dimensional data? Fast techniques and algorithms, able to deal with larger and larger amounts of data with high dimension are required.

This part consists in methodological developments to respond to the aforementioned issues and appropriate for the analysis of grasslands. The first chapter (Chapter 2) introduces and compares techniques for the smoothing of dense inter-annual satellite image time series. The second chapter (Chapter 3) presents a similarity measure that was developed for the supervised classification of grasslands modeled by a Gaussian distribution. In the last chapter (Chapter 4), a similarity measure based on a flexible kernel that encompasses several similarity measures known in the literature is developed.

2. Time series reconstruction

2.1. Introduction

Missing or noisy data can be encountered when analyzing dense optical satellite image time series (SITS), due to the occurrence of clouds and their shadows in parts or in the whole images [Goward et al., 1991]. For instance, Figure 2.1 shows a Formosat-2 acquisition disturbed by clouds and shadows. We can see that the reflectance of cloudy pixels is completely changed while shadowed pixels have a lower reflectance. Figure 2.2 represents the temporal profile of a given vegetation pixel in the near infrared band. The red dots correspond to noisy temporal measurements, *i.e.*, tagged as clouds or shadows by the mask issued from [Hagolle et al., 2010].

Usually, the reflectance in the visible and NIR bands increases with the presence of clouds, while it decreases with the shadows. Hence, the noisy temporal measurements introduce pseudo-hikes and pseudo-lows in the SITS [Shao et al., 2016] and they could deteriorate the analysis conducted on the observed SITS. Knowing this phenomenon, several ways of dealing with the noisy SITS were proposed in the literature:

1. Use the noisy SITS as it is [Halabuk et al., 2015],
2. Remove from the SITS the images affected by clouds [Franke et al., 2012],
3. Filter or smooth the time series to clean the data [Shao et al., 2016].

The first option is risky as it will induce uncertainties in the SITS and thus in the analysis [Cihlar and Howarth, 1994]. The second option can drastically reduce the number of observations depending on the clouds/shadows cover of the study area. A solution would be to remove the noisy data at the pixel scale. However, this will result in irregular time intervals between pixels which is difficult to manage. Moreover, removing the images affected by clouds in large scale scenarios (*e.g.*, national scale) where different tiles are exploited seems fastidious. Hence, in order to exploit the full SITS, the reconstruction of the missing data is required and it is usually performed with a temporal filter.

Many smoothing algorithms have been developed to reduce the noise in SITS [Shao et al., 2016]. They recover missing values from the available data. They can be classified into two model categories:

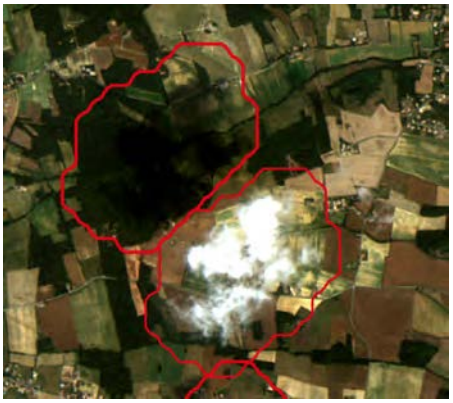

Figure 2.1.: A cloud and its shadow causing noise in the image. The red lines correspond to the contours of the cloud mask [Hagolle et al., 2010] (© CNES/Kalideos NSPO - Distribution Airbus DS).

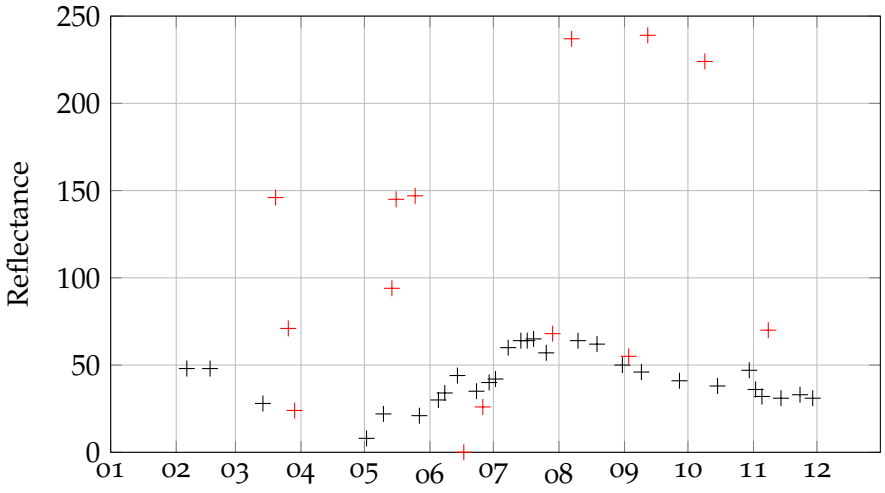

Figure 2.2.: Example of a temporal profile of a vegetation pixel in the NIR band of Formosat-2. The black crosses correspond to not noisy data and the red ones correspond to missing/noisy data due to the clouds/shadows.

- Parametric models
  - Linear models: Linear interpolation [Inglada et al., 2015]. The non-noisy tagged data is not smoothed and it is used to interpolate the missing data. In [Inglada et al., 2015], very large areas implying several satellite tracks and thus different observation dates among the tracks were processed. All image tracks were resampled on the same temporal grid. The time series of

every pixel were linearly interpolated using only the non-noisy tagged data. The results showed the temporal resampling did not significantly influence the crop classification accuracy.

- Non-linear / curve fitting models: Assymetric Gaussian [Jönsson and Eklundh, 2004], Double logistic [Jönsson and Eklundh, 2004, Beck et al., 2006]. A specific functional form is imposed to the temporal profile. These methods are used on even interval NDVI time series of vegetation. They are appropriate to model the annual vegetation cycle (phenology) and are generally used to extract seasonal metrics.

- Non-parametric models
  - Kernel and polynomial fitting: Savitzky-Golay filter (local polynomial regression) [Jönsson and Eklundh, 2004, Chen et al., 2004, Pan et al., 2015], Whittaker filter [Atzberger and Eilers, 2011a]. No specific form is imposed but the roughness of the smooth curve is controlled by a roughness parameter. These methods are particularly useful when dealing with unequally spaced time series. They have also been used under the assumption that NDVI was negatively biased by clouds and they were modified to fit the upper envelope of the data.
  - Basis functions: Splines [Bradley et al., 2007, Hermance et al., 2007], Fourier transform [Moody and Johnson, 2001, Hermance et al., 2007], Wavelet transform [Sakamoto et al., 2005]. Data are projected on basis. Thse methods have been used when periodicity of data is assumed, usually for inter-annual analysis.

The smoothing algorithm must be selected with care and depends on the nature of the time series to smooth [Hird and McDermid, 2009]. In our case, the use of dense optical SITS with high spatial resolution, such as Sentinel-2, to analyze semi-natural elements carry some constraints:

- The local extrema are important in the analysis because they correspond to phenological events. The smoothing algorithm must preserve the original extrema of the temporal profile.

- The mask of clouds can be incomplete because of undetected/non-tagged clouds or shadows (Figure 2.3). The data tagged as non-noisy must be smoothed a little.

- Possibly consecutive noisy observations which imply unequally-spaced intervals of non-missing data. The smoothing algorithm must handle properly the unequally-spaced intervals of time.

- A large number of pixels needs to be smoothed. The algorithm must be computationally efficient.

Figure 2.3.: Example of incomplete mask of clouds. The red lines correspond to the contours of the cloud mask [Hagolle et al., 2010]

Therefore, a smoothing algorithm which combines efficient computation, fidelity to the data, low roughness and appropriate for unequally-spaced intervals of time is required. The linear models and the parametric models were excluded from our selection because they did not meet these requirements. Three algorithms potentially meeting these requirements were retained from the literature and benchmarked in order to select the most appropriate one: the splines, the Kernel smoother and the Whittaker filter. Their principle is developed and their characteristics are discussed in the following.

2.2. Smoothing algorithms for satellite image time series of grasslands

Let T be the length of the time series to smooth, *i.e.*, the total number of temporal observations/images. Let $\mathbf{x} = [x(t_1), \ldots, x(t_T)]^\top$ be the (noisy) temporal vector of one pixel composed of each observed value $x(t_i)$ at time t_i during the time series, with $i \in \{1, \ldots, T\}$. For simplicity reasons, only one spectral band (or vegetation index) will be considered.

The mask of clouds for each image of the time series enables the definition of a temporal vector of weights $\mathbf{w} = [w(t_1), \ldots, w(t_T)]^\top$ for each pixel, with $w(t_i) = 0$ for missing (*i.e.* noisy) values and $w(t_i) = 1$ for non-missing values at time t_i. Note that even if the mask provides different values for clouds and shadows, the vector of weights is binary. No difference is made between a thin cloud, a thick cloud and a shadow.

The objective is to fit a smooth time series $\hat{\mathbf{x}} = [\hat{x}(t_1), \ldots, \hat{x}(t_T)]^\top$ from the series $\mathbf{x}$.

2.2.1. Splines

Splines are a linear basis expansions model for fitting curves. They are piecewise polynomial functions between knots. Knots are particular points of the input temporal domain used to split it into several parts. A simple model is then learned on each part while particular condition can be imposed for the global model. Continuity between knots can be imposed with derivatives constraints at the knots. The model is expressed as:

$$\hat{\mathbf{x}}(t) = \sum_{i=1}^{Q} \beta_i s_i(t) \tag{2.1}$$

where $\hat{\mathbf{x}}(t)$ is the smoothed time series, $s_i(t)$ are the basis depending on the time intervals, β_i are the basis coefficients, Q is the number of basis functions, which is related to K the number of knots, M the order of the basis (degree of the spline) and the type of basis used.

The estimation of the coefficients is conventionally done using least square approximation. It is done by solving the following optimization problem:

$$\min_{\beta} \left[\sum_{j=1}^{T} \left(\mathbf{x}(t_j) - \mathbf{s}(t_j)^\top \boldsymbol{\beta} \right)^2 \mathbf{w}(t_j) \right] \tag{2.2}$$

with $\mathbf{s}(t_j) = \left[s_1(t_j), \ldots, s_Q(t_j) \right]$ and $\boldsymbol{\beta} = [\beta_1, \ldots, \beta_Q]$.

The solution is given, in matrix form, by:

$$\hat{\boldsymbol{\beta}} = (\mathbf{S}^\top \mathbf{S})^{-1} \mathbf{S}^\top \mathbf{x} \tag{2.3}$$

with

$$\mathbf{S} = \begin{pmatrix} \mathbf{s}_1(t_1) & \ldots & \mathbf{s}_Q(t_1) \\ \mathbf{s}_1(t_2) & \ldots & \mathbf{s}_Q(t_2) \\ & \vdots & \\ \mathbf{s}_1(t_T) & \ldots & \mathbf{s}_Q(t_T) \end{pmatrix}.$$

The quality of the reconstruction depends on several factors, the number of knots and their positions, the order of local basis function and the types of basis used. Some parameters can be cross-validated, for instance the number of knots K. Other parameters can be tuned with prior information. For instance, to have a smooth second derivative, the order of the splines should be $M = 2 + 2 = 4$. For an intra-annual time series of vegetation, the splines should be linear and their order should be 2. Finally, some parameters can be tuned empirically from the data, for instance, the position of knots. Given their numbers, one can use equally space knots in $[t_1, t_T]$ or use

percentiles.

2.2.2. Kernel smoother

A Kernel smoother method is a regression technique that estimates a smooth function $\hat{\mathbf{x}}(t)$ from $\mathbf{x}(t)$ by fitting a simple model separately at each query point t_0 belonging to $[t_1, t_T]$. The observations t_i close to t_0 are used to fit the simple model. Closeness is defined using a kernel function $K_\lambda(t_0, t_i)$ which assigns a weight to t_i based on its temporal distance from t_0. There are different kernels which give a different weight to each point in the neighborhood of t_0, but it has been shown that the influence of the kernel is not significant. Therefore, we chose a simple kernel, the Epanechnikov quadratic kernel (Figure 2.4):

$$K_\lambda(t_0, t) = D\left(\frac{|t - t_0|}{\lambda}\right) \tag{2.4}$$

with

$$D(z) = \begin{cases} \frac{3}{4}(1 - z^2) & \text{if } |z| \leq 1 \\ 0 & \text{otherwise.} \end{cases} \tag{2.5}$$

The parameter λ controls the width of the neighborhood.

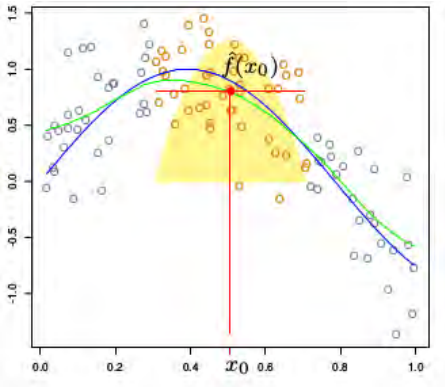

Figure 2.4.: Illustration of Kernel smoother with Epanechnikov kernel taken from [Hastie et al., 2009]. The green curve is the kernel-weighted average of the 100 circles generated from the blue curve, using Epanechnikov kernel with window width $\lambda = 0.2$. The red point is the fitted constant $\hat{f}(x_0)$ and the red circles indicate the observations contributing to the fit at x_0. The solid yellow region indicates the weights assigned to observations.

Locally weighted polynomial regression solves a separate weighted least squares problem at each target point t_0 to learn a polynomial function. At any order p, the

polynomial is fitted locally by:

$$\min_{\beta_0,...,\beta_p} \sum_{i=1}^{T} K_\lambda(t_i, t_0)[\mathbf{x}(t_i) - \beta_0 - \beta_1(t_i - t_0) - ... - \beta_p(t_i - t_0)^p]^2 \mathbf{w}(t_i) \tag{2.6}$$

with t_i is in the neighborhood of t_0, controlled by λ. The solution is given by $\hat{\beta}_0, ..., \hat{\beta}_p$ and $\hat{\mathbf{x}}(t_0)$ is approximated by $\hat{\beta}_0$. The estimated curve is obtained computing the regression polynomial for each t_0.

At order $p = 0$, the solution of the local linear regression is called the Nadaraya-Watson kernel weighted average:

$$\hat{\mathbf{x}}(t_0) = \hat{\beta}_0 = \frac{\sum_{i=1}^{T} K_\lambda(t_0, t_i)\mathbf{x}(t_i)\mathbf{w}(t_i)}{\sum_{i=1}^{T} K_\lambda(t_0, t_i)}. \tag{2.7}$$

At order $p = 2$, the local quadratic regression is equivalent to the Savitzky-Golay filter except that the Kernel smoother has a flexible window size, meaning that it can deal with irregular temporal intervals and with unequally-spaced missing data.

Two parameters need to be determined: the order of the polynomial p and the width of the neighborhood λ. The order of the polynomial can be tuned empirically with the input data. When the temporal profile has a local parabolic form with minima and maxima, it can be estimated with a polynomial of order 2 (Figure 2.5). λ can be found by cross-validation as discussed in section 2.2.3.2. Larger λ values imply higher smoothness (averages over more observations) but at the cost of a worse fit to the data (higher bias) [Hastie et al., 2009].

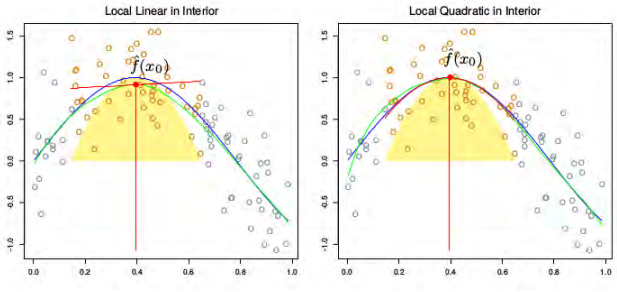

Figure 2.5.: Left panel: Local linear fits (green curve) exhibit bias in regions of curvature of the true function (blue curve). Right panel: Local quadratic fits tend to eliminate this bias. Illustration taken from [Hastie et al., 2009].

2.2.3. Whittaker smoother

2.2.3.1. Principle

The Whittaker smoother is based on penalized least squares [Eilers, 2003]: the smoothing must be a tradeoff between fidelity to the data (S) and roughness of the reconstructed series (R_d). We are looking for the smooth time series $\hat{\mathbf{x}}$ such that:

$$\hat{\mathbf{x}} = \arg\min_{z} S(\mathbf{z}) + \lambda R_d(\mathbf{z}).$$

λ is the positive smoothing parameter that controls the compromise between the fidelity and the roughness. The larger it is, the smoother $\hat{\mathbf{x}}$ will be, increasing the lack of fit to the data.

The fidelity to the data S is expressed as the sum of squares of differences and it measures the lack of fit to the data:

$$S(\hat{\mathbf{x}}) = \sum_{i=1}^{T} \left[\mathbf{x}(t_i) - \hat{\mathbf{x}}(t_i)\right]^2 \mathbf{w}(t_i). \tag{2.8}$$

In its matrix form,

$$S = \|\mathbf{x} - \hat{\mathbf{x}}\|^2 = (\mathbf{x} - \hat{\mathbf{x}})^\top \mathbf{W} (\mathbf{x} - \hat{\mathbf{x}}), \tag{2.9}$$

with $\mathbf{W}$ is the diagonal matrix with $\mathbf{w}$ on its diagonal.

The roughness of the data R_d is expressed as the norm of derivatives of order d with respect to the time:

$$R_d(\hat{\mathbf{x}}) = \sum_{i=d+1}^{T} \left(\Delta_d \hat{\mathbf{x}}(t_i)\right)^2 \tag{2.10}$$

with Δ_d is the d^{th} order divided differences which accounts for the intervals of time between the acquisitions. It is suitable for unequally spaced intervals. In its matrix form,

$$R_d = \|\mathbf{D}_d \hat{\mathbf{x}}\|^2 = (\mathbf{D}_d \hat{\mathbf{x}})^\top \mathbf{D}_d \hat{\mathbf{x}} = \hat{\mathbf{x}}^\top \mathbf{D}_d^\top \mathbf{D}_d \hat{\mathbf{x}} \tag{2.11}$$

where $\mathbf{D}_d$ is the derivative matrix of order d.

Finding the smooth time series $\hat{\mathbf{x}}$ is equivalent to minimizing:

$$\mathbf{S} + \lambda \mathbf{R}_d = (\mathbf{x} - \hat{\mathbf{x}})^\top \mathbf{W} (\mathbf{x} - \hat{\mathbf{x}}) + \lambda \hat{\mathbf{x}}^\top \mathbf{D}_d^\top \mathbf{D}_d \hat{\mathbf{x}}. \tag{2.12}$$

Eq. (2.12) is a regularized least-square problem. Its solution is given by computing the derivative with respect to $\hat{\mathbf{x}}$ and setting it to zero:

$$\hat{\mathbf{x}} = (\mathbf{W} + \lambda \mathbf{D}_d^\top \mathbf{D}_d)^{-1} \mathbf{W} \mathbf{x}. \tag{2.13}$$

Two parameters need to be tuned: the order of the derivatives d and the smoothing parameter λ. d can be tuned according to the degree of smoothness we want to impose. If we want the original SITS to be smoothed, the order of the derivatives will be 2.

2.2.3.2. Selection of the smoothing parameter

The optimal parameter λ (*i.e*, which gives a good fit to the data while reducing the roughness) can be estimated by cross-validation. It consists in minimizing the average residual sum of squares between the original time series and its smoothed counterpart, that is called the "Ordinary Cross-Validation" (OCV, or Leave One Out Cross Validation):

$$OCV(\lambda) = \frac{1}{\sum_i \mathbf{w}(t_i)} \sum_{i=1}^{T} \mathbf{w}(t_i) \left(\mathbf{x}(t_i) - \hat{\mathbf{x}}(t_i)^{-i} \right)^2 \tag{2.14}$$

with $\hat{\mathbf{x}}(t_i)^{-i}$ is the estimated value of $\mathbf{x}(t_i)$ after removing the i^{th} observation.

From the previous section, we know that $\hat{\mathbf{x}} = \mathbf{A}^{-1}\mathbf{W}\mathbf{x}$ with $\mathbf{A} = \mathbf{W} + \lambda \mathbf{D}_d^\top \mathbf{D}_d$. We introduce the hat matrix $\mathbf{H}$ (or the smoother matrix [Hastie and Tibshirani, 1986]) such that $\hat{\mathbf{x}} = \mathbf{H}\mathbf{x}$ (solving $\mathbf{A}\mathbf{H} = \mathbf{W}$ to find $\mathbf{H}$). Hastie and Tibshirani [Hastie et al., 2009] proved the following relationship:

$$\mathbf{x}(t_i) - \hat{\mathbf{x}}(t_i)^{-i} = \frac{\mathbf{x}(t_i) - \hat{\mathbf{x}}(t_i)}{1 - h_{ii}} \tag{2.15}$$

where h_{ii} is the i^{th} element on the diagonal of $\mathbf{H}$.

Therefore:

$$OCV(\lambda) = \frac{1}{\sum_i \mathbf{w}(t_i)} \sum_{i=1}^{T} \mathbf{w}(t_i) \left[\frac{\mathbf{x}(t_i) - \hat{\mathbf{x}}(t_i)}{1 - h_{ii}} \right]^2. \tag{2.16}$$

In the matrix form:

$$OCV(\lambda) = \frac{(\mathbf{x} - \hat{\mathbf{x}})^\top \tilde{\mathbf{W}} (\mathbf{x} - \hat{\mathbf{x}})}{\sum_i \mathbf{w}(t_i)} \text{ with } \tilde{w}_{ii} = \frac{\mathbf{w}(t_i)}{(1 - h_{ii})^2}. \tag{2.17}$$

The optimal λ is the value which results in the minimum of OCV.

OCV can be computed for the splines and the Kernel smoother in a similar way than for the Whittaker smoother since they all are linear estimators.

2.2.3.3. Illustrations

Figure 2.6 illustrates the reconstruction every 5 days of the NIR time series showed in Figure 2.2 for different values of the Whittaker smoothing parameter. The OCV values associated with different values of λ are shown in Figure 2.7.

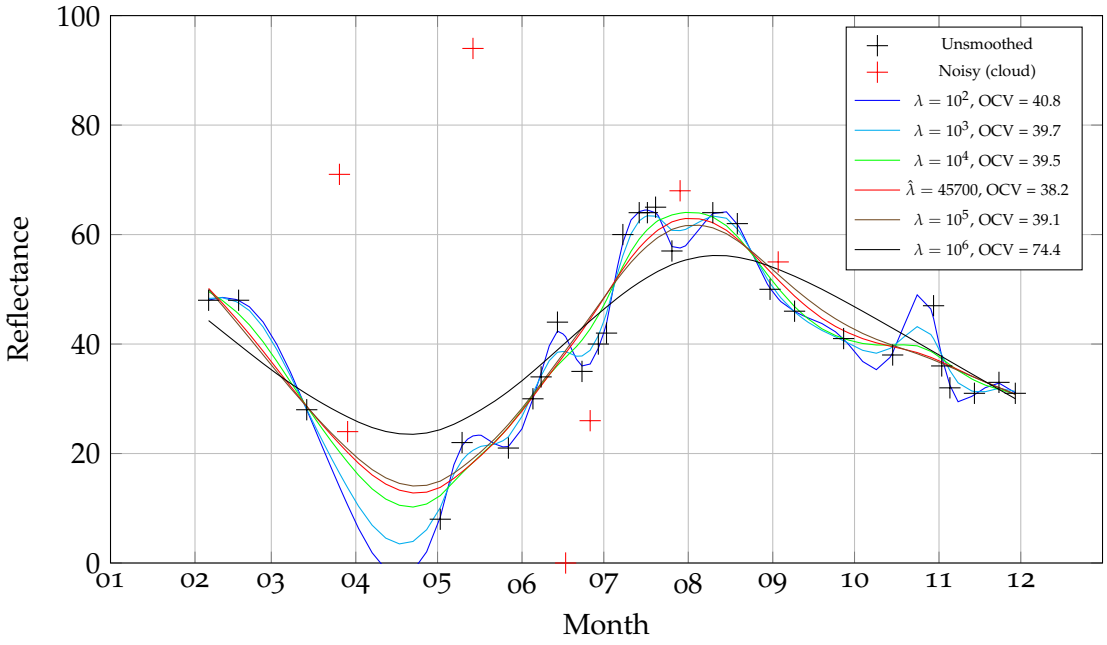

Figure 2.6.: Example of a time series reconstruction resampled every 5 days with different smoothing parameters of the Whittaker smoother for a pixel in the NIR spectral band.

OCV seems to choose the optimal λ value ($\hat{\lambda} = 45700$). Indeed, a low λ results in aberrant values at the periods of the time series when there are a lot of consecutive no data, while higher values result in a too smoothed time series.

2.2.4. Comparison

An example of smoothing with optimal parameters found by cross-validation for each method is shown in Figure 2.8, with the time intervals resampled every 5 days. The Kernel smoother at order $p = 2$ does not behave well in the case of several consecutive noisy dates with the width of the neighborhood found by cross-validation ($\hat{\lambda} = 44$). Splines, at order $M = 2$ have a high number of knots found by cross-validation ($\hat{K} = 11$). Hence, they are influenced by most of the local extrema and result in a rough time series. The Whittaker smoother at order $d = 2$ is more stable compared the Kernel smoother and the splines, with the smoothing parameter found by OCV ($\hat{\lambda} = 45700$).

The main characteristics of the methods are synthesized in Table 2.1. The Whittaker Smoother was chosen because of its fast execution, its combination of fidelity to the data and low roughness of the smoothing curve.

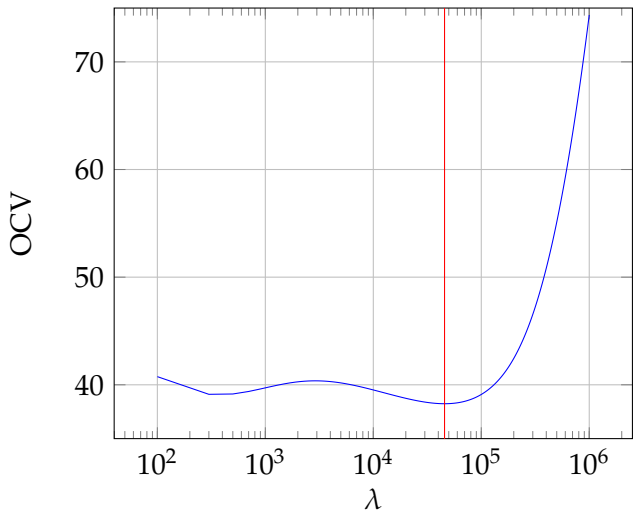

Figure 2.7.: OCV values depending on the smoothing parameter λ, on the 5-day-resampled time series with Whittaker smoother. The red line corresponds to the minimum of OCV: $\hat{\lambda} = 45700$.

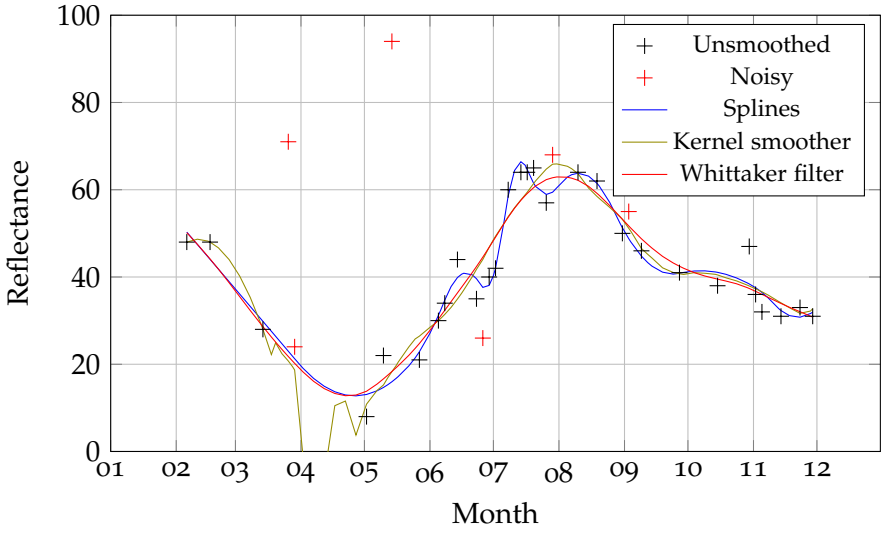

Figure 2.8.: Comparison of algorithms to smooth a resampled time series every 5 days. Parameters found by OCV and computing times: Splines, $Q = 3$, $M = 2$, $\hat{K} = 11$, 7ms; Kernel smoother, $p = 2$, $\hat{\lambda} = 44$, 20ms; Whittaker filter, $d = 2$, $\hat{\lambda} = 45700$, 3ms.

Table 2.1.: Characteristics of the selected smoothing algorithms. + indicates a high property while - indicates a low one.

Algorithm	Nb of param.	Speed	Fidelity	Roughness	Reference
Whittaker smoother	2	+	+	-	[Eilers, 2003]
Kernel smoother	2	-	-	-	[Fan and Gijbels, 1996, Hastie et al., 2009]
Splines	2	+	+	+	[Hermance et al., 2007]

2.3. Outlook

In this work, the smoothing is done temporally pixel per pixel and band per band. One could imagine adding a spatial smoothing [Shen et al., 2015], which accounts for the neighborhood of the smoothed pixels, such as non-local means [Buades et al., 2011] or context-based methods [Melgani, 2006]. A spectral smoothing could be considered too because of the correlation between the spectral bands [Shen et al., 2015].

3. High Dimensional Kullback-Leibler Divergence for grassland management practices classification from high resolution satellite image time series

High Dimensional Kullback-Leibler Divergence for grassland management practices classification from high resolution satellite image time series

Published in *2016 IEEE International Geoscience and Remote Sensing Symposium (IGARSS)*, Beijing, 2016, pp. 3342-3345; doi: 10.1109/IGARSS.2016.7729864.

Mailys Lopes[1], Mathieu Fauvel[1], Stéphane Girard[2], David Sheeren[1]

[1]DYNAFOR, University of Toulouse, INRA, INPT, France
[2]Team MISTIS, University of Grenoble, INRIA, LJK, France

Abstract

The aim of this study is to build a model suitable to classify grassland management practices using satellite image time series with high spatial resolution. The study site is located in southern France where 52 parcels with three management types were selected. The NDVI computed from a Formosat-2 intra-annual time series of 17 images was used. To work at the parcel scale while accounting for the spectral variability inside the grasslands, the pixels signal distribution is modeled by a Gaussian distribution. To deal with the small ground sample size compared to the large number of variables, a parsimonious Gaussian model is used. A high dimensional symmetrized Kullback-Leibler divergence (KLD) is introduced to compute the similarity between each pair of grasslands. Our proposed model provides better results than the conventional KLD in terms of classification accuracy using SVM.

Keywords: Satellite image time series, high dimension, Kullback-Leibler divergence, grassland management practice, classification.

3.1. Introduction

In the frame of sustainable development, the study of landscape state and its evolution are required to understand environmental changes and biodiversity loss. To this aim, research in landscape ecology is devoted to understanding how the landscape configuration and composition impact on biodiversity and services provided. This research requires the identification and the characterization of semi-natural elements in the landscape. Indeed, semi-natural habitats are perennial and less inclined to be disturbed. They are sources of biodiversity in farmed landscapes. Particularly, permanent grasslands, as they represent one of the largest terrestrial landscape (they cover 18% of France territory [Eurostat, 2010]), are a source of significant animal and plant biodiversity [Gardi et al., 2002, Sullivan et al., 2010], providing many ecosystem services such as carbon storage, erosion regulation, crop pollination, biological

regulation of ravagers [Werling et al., 2014]. Although policies have been adopted to protect biodiversity in semi-natural landscapes (European Union Habitats Directive, 92/43/EEC), the permanent grasslands area is continuously decreasing, leading to a loss of biodiversity [Sullivan et al., 2010].

Grasslands being the main livestock feeding resource, the species composition in semi-natural grasslands is also impacted by the management practices [Zechmeister et al., 2003]. Indeed, the anthropic events in the grasslands, like mowing and/or casual grazing, disturb the natural cycle and the structure of the vegetation. Therefore, it is essential to identify the management practices in each parcel to predict their effect on biodiversity and related ecosystem services.

In this context, remote sensing appears to be an appropriate tool to characterize grasslands at the landscape scale, because of the large spatial coverage and revisit frequency of satellite sensors. However, the reflected signal of the grasslands is more difficult to interpret compared to mono-specific lands like crops, due to the diversity and the mix of grassland species. Furthermore, grasslands are relatively small elements of the landscape (in average 1 hectare), which require high spatial resolution data to be detectable [Corbane et al., 2015]. Given their phenological cycle and the punctuality of the anthropic events (*e.g.*, mowing), very dense time series through the vegetation cycle are necessary to identify the management types [Schuster et al., 2015].

Until recently, satellite missions offering high revisit frequency had low spatial resolution (*i.e.*, MODIS), and high spatial resolution missions did not provide dense time series. New missions like Sentinel-2, with very high revisit frequency (5 days) and high spatial resolution (10 meters) enable new possibilities for grassland monitoring [Hill, 2013].

In this study, a statistical model is proposed to identify grassland management practices using time series of a spectral vegetation index (NDVI) with high temporal resolution. Management practices are defined at the parcel scale. Conventional pixel-oriented approaches result in the appearance of misclassified pixels within a class [Bock et al., 2005], leading to non-homogeneous objects that are ecologically unrealistic. Thus, an object-oriented method is developed in this paper.

The first contribution of the method was to account for the spectral variability in a grassland. We considered that the distribution of the pixel spectral reflectance in a given grassland can be modeled by a Gaussian distribution. Then, the Kullback-Leibler divergence was used to compute the distance between each pair of grasslands. To deal with the small sample size compared to the number of temporal variables, a parsimonious Gaussian model was proposed as a second contribution.

The object-oriented approach was compared to a pixel-based approach, through supervised classification.

In section 3.2, the dataset is introduced. Then, the high dimensional Kullback-

Leibler divergence method that we developed is described in section 3.3. In section 3.4, the experimental results on real satellite image time series are presented. Finally, conclusions and perspectives conclude this paper.

3.2. Dataset

3.2.1. Study site

The study site is located in south-west France, near Toulouse, in a semi-rural area where livestock farming is in decline in favor of field crops. Grasslands are mostly used for forage or silage production. The extent of the area corresponds to the satellite image extent (4400 km^2).

3.2.2. Field Data

The dataset is composed of 52 parcels with their management methods. The homogeneity has been controlled during a field survey in May, 2015, where the past and current management practices were also determined, by interviewing the farmers or grassland owners. We identified 3 management types during the vegetation cycle: one mowing (34 parcels), grazing (10 parcels) and mixed management (mowing then grazing, 8 parcels). We used them as classes for the classification. The grasslands have been digitalized by hand.

3.2.3. Satellite data

The satellite image time series (SITS) is composed of 17 multispectral Formosat-2 images (8 meters spatial resolution) from 2013. The images are provided with a mask of clouds and shadows [Hagolle et al., 2010]. The Normalized Difference Vegetation Index (NDVI) was used during this study. Each pixel $\mathbf{x}$ is represented by a vector of size 17.

To remove the noise due to clouds and shadows in the SITS, the NDVI was smoothed applying the Whittaker filter pixel-by-pixel [Eilers, 2003].

3.3. High Dimensional Kullback-Leibler divergence

3.3.1. Symmetrized Kullback-Leibler divergence

The pixel reflectance distribution of grasslands is modeled by a Gaussian distribution, *i.e.* the density function of pixels $\mathbf{x}$ is, conditionally to grassland g_i, a Gaussian distribution. To compute the similarity of the distribution between two grasslands,

we used the symmetrized Kullback-Leibler divergence (KLD) [Kullback, 1987]. The symmetrized KLD between two Gaussian distributions can be written as:

$$KLD(g_i, g_j) = \frac{1}{2}\Big[\mathrm{Tr}\left[\boldsymbol{\Sigma}_i^{-1}\boldsymbol{\Sigma}_j + \boldsymbol{\Sigma}_j^{-1}\boldsymbol{\Sigma}_i\right] + (\boldsymbol{\mu}_i - \boldsymbol{\mu}_j)^\top\left(\boldsymbol{\Sigma}_i^{-1} + \boldsymbol{\Sigma}_j^{-1}\right)(\boldsymbol{\mu}_i - \boldsymbol{\mu}_j)\Big] - d \quad (3.1)$$

where $\boldsymbol{\Sigma}_i$ is the covariance matrix, $\boldsymbol{\mu}_i$ is the mean vector of the signal, d the number of variables and Tr is the trace operator. The parameters are estimated by their empirical counterparts $\hat{\boldsymbol{\mu}}_i = \frac{1}{n_i}\sum_{l=1}^{n_i}\mathbf{x}_l$ and $\hat{\boldsymbol{\Sigma}}_i = \frac{1}{n_i}\sum_{l=1}^{n_i}(\mathbf{x}_l - \hat{\boldsymbol{\mu}}_i)(\mathbf{x}_l - \hat{\boldsymbol{\mu}}_i)^\top$ with n_i the number of pixels in grassland g_i, $g_i \in \{1, ..., G\}$ and G is the total number of grasslands.

Unfortunately, the number of pixels used in the estimation is low compared to the number of variables. Figure 3.1 shows that the number of pixels of most grasslands is lower than the number of parameters to estimate. Thus, the covariance matrix is non invertible for these grasslands. Furthermore, for the other grasslands, the estimated covariance matrices in eq.(3.1) are ill-conditioned making the computation of their inverse numerically unstable. To cope with this issue, specific derivations are considered in the next section.

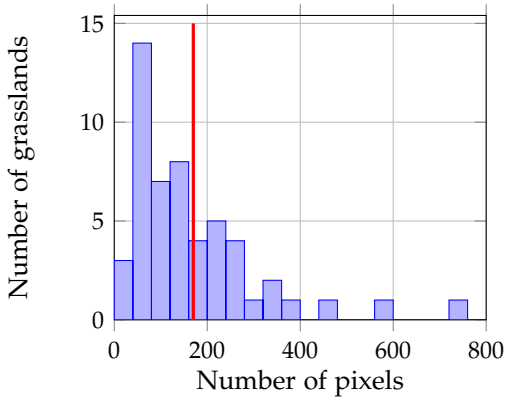

Figure 3.1.: Distribution of the number of pixels per grassland. The red line corresponds to the number of parameters to be estimated for each grassland for a conventional multivariate Gaussian model. This number is derived from the number of variables using the formula $d(d+3)/2 = 170$ for $d = 17$.

3.3.2. High Dimensional Symmetrized KLD

In this work, a high dimensional model is used to model the Gaussian distribution of grasslands [Bouveyron et al., 2007b]. The model assumes that the last (lowest) eigenvalues of the covariance matrix are equal. According to this model, the covariance matrix of grassland g_i can be written as:

$$\mathbf{\Sigma}_i = \mathbf{Q}_i \mathbf{\Lambda}_i \mathbf{Q}_i^\top + \lambda_i \mathbf{I}_d \tag{3.2}$$

where: $\mathbf{I}_d$ is the identity matrix of size $d = 17$, $\mathbf{Q}_i = \left[\mathbf{q}_{i1}, \ldots, \mathbf{q}_{ip_i}\right]$, $\mathbf{\Lambda}_i = \text{diag}\left[\lambda_{i1} - \lambda_i, \ldots, \lambda_{ip_i} - \lambda_i\right]$, $\mathbf{q}_{ij}, \lambda_{ij}$ are the j^{th} eigenvalues/eigenvectors of the covariance matrix $\mathbf{\Sigma}_i$, $j \in \{1, \ldots, d\}$ such as $\lambda_{i1} \geq \ldots \geq \lambda_{id}$, p_i is the number of non-equal eigenvalues, λ_i is the multiple eigenvalue corresponding to the noise term (last and equal eigenvalues).

Following this model, the inverse of the covariance matrix can be computed explicitly:

$$\mathbf{\Sigma}_i^{-1} = -\mathbf{Q}_i \mathbf{V}_i \mathbf{Q}_i^\top + \lambda_i^{-1} \mathbf{I}_d \tag{3.3}$$

with $\mathbf{V}_i = \text{diag}\left[\frac{1}{\lambda_i} - \frac{1}{\lambda_{i1}}, \ldots, \frac{1}{\lambda_i} - \frac{1}{\lambda_{ip_i}}\right]$, and eq.(3.1) can be written as:

$$\begin{aligned} HDKLD(g_i, g_j) = \\ \frac{1}{2}\Big[&- \|\mathbf{\Lambda}_j^{\frac{1}{2}} \mathbf{Q}_j^\top \mathbf{Q}_i \mathbf{V}_i^{\frac{1}{2}}\|_F^2 - \|\mathbf{\Lambda}_i^{\frac{1}{2}} \mathbf{Q}_i^\top \mathbf{Q}_j \mathbf{V}_j^{\frac{1}{2}}\|_F^2 \\ &+ \lambda_i^{-1} \text{Tr}\left[\mathbf{\Lambda}_j\right] - \lambda_j \text{Tr}\left[\mathbf{V}_i\right] + \lambda_j^{-1} \text{Tr}\left[\mathbf{\Lambda}_i\right] - \lambda_i \text{Tr}\left[\mathbf{V}_j\right] \\ &- \|\mathbf{V}_i^{\frac{1}{2}} \mathbf{Q}_i^\top (\boldsymbol{\mu}_i - \boldsymbol{\mu}_j)\|^2 - \|\mathbf{V}_j^{\frac{1}{2}} \mathbf{Q}_j^\top (\boldsymbol{\mu}_i - \boldsymbol{\mu}_j)\|^2 \\ &+ \frac{\lambda_i + \lambda_j}{\lambda_i \lambda_j} \|(\boldsymbol{\mu}_i - \boldsymbol{\mu}_j)\|^2 + \frac{\lambda_i^2 + \lambda_j^2}{\lambda_i \lambda_j} d\Big] - d \end{aligned} \tag{3.4}$$

where $\|L\|_F^2 = \text{Tr}(L^\top L)$ is the Frobenius norm.

3.3.3. Estimation

The parameters of eq.(3.4) are estimated for each grassland g_i from the empirical mean vector and covariance matrix such as [Bouveyron et al., 2007b]:

- $\hat{\lambda}_{ij}$ and $\hat{\boldsymbol{q}}_{ij}$ are the first eigenvalues/eigenvectors of $\hat{\mathbf{\Sigma}}_i$, $j \in \{1, \ldots, p_i\}$. Thus, only the p_i first eigenvalues/eigenvectors are required and the unstable estimation of the eigenvectors associated to small eigenvalues is avoided,
- $\hat{p}_i$ corresponds to the number of eigenvalues needed to reach a given percentage of variance t, $\frac{\sum_{i=1}^{\hat{p}_i} \hat{\lambda}_i}{\sum_{i=1}^{d} \hat{\lambda}_i} \geq t$, t being tuned during learning,
- $\hat{\lambda}_i = \frac{\text{Tr}(\hat{\mathbf{\Sigma}}_i) - \sum_{j \leq \hat{p}_i} \hat{\lambda}_{ij}}{d - \hat{p}_i}$.

3.3.4. Construction of a positive definite kernel with HDKLD

The (HD)KLD measure is a semi-metric, *i.e.*, it satisfies only three first axioms of a metric [Abou–moustafa and Ferrie, 2012]: $(HD)KLD(g_i, g_j) \geq 0$, $(HD)KLD(g_i, g_i) = 0$ and $(HD)KLD(g_i, g_j) = (HD)KLD(g_j, g_i)$. This semi-metric can be turned to a positive definite kernel function by plugging it into a radial basis function [Haasdonk and Bahlmann, 2004]: $K(g_i, g_j) = \exp\left[-\frac{(HD)KLD(g_i,g_j)^2}{\sigma}\right]$ with $\sigma \in \mathbb{R}_+^*$. This kernel is used in the experimental section with a SVM.

3.4. Experimental results

3.4.1. Competitive method

In order to test the effectiveness of the proposed approach, the kernel built in the previous section was used to classify the data using SVM, both for the conventional KLD and the HDKLD. In order to make tractable the inverse problem in KLD, a small (10^{-9}) ridge regularization was done for the covariance matrices. The Gaussian modeling was further compared to the simple case where the pixel reflectance distribution of a grassland is modeled by the mean vector value. Then grasslands are classified by SVM with a conventional RBF kernel. Finally, a pixel-wise SVM classification with a RBF kernel was performed and a majority rule inside each grassland was done to extract one class label at the grassland scale. The SVM and the HDKLD were implemented in Python through the Scikit library. In the remaining of the paper, the methods are denoted, KLD-SVM, HDKLD-SVM, $\boldsymbol{\mu}$-SVM and P-SVM, respectively.

3.4.2. Protocol

All the parameters of each method were optimized using cross-validation. The search ranges were $\sigma \in \{2^{-5}, 2^{-4}, \ldots, 2^5\}$ for P-SVM and $\boldsymbol{\mu}$-SVM, $\sigma \in \{2^8, 2^9, \ldots, 2^{12}\}$ for KLD-SVM and HDKLD-SVM, $C \in \{1, 10, 100\}$ (penalty parameter) for all the methods and $t \in \{0.80, 0.85, 0.90, 0.95, 0.99\}$ for HDKLD-SVM.

Given the small size of the reference data, a Leave One Out procedure was chosen. One grassland is iteratively classified given all the other grasslands. The confusion matrix is built during the process. The classification accuracy is assessed with the overall accuracy (OA) and the Kappa coefficient. The statistical significance of the observed differences are computed using the Z-test.

3.4.3. Results

Table 3.1 gives the confusion matrices associated to each method, their overall accuracy (OA) and Kappa coefficient.

		P-SVM			**μ-SVM**			**KLD-SVM**			**HDKLD-SVM**		
		REF			REF			REF			REF		
PRED		32	4	2	31	6	3	32	8	8	33	4	4
		1	4	1	1	0	0	1	0	0	0	3	0
		1	0	7	2	2	7	1	0	2	1	1	6
OA		0.83			0.73			0.66			0.81		
Kappa		**0.64**			**0.41**			0.09			**0.57**		

Table 3.1.: Confusion matrices for each classification method. Bold numbers correspond to the best results in terms of Kappa. The observed differences are not significant according to the Z-test and the 95% confidence level.

The KLD-SVM is the worst method in terms of Kappa coefficient. The conventional KLD does not perform well in this small sample size context. The proposed parsimonious model is robust to this configuration and it outperforms the conventional KLD.

However, with this dataset, the classifications based on object and pixel-wise approaches are equivalent since the Kappa coefficients between HDKLD-SVM and P-SVM are not significantly different. As an example, there was only one more well-classified grassland with P-SVM compared to HDKLD-SVM. Thus, at this step, no conclusion can be drawn about the performance of HDKLD against P-SVM. Indeed, for HDKLD-SVM, G grasslands instead of n pixels are processed, with $G \ll n$ (here $G = 52$ and $n = 8741$). Moreover, the proposed model provides a statistical description of the grasslands through the distribution parameters: mean and covariance.

3.5. Conclusion

A suitable model for high dimensional data was developed to deal with the dense images time series which will be provided by Sentinel-2 mission. This model is able to classify grassland management practices from dense time series in a small ground sample size context. We proposed to account for the spectral variability in grasslands by modeling the pixels value distribution with a parsimonious Gaussian model. This model is used to define a semi-metric between two grasslands that is used in a supervised classifier.

From the experimental results, HDKLD-SVM is the most-efficient object-oriented method compared to KLD-SVM and to μ-SVM. No significant differences have been observed with the pixel-wise approach. However this model enables a proper modeling of the grassland at the parcel scale.

This model was investigating for future Sentinel-2 image time series. At this step,

our model has been tested with a spectral vegetation index only. We will further extend the method for multispectral data to account for all the spectral information provided by the SITS.

4. Object-based classification of grasslands from high resolution satellite image time series using Gaussian Mean Map Kernels

Object-Based Classification of Grasslands from High Resolution Satellite Image Time Series Using Gaussian Mean Map Kernels

Published in *Remote Sensing* 2017, 9(7), 688; doi:10.3390/rs9070688.

Mailys Lopes[1], Mathieu Fauvel[1], Stéphane Girard[2] and David Sheeren[1]

[1] Dynafor, University of Toulouse, INRA, INPT, INPT-EI PURPAN, 31326 Castanet Tolosan, France
[2] Team Mistis, INRIA Rhône-Alpes, LJK, 38334 Montbonnot, France

Abstract

This paper deals with the classification of grasslands using high resolution satellite image time series. Grasslands considered in this work are semi-natural elements in fragmented landscapes, i.e., they are heterogeneous and small elements. The first contribution of this study is to account for grassland heterogeneity while working at the object level by modeling its pixels distributions by a Gaussian distribution. To measure the similarity between two grasslands, a new kernel is proposed as a second contribution: the α-Gaussian mean kernel. It allows one to weight the influence of the covariance matrix when comparing two Gaussian distributions. This kernel is introduced in support vector machines for the supervised classification of grasslands from southwest France. A dense intra-annual multispectral time series of the Formosat-2 satellite is used for the classification of grasslands' management practices, while an inter-annual NDVI time series of Formosat-2 is used for old and young grasslands' discrimination. Results are compared to other existing pixel- and object-based approaches in terms of classification accuracy and processing time. The proposed method is shown to be a good compromise between processing speed and classification accuracy. It can adapt to the classification constraints, and it encompasses several similarity measures known in the literature. It is appropriate for the classification of small and heterogeneous objects such as grasslands.

Keywords: supervised classification; SVM; Gaussian mean map kernels; kernel methods; object analysis; grasslands

4.1. Introduction

Grasslands are semi-natural elements that represent a significant source of biodiversity in farmed landscapes [Eriksson et al., 1995, Cousins and Eriksson, 2002, Gardi et al., 2002, Critchley et al., 2004]. They provide many ecosystem services such as carbon storage, erosion regulation, food production, crop pollination and biological

regulation of pests [Werling et al., 2014], which are linked to their plant and animal composition.

Different factors impact grassland biodiversity conservation. Among them, the age of a grassland (i.e., the time since last ploughing/sowing) is directly related to its plant and animal composition. Old "permanent" grasslands, often called semi-natural grasslands, hold a richer biodiversity than temporary grasslands [Austrheim and Olsson, 1999, Norderhaug et al., 2000, Cousins and Eriksson, 2002, Waldhardt and Otte, 2003]. Indeed, they had time to establish and stabilize their vegetation cover, contrarily to temporary grasslands, which are part of a crop rotation. Additionally, agricultural management of grasslands (i.e., mowing, grazing, fertilizing, reseeding, etc.) influences their structure and composition [Hansson and Fogelfors, 2000, Moog et al., 2002, Zechmeister et al., 2003, Plantureux et al., 2005]. Management is essential for their biodiversity conservation because its prevents woody establishment. Conversely, an intensive use constitutes a threat for this biodiversity [Muller, 2002, Plantureux et al., 2005]. Therefore, it is important to know the age of a grassland and to identify the management practices in order to monitor their effect on biodiversity and related services. However, these factors are defined at different temporal scales: over the years for the age of a grassland and during a vegetation season (i.e., a year) for the management practice.

Usually, ecologists and agronomists characterize grasslands at the parcel scale through field surveys. However, these surveys require important human and material resources, the knowledge of the assessor and a sampling strategy, which make them expensive and time consuming [Rocchini et al., 2016]. They are thus limited in spatial extent and in temporal frequency, limiting grassland characterization to a local scale and over a short period of time.

Conversely, remote sensing offers the possibility to provide information on landscapes over large extents, thanks to the broad spatial coverage and regular revisit frequency of satellite sensors [Pettorelli et al., 2014]. In this context, satellite images have already appeared to be an appropriate tool to monitor vegetation over large areas with a high temporal resolution.

In the remote sensing literature, grasslands have relatively not been studied much compared to other land covers like crops or forest [Newton et al., 2009]. Most of the studies focusing on grasslands have agronomic applications, such as estimating biomass productivity and growth rate [Gu et al., 2013, Li et al., 2013, Gu and Wylie, 2015] or derivating biophysical parameters like the Leaf Ara Index (LAI), the Fraction of Photosynthetically Active Radiation (fPAR) and the chlorophyll content [Friedl et al., 1994, Wylie et al., 2002, Darvishzadeh et al., 2008, He et al., 2009, Asam et al., 2013]. Studies having biodiversity conservation schemes such as assessing plant diversity and plant community composition in a grassland are usually based on ground spectral

measurements or airborne acquisitions at a very high spatial resolution [Schmidtlein and Sassin, 2004, Ishii et al., 2009, Fava et al., 2010, Oldeland et al., 2010, Feilhauer et al., 2011, Duniway et al., 2012, Punalekar et al., 2016]. However, such acquisitions are time consuming and expensive, and thus, they do not allow for continuous monitoring of grasslands over the years.

Using satellite remote sensing images, grasslands have been much studied at a regional scale with medium spatial resolution sensors (i.e., MODIS, 250 m/pixel [Li et al., 2013, Gu et al., 2013, Hilker et al., 2014]), where the Minimum Mapping Unit (MMU) is at least of hundreds of meters. This scale is suitable for large, extensive, homogeneous and contiguous regions like steppes [Cao et al., 2015], but not for fragmented landscapes, which are usually found in Europe and in France particularly [Eriksson et al., 2002, Zillmann et al., 2014]. These fragmented landscapes are made of a patchwork of different land covers, which have a small area [Zillmann et al., 2014]. In these types of landscapes, grasslands can be smaller (less than 10,000 m^2) than the pixel resolution [Ali et al., 2016] (see Figure 4.1 for a graphical example). As a consequence, pixels containing grasslands are usually a mixture of other contributions, which can limit the analysis [Nagendra, 2001, Blaschke et al., 2014]. As examples, Poças et al. [Poças et al., 2012] had to select large contiguous areas of semi-natural grasslands in a mountain region of Portugal to be able to use SPOT-VEGETATION data (1-km resolution). Halabuk et al. [Halabuk et al., 2015] also had to select only one MODIS pixel per homogeneous sample site in Slovakia to detect cutting in hay meadows. A 30-m pixel resolution is still not sufficient for grassland characterization. Indeed, Lucas et al. [Lucas et al., 2007] and Toivonen and Luoto [Toivonen and Luoto, 2003] showed that it was more difficult to classify fragmented and complex elements [Nagendra et al., 2013], like semi-natural grasslands, than homogeneous habitats, using Landsat imagery. Price et al. [Price et al., 2002] classified six grassland management types in Kansas using six Landsat images, but the accuracy of the classification was not satisfying (less than 70%). Therefore, to detect small grasslands in fragmented landscapes, high spatial resolution images are required [Gamon et al., 1993, Corbane et al., 2015, Ali et al., 2016].

For high spatial resolution images (about 10 m/pixel), few intra-annual images are usually available for a given location [Wulder et al., 2004]. However, Buck et al. [Buck et al., 2015] concluded that three RapidEye images per year were not enough to detect the mowing practices in grasslands. It was confirmed by Franke et al. [Franke et al., 2012] who classified grassland use intensity into four categories: semi-natural grassland, extensively-used grassland, intensively-used grassland and tilled grassland. They increased the classification accuracy when increasing the number of RapidEye images from three to five scenes. Additionally, Schmidt et al. [Schmidt et al., 2014] concluded that about seven to ten images, depending on the vegetation index used,

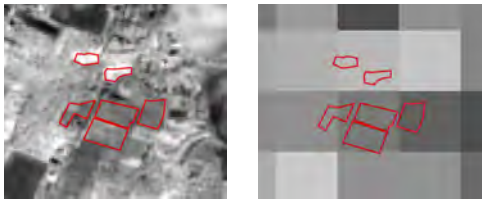

(**a**) (**b**)

Figure 4.1.: Digitalized grasslands (in red) from the dataset used in this study on (**a**) a Sentinel-2 image (10-m pixel resolution) and (**b**) a MODIS image (250 m).

are a good tradeoff between the amount of satellite data and classification accuracy of grassland use intensity. Some works report results with few images per year, such as Dusseux et al. [Dusseux et al., 2014b], but they worked on LAI. In their study for mapping grassland habitat using intra-annual RapidEye imagery, Schuster et al. [Schuster et al., 2015] concluded the more acquisition dates used, the better the mapping quality.

Given the heterogeneity of grasslands in fragmented landscapes, their phenological cycle and the punctuality of the anthropogenic events (e.g., mowing), dense high spatial resolution intra-annual time series are necessary to identify the grassland management types [Psomas et al., 2011, Hill, 2013, Schuster et al., 2015, Ali et al., 2016]. Moreover, to discriminate semi-natural grasslands from temporary grasslands, inter-annual time series are necessary. Until recently, satellite missions offering high revisit frequency (1–16 days) had coarse spatial resolution (i.e., NOAA AVHRR, 1 km; MODIS, 250/500 m). Conversely, high spatial resolution missions did not provide dense time series and/or were costly (i.e., QuickBird, RapidEye). For these reasons and compared to crops, grasslands' differentiation through Earth observations is still considered as a challenge [Schuster et al., 2015]. However, new missions like Sentinel-2 [Drusch et al., 2012], with a very high revisit frequency (five days) and high spatial resolution (10 m in four spectral channels, 20 m in six channels), provide new opportunities for grasslands' monitoring over the years in fragmented landscapes [Hill, 2013] at no cost, thanks to the ESA free data access policy. For instance, the high spatial resolution is assumed to make possible the identification of grassland-only pixels in the image, and several pixels can belong to the same grassland plot. Hence, the analysis can be done at the object level, not at the pixel level, which is suitable for landscape ecologists and agronomists who usually study grasslands at the parcel scale [Laliberte et al., 2007]. Thus, object-oriented approaches are more likely to characterize grasslands ecologically [Brenner et al., 2012, Stenzel et al., 2017]. Yet, many works consider pixel-based approaches without any spatialconstraints [Schuster et al., 2015, Price et al., 2002, Toivonen and Luoto, 2003, Evans and Geerken, 2006, Franke et al., 2012, Gu et al.,

2013, Buck et al., 2015].

At the object level, grasslands are commonly represented by their mean NDVI [Li et al., 2013]. However, such a representation might be too simple since it does not account for the heterogeneity in a grassland. Sometimes, distributions of pixels as individual observations are still better than the mean value to represent grasslands, as in [Hill, 2013]. Lucas et al. [Lucas et al., 2007] used a rule-based method on segmented areas for habitat mapping, but it did not work well on complex and heterogeneous land covers. Esch et al. [Esch et al., 2014] also used an object-oriented method on segmented elements then represented by their mean NDVI. These methods based on mean modeling do not capture grasslands' heterogeneity well. Other representations can be found in the literature, taking the standard deviation and object texture features as variables [Duro et al., 2012], but they were not applied to time series. To our knowledge, these methods do not use the high spatial and the high temporal resolutions jointly. Moreover, all of these studies used vegetation indices as a variable, although it has been shown that classification results are better when using more spectral information [Zillmann et al., 2014, Sheeren et al., 2016].

To deal with the high spatio-spectro-temporal resolutions new satellite sensors are now offering, dimension reduction is usually performed through the use of a vegetation index such as NDVI [Ding et al., 2014, Pan et al., 2015, Schmidt et al., 2014, Schuster et al., 2015], PCA [Cingolani et al., 2004] or spectro-temporal metrics [Zillmann et al., 2014, Müller et al., 2015]. However, a large amount of spectro-temporal information is lost with these solutions. Franke et al. [Franke et al., 2012] developed an indicator of the spectral variability of a pixel over the time series, the mean absolute spectral dynamics, but its efficiency was assessed using a decision tree algorithm. Decision trees are usually not recommended because they tend to over-fit the data [Mitchell, 1997]. Therefore, the high spatio-spectro-temporal resolutions have not really been addressed in the literature of remote sensing classification. Indeed, such time series bring new methodological and statistical constraints given the high dimension of data (i.e., number of pixels and number of spectral and temporal measurements). Dealing with more variables increases the number of parameters to estimate, increasing the computation time and making the computation unstable (i.e., ill-conditioned covariance matrices, etc.) [Donoho, 2000, Fauvel et al., 2013]. Hence, conventional models are not appropriate if one wants to use all of the spectro-temporal information of time series with high spatial and temporal resolutions. Thus, classifying grasslands with this type of data is still considered as a challenge [Schuster et al., 2015].

In the present study, we introduce a model suitable for the classification of grasslands using Satellite Image Time Series (SITS) with a high number of spectro-temporal variables (e.g., Sentinel-2 data). Two temporal scales are considered in this work: (i) an inter-annual time series of three years to discriminate old grasslands from young

grasslands and (ii) an intra-annual time series to identify the management practices. Note that in this work, the objects are not found from segmentation [Blaschke et al., 2014], but from the existing dataset in a polygon form.

The first contribution of this study is to model a grassland at the object level while accounting for the spectral variability within a grassland. We consider that the distribution of the pixel spectral reflectance in a given grassland can be modeled by a Gaussian distribution. The second contribution is to propose a measure of similarity between two Gaussian distributions that is robust to the high dimension of the data. This method is based on the use of covariance through mean maps. The last contribution is the application of the method to old and young grasslands' discrimination and of management practices' classification, which are non-common applications in remote sensing. Moreover, to our knowledge, mean maps have not yet been used on Gaussian distributions for supervised classification of SITS at the object level.

In the next section, the materials used for the experimental part of this study are presented. Then, the methods, including the different types of grassland modeling and the measures of similarity between distributions, are introduced in Section 4.3. Following that, we experiment with the proposed methods on the classification of a real dataset in Section 4.4. Finally, conclusions and prospects are given in Section 4.5.

4.2. Materials

4.2.1. Study Site

The study site is located in southwest France, near the city of Toulouse (about 30 km), in a semi-rural area (center coordinates: 43°27′36″N 1°8′24″E; Figure 4.2). This region is characterized by a temperate climate with oceanic and Mediterranean influences. The average annual precipitation is 656 mm, and the average temperature is 13 °C. The north of the site, closer to the urban area of Toulouse, is flat, whereas the southwest of the site is hilly. The eastern part corresponds to the Garonne River floodplain, and this location is dominated by crop production. Within this study site, livestock farming is declining in favor of annual crop production. Grasslands are mostly used for forage or silage production. Some grasslands, located in the southwestern part of the area, are pastures for cattle or sheep. The extent of the area is included in the satellite image extent (Figure 4.2) and is about 24×24 km².

4.2.2. Satellite Data

Time series of Formosat-2 were used in this experiment. Formosat-2 has four spectral bands with an 8-m spatial resolution: B1 "Blue" (0.45–0.52 μm), B2 "Green" (0.52–0.6 μm), B3 "Red" (0.63–0.69 μm), B4 "Near Infra-Red (NIR)" (0.76–0.9 μm). The ex-

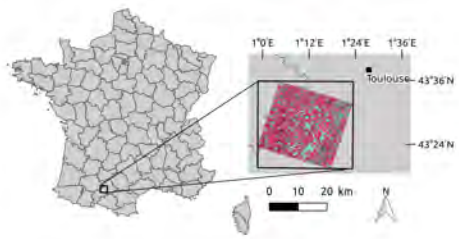

Figure 4.2.: Study site location in southwest France. It is included in the satellite image extent.

tent of an acquisition is 24 km × 24 km. The images were all acquired with the same viewing angle. They were orthorectified, radiometrically and atmospherically corrected by the French Spatial Agency (CNES). They were provided by the Center for the Study of the Biosphere from Space (CESBIO) in reflectance with a mask of clouds and shadows issued from the MACCS (Multi-sensor Atmospheric Correction and Cloud Screening) processor [Hagolle et al., 2010], in the frame of the Kalideos project.

For the inter-annual analysis, we used all of the acquisitions of the consecutive years 2012 (13 observations), 2013 (17 observations) and 2014 (15 observations) (Figures 4.3 and S1 in the Supplementary Materials). The acquisitions of the year 2013 and of the year 2014 were used separately for the classification of management practices.

To reconstruct the time series due to missing data (clouds and their shadows), the Whittaker filter [Eilers, 2003] was applied pixel-by-pixel on the reflectances in each spectral band for each year independently. The Whittaker filter is a non-parametric filter that has a smoothing parameter that controls the roughness of the reconstructed curve. It has been successfully applied to smooth NDVI time series in the literature [Atzberger and Eilers, 2011a, Atzberger and Eilers, 2011b, Nitze et al., 2015, Shao et al., 2016]. The smoother was adapted for unequally-spaced intervals and accounted for missing data (see [Sheeren et al., 2016] for a detailed description of the method). The smoothing parameter was the same for all of the pixels. It was equal to 10^5 for the year 2013 and to 10^4 for 2012 and 2014, after an ordinary cross-validation done on a subset of the pixels for each year. An example of smoothing on a grassland pixel is provided in Figure 4.4. This pixel is hidden by a light cloud during one image acquisition (red cross). Notice that the smoothing is done at the cost of under-estimating the local maxima of the temporal profile.

For the intra-annual time series, we used all of the spectral information. Therefore, the smoothed time series associated with each of the four spectral bands were concatenated to get a unique time series per pixel. For the inter-annual time series, as using all of the spectral bands would result in a too large number of variables to process, we

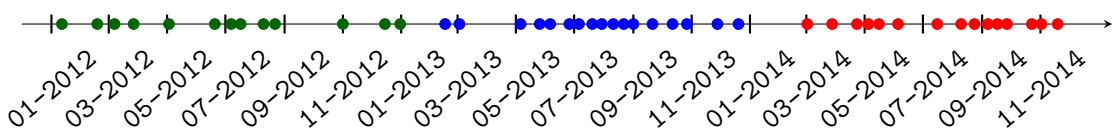

Figure 4.3.: Formosat-2 acquisition dates in 2012 (green dots), 2013 (blue dots) and 2014 (red dots) used in this experiment.

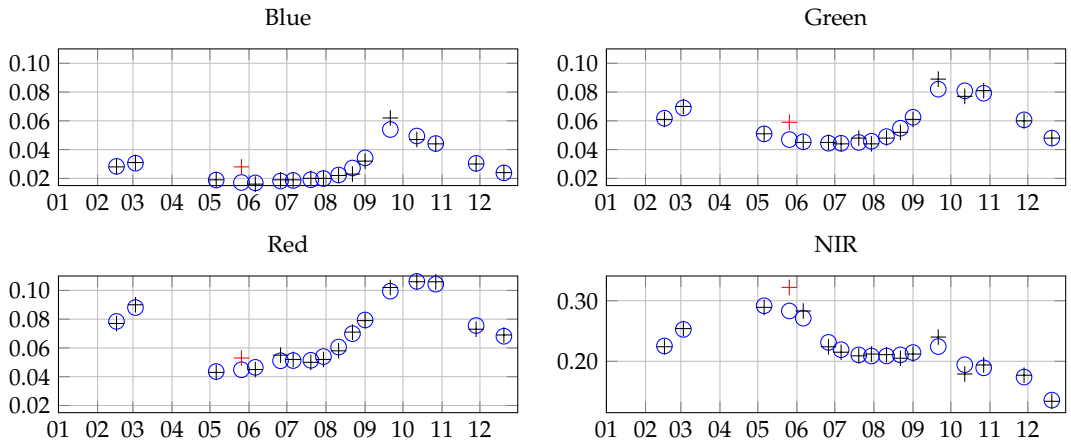

Figure 4.4.: Example of time series reconstruction (blue dots) with the Whittaker smoother for a pixel of a grassland in the four spectral bands. The black crosses correspond to the original 2013 Formosat-2 time series, and the red ones correspond to missing/noisy data due to the clouds. The x-axis represents the month of year 2013, and the y-axis is the reflectance.

worked on the NDVI, computed from the red and NIR bands.

4.2.3. Reference Data

4.2.3.1. Old and Young Grasslands

In this study, "old" grasslands are 14 years old or more, whereas "young" grasslands are less than five years old. The French agricultural land use database (Registre Parcellaire Graphique) was used to extract the grasslands depending on their age. It registers on an annual basis the cultivated areas declared by the farmers in a GIS. Grasslands are declared as "permanent" or "temporary". Permanent grasslands are at least five years old, whereas temporary grasslands are less than five years old (Commission Regulation EU No. 796/2004). For every plot declared as a grassland in 2014, its age

was computed from the previous years' declarations. We kept only the grasslands that were at least 14 years old in 2014 ("old") and the grasslands that were less than 5 years old in 2014 ("young"). A negative buffer of 8 m was then applied to all of the polygons to eliminate the edge effects (Figure 4.5). Then, they were rasterized using the GDAL command gdal_rasterize (http://www.gdal.org/gdal_rasterize.html) to obtain the pixels inside each grassland. Only the grasslands having an area of at least 1000 m² were kept to ensure a minimum number of 16 pixels to represent each grassland. In the end, there were 59 old grasslands (at least 14 years old) and 416 young grasslands (Table 4.1), for an average area of about 26,600 m².

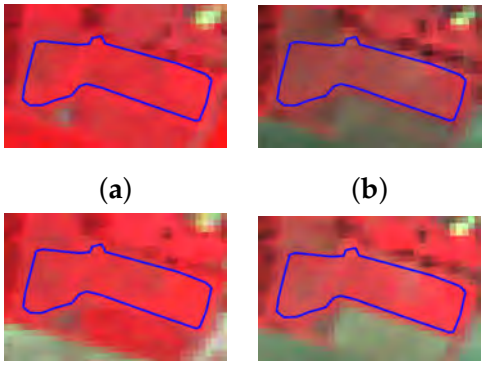

(**a**) (**b**)

(**c**) (**d**)

Figure 4.5.: False color Formosat-2 images of the same grassland on two close dates (June and October) in 2013 and 2014 with the same color scale. (**a**) 6 June 2013, (**b**) 27 October 2013, (**c**) 5 June 2014, (**d**) 23 October 2014. The blue line represents the polygon limits of the grassland.

Table 4.1.: Composition of the old and young grasslands' dataset.

Class	**No. of Grasslands**	**No. of Pixels**
Old	59	31,166
Young	416	129,348
Total	475	160,514

4.2.3.2. Management Practices

The information of the agricultural practices performed in the crops is not featured in the land use database. Therefore, this dataset comes exclusively from field data.

As mentioned in the Introduction, ground data are difficult to obtain in ecology since field work is fastidious. A field survey was conducted in May 2015 to determine the past and current management practices of 52 grasslands by interviewing the farmers or grasslands' owners. The practices remained stable for the years 2013 and 2014. Four management types during a vegetation cycle were identified: one mowing, two mowings, grazing and mixed (mowing then grazing). We eliminated the type "two mowings" of the dataset because of its under-representation (only three grasslands).

The management types were used as classes for the classification (Table 4.2). The grasslands were digitalized manually after field work. A negative buffer of 8 m was then applied to eliminate the edge effects, before rasterizing the polygons. The average grasslands surface area is about 10,000 m². The smallest grassland is 1632 m² (which represents 25 Formosat-2 pixels), and the largest is 47,111 m² (735 pixels) (Figure 4.6).

Table 4.2.: Grassland management types and composition of the dataset.

Class	**No. of Grasslands**	**No. of Pixels**
Mowing	34	6265
Grazing	10	1193
Mixed	8	1170
Total	52	8628

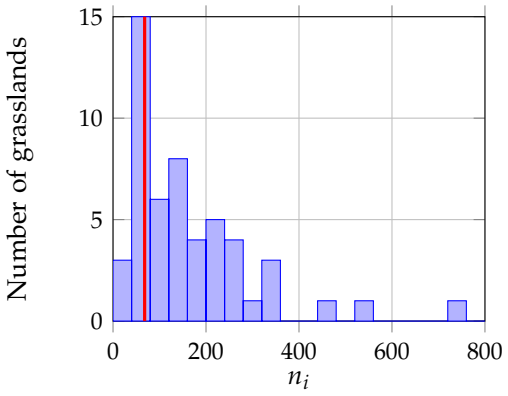

Figure 4.6.: Histogram of grasslands' size in the number of pixels n_i. The red line corresponds to the number of spectro-variables $d = 68$ in 2013.

4.3. Methods

4.3.1. Grassland Modeling

In this work, each grassland g_i is composed of a given number n_i of pixels $\mathbf{x}_{ik} \in \mathbb{R}^d$, where k is the pixel index such as $k \in \{1, ..., n_i\}$, $i \in \{1, \ldots, G\}$, G is the total number of grasslands, $N = \sum_{i=1}^{G} n_i$ is the total number of pixels, $d = n_B n_T$ is the number of spectro-temporal variables, n_B is the number of spectral bands and n_T is the number of temporal acquisitions. In the experimental part, when working on the intra-annual time series of 2013 using the four spectral bands, $d = 4 \times 17 = 68$. In 2014, $d = 4 \times 15 = 60$. When working on the inter-annual times series using NDVI, $d = 1 \times (13 + 17 + 15) = 45$. With each grassland g_i is associated a matrix $\mathbf{X}_i$ of size $(n_i \times d)$ and a response variable $y_i \in \mathbb{R}$, which corresponds to its class label.

In the following, two types of grassland modeling are discussed, at the pixel level and at the object level. A more informative object level modeling is then proposed. Then, similarity measures are discussed.

4.3.1.1. Pixel Level

The representation of a grassland at the pixel level has been much used in the remote sensing literature [Schuster et al., 2015, Price et al., 2002, Toivonen and Luoto, 2003, Evans and Geerken, 2006, Franke et al., 2012, Gu et al., 2013, Buck et al., 2015]. The grassland can either be represented by all of its pixels or by one pixel when the spatial resolution of the pixel is too coarse; see, for instance, [Poças et al., 2012, Halabuk et al., 2015]. In this representation, a sample is a pixel. Therefore, with each $\mathbf{x}_{ik}$ is associated the response variable y_i of g_i, but $\mathbf{x}_{ik}$ is processed independently of all other $\mathbf{x}_{ik'}$ of g_i. However, this representation usually leads to aberrant classification results (e.g., salt and pepper effect) [Blaschke et al., 2014], which are not expected when working at the grassland level.

4.3.1.2. Object Level

At the object level, the mean vector $\boldsymbol{\mu}_i$ of the pixels belonging to g_i is generally used to represent g_i. It is estimated empirically by:

$$\hat{\boldsymbol{\mu}}_i = \frac{1}{n_i} \sum_{l=1}^{n_i} \mathbf{x}_{il}. \tag{4.1}$$

In this case, a vector $\hat{\boldsymbol{\mu}}_i \in \mathbb{R}^d$ and a response variable $y_i \in \mathbb{R}$ are associated with each grassland. This representation might be limiting for heterogeneous objects such as grasslands since the spectro-temporal variability is not encoded. To illustrate this bias, Figure 4.7 shows on the left the set of pixel values in the NIR band for two

grasslands (a and b). From this figure, it can be seen that if the mean vector captures the average behavior, higher variability can be captured by including the variance/covariance (middle and right plots). The figure shows that the first and second eigenvectors of the covariance matrix capture well the general trend in the grassland and the main variations due to different phenological behaviors in the grassland. This information cannot be recovered by considering the variance feature only: covariance must also be included.

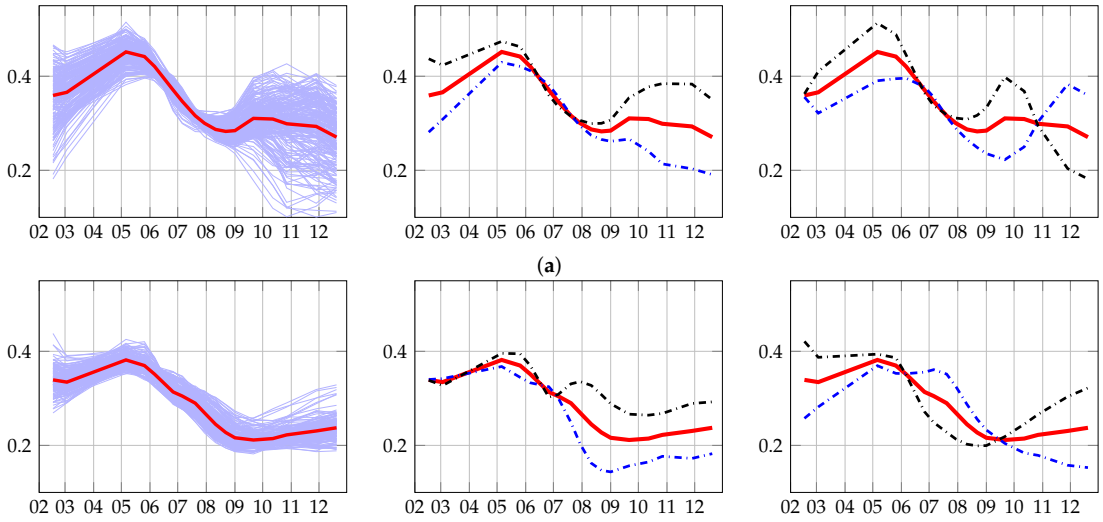

Figure 4.7.: Examples of 2013 time series evolution in the NIR reflectance band of Formosat-2 for a grassland of management practice (**a**) "mowing" and (**b**) "grazing". The x-axis is the month of the year. The y-axis is the NIR reflectance value. The plot on the left shows the evolution of all of the pixels in the grassland and the temporal mean of these pixels in red. The plot in the middle shows the temporal mean in red, the temporal mean $+0.2\times$ the first eigenvector in blue and the temporal mean $-0.2\times$ the first eigenvector in black. The plot on the right shows the temporal mean in red, the temporal mean $+0.2\times$ the second eigenvector in blue and the temporal mean $-0.2\times$ the second eigenvector in black.

In this study, to account for the spectro-temporal variability, we assume that the distribution of pixels $\mathbf{x}_i$ is, conditionally to grassland g_i, a Gaussian distribution $\mathcal{N}(\boldsymbol{\mu}_i, \boldsymbol{\Sigma}_i)$, where $\boldsymbol{\Sigma}_i$ is the covariance matrix estimated empirically by:

$$\hat{\boldsymbol{\Sigma}}_i = \frac{1}{n_i - 1} \sum_{l=1}^{n_i} (\mathbf{x}_{il} - \hat{\boldsymbol{\mu}}_i)(\mathbf{x}_{il} - \hat{\boldsymbol{\mu}}_i)^\top. \tag{4.2}$$

In this case, we associate with each g_i its estimated distribution $\mathcal{N}(\hat{\boldsymbol{\mu}}_i, \hat{\boldsymbol{\Sigma}}_i)$ and a response variable $y_i \in \mathbb{R}$. The Gaussian modeling encodes first and second order information on the grassland by exploiting the variance-covariance information. It is worth noting that if we constrain $\hat{\boldsymbol{\Sigma}}_i = \mathbf{I}_d$, the identity matrix of size d, for $i \in [1, \ldots, G]$, the Gaussian modeling is reduced to the mean vector. In the following, $\mathcal{N}(\hat{\boldsymbol{\mu}}_i, \hat{\boldsymbol{\Sigma}}_i)$ is denoted by $\mathcal{N}_i$.

4.3.2. Similarity Measure

4.3.2.1. Similarity Measure between Distributions

For classification purposes, a similarity measure between each pair of grasslands is required. With pixel-based or mean modeling approaches, conventional kernel methods such as Support Vector Machine (SVM) with a Radial Basis Function (RBF) kernel can be used since the explanatory variable is a vector. However for a Gaussian modeling, i.e., when the explanatory variable is a distribution, specific derivations are required to handle the probability distribution as an explanatory variable.

Many similarity functions generally used to compare two Gaussian distributions (e.g., Kullback–Leibler divergence [Kullback, 1987] and Jeffries–Matusita distance, which is based on Bhattacharyya distance [Richards and Jia, 1999]) require the inversion of the covariance matrices and the computation of their determinants. For a conventional multivariate Gaussian model, the number of parameters to estimate for each grassland is $d(d+3)/2$ (d parameters for the mean vector and $d(d+1)/2$ parameters for the symmetric covariance matrix). In the case where d is large, the number of parameters to estimate can be much larger than the number of samples, making the inverse problem ill-posed. This issue is faced in this study because grasslands are small elements of the landscape. They are characterized by a number of spectro-temporal variables, which is about of the same order as the number of pixels n_i (see Figure 4.6). Therefore, most of the estimated covariance matrices are singular, and their determinants are null. Hence, conventional similarity measures used for moderate dimensional Gaussian distributions are not suitable for high dimensional Gaussian distributions. In the following, we propose to use mean map kernels, and we introduce a derivation of mean map kernels to weight the influence of the covariance matrix.

4.3.2.2. Mean Map Kernels between Distributions

Mean map kernels are similarity measures that operate on distributions [Mehta and Gray, 2010]. They have been used in remote sensing for semi-supervised pixel-based learning in [Gomez-Chova et al., 2010]. In their work, the authors define the similarity between two distributions p_i and p_j as the average of all pairwise kernel evaluations over the available realizations of p_i and p_j (i.e., pixels that belong to grasslands g_i

or g_j). It corresponds to the empirical mean kernel (Equation (8) [Gomez-Chova et al., 2010]):

$$K^e(p_i, p_j) = \frac{1}{n_i n_j} \sum_{l,m=1}^{n_i,n_j} k(\mathbf{x}_{il}, \mathbf{x}_{jm}), \tag{4.3}$$

where n_i and n_j are the number of pixels associated with p_i and p_j, respectively, $\mathbf{x}_{il}$ is the l-th realization of p_i, $\mathbf{x}_{jm}$ is the m-th realization of p_j and k is a semi-definite positive kernel function.

It is possible to include prior knowledge on the distributions by considering the generative mean kernel [Mehta and Gray, 2010]:

$$K^g(p_i, p_j) = \int_{\mathbb{R}^d} \int_{\mathbb{R}^d} k(\mathbf{x}, \mathbf{x}') \hat{p}_i(\mathbf{x}) \hat{p}_j(\mathbf{x}') d\mathbf{x} d\mathbf{x}'. \tag{4.4}$$

Note that Equation (4.3) acts on the realizations of p_i, while Equation (4.4) acts on its estimation. When dealing with a large number of samples, the latter can drastically reduce the computational load with respect to the former.

In our grassland modeling, p_i and p_j are assumed to be Gaussian distributions. In that case, if k is a Gaussian kernel such as $k(\mathbf{x}, \mathbf{x}') = \exp(-\frac{\gamma}{2}\|\mathbf{x} - \mathbf{x}'\|^2)$, Equation (4.4) reduces to the so-called Gaussian mean kernel [Muandet et al., 2012]:

$$K^G(\mathcal{N}_i, \mathcal{N}_j) = \frac{\exp\left\{-0.5(\hat{\boldsymbol{\mu}}_i - \hat{\boldsymbol{\mu}}_j)^T \left(\hat{\boldsymbol{\Sigma}}_i + \hat{\boldsymbol{\Sigma}}_j + \gamma^{-1}\mathbf{I}_d\right)^{-1} (\hat{\boldsymbol{\mu}}_i - \hat{\boldsymbol{\mu}}_j)\right\}}{|\hat{\boldsymbol{\Sigma}}_i + \hat{\boldsymbol{\Sigma}}_j + \gamma^{-1}\mathbf{I}_d|^{0.5}}, \tag{4.5}$$

where γ is a positive regularization parameter coming from the Gaussian kernel k and $|\cdot|$ stands for the determinant.

This kernel is not normalized, i.e., $K^G(\mathcal{N}_i, \mathcal{N}_i) \neq 1$, but the normalization can be achieved easily:

$$\begin{aligned} \tilde{K}^G(\mathcal{N}_i, \mathcal{N}_j) &= \frac{K^G(\mathcal{N}_i, \mathcal{N}_j)}{K^G(\mathcal{N}_i, \mathcal{N}_i)^{0.5} K^G(\mathcal{N}_j, \mathcal{N}_j)^{0.5}} \\ &= K^G(\mathcal{N}_i, \mathcal{N}_j) |2\hat{\boldsymbol{\Sigma}}_i + \gamma^{-1}\mathbf{I}_d|^{0.25} |2\hat{\boldsymbol{\Sigma}}_j + \gamma^{-1}\mathbf{I}_d|^{0.25}. \end{aligned} \tag{4.6}$$

With respect to the Kullback–Leibler Divergence (KLD) and the Jeffries–Matusita Distance (JMD), the Gaussian mean kernel introduces a ridge regularization term $\gamma^{-1}\mathbf{I}_d$ in the computation of the inverse and of the determinant [Tarantola, 2005]. Thus, the Gaussian mean kernel is more suitable to measure the similarity in a high dimensional space than KLD and JMD. The value of γ tunes the level of regularization. It is tuned during the training process as a conventional kernel parameter.

However, in the case of very small grasslands, two problems remain. The first lies in the ridge regularization: in this case, so low γ values are selected that it becomes too regularized, and it deteriorates the information. The second problem is that the estimation of the covariance matrix has a large variance when the number of samples used for the estimation is lower than the number of variables. Therefore, the covariance matrix becomes a poorly-informative feature. In the following, we propose a new kernel function that allows one to weight the covariance features with respect to the mean features.

4.3.2.3. α-Gaussian Mean Kernel

Depending on the level of heterogeneity and the size of the grassland, the covariance matrix could be more or less important for the classification process. We propose a kernel including an additional positive parameter α, which allows one to weight the influence of the covariance matrix, the α-generative mean kernel:

$$K^{\alpha}(p_i, p_j) = \int_{\mathbb{R}^d} \int_{\mathbb{R}^d} k(\mathbf{x}, \mathbf{x}') \hat{p}_i(\mathbf{x})^{(\alpha^{-1})} \hat{p}_j(\mathbf{x}')^{(\alpha^{-1})} d\mathbf{x} d\mathbf{x}'. \tag{4.7}$$

When p_i and p_j are Gaussian distributions, k is a Gaussian kernel and the normalization is applied, the expression gives rise to the α-Gaussian mean kernel:

$$\tilde{K}^{\alpha}(\mathcal{N}_i, \mathcal{N}_j) = \frac{\exp\left\{-0.5(\hat{\boldsymbol{\mu}}_i - \hat{\boldsymbol{\mu}}_j)^T \left(\alpha(\hat{\boldsymbol{\Sigma}}_i + \hat{\boldsymbol{\Sigma}}_j) + \gamma^{-1}\mathbf{I}_d\right)^{-1} (\hat{\boldsymbol{\mu}}_i - \hat{\boldsymbol{\mu}}_j)\right\}}{|\alpha(\hat{\boldsymbol{\Sigma}}_i + \hat{\boldsymbol{\Sigma}}_j) + \gamma^{-1}\mathbf{I}_d|^{0.5}} |2\alpha\hat{\boldsymbol{\Sigma}}_i + \gamma^{-1}\mathbf{I}_d|^{0.25} |2\alpha\hat{\boldsymbol{\Sigma}}_j + \gamma^{-1}\mathbf{I}_d|^{0.25}. \tag{4.8}$$

The proof is given in the Appendix. It is interesting to note that particular values of α and γ lead to known results:

1. $\alpha = 0$: In this case, Equation (4.8) reduces to the Gaussian kernel between the mean vectors. It becomes therefore equivalent to an object modeling where only the mean is considered.

2. $\alpha = 1$: It corresponds to the Gaussian mean kernel defined in Equation (4.6).

3. $\alpha \to +\infty$: We get a distance, which works only on the covariance matrices. It is therefore equivalent to an object modeling where only the covariance is considered.

4. $\gamma \to +\infty$ and $\alpha = 2$: The α-Gaussian mean kernel simplifies to an RBF kernel built with the Bhattacharyya distance computed between $\mathcal{N}_i$ and $\mathcal{N}_j$.

This proposed kernel thus includes several similarity measures known in the literature. Furthermore, new similarity measures can be defined by choosing different parameters' configuration. The α-Gaussian mean kernel (αGMK) is therefore more flexible since it can adapt to the classification constraints:

- Whether the heterogeneity of the object is relevant or not,
- Whether the ratio between the number of pixels and the number of variables is high or low.

4.4. Experiments on Grasslands' Classification

In this section, the experiments for grassland classification are detailed. We first introduce the seven competitive methods, then the classification protocol is described, and we finally present and discuss the results.

4.4.1. Competitive Methods

Several existing pixel-based and object-based classification methods using SVM are presented below. They are compared to assess the effectiveness of the proposed object-based method, which relies on the weighted use of the covariance matrix, αGMK, for the classification of grasslands.

4.4.1.1. Pixel-Based and Mean Modeling

These conventional methods use a RBF kernel.

- PMV (Pixel Majority Vote): The pixel-based method was described in Section 4.3.1.1. It classifies each pixel with no a priori information on the object to which the pixel belongs. In order to compare to other object level methods, one class label is extracted per grassland by a majority vote done among the pixels belonging to the same grassland.
- $\boldsymbol{\mu}$ (mean): The distribution of the pixels reflectance of g_i is modeled by its mean vector $\boldsymbol{\mu}_i$ (see Section 4.3.1.2).

4.4.1.2. Divergence Methods

These methods are based on a distance D between two Gaussian distributions. They are used in a Gaussian kernel such as $K_D(\mathcal{N}_i, \mathcal{N}_j) = \exp(-\frac{D_{ij}^2}{\sigma})$, with $\sigma > 0$:

- HDKLD (High Dimensional Kullback–Leibler Divergence): This method uses the Kullback–Leibler divergence for Gaussian distributions with a regularization on covariance matrices such as described in [Lopes et al., 2016].

- BD (Bhattacharyya Distance): This method uses the Bhattacharyya distance in the case of Gaussian distributions:

$$B(\mathcal{N}_i, \mathcal{N}_j) = \frac{1}{8}(\hat{\boldsymbol{\mu}}_i - \hat{\boldsymbol{\mu}}_j)^\top \left(\frac{\hat{\boldsymbol{\Sigma}}_i + \hat{\boldsymbol{\Sigma}}_j}{2}\right)^{-1} (\hat{\boldsymbol{\mu}}_i - \hat{\boldsymbol{\mu}}_j) + \frac{1}{2} \ln \left(\frac{\left|\frac{\hat{\boldsymbol{\Sigma}}_i + \hat{\boldsymbol{\Sigma}}_j}{2}\right|}{|\hat{\boldsymbol{\Sigma}}_i|^{0.5} |\hat{\boldsymbol{\Sigma}}_j|^{0.5}} \right).$$

  Small eigenvalues of the covariance matrices are shrinked to the value 10^{-5} to make the computation tractable [Ledoit and Wolf, 2004].

4.4.1.3. Mean Map Kernel-Based Methods

These methods are based on mean map kernels presented in Section 4.3.2:

- EMK (Empirical Mean Kernel): This method uses the empirical mean map kernel of Equation (4.3) and it is pixel-based.

- GMK (Gaussian Mean Kernel): This method is based on the normalized Gaussian mean kernel (Equation (4.6)).

- αGMK (α-Gaussian Mean Kernel): This method is based on the proposed normalized α-Gaussian mean kernel (Equation (4.8)).

Figure 4.8 illustrates the relationships between the different methods. The characteristics of each method are synthesized in Table 4.3.

For memory issues during the SVM process, the number of pixels processed for the old and young grasslands' classification was divided by 10 for the two methods based on pixels (PMV and EMK). Only one pixel out of 10 was kept per grassland.

Table 4.3.: Characteristics of the methods used in this study.

Method	**PMV**	**EMK**	$\boldsymbol{\mu}$	**HDKLD**	**BD**	**GMK**	α**GMK**
Level	Pixel	Object	Object	Object	Object	Object	Object
Explanatory variable	$\mathbf{x}_{ik}$	$\mathbf{x}_{ik}$	$\boldsymbol{\mu}_i$	$\mathcal{N}_i$	$\mathcal{N}_i$	$\mathcal{N}_i$	$\mathcal{N}_i$
Kernel	RBF	RBF	RBF	K_{HDKLD}	K_{B}	$\tilde{K}^G$	$\tilde{K}^\alpha$
Parameters	σ, C	σ, C	σ, C	σ, C	σ, C	γ, C	γ, α, C
No. of samples	16,250/8628	16,250/8628	475/52	475/52	475/52	475/52	475/52

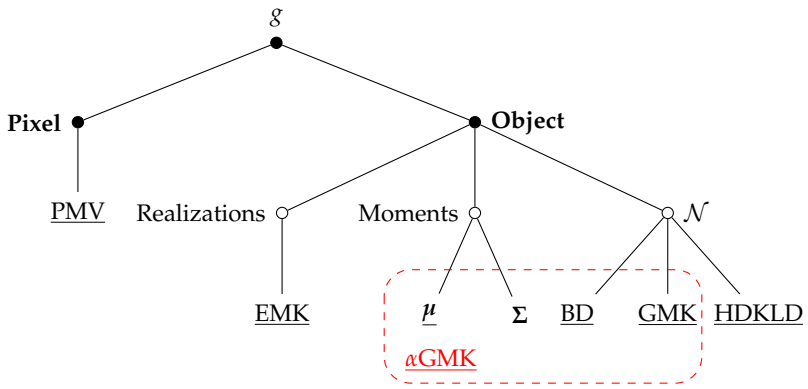

Figure 4.8.: Contribution of the proposed method in grassland analysis for supervised classification. αGMK consists of a general modeling of the grassland at the object level, and it encompasses several known modelings. The underlined methods are tested in this study. PMV, EMK and $\boldsymbol{\mu}$ are not based on Gaussian modeling, while the others are.

4.4.2. Classification Protocol

We compared the efficiency in terms of classification accuracy and processing time of all of the presented methods by classifying the two grassland datasets on inter-annual and intra-annual time series (Section 4.2).

For each method, a Monte Carlo procedure was performed for 100 runs. For each run, the dataset was split randomly into training and testing datasets (75% for training and 25% for testing), preserving the initial proportions of each class. The same grasslands were selected for a given Monte Carlo repetition regardless of the method.

During each repetition, the optimal parameters were tuned by cross-validation based on the best F1 score. Table 4.4 contains the parameters grid search for all of the methods. Note that a wide grid was searched for the parameter α of αGMK to further analyze the distribution of selected values. The penalty parameter C of the SVM process was chosen empirically and fixed to $C = 10$, after running several simulations. The classification accuracy for each repetition was assessed by the F1 score computed from the confusion matrix. The Overall Accuracy (OA) was computed, but it is not presented here, because it does not reflect the accuracy of the classification well since unbalanced datasets were used.

In order to compare each pair of methods, a Wilcoxon rank-sum test was processed on the pair of distributions of the 100 F1 scores. This nonparametric test is designed for two independent samples that are not assumed to be normally distributed [Wilcoxon, 1945]. It tests if the two samples are drawn from populations having the same distribution.

The kernels and the SVM were implemented in Python through the Scikit library [Pedregosa et al., 2011].

Table 4.4.: Parameters tested for each method during cross-validation.

Method	Parameters Values	
	Inter-Annual Analysis	**Intra-Annual Analysis**
PMV	$\sigma \in \{2^0, 2^1, \ldots, 2^{10}\}$	$\sigma \in \{2^{-17}, 2^{-16}, \ldots, 2^{-10}\}$
EMK	$\sigma \in \{2^0, 2^1, \ldots, 2^{10}\}$	$\sigma \in \{2^{-18}, 2^{-17}, \ldots, 2^{-10}\}$
μ	$\sigma \in \{2^0, 2^1, \ldots, 2^{10}\}$	$\sigma \in \{2^{-18}, 2^{-17}, \ldots, 2^{-10}\}$
HDKLD	$\sigma \in \{2^{10}, 2^{11}, \ldots, 2^{20}\}$	$\sigma \in \{2^{15}, 2^{16}, \ldots, 2^{25}\}$
BD	$\sigma \in \{2^0, 2^1, \ldots, 2^{10}\}$	$\sigma \in \{2^{10}, 2^{11}, \ldots, 2^{18}\}$
GMK	$\gamma \in \{2^0, 2^1, \ldots, 2^{10}\}$	$\gamma \in \{2^{-17}, 2^{-18}, \ldots, 2^{-10}\}$
α**GMK**	$\gamma \in \{2^0, 2^1, \ldots, 2^{10}\}$	$\gamma \in \{2^{-18}, 2^{-17}, \ldots, 2^{-13}\}$
	$\alpha \in \{0, 0.1, 0.5, 1, 2, 5, 10, 15, 20, 25, 50\}$	$\alpha \in \{0, 10^{-3}, 10^{-2}, 10^{-1}, 0.3, 0.5, 0.7, 0.9, 1, 2, 5, 10, 15, 20, 25\}$

4.4.3. Results

4.4.3.1. Old and Young Grasslands: Inter-Annual Time Series

Figure 4.9 sums up the old and young grasslands' classification results for each method over the 100 repetitions as a boxplot of F1 scores. The Kappa coefficients can be found in Figure S2 in the Supplementary Materials. Since the cross-validation was not based on the Kappa coefficient, the results are discussed in terms of F1 scores. The method reaching the best scores is αGMK with a F1 average of 0.71 followed by PMV and GMK with an average of 0.69.

Table 4.5 contains the Wilcoxon rank-sum test statistics between each pair of methods. It tests the null hypothesis that the two sets of observations are drawn from the same distribution. The null hypothesis is rejected if the test statistics is greater than 1.96 with a confidence level of 5% (p-value < 0.05). In this case, it accepts the alternative hypothesis that values in one population are more likely to be larger than the values from the other. The two best methods, αGMK and PMV are not significantly different. However, αGMK is significantly better than all of the other methods, whereas PMV is not significantly different than the mean map methods (EMK and GMK). The worst method is HDKLD with a mean F1 of 0.59.

In terms of processing load and time, the pixel-based methods are clearly the most demanding. Indeed, processing the 160,514 pixels was not possible with SVM, so we had to reduce the number of samples. These issues are not faced with object-oriented methods. The fastest methods are μ and HDKLD, but they did not reach acceptable

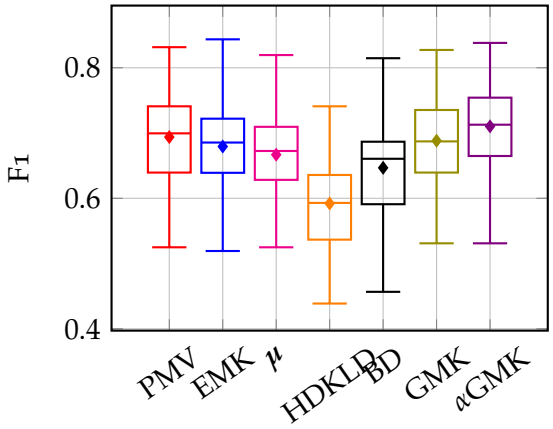

Figure 4.9.: Boxplot of F1 score repartitions for the classification of the old and young grasslands. The line in the box stands for the median, whereas the dot stands for the mean.

Table 4.5.: Absolute value of Wilcoxon rank-sum test statistics on the F1 score for the old and young grasslands' classification. ** indicates that the results are significantly different, i.e., p-value < 0.05.

Method	PMV	μ	HDKLD	BD	EMK	GMK	αGMK
PMV	-	3.52 **	8.66 **	4.83 **	1.93	0.98	1.32
μ		-	7.48 **	1.76	1.55	2.28 **	4.80 **
HDKLD			-	5.68 **	8.26 **	8.65 **	9.77 **
BD				-	3.23 **	3.95 **	6.09 **
EMK					-	0.94	3.35 **
GMK						-	2.42 **
α**GMK**							-

classification accuracies. The best method in terms of ratio accuracy/processing time is αGMK. It is appropriate for processing a large number of grasslands.

4.4.3.2. Management Practices: Intra-Annual Time Series

The classifications accuracies for management practices are shown in Figure 4.10 (F1 score) and in Figure S3 in the Supplementary Materials (Kappa coefficient) for year 2013 and for year 2014.

In terms of classification accuracy, methods based on divergences (BD and HDKLD) provided the worst results. Pixel-based methods, the mean modeling method and mean generative kernel methods provided similar results in terms of F1 score, except for PMV, which was significantly worse than the others for the year 2013. αGMK provided the highest values in 2013 (average F1 of 0.65), but it was not significantly better than the others for this dataset. Indeed, due to the very low number of grasslands composing this dataset, confusion matrices were quite similar whatever the method. It is therefore difficult to compare the methods' efficiency in this configuration.

Nevertheless, this dataset makes possible the comparison in terms of processing times, because the same spectral information was used for all of the methods. Figure 4.11 illustrates the training processing time relative to the one of PMV versus the average F1 score for each method. In terms of computational time, the pixel-based methods required the largest processing times. BD was also very long, mainly because of the shrinkage procedure. Mean modeling was the fastest, followed closely by HDKLD. αGMK and GMK were equivalent in terms of computational times. For this configuration with a low number of grasslands, the mean modeling was the most efficient in terms of accuracy/processing time ratio.

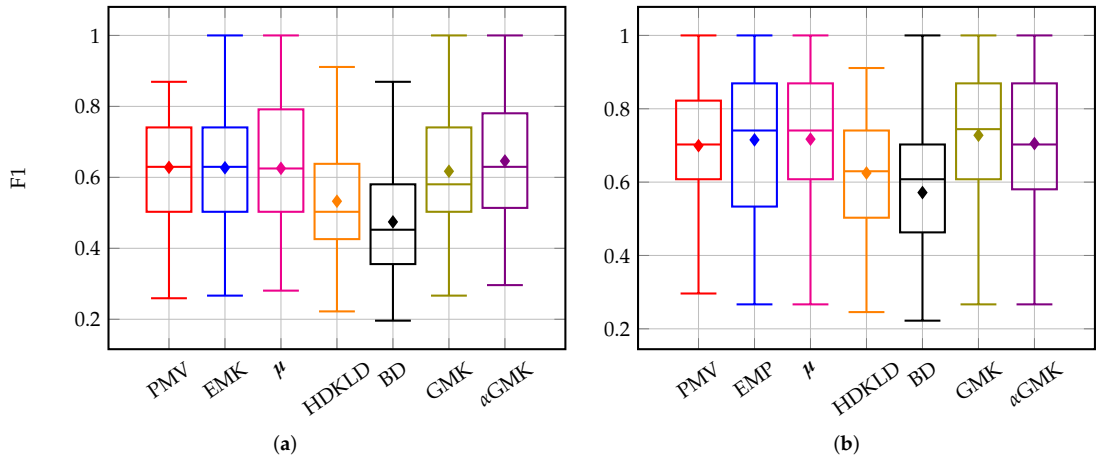

Figure 4.10.: Boxplot of F1 score repartitions for classification of management practices using time series of year (**a**) 2013 and (**b**) 2014. The line in the box stands for the median, whereas the dot stands for the mean.

It is worth noting that the times series of 2014 produced higher classification accuracies (maximum F1 average of 0.73 for GMK) than the time series of 2013 (maximum F1 average of 0.65 for αGMK).

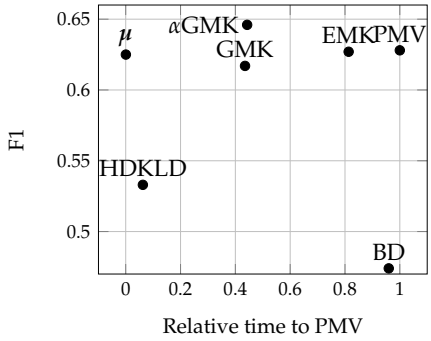

Figure 4.11.: Relative training processing times to PMV and average F1 of each method for intra-annual time series of 2013.

4.4.4. Discussion

The purpose of this work was to develop a model suitable for the classification of grasslands from dense inter- or intra-annual SITS and robust to the dimension of the data. The proposed method based on a weighted use of the covariance, namely αGMK, was compared to several competitive methods.

4.4.4.1. Methods' Efficiency

The methods' efficiency is discussed for the old and young grasslands' classification, since the results provided with the other dataset are not significantly different, mostly because of the small dataset size.

The divergence methods (BD and HDKLD) provided the worst results, showing that they are not robust enough to a high dimensional space.

Although they provided results close to the best results, pixel-based methods (PMV and EMK) are the most demanding in terms of computational time, and they do not scale well with the number of pixels. Indeed, they have to process N pixels instead of G grasslands with $G \ll N$. Therefore, we had to reduce the number of pixels used for the classification. Using them on a large area might be difficult, as the old and young grasslands' dataset showed.

Representing grasslands by the estimated distribution of their set of pixels decreases the complexity during the SVM process. Therefore, the object level methods offer a lower computational load when compared to empirical mean kernels and pixel-based methods.

The mean generative kernel methods performed significantly better than the mean-only method (μ). Among them, αGMK performed better than GMK. It was also one of the most stable methods.

In this context, including the covariance information helps to discriminate grasslands. However, if the dimensionality is not properly handled, it deteriorates the process (e.g., BD and HDKLD). In this case, it is preferable to use the mean values only. αGMK offers the possibility to weight the influence of the covariance information compared to the mean. As a result, it provided better results than the mean modeling and than GMK, since it encompasses both.

It is furthermore interesting to analyze the optimal values of the weighting parameter α found during the cross-validation and the average of associated F1 scores (Figure 4.12). The highest F1 scores were reached for high values of $\hat{\alpha}$. The worst F1 scores were obtained with $\hat{\alpha} < 2$, and the value $\hat{\alpha} = 0$ was never selected. It shows the importance of the covariance information in grasslands' modeling: the heterogeneity in a grassland must be accounted for, and it is not entirely well represented by the mean only.

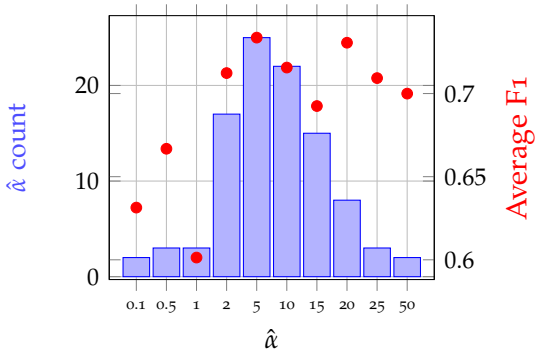

Figure 4.12.: Bar plot of $\hat{\alpha}$ values chosen by cross-validation and the average of associated F1 scores (red dots) for the classification of old and young grasslands using αGMK. Nota Bene : The value $\hat{\alpha} = 0$ was never selected.

4.4.4.2. Grassland Modeling

Following on from the methods' discussion, the choice of modeling grasslands pixels' distribution by a Gaussian distribution makes sense in this context. It is particularly appropriate for semi-natural grasslands, which are very heterogeneous, contrary to crops or annual "artificial" grasslands, which can be assimilated to crops.

However, modeling grasslands by the mean only produced equivalent results to the methods based on Gaussian modeling for the classification of management practices, contrary to the old and young grassland discrimination. Indeed, management practices are supposed to be uniform at the grassland scale. Therefore, the mean appears to be sufficient for this application, contrary to the old and young grasslands' discrimination, which requires capturing more variations between the grasslands. The best

modeling might be different depending on the application. Moreover, some grasslands are so small that the covariance matrix is too badly estimated.

In the proposed kernel, this modeling was made flexible by regularizing the weight given to the covariance matrix. αGMK benefits from its high level of adaptability in front of the object configuration: no choice has to be made between a Gaussian or a mean modeling since the method encompasses both. It also includes several object level methods known in the literature. However, this is at the cost of one more parameter to tune. Therefore, the classification process takes more time than GMK, for instance.

Above all, although it is the first application of generative mean kernels in remote sensing classification, the α-Gaussian mean kernel proved its efficiency and stability in these experiments. The results suggest it is appropriate for grasslands' classification.

4.4.4.3. Acquisition Dates

For the management practice classification, using time series of 2014 produced better results than using 2013. This might be explained by the acquisition dates in the time series. Although 2014 has less images, more clear images were acquired during spring compared to 2013, which has a lack of acquisitions in April and May (Figure 4.3). Indeed, many studies showed that the best season to discriminate grasslands is during the growing season [Psomas et al., 2011, Franke et al., 2012, Hill, 2013, Ali et al., 2016]. Spring is the period of the vegetation cycle where the management practices begin. Therefore, it is easier to differentiate the practices during this period. It might thus affect the accuracy of the classification of the year 2013.

It is not shown in this experiment, but using only one or two years of acquisitions to discriminate old from young grasslands did not produce sufficient classification accuracies. This is the reason why three years of data were used. Old "permanent" grasslands are supposed to have a more stable phenology over the years than the young "temporary" grasslands, which have been recently sown (less than five years) [Austrheim and Olsson, 1999]. The young grasslands phenology is closer to crops in their very first years. We suppose this makes possible their discrimination with inter-annual SITS. However, the optimal number of years needed to discriminate these types of grasslands could constitute a research topic.

In general, the results could also be enhanced by removing some winter images, which can have a negative influence on the entire annual time series [Halabuk et al., 2015]. However, the scope of this study was to develop a method that is able to use a given time series, without having to process a date selection.

4.4.4.4. Grassland Typology

On the whole, the classification did not reach high accuracies (F1 maximum average of 0.73 for management practices and of 0.71 for old and young grasslands' classification). This can be explained by the unbalanced dataset with under-representation of grazing and mixed grasslands in the first application and under-representation of old grasslands in the second one. These classes obtained the lowest producer and user accuracies (cf. Tables S1 and S2 in the Supplementary Materials) because of their limited number of samples for training the models. The methods should be tested on a more balanced dataset of grasslands' classes.

Moreover, as many times emphasized, semi-natural grasslands (which are present in these datasets) are characterized by their high level of heterogeneity. Therefore, there might be a large amount of intra-class variability because of grasslands' diversity. The discrimination might be improved by using more distinct classes: intensively-used grasslands against extensively-used grasslands, artificial (monospecific) grasslands against semi-natural grasslands, for instance.

4.4.4.5. Comparison with Existing Works

To our knowledge, only the work of Möckel et al. [Möckel et al., 2014] relates to the classification of grasslands' age using remote sensing data. They reached a Kappa value of 0.77 in classifying three different grassland age-classes. However, they used airborne hyperspectral data from a single date. Their recommendation was to use multitemporal data to improve the classification or to use satellite hyperspectral data to monitor grasslands over wider areas. Our study was based on using multi-spectro-temporal satellite data, but our proposed method would also work with hyperspectral data.

As described in the Introduction, few studies have been carried out on the analysis of semi-natural grasslands using high spatio-spectro-temporal resolution SITS. Usually, methods were pixel-based, and they were applied on a few images or on a precise date selection to avoid dealing with the high dimension of data [Price et al., 2002, Toivonen and Luoto, 2003, Franke et al., 2012]. Schuster et al. [Schuster et al., 2015] successfully classified grassland habitat using 21 RapidEye images on a pixel basis, but there was no mention of the processing times.

At the object level using a time series, grasslands were often represented by their mean NDVI, such as in [Esch et al., 2014], who noticed the difficulty to discriminate grasslands from crops because of mean seasonal NDVI similarities. The closest configuration might be the work of Zillman et al. [Zillmann et al., 2014], who used an object-based analysis and spectral reflectances combined with seasonal statistics of vegetation indices for mapping grasslands across Europe. The seasonal statistics

were particularly relevant in the classification, because they captured well the spectral diversity of the grassland phenology. The use of these metrics could be considered for discriminating grassland management practices, which impact on the phenology. The authors also concluded that the object-based analysis improves the classification compared to a pixel-based classification. However, the objects were determined by segmentation.

4.4.5. Prediction of Management Practices on the Land Use Database Grasslands

To show the efficiency of αGMK, we classified all of the grasslands from the French agricultural land use database (Registre Parcellaire Graphique) covered by the Formosat-2 time series to predict their management practice in 2014. All of the plots declared as grasslands in 2014, i.e., "permanent grassland" and "temporary grassland" regardless of their age, were selected. After applying a negative buffer of 8 m and rasterizing the polygons, we removed the plots representing less than 10 Formosat-2 pixels. In the end, there were 797 grassland plots covered by the extent of Formosat-2 for a total of 252,472 pixels.

The multispectral SITS of 2014 was used. The SVM was trained on the whole field data (Section 4.2.3.2) using the same grid search as in the experiments. The parameters chosen after cross-validation based on F1 score were $\hat{\alpha} = 5$ and $\hat{\gamma} = 2^{-15}$. Then, the model was used to predict the management practices of the 797 grasslands of the land use database.

The classification accuracy could not be assessed since the true labels of the grasslands are not known. However, as described in the study site, a spatial distribution of the classes could be expected. Indeed, grazed and mixed grasslands should be found in the southwest of the site, whereas more mown grasslands should be in the north.

An extract of the classification result is shown in Figure 4.13. It represents the classified grasslands in their raster format. As expected, most of the grazed and mixed grasslands are located in the southwest of the image, whereas the north of the image is mostly composed of mown grasslands. Therefore, αGMK was very likely able to classify with an acceptable accuracy the grasslands management practices without any a priori geographic information. However, specific care should be considered, as not all of the possible management practices were predicted. For instance, grasslands mown twice or unused grasslands were not in the training dataset, but it does not mean these managements do not exist in the rest of the data. The method deserves to be tested with an exhaustive grassland typology to produce more detailed grasslands maps.

In terms of processing times, the proposed method is able to classify 800 grasslands, representing more than 250,000 pixels, at the object level from a high spatial resolution

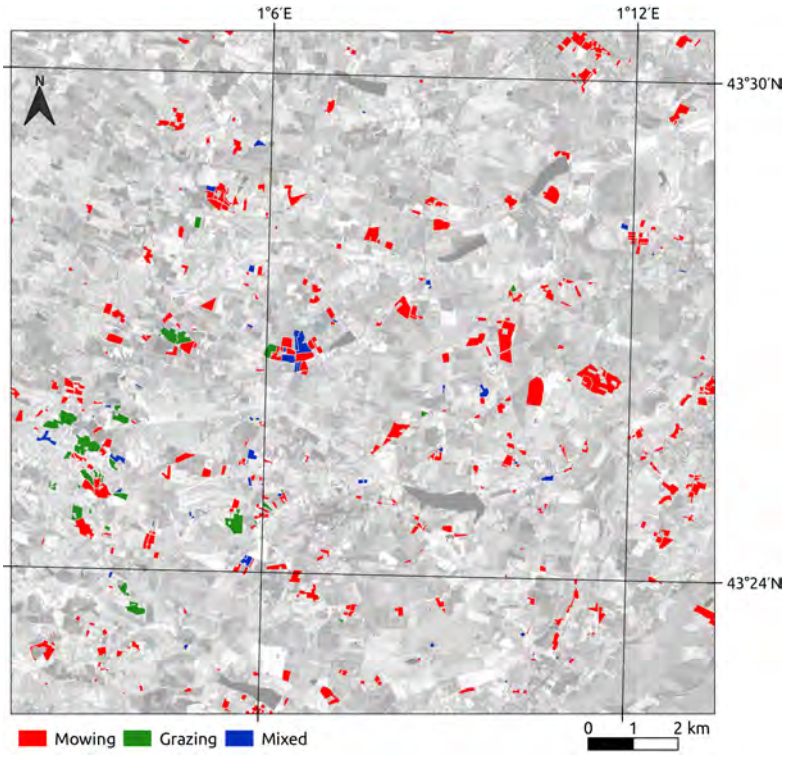

Figure 4.13.: Extract of the management practices classification of the grasslands from the French agricultural land use database (Registre Parcellaire Graphique) in 2014. The background is a May, 2014 Formosat-2 image in the NIR channel.

SITS within a few seconds on a conventional personal computer.

4.5. Conclusions

This study aimed at developing a model for the classification of grasslands using satellite image time series with a high number of spectro-temporal variables. A grassland modeling at the object level was proposed. To deal with grasslands' heterogeneity, their pixels distribution was modeled by a Gaussian distribution. Then, to measure the similarity between two grasslands, i.e., two Gaussian distributions, a kernel function based on mean maps was introduced, namely the α-Gaussian mean kernel. The proposed method was compared to existing pixel-based and object-based classification methods for the supervised classification of grassland using inter- and intra-annual SITS. The Gaussian mean kernels provided the highest classification accuracies, showing that the covariance information must be accounted for. In terms of processing

times, the object-based methods were much faster than pixel-based methods.

Several contributions have been made in this work. The first lies in the grasslands' pixel distribution modeling at the object level. A flexible kernel was proposed to encompass both the Gaussian and mean modeling of grasslands, so no choice has to be made between these two modelings. It can therefore be used on homogeneous objects such as artificial grasslands or on very small objects, as well as on heterogeneous semi-natural grasslands. The second contribution is that this kernel is suitable for high dimensional data in a small ground sample size context. It enables the use of all of the multispectral data instead of a single vegetation index or the use of a long time series. Furthermore, it can be used on a whole time series without date selection. Indeed, this new kernel offers very low computational load. It can therefore be applied on a large dataset. With this kernel, we were able to process and to classify more than 250,000 pixels on a conventional personal computer within a few seconds. Even if it is the first application of generative mean kernels in remote sensing classification, the αGMK proved its efficiency and stability in these experiments. It is a good compromise between processing speed and accuracy for the classification of grasslands.

The αGMK deserves to be tested on a larger dataset with more balanced classes. Seasonal statistics could be used to improve the representation of grassland phenology. These ideas will be considered in the future. This method was designed to deal with the dense SITS, which will be provided by Sentinel-2 and to efficiently produce maps from this type of data. Other applications of the method are still possible (e.g., small and heterogeneous objects, such as peatlands, urban areas, etc.).

Supplementary Materials

The supplementary materials can be found in Appendix C.

Appendix

Proof of Equation (4.8). First, let us write the Gaussian distribution p_i to the power of α^{-1}:

$$\begin{aligned}
p_i(\mathbf{x}|\boldsymbol{\mu}_i, \boldsymbol{\Sigma}_i)^{\alpha^{-1}} &= \frac{1}{(2\pi)^{d/2\alpha}} \times \frac{1}{|\boldsymbol{\Sigma}_i|^{1/2\alpha}} \times \exp\left\{-0.5(\mathbf{x}-\boldsymbol{\mu}_i)^\top (\alpha\boldsymbol{\Sigma}_i)^{-1} (\mathbf{x}-\boldsymbol{\mu}_i)\right\} \\
&= \frac{(2\pi)^{\frac{d}{2}(1-\frac{1}{\alpha})}}{(2\pi)^{d/2}} \times \alpha^{1/2} \times \frac{|\boldsymbol{\Sigma}_i|^{\frac{1}{2}(1-\frac{1}{\alpha})}}{|\alpha\boldsymbol{\Sigma}_i|^{1/2}} \times \exp\left\{-0.5(\mathbf{x}-\boldsymbol{\mu}_i)^\top (\alpha\boldsymbol{\Sigma}_i)^{-1} (\mathbf{x}-\boldsymbol{\mu}_i)\right\} \\
&= \alpha^{1/2}(2\pi)^{\frac{d}{2}(1-\frac{1}{\alpha})} |\boldsymbol{\Sigma}_i|^{\frac{1}{2}(1-\frac{1}{\alpha})} \times p(\mathbf{x}|\boldsymbol{\mu}_i, \alpha\boldsymbol{\Sigma}_i) \\
&= C(\boldsymbol{\Sigma}_i, \alpha) p(\mathbf{x}|\boldsymbol{\mu}_i, \alpha\boldsymbol{\Sigma}_i). \qquad (4.9)
\end{aligned}$$

Then, plugging Equation (4.9) in Equation (4.7), we get:

$$K^{\alpha}(\mathcal{N}_i, \mathcal{N}_j) = C(\boldsymbol{\Sigma}_i, \alpha) C(\boldsymbol{\Sigma}_j, \alpha) \frac{\exp\left\{-0.5(\hat{\boldsymbol{\mu}}_i - \hat{\boldsymbol{\mu}}_j)^T \left(\alpha\hat{\boldsymbol{\Sigma}}_i + \alpha\hat{\boldsymbol{\Sigma}}_j + \gamma^{-1}\mathbf{I}_d\right)^{-1} (\hat{\boldsymbol{\mu}}_i - \hat{\boldsymbol{\mu}}_j)\right\}}{|\alpha\hat{\boldsymbol{\Sigma}}_i + \alpha\hat{\boldsymbol{\Sigma}}_j + \gamma^{-1}\mathbf{I}_d|^{0.5}},$$

which is Equation (4.5) with the covariance matrix of the Gaussian distribution scaled with α. The constants $C(\boldsymbol{\Sigma}_i, \alpha)$ and $C(\boldsymbol{\Sigma}_j, \alpha)$ are removed when normalizing the kernel, and we get Equation (4.8). □

Acknowledgements

This work was partially supported by a French National Institute for Agricultural Research (INRA) and French National Institute for Research in Computer Science and Automation (INRIA) Young Scientist Contract (CJS INRA-INRIA) and by the grant Défi Mastodons-CNRS. The authors would like to thank CNES and CESBIO for providing the pre-processed Formosat-2 data. Special thanks to Marc Lang for playing a major role in the field work, to Donatien Dallery for designing the processing chain to compute the grasslands age from the RPG and to Romain Carrié for his careful reviewing of the Introduction. We would like to thank the anonymous reviewers for their constructive comments.

Conclusion of Part II

This part developed methods for the supervised analysis of grasslands using dense satellite image time series. In the first chapter, we proposed a smoothing algorithm to reconstruct and smooth the time series due to noise caused by clouds and their shadows. The Whittaker smoother was chosen because it combines fidelity to the data and low roughness and it is fast to execute.

Then, we emphasized the need to account for the heterogeneity of the grassland while working at the grassland level. We proposed to model the grassland's pixels distribution by a Gaussian distribution. Two similarity measures based on a Gaussian modeling that can be plugged in the kernel of SVM for the supervised classification of grasslands were introduced: the High Dimensional Kullback-Leibler Divergence and the α-Gaussian Mean Kernel that encompasses several similarity measures. These measures are robust to high dimensional data and they are fast to compute. They have been applied using intra- and inter-annual NDVI or multispectral time series to classify the grasslands according to their management practices (mowing, grazing, mixed) and to their age (less than five years or more than 14 years).

The next part will focus on thematic applications of the methods to define continuous ecological indicators of grasslands from remote sensing data.

Part III.

Definition of ecological indicators of grasslands from satellite image time series

Introduction of Part III

In the previous part, methodological developments were conducted for the supervised classification at the grassland level using satellite image time series with high spatial and temporal resolutions. These methods were applied to classify grasslands' management practices and age, which provide information on the type of grasslands in a discrete way.

Plant species diversity is influenced by grassland's management practices and age, but this diversity is usually quantified with continuous measures. Hence, continuous indicators of grasslands' biodiversity issued from satellite data should be defined to monitor the biodiversity over large extents.

In this part, the methodological developments are applied to the thematic needs for ecological indicators of grasslands. In Chapter 5, we assess the potential of SITS with a high spatial and a high temporal resolutions to predict two biodiversity indices in grasslands through a kernel least-mean square regression. Chapter 6 is based on the Spectral Variation Hypothesis that assumes that the spectral heterogeneity measured in a habitat can be used as a proxy for its species diversity. We made the hypothesis that the species differ in their phenology and hence, that the temporal variations could be used in addition to the spectral variation. We propose several spectro-temporal heterogeneity measures based on the unsupervised clustering of grasslands from dense SITS with a high spatial resolution. Then, we assess the relationship between these measures and the species diversity in grasslands represented by the Shannon index.

5. Potential of Sentinel-2 and SPOT5 (Take5) time series for the estimation of grasslands biodiversity indices

Potential of Sentinel-2 and SPOT5 (Take5) time series for the estimation of grasslands biodiversity indices

Published in *2017 9th International Workshop on the Analysis of Multitemporal Remote Sensing Images (MultiTemp)*, Brugge, Belgium, 2017, pp. 1-4; doi: 10.1109/Multi-Temp.2017.8035206.

Mailys Lopes[(1)], Mathieu Fauvel[(1)], Annie Ouin[(1)] and Stéphane Girard[(2)]

[(1)]DYNAFOR, University of Toulouse, INRA, INPT, France
[(2)]Team MISTIS, University of Grenoble, INRIA, LJK, France

Abstract

The aim of this study is to assess the potential of satellite image time series with high spatial and high temporal resolutions for the prediction of grasslands plant biodiversity. The grasslands are modeled at the object scale to be consistent with ecological measurements (one biodiversity index per grassland). A kernel regression is used to predict the biodiversity index of a grassland from its spectro-temporal reflectance. The method is applied using two intra-annual multispectral or NDVI time series of SPOT5 Take5 (18 dates) and Sentinel-2 (7 dates) to predict the Shannon and the Simpson indices of about 200 grasslands in south-west France. The best coefficient of determination for the prediction of the Shannon index is 0.13 and it is 0.17 for the Simpson index prediction. The unsatisfactory results suggest that a high temporal resolution combined with a high spatial resolution and multispectral bands are not sufficient to estimate grassland biodiversity at the grassland scale.

Keywords: Kernel regression, high resolution time series, SPOT5 (Take5), Sentinel-2, biodiversity, grasslands.

5.1. Introduction

Grasslands are one of the most largest land covers on Earth. They represent a significant source of biodiversity in farmed landscapes, because of their plant and animal composition [Eriksson et al., 1995, Critchley et al., 2004]. Thanks to this diversity, they provide many ecosystem services such as carbon and erosion regulation, pest control, crop pollination [O'Mara, 2012]. However, global grassland surface area is decreasing and grassland diversity is declining because of agriculture intensification and urbanization [O'Mara, 2012]. To understand these effects, it is of utmost matter to determine and monitor grassland diversity and composition at a large extent.

In ecology, grasslands are usually monitored through ground surveys. But they are limited in time and space, since they are time-consuming and require important

human and materials resources [Rocchini et al., 2010]. Remote sensing is a tool which has already proven its ability for habitat mapping [Kerr and Ostrovsky, 2003, Pettorelli et al., 2014]. However, the study of grasslands in fragmented landscapes, such as found in Europe, has been limited because of sensors resolutions. Indeed, grasslands are rather small elements in the landscape which require a high spatial resolution to be detectable [Corbane et al., 2015]. Moreover, for biodiversity related applications, very high spatial resolution (less than 1 meter) is more relevant to discriminate the species communities [Turner et al., 2003, Corbane et al., 2015, Rocchini et al., 2016].

For biodiversity application, most of the remote sensing research is based on the Spectral Variation Hypothesis [Palmer et al., 2002, Oldeland et al., 2010, Rocchini et al., 2016]. It supposes that the spatio-spectral variability in the image is related to the spatial heterogeneity in the environment, and therefore it can be used as a proxy for species diversity. Hence, the study of grasslands biodiversity is usually performed with hyperspectral data issued from a field spectroradiometer or an airborne sensor (around 1-m spatial resolution) [Schmidtlein and Sassin, 2004, Oldeland et al., 2010, Feilhauer et al., 2011, Möckel et al., 2014]. Although these works showed good results, they were limited to a very local scale, because of the costs involved by such a mission. When this type of data is not accessible and when a larger extent is required, a tradeoff can be considered by using time series with high temporal resolution. Indeed, species communities differ in their temporal behavior, *i.e.*, their phenology. In addition, new satellite missions for continuous vegetation monitoring, such as Sentinel-2, provide freely multispectral time series with high spatial and high temporal resolutions.

In this context, this study aims at evaluating the potential of multispectral satellite image time series (SITS) to determine grassland plant biodiversity at the grassland scale. Two intra-annual SITS with high spatial and high temporal resolutions are compared.

In this experiment, grasslands are modeled at the object scale to be consistent with ecological studies which usually characterize grasslands at the parcel scale. A non-parametric regression method to predict grasslands biodiversity index is used. The method is experimented to predict the Shannon index and the Simpson index of grasslands in south-west France using a SPOT5 (Take5) and a Sentinel-2 time series. Results are analyzed in terms of prediction accuracy and stability.

5.2. Data

5.2.1. Study site

The study site is part of a Long-Term Ecological Research site located in Gascony ("Coteaux et Vallées de Gascogne", LTER_EU_FR_003), in south-west France near the city of Toulouse (43°17′N, 0°54′E). This hilly area of around 900km² is characterized

by a mosaic of crops, small woods and grasslands. It is dominated by mixed crop-livestock farming. Grasslands provide food for cattle by grazing and/or producing hay or silage. They are mainly located on steep slopes whereas annual crops are in the valleys on the most productive lands. The climate is sub-Atlantic with sub-Mediterranean and mountain influences (mean annual temperature, 12.5°C; mean annual precipitation, 750 mm) [Carrié et al., 2017].

5.2.2. Dataset

The dataset is composed of more than 200 grasslands. A botanical survey was conducted in the Springs 2015 (on 171 grasslands) and 2016 (on 45 grasslands), after the flowering and before the mowing (April-May), to record the botanical composition of all these grasslands. From this floristic record, several biodiversity indices can be computed. They represent the biodiversity in the grassland at the grassland scale, and not at the plot scale. The Shannon index (H) and the Simpson index (D) were chosen because of their wide-spread utilization in ecology: $H = -\sum_{i=1}^{R} p_i \ln p_i$ and $D = \sum_{i=1}^{R} p_i^2$ where p_i is the proportion of the i^{th} species and R is the total number of species in the grassland (species richness). H values are usually between 0 and 4, and D always ranges between 0 and 1. H increases and D decreases as the diversity increases. The statistics of the dataset for each variable are presented in Table 5.1. Three examples of grasslands temporal profiles along the H and D axis, from very poor to very rich in biodiversity, are shown in Fig. 5.1.

The grasslands were digitalized in a GIS from aerial photographs (BD Ortho database, IGN). For this study, a negative buffer of 10m was applied to all the grassland polygons to avoid edge effects due to mixed pixels at the edges. Only the grasslands composed of at least 10 pixels of 10-m resolution, *i.e.* having an area higher than 1000m², were kept, to ensure a minimum number of pixels in a grassland. In the end, there were 192 grasslands.

Table 5.1.: Summary of biodiversity indices of the dataset. H = Shannon index, D = Simpson index, G = number of grasslands, SD = standard deviation, CV = coefficient of variation.

Variable	G	Min	Max	Mean	SD	CV
H	192	0.096	3.512	2.274	0.491	0.216
D	192	0.049	0.973	0.168	0.126	0.752

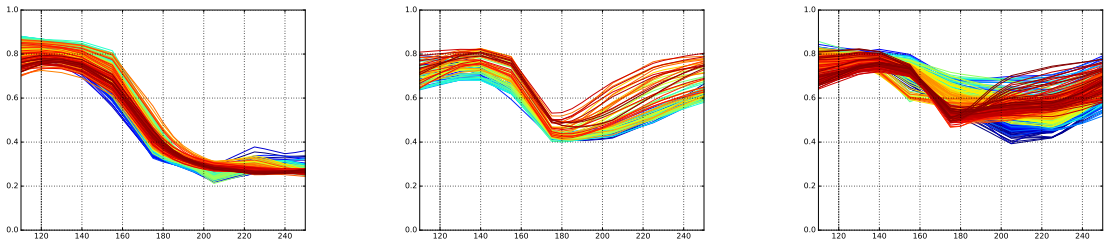

(a) H = 0.10, D = 0.97 (b) H = 1.66, D = 0.29 (c) H = 2.89, D = 0.09

Figure 5.1.: NDVI temporal profiles from SPOT5 time series of all the pixels belonging to three grasslands along the H and D gradients: (a) grassland poor in biodiversity, (b) grassland quite rich and (c) grassland very rich. The x-axis corresponds to the day of year of 2015 and the y-axis corresponds to the NDVI. Grasslands have been voluntarily chosen on their high number of pixels for better visualization.

5.2.3. Satellite images

The SPOT5 (Take5) time series was used in this experiment (www.spot-take5.org). 18 images were available over the present study site from April to September 2015 (Fig. 5.2). SPOT5 has a spatial resolution of 10 meters in four spectral channels (visible to near infrared (NIR)).

The Sentinel-2 [Drusch et al., 2012] time series acquired over the year of 2016 was also used for comparison in this experiment. We used the available images from April to September 2016 (Fig. 5.3). The four 10-m spectral bands were used as well as the four 20-m spectral bands corresponding to the red edge and NIR bands. The 20-m bands were resampled at 10 meters with a bilinear resampling algorithm, using the *gdalwarp* function of GDAL (http://www.gdal.org/gdalwarp.html). It resulted in a time series of seven dates with eight spectral bands. Therefore, this time series is characterized by less dates than SPOT5 series but with a higher number of spectral bands.

Figure 5.2.: Dates of SPOT5 (Take5) images used in this study (2015).

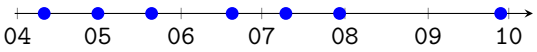

Figure 5.3.: Dates of Sentinel-2 images used in this study (2016).

5.3. Methodology

5.3.1. Grassland modeling

In this work, each grassland g_i is composed of a given number n_i of pixels represented by a spectro-temporal vector $\mathbf{x}_{ik} \in \mathbb{R}^d$, where k is the pixel index such as $k \in \{1, ..., n_i\}$, $i \in \{1, \ldots, G\}$, G is the total number of grasslands, $d = n_B n_T$ is the number of spectro-temporal variables, n_B is the number of spectral bands and n_T is the number of temporal acquisitions (here, $n_B = 4$ and $n_T = 18$ for SPOT5, $n_B = 8$ and $n_T = 7$ for Sentinel-2, but $n_B = 1$ if using a single vegetation index). Two grassland representations are proposed, at the pixel and at the object scales.

At the pixel scale, with each grassland g_i are associated a matrix $\mathbf{X}_i = [\mathbf{x}_{i1}, \ldots, \mathbf{x}_{in_i}]^\top$ of size $(n_i \times d)$ and a response variable $y_i \in \mathbb{R}$ (its biodiversity index).

At the object scale, the mean spectro-temporal vector $\boldsymbol{\mu}_i$ of the pixels belonging to g_i is used to represent g_i. It is estimated empirically by $\hat{\boldsymbol{\mu}}_i = \frac{1}{n_i} \sum_{k=1}^{n_i} \mathbf{x}_{ik}$. In this case, a vector $\hat{\boldsymbol{\mu}}_i \in \mathbb{R}^d$ and a response variable $y_i \in \mathbb{R}$ are associated with each grassland.

5.3.2. Kernel least mean square regression

In order to predict the response variable (H or D) for each grassland represented by its reflectance, a kernel least mean square (KLMS) regression was used. The KLMS regression [Liu et al., 2008] consists in solving:

$$\min_f \sum_{i=1}^{G} \Big(y_i - f(g_i) \Big)^2 + \theta \|f\|^2 \tag{5.1}$$

with y_i is the response variable associated with grassland g_i, f is the regression function such as $f(g_i) = \hat{y}_i$, $\hat{y}_i$ is the predicted variable of g_i, $f(g_i) = \sum_{j=1}^{G} \beta_j K(g_i, g_j) + b$, K is the kernel function, β_j's are the parameters of f, b is the intercept and θ is the regularization hyperparameter.

The solution to this problem is given by:

$$\hat{\boldsymbol{\beta}} = (\mathbf{K} + \theta \mathbf{I})^{-1} \mathbf{y}, \; \hat{b} = \bar{y} \tag{5.2}$$

where $\boldsymbol{\beta}$ is the vector of linear coefficients β_j, $\mathbf{K}$ is the kernel matrix issued from the kernel function K applied between each pair of grasslands g_i, $\mathbf{I}$ is the identity matrix,

$\mathbf{y}$ is the response vector made of y_i and $\bar{y}$ is the mean value of y_i.

In this experiment, two kernels were tested. For the representation at the object scale, the conventional RBF kernel was used between two grasslands g_i and g_j modeled by their mean vectors $\boldsymbol{\mu}_i$ and $\boldsymbol{\mu}_j$:

$$K_{\text{RBF}}(g_i, g_j) = \exp(-\sigma \|\boldsymbol{\mu}_i - \boldsymbol{\mu}_j\|^2) \tag{5.3}$$

with $\sigma > 0$. This method is denoted by "μ-KLMS" in the following.

The second kernel tested is the empirical mean kernel between two distributions p_i and p_j [Gomez-Chova et al., 2010] for the grassland representation at the pixel scale. It corresponds to the average of all pairwise RBF kernel evaluations over the realizations of the two distributions (*i.e.*, pixels that belong to grasslands g_i or g_j):

$$K_{\text{EMK}}(g_i, g_j) = \frac{1}{n_i n_j} \sum_{k,l=1}^{n_i,n_j} K_{\text{RBF}}(\mathbf{x}_{ik}, \mathbf{x}_{jl}), \tag{5.4}$$

where n_i and n_j are the number of pixels associated with g_i and g_j respectively and $\mathbf{x}_{ik}$ is the k^{th} realization (pixel) of g_i. This method is denoted by "EMK-KLMS" in the following.

In these two cases, two hyperparameters must be tuned during the regression process: the kernel parameter σ and the regression regularization parameter θ.

5.3.3. Regression protocol

The regression was investigated for two reflectance configurations: the Normalized Difference Vegetation Index (NDVI) and the four (SPOT5) or eight (Sentinel-2) concatenated multispectral bands (MS).

For each configuration, the regression process was repeated 10 times through a Monte Carlo procedure. For each repetition, the dataset was split randomly into two subsets: 80% for training and 20% for testing. The optimal hyperparameters (σ and θ) were tuned during a 5-fold cross-validation based on the highest coefficient of determination (r^2) to minimize the prediction error: $r^2 = 1 - \dfrac{\sum_i (y_i - \hat{y}_i)^2}{\sum_i (y_i - \bar{y})^2}$.

The efficiency of each configuration (*i.e.*, kernel, spectral information and sensor) to predict the responses variables was compared in terms of regression accuracy, stability and processing time.

The kernels and the regression were implemented in Python through the Scikit library (http://scikit-learn.org).

5.4. Experimental results

Table 5.2.: Mean (standard deviation) r^2 for H prediction over the 10 repetitions.

Method	μ-KLMS		EMK-KLMS	
Data	train	test	train	test
SITS	SPOT5			
NDVI	0.10 (0.06)	0.08 (0.08)	0.12 (0.06)	0.10 (0.09)
MS	0.11 (0.08)	0.12 (0.10)	0.12 (0.09)	**0.13** (0.13)
SITS	Sentinel-2			
NDVI	0.06 (0.06)	0.07 (0.05)	0.04 (0.06)	0.04 (0.07)
MS	-0.02 (0.03)	0.01 (0.05)	-0.01 (0.03)	0.04 (0.06)

Table 5.3.: Mean (standard deviation) r^2 for D prediction over the 10 repetitions.

Method	μ-KLMS		EMK-KLMS	
Data	train	test	train	test
SITS	SPOT5			
NDVI	0.11 (0.09)	0.13 (0.08)	0.13 (0.09)	0.12 (0.11)
MS	0.14 (0.11)	**0.17** (0.13)	0.15 (0.10)	0.14 (0.14)
SITS	Sentinel-2			
NDVI	0.05 (0.06)	0.15 (0.10)	0.04 (0.07)	0.14 (0.12)
MS	-0.05 (0.04)	0.01 (0.04)	-0.01 (0.05)	0.05 (0.06)

The mean coefficient of determination and its standard deviation over the 10 repetitions during training and testing phases of the regression model for each method to predict the Shannon index and the Simpson index, respectively, are synthesized in Tables 5.2 and 5.3.

With SPOT5, results were improved when using the MS data (four bands) instead of the NDVI, regardless of the method. It increased the $\bar{r}^2$ of about up to 0.04. For H prediction, the EMK-KLMS method was better than μ-KLMS in all configurations. The best results were obtained with the EMK-KLMS method with MS data ($\bar{r}^2 = 0.13$). For D prediction, μ-KLMS was always better than EMK-KLMS. The best result was achieved with μ-KLMS on MS data ($\bar{r}^2 = 0.17$).

With Sentinel-2, the results were worse than with SPOT5 for H prediction (best score is $\bar{r}^2 = 0.07$, μ-KLMS with NDVI). However, the regression was better for D

prediction using Sentinel-2 NDVI (best $\bar{r}^2 = 0.15$, μ-KLMS) than SPOT5 NDVI ($\bar{r}^2 = 0.13$). Sentinel-2 showed opposite results to SPOT5: results are worse using MS data than using NDVI, regardless of the method and the variable. It seems that accuracies are decreased when using the 20-m bands. Indeed, results were better when using only the four Sentinel-2 10-m bands with μ-KLMS. It could explain why the MS data did not perform better than NDVI.

No conclusion can be drawn about the performance of the μ-KLMS method against EMK-KLMS. However, EMK-KLMS did not provide the most stable results (high standard deviation compared to mean value). It is also more time consuming than the mean modeling.

Globally, the Simpson index D was more accurately predicted than the Shannon index H. Nevertheless, the prediction results for both indices are not satisfying.

5.5. Discussion and Conclusion

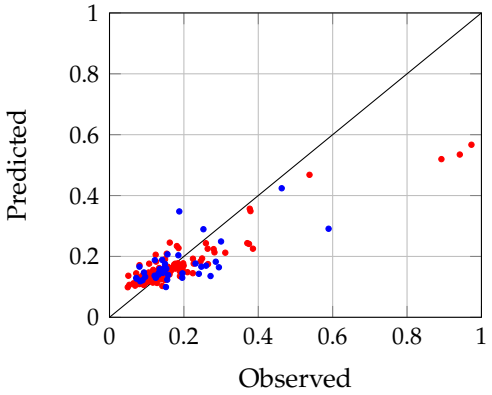

Figure 5.4.: Observed vs. predicted D for the best run ($r^2_{\text{test}} = 0.43$), μ-KLMS using SPOT5 MS data. Red dots corresponds to elements of the training phase. Blue dots corresponds to predicted elements of the testing phase.

A scatter plot of observed vs. predicted D value for the best run of the μ-KLMS method using SPOT5 MS data is plotted in Fig. 5.4. There is a lack of variance in the predicted dataset, either for H or D. The model predicts always the same range of values. Extreme, and especially higher D values/lower H values (they correspond to grasslands very poor in biodiversity, almost monospecific) are less represented in the dataset (only three grasslands with D > 0.8), and are less represented in the training dataset. Thus, they are badly learned during the training phase, compared to richer grasslands. The regression quality could be improved if having more grasslands with

high D values (low H values), making the dataset more balanced along the biodiversity indices gradients.

There might also be more variability inter-grasslands than along the H or D gradients. Grasslands can be managed differently (one or two mowings, grazing, mowing and grazing, or no utilization) with a different use intensity. These disturbances might have a higher impact on the signal than the species composition. This was confirmed by Feilhauer *et al.* [Feilhauer et al., 2013] who assessed the floristic composition with simulated Sentinel-2 data from field hyperspectral data. They showed that multiseasonal data decreased the model fit compared to monotemporal data. Therefore, it would be of interest to separate grasslands depending on their management.

Accuracies of prediction were much lower than those found using hyperspectral imagery at the plot scale (r^2 of 0.4 and 0.45 for inverse Simpson's diversity in [Möckel et al., 2016], and up to 0.62 for Shannon index in [Oldeland et al., 2010] with spectral variability measure). However, these studies were conducted at the plot scale for the floristic record and the associated spectral information. They used the pixels corresponding only to the sampling unit. Our protocol was different, since the botanical survey was conducted at the grassland scale by a random walk strategy and only one biodiversity index was computed from it. In this case, there is no direct correspondence between a given pixel and the floristic record. Indeed, even if one grassland is a homogeneous unit from an agronomic viewpoint (one field, same practices), because of topography, soil depth, presence of a stream, it can present very different ecological sub-units with different plant compositions.

Despite the unsatisfactory results, the Simpson index (D) was always better predicted than the Shannon index (H). D is a measure of the dominance in a community, while H is more sensible to rare species [Magurran, 1988]. Thus, one can suppose that dominance in a plant community is more predictable by satellite remote sensing than the presence of rare species, and dominance-based indices should be favored.

The lack of a balanced dataset along the biodiversity gradients does not allow a formal conclusion on the actual potential of multispectral SITS with a high temporal and a high spatial resolutions to predict the biodiversity indices of grasslands. However, current results suggest that this type of data is not suitable to predict such indices measured at the scale of the grassland. Indeed, the species composition of grasslands does typically fall in the hyperspectral domain. As future prospects, the use of spectral heterogeneity [Rocchini et al., 2010] as a proxy for species diversity should be considered [Oldeland et al., 2010]. It could be adapted to temporal data.

6. Spectro-Temporal Heterogeneity Measures from Dense High Spatial Resolution Satellite Image Time Series: Application to Grassland Species Diversity Estimation

Spectro-Temporal Heterogeneity Measures from Dense High Spatial Resolution Satellite Image Time Series: Application to Grassland Species Diversity Estimation

Published in *Remote Sensing* 2017, 9(10), 993; doi:10.3390/rs9100993.

Mailys Lopes[1], Mathieu Fauvel[1], Annie Ouin[1] and Stéphane Girard[2]

[1] Dynafor, University of Toulouse, INRA, INPT, INPT-EI PURPAN, Chemin de Borde-Rouge, 31326 Castanet Tolosan, France

[2] Team Mistis, Inria Grenoble Rhône-Alpes, LJK, 655 Avenue de l'Europe, 38334 Montbonnot, France

Abstract

Grasslands represent a significant source of biodiversity that is important to monitor over large extents. The Spectral Variation Hypothesis (SVH) assumes that the Spectral Heterogeneity (SH) measured from remote sensing data can be used as a proxy for species diversity. Here, we argue the hypothesis that the grassland's species differ in their phenology and, hence, that the temporal variations can be used in addition to the spectral variations. The purpose of this study is to attempt verifying the SVH in grasslands using the temporal information provided by dense Satellite Image Time Series (SITS) with a high spatial resolution. Our method to assess the spectro-temporal heterogeneity is based on a clustering of grasslands using a robust technique for high dimensional data. We propose new SH measures derived from this clustering and computed at the grassland level. We compare them to the Mean Distance to Centroid (MDC). The method is experimented on 192 grasslands from southwest France using an intra-annual multispectral SPOT5 SITS comprising 18 images and using single images from this SITS. The combination of two of the proposed SH measures—the within-class variability and the entropy—in a multivariate linear model explained the variance of the grasslands' Shannon index more than the MDC. However, there were no significant differences between the predicted values issued from the best models using multitemporal and monotemporal imagery. We conclude that multitemporal data at a spatial resolution of 10 m do not contribute to estimating the species diversity. The temporal variations may be more related to the effect of management practices.

Keywords: Spectral Variation Hypothesis; Spectral heterogeneity; Dense satellite image time series; Alpha-diversity; Grasslands.

6.1. Introduction

Grasslands represent one of the largest land covers on Earth. They are an important source of biodiversity in farmed landscapes, thanks to their plant and animal composition [Eriksson et al., 1995, Critchley et al., 2004]. This biodiversity supports many ecosystem services such as carbon regulation, erosion regulation, food production, biological control of pests and crop pollination [O'Mara, 2012, Werling et al., 2014]. However, global grassland surface area is decreasing, and grassland diversity is declining because of agriculture intensification, abandonment and urbanization [O'Mara, 2012], leading to a loss of biodiversity and associated services. To understand these effects, it is of utmost importance to determine and monitor grassland species diversity and composition over large extents.

Biodiversity can be characterized by alpha-diversity [Magurran, 1988], which is related to the diversity in species of a community. Alpha-diversity is commonly measured by the species richness (number of species in the sampling area). However, this diversity can also be quantified with heterogeneity measures, such as the Shannon index [Shannon, 1948], which combines richness and evenness (even abundance between species), and the Simpson index [Simpson, 1949], which measures the dominance of species over the others.

Usually, ecologists measure and monitor biodiversity during field surveys. However, these surveys are time consuming, and they require important human and material resources, making them costly and limited in time and space [Rocchini et al., 2010, Skidmore et al., 2015]. Moreover, they tend to be influenced by the assessor [Rocchini et al., 2016], which can make the comparison between study areas difficult. Ecological field surveys are thus limited to a local scale, whereas there is an important need to monitor biodiversity over larger extents (national to international scales). To circumvent this issue, remote sensing appears to be an appropriate tool. Indeed, thanks to the broad spatial coverage and regular revisit frequency of satellite sensors, remote sensing provides continuous, regular and repeatable observations over large extents [Pettorelli et al., 2014, Cord et al., 2017]. It has already proven its ability for habitat mapping [Kerr and Ostrovsky, 2003, Pettorelli et al., 2014], and it can be seen as an indirect approach for biodiversity estimation [Rocchini et al., 2010, Skidmore et al., 2015].

Considerable progress has been made in the remote sensing of biodiversity during the last few decades [Rocchini et al., 2016]. Many works are based on the Spectral Variation Hypothesis (SVH) [Gould, 2000, Palmer et al., 2002], which assumes that the spectral heterogeneity in the image is correlated with the heterogeneity of the habitat. The diversity of species being related to the heterogeneity of the habitat [Wilson et al., 2002, Tews et al., 2004], the spectral heterogeneity can be used as a proxy for species diversity [Rocchini et al., 2016].

The measures of grasslands' species diversity in the context of SVH have been discussed in the work of Oldeland et al. [Oldeland et al., 2010]. Most of the studies are based on species richness. However, this measure gives equal weight to every species, regardless of their proportion in the community. The contribution of rare individuals in the spectral heterogeneity can be doubtful. Abundance-based measures of species diversity, such as the Shannon index, give more weight to species with higher proportions. Therefore, these measures should be preferred to species richness in the context of SVH [Oldeland et al., 2010, Möckel et al., 2016].

Many ways to quantify the Spectral Heterogeneity (SH) and to relate it to alpha-diversity have been developed in the remote sensing community [Rocchini et al., 2010]. SH has been quantified with the standard variation or the coefficient of variation of the Normalized Difference Vegetation Index (NDVI) [Gould, 2000, Oindo and Skidmore, 2002], using Principal Components Analysis (PCA) [Fairbanks and McGwire, 2004, Oldeland et al., 2010] and with the mean Euclidean distance to the spectral centroid [Palmer et al., 2002, Rocchini, 2007, Oldeland et al., 2010, Möckel et al., 2016]. However, these measures do not describe well the variability in the spectral space. Recently, Féret and Asner [Féret and Asner, 2014] developed an original approach to account for both the spatial and the spectral information of imaging spectroscopy. Their approach is based on the hypothesis that species can be categorized according to their spectral reflectance. They performed an unsupervised clustering using the *k*-means algorithm, assigning each pixel of the image to a cluster called a "spectral species". Then, they computed the "spectral species distribution", which is the entropy (Shannon index) of the spectral species and which was found highly correlated with the ground Shannon index of a tropical forest. However, since they were using hyperspectral data with very high spatial resolution (2 m), simplifying steps were necessary prior to the clustering because *k*-means is not suitable for high dimensional data, resulting in a significant loss of spectral information and possibly of the heterogeneity.

Most of the aforementioned works were performed with hyperspectral data issued from a field spectroradiometer or an airborne sensor, thus with a very high spatial resolution. Although these works showed good results, they were limited to a very local scale, because of the costs involved by such a mission. Conversely, new satellite missions for continuous vegetation monitoring, such as Sentinel-2 [Drusch et al., 2012], provide freely multispectral time series with high spatial and high temporal resolutions. Therefore, a tradeoff could be considered by using time series of satellite images to monitor grasslands biodiversity over large extents. Indeed, species communities differ in their temporal and seasonal behaviors, i.e., their phenology, making the phenological diversity related to the species diversity [Hooper, 1998, Sakai, 2001]. Therefore, in this study, we argue the hypothesis that the spectro-temporal heterogeneity of a community can be related to its species diversity, such as suggested by

Rocchini et al. [Rocchini et al., 2016]: "Multispectral satellite sensors with high to very high spatial resolution and short revisit period, such as Sentinel-2, Venμs, and other high spatial resolution multispectral sensors may be good candidates for biodiversity mapping based on spectro-temporal variations". We could name this hypothesis the "Spectro-Temporal Variation Hypothesis" (STVH) in reference to the SVH.

However, the use of both the spectral and the temporal information in dense time series involves big data issues. Indeed, we have to deal with a high number of spectro-temporal variables, but with a small number of samples, because grasslands in Europe are relatively small objects in the landscape (around one hectare). Even with high spatial resolution sensors (around 10 m), on average, only a hundred pixels compose these grasslands, while there is about the same number of spectro-temporal variables during a year of acquisitions. Clustering algorithms and measures of spectral heterogeneity that are suitable for high dimensional data are thus required.

The objective of this study is to verify if the spectro-temporal variations in grasslands are related to their species diversity, using dense Satellite Image Time Series (SITS) with a high spatial resolution (10 m). To verify this hypothesis, we propose to link spectro-temporal and spectral-only heterogeneity measures derived from the unsupervised clustering of grasslands to their species diversity through linear regression models. To address the high dimensional issue, we propose to use a robust clustering algorithm that does not require dimension reduction prior to the clustering. We introduce new SH measures derived from the clustering and computed at the grassland level, to be consistent with ecological studies that usually estimate the biodiversity at the grassland level. The SH measures make possible the comparison of grasslands of varying sizes.

The proposed method is experimented on the Shannon index measured in 192 grasslands from southwest France with a dense intra-annual SPOT5 (Take5) multispectral time series and with single images extracted from this SITS. Note that contrary to [Féret and Asner, 2014], the spatial units are determined by the grasslands' spatial limits that are defined in a GIS, such as a land cover database.

In the next section, we present the materials used in this study. Then, the method proposed to measure the spectro-temporal heterogeneity is detailed in Section 6.3. Finally, the results are given in Section 6.4 and discussed in Section 6.5. Conclusions are given in Section 6.6.

6.2. Materials

6.2.1. Study Area

The study area is part of the Long-Term Ecological Research site "Coteaux et Vallées de Gascogne" (LTER_EU_FR_003), located in Gascony, in southwest France near the

city of Toulouse (43°17′N, 0°54′E, Figure 6.1). This hilly area of around 900 km² is characterized by a mosaic of crops, small woods and grasslands. It is dominated by mixed crop-livestock farming. Grasslands provide food for cattle by grazing and/or producing hay or silage. They range from monospecific grasslands sown with ryegrass (improved with mineral fertilizing and mown up to three times a year) to semi-natural grasslands composed of spontaneous plant species (not fertilized and mown once a year). Grasslands are mainly located on steep slopes, whereas annual crops are in the valleys on the most productive lands. The climate is sub-Atlantic with sub-Mediterranean and mountain influences (mean annual temperature, 12.5 °C; mean annual precipitation, 750 mm) [Ryschawy et al., 2012, Carrié et al., 2017].

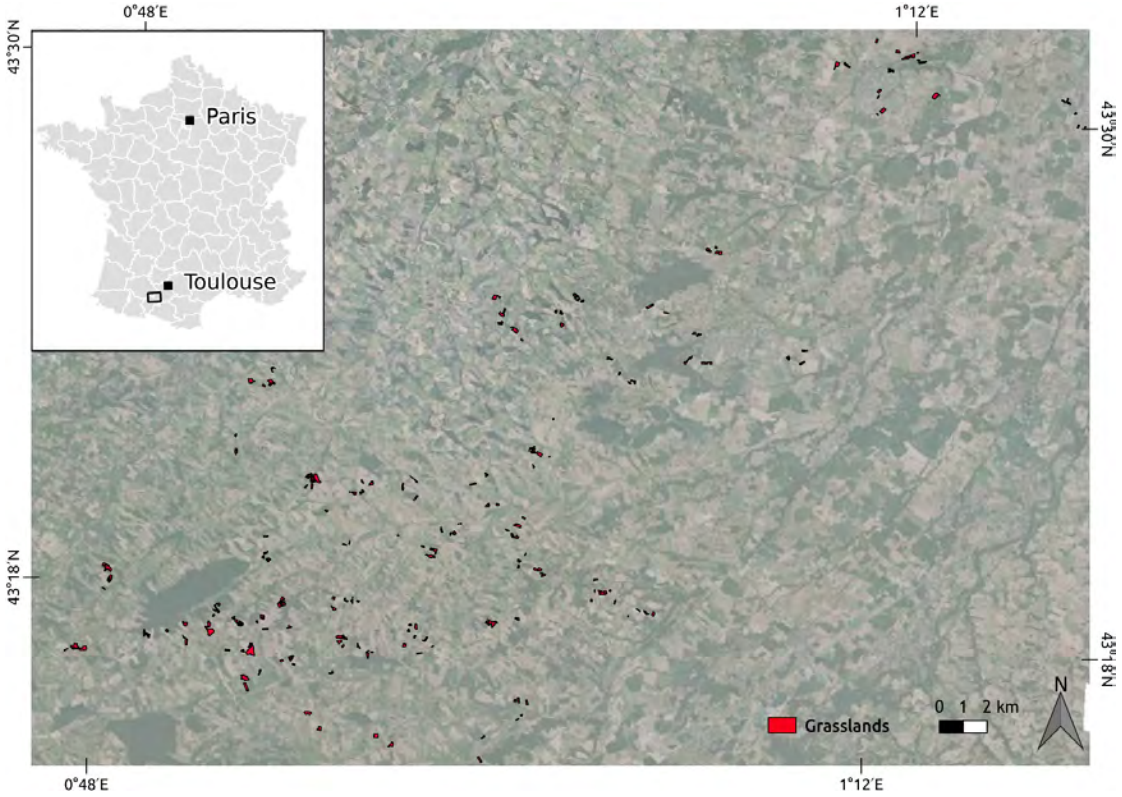

Figure 6.1.: Location of the study area in southwest France and of the grasslands within the study area. The background is an aerial photograph issued from the French orthophoto database "BD ORTHO® " (©IGN).

6.2.2. Satellite Image Time Series

The time series issued from the SPOT5 (Take5) mission (https://www.spot-take5.org) was used in this study. Eighteen images at a spatial resolution of 10 m were available from April–September 2015 (Table 6.1).

Table 6.1.: Characteristics of SPOT5 (Take5) imagery used in this study.

Pixel Size	10 m
Spectral bands	B1 "Green" (500–590 nm) B2 "Red" (610–680 nm) B3 "Near-Infrared" (780–890 nm) B4 "Short Wave Infrared" (1580–1750 nm)
Acquisition dates	20-04-2015, 25-04-2015, 30-04-2015, 10-05-2015, 20-05-2015, 04-06-2015, 24-06-2015, 29-06-2015, 04-07-2015, 09-07-2015, 14-07-2015, 19-07-2015, 24-07-2015, 13-08-2015, 18-08-2015, 28-08-2015, 02-09-2015, 07-09-2015

The images were orthorectified, radiometrically and atmospherically corrected by the French Spatial Agency (CNES). They were provided in reflectance with a mask of clouds and shadows issued from the MACCS (Multi-sensor Atmospheric Correction and Cloud Screening) processor [Hagolle et al., 2010].

To reconstruct the time series due to missing data (clouds and their shadows), the Whittaker filter [Eilers, 2003, Atzberger and Eilers, 2011b] was applied pixel-by-pixel on the reflectances in each spectral band. The smoothing parameter was the same for all the pixels and all the spectral bands. It was fixed to 10^4 after an ordinary cross-validation done on a subset of the pixels.

The smoothed time series associated with each of the spectral bands were concatenated to get a unique spectro-temporal vector $\mathbf{x}_k$ per pixel k, such as

$$\mathbf{x}_k = [\mathbf{x}_{k\mathrm{B}_1}(t_1), \ldots, \mathbf{x}_{k\mathrm{B}_1}(t_T), \mathbf{x}_{k\mathrm{B}_2}(t_1), \ldots, \mathbf{x}_{k\mathrm{B}_2}(t_T), \mathbf{x}_{k\mathrm{B}_3}(t_1), \ldots, \mathbf{x}_{k\mathrm{B}_1}(t_T), \mathbf{x}_{k\mathrm{B}_4}(t_1), \ldots, \mathbf{x}_{k\mathrm{B}_4}(t_T)]^\top,$$

where $\mathbf{x}_{k\mathrm{B}_1}(t_j)$ is the value of pixel k in band $B1$ at the j-th acquisition, and $T = 18$ is the number of acquisitions.

6.2.3. Field Data

Grasslands composing the dataset have been monitored for several years in the frame of different research projects. They represent more than 200 managed grass-

lands. The management practices and their intensity (i.e., number of mowings, intensity of grazing) are known for some grasslands.

The grasslands were digitalized in a GIS from aerial photographs ("BD ORTHO® " French database of orthophotos, ©IGN). For this study, an inner buffer of 10 m was removed from all the grasslands' polygons to avoid edge effects due to mixed pixels at the parcel edges. After rasterizing the polygons, only the grasslands composed of at least 10 pixels of 10-m resolution, i.e., having an area higher than 1000 m², were kept to ensure a minimum number of pixels per grassland. After this treatment, the dataset is composed of 192 grasslands. Their location can be seen in Figure 6.1.

A botanical survey was conducted in the spring of 2015 and 2016 after the flowering and before the mowing (April–May), to record the botanical composition of these grasslands. The grassland composition is supposed to remain stable from one year to the following year. The survey consisted of an exhaustive visual recording of all the species present in the grassland. The recording was processed while walking on a "W-shaped" transect, and the percentage of cover of each species was estimated at the grassland scale. The cover was estimated with the Braun-Blanquet abundance-dominance coefficients [Braun-Blanquet et al., 1932] for each present species (*: one individual, +: cover <1%, 1: 1–5%, 2: 5–25%, 3: 25–50%, 4: 50–75%, 5: 75–100%). An average abundance was kept for each coefficient (*: 0.1%, +: 0.2%, 1: 2.5%, 2: 15%, 3: 37.5%, 4: 62.5%, 5: 87.5%). From these absolute abundance-dominance covers, relative proportions of cover in the grassland can be retrieved for each species.

In this study, the species richness (number of species in the plot) was not considered because it accounts for rare species in the grassland, which might impact its functional diversity, but which do not have an impact on the spatio-spectral heterogeneity [Oldeland et al., 2010]. Therefore, an abundance-based biodiversity index was preferred to measure the alpha-diversity, the Shannon index (H):

$$\mathrm{H} = -\sum_{s=1}^{R} p_s \ln p_s \tag{6.1}$$

where p_s is the proportion of the s-th species with $\sum_{s=1}^{R} p_s = 1$ and R is the total number of species in the grassland (species richness). H values usually range between 0 and 5, increasing as the diversity increases. The Shannon index is a measure of the entropy in the grassland. It reflects the evenness of a population: a community with one or two dominating species is considered less diverse than a community that has different species with a similar number of individuals [Oldeland et al., 2010].

Most of the grasslands are semi-natural grasslands with a medium to high level of biodiversity (H > 2) (Figure 6.2a). Only a few are monospecific grasslands (sown with one species, H < 0.5). Three examples of grasslands' temporal profiles along the H axis, from a low to a high level of biodiversity, are shown in Figure 6.3.

The average grassland size in pixels is 135 pixels, and the median is 94 pixels (Figure 6.2b). In total, there are 25,903 pixels in the dataset.

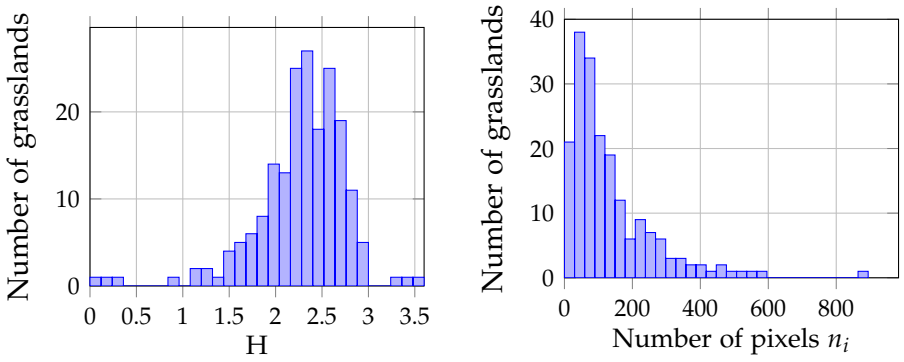

(**a**) (**b**)

Figure 6.2.: Histogram of (**a**) Shannon index H and (**b**) grasslands' size in number of pixels n_i.

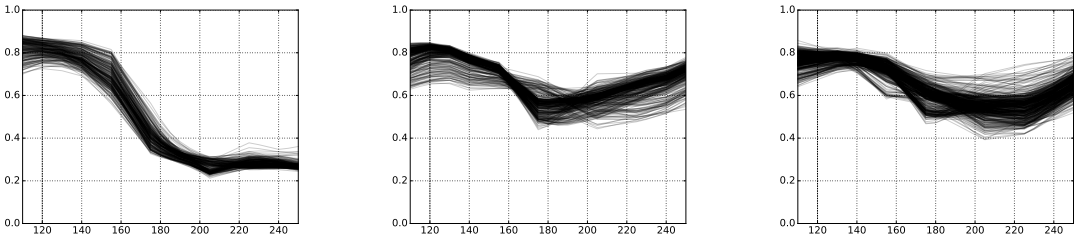

(**a**) H = 0.10 (**b**) H = 1.57 (**c**) H = 2.89

Figure 6.3.: SPOT5 NDVI temporal profiles of all the pixels belonging to three grasslands along the H gradient: (**a**) grassland with a low level of biodiversity, (**b**) grassland with a medium level of biodiversity and (**c**) grassland with a high level of biodiversity. The floristic record of these three grasslands can be found in Appendix, Table 6.3. The x-axis corresponds to the day of the year of 2015, and the y-axis corresponds to the NDVI. Grasslands have been voluntarily chosen by their high number of pixels for better visualization.

6.3. Method

The objective of this part is to describe the proposed method to measure the spectro-temporal heterogeneity in the grasslands from SITS and to link it with the Shannon index measured in the field in order to verify the STVH.

Each pixel k is represented by a vector $\mathbf{x}_k$ of dimension d, d being the number of variables. For instance, in the case of hyperspectral data, d is the number of spectral bands, which is a few hundred. In the case of multitemporal data, usually a vegetation index is used, and d corresponds to the number of temporal measurements. In this study, where we use both the spectral and the temporal information, $d = n_B n_T$, with n_B the number of spectral bands and n_T the number of temporal acquisitions, as presented in Section 6.2.2.

6.3.1. Measures of Spectral Heterogeneity in the Literature

In the literature, the measure of spectral heterogeneity is based on measures of dispersion [Rocchini et al., 2010] such as the standard deviation [Gould, 2000] or the coefficient of variation [Oindo and Skidmore, 2002]. However, these measures require selecting single bands or performing band reduction, such as using a vegetation index or using ordination methods like Principal Components Analysis (PCA), and thus, they lose some relevant information. To enable the use of all the spectral information, Rocchini [Rocchini, 2007] proposed the mean of the pairwise Euclidean distances from the spectral centroid (MDC) [Palmer et al., 2002] for all the pixels covering the sampling plot:

$$\mathrm{MDC}_i = \frac{1}{n_i} \sum_{k=1}^{n_i} \|\mathbf{x}_{ik} - \boldsymbol{\mu}_i\|^2 \tag{6.2}$$

where n_i is the number of pixels in the plot i, $\mathbf{x}_{ik}$ is the spectral vector associated with pixel k, $\boldsymbol{\mu}_i$ is the plot's spectral centroid and $\|\cdot\|^2$ stands for the Euclidean distance. In our case, the plot is the grassland. Hence, the centroid is the grassland's pixels' centroid, i.e., the mean spectro-temporal value of the grassland's pixels.

To reduce the dimensional-space, some studies compute the MDC on the first few components of PCA performed on the spectral variables [Rocchini, 2007, Oldeland et al., 2010,Möckel et al., 2016]. Theoretically, it is almost equivalent to the original MDC.

MDC is in fact the trace of the pixels' empirical covariance matrix $\mathbf{V}_i$, which measures the spectral variability in the plot:

$$\mathbf{V}_i = \frac{1}{n_i} \sum_{k=1}^{n_i} (\mathbf{x}_{ik} - \boldsymbol{\mu}_i)(\mathbf{x}_{ik} - \boldsymbol{\mu}_i)^\top \tag{6.3}$$

and:

$$\text{trace}(\mathbf{V}_i) = \frac{1}{n_i} \sum_{k=1}^{n_i} \|\mathbf{x}_{ik} - \boldsymbol{\mu}_i\|^2. \tag{6.4}$$

However, several drawbacks can be raised from the MDC. This measure is flawed because it assumes homoscedasticity of the variables (same variance), and it does not differentiate between monomodal and multimodal distributions in the spectral space. Different spectral configurations can have the same distance to the centroid [Féret and Asner, 2014] as illustrated in a two-dimensional space in Figure 6.4.

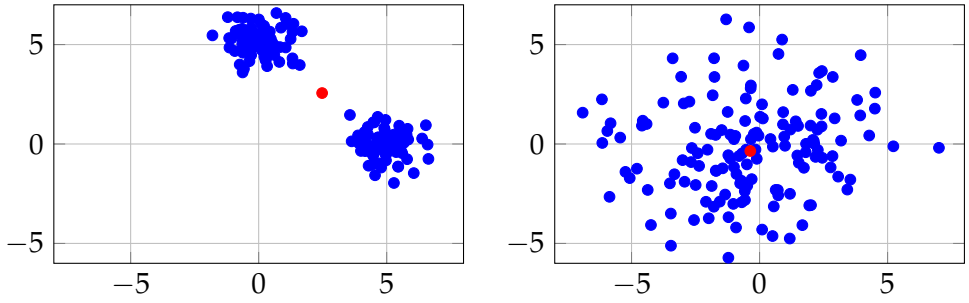

(a) MDC = 13.9 **(b)** MDC = 13.6

Figure 6.4.: Simulated pixels' distributions for two different plots (**a**) and (**b**). Pixels are displayed in blue, and the centroids of the plots are displayed in red. The estimated MDC are very close while the spectral distributions of the plots are clearly different.

To address this issue, Féret and Asner [Féret and Asner, 2014] introduced a clustering step to account for the global distribution in the spectral space. The unsupervised clustering is used to obtain "spectral species" (clusters), which are related to one or several species sharing similar spectral signatures. The clusters were estimated through a PCA and a k-means procedure. Although this clustering algorithm is often used, it is not robust in a high dimensional space [Parsons et al., 2004]. Moreover, it assumes homoscedasticity of the clusters (same variance for each cluster), and it does not reflect well the distribution in the spectral space. An illustration can be seen in Figure 6.5 where (a) a simulated plot made of three different spectral species was clusterized by (b) the pipeline PCA + k-means and (c) by Gaussian mixture models. With PCA + k-means, the spectral species (clusters) are not well found contrary to the clustering using Gaussian mixture models.

Thus, in the following, we propose a clustering technique that is robust to high dimensional data. Hence, no dimension reduction such as PCA is necessary. Moreover, it assumes heteroscedasticity of the clusters, i.e., each cluster could have a different

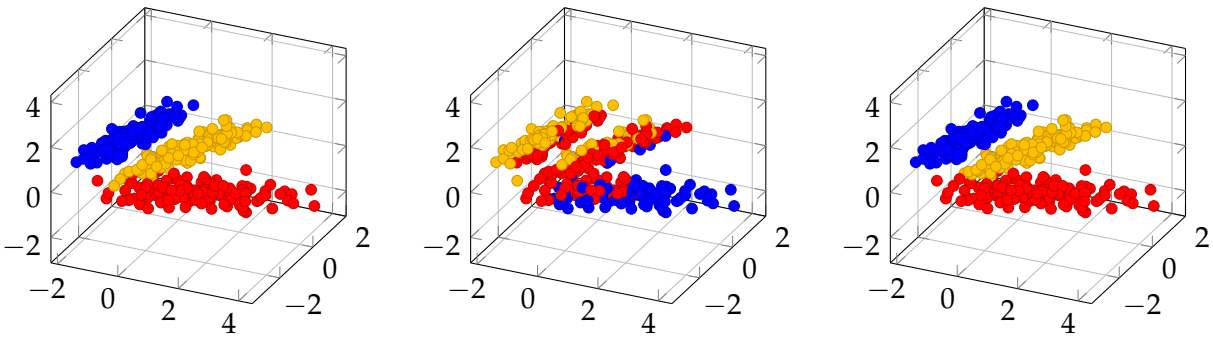

Figure 6.5.: (**a**) Simulated distributions of three spectral species (blue, yellow, red) in a 3-dimensional space. (**b**) Clustering of the three distributions with PCA and k-means. (**c**) Clustering of the three distributions with Gaussian mixture models.

variability. This clustering algorithm enables the computation of other measures of spectral heterogeneity.

6.3.2. Spectral Clustering Algorithm for High Dimensional Data and Derived Measures of Spectral Heterogeneity

We suggest to use a robust clustering algorithm that encompasses k-means, but that is suitable in a context of a small sample size with a large number of variables: the High Dimensional Data Clustering (HDDC) [Bouveyron et al., 2007a] (available in the R package at https://cran.r-project.org/web/packages/HDclassif/index.html). HDDC is based on a mixture model where each mixture component follows a Gaussian distribution. Under this model, a given sample (i.e, pixel) $\mathbf{x}$ is the realization of a random vector, for which distribution p is such that [Lagrange et al., 2017]:

$$p(\mathbf{x}) = \sum_{c=1}^{C} \pi_c f_c(\mathbf{x}|\boldsymbol{\mu}_c, \boldsymbol{\Sigma}_c) \tag{6.5}$$

where C is the number of clusters, π_c is the proportion of cluster c and $f_c(\mathbf{x}|\boldsymbol{\mu}_c, \boldsymbol{\Sigma}_c)$ is a Gaussian distribution with parameters $\boldsymbol{\mu}_c$ and $\boldsymbol{\Sigma}_c$, i.e.,

$$f_c(\mathbf{x}|\boldsymbol{\mu}_c, \boldsymbol{\Sigma}_c) = \frac{1}{(2\pi)^{\frac{d}{2}}|\boldsymbol{\Sigma}_c|^{\frac{1}{2}}} \exp\left(-\frac{1}{2}(\mathbf{x}-\boldsymbol{\mu}_c)^\top \boldsymbol{\Sigma}_c^{-1}(\mathbf{x}-\boldsymbol{\mu}_c)\right). \tag{6.6}$$

The parameters of the mixture model are estimated using a conventional expectation-maximization algorithm. Once the optimal parameters are found, each sample $\mathbf{x}$ is

assigned to the cluster c for which the log-probability $Q_c(\mathbf{x})$ is maximal. $Q_c(\mathbf{x})$ is computed as:

$$Q_c(\mathbf{x}) = \frac{1}{2} \times \left(-(\mathbf{x} - \boldsymbol{\mu}_c)^\top \boldsymbol{\Sigma}_c^{-1} (\mathbf{x} - \boldsymbol{\mu}_c) - \log(|\boldsymbol{\Sigma}_c|) + 2\log(\pi_c) - d\log(2\pi) \right). \quad (6.7)$$

The computation of Equation (6.7) requires the inversion of the covariance matrix $\boldsymbol{\Sigma}_c$ and the computation of the logarithm of its determinant, which can be numerically unstable in a high dimensional context. To circumvent these issues, HDDC assumes that the last (lowest) eigenvalues of the covariance matrix are equal. It results that the inverse of the covariance matrix and its determinant can be computed explicitly while the numerical stability is controlled [Bouveyron et al., 2007b].

In this study, the clustering is applied to all the grasslands' pixels $\mathbf{x}_k \in \mathbb{R}^d$, regardless of the grassland to which they belong. The clustering splits all the pixels into C clusters. Then, for each grassland g_i, its corresponding pixels $\mathbf{x}_{ik}$ are assigned to C_i clusters with $k \in \{1, ..., n_i\}$; n_i is the number of pixels in g_i, $C_i \in \{1, \ldots, C\}$ and $C_i \ll C$.

For each cluster c in the grassland, the mean vector $\boldsymbol{\mu}_{ic}$ and the covariance matrix associated with the pixels belonging to this cluster are updated from the initial clustering on all the pixels. The proportion of this cluster p_{ic} is also updated, $p_{ic} = \frac{n_{ic}}{n_i}$ with n_{ic} the number of pixels of g_i associated with c. Hence, by considering several clusters inside a given grassland, it is possible to assess the between-class variability, the within-class variability and the entropy within the grassland. They provide additional information with respect to MDC to assess the spectral heterogeneity, and they are defined in the next subsections.

6.3.2.1. Between- and Within-Class Variabilities

The covariance matrix of g_i can be decomposed as [Girard and Saracco, 2016]:

$$\mathbf{V}_i = \mathbf{B}_i + \mathbf{W}_i \quad (6.8)$$

with:

- $\mathbf{B}_i = \sum_{c=1}^{C_i} p_{ic}(\boldsymbol{\mu}_{ic} - \boldsymbol{\mu}_i)(\boldsymbol{\mu}_{ic} - \boldsymbol{\mu}_i)^\top$ is the between-class covariance matrix,
- $\boldsymbol{\mu}_{ic}$ is the spectro-temporal mean of pixels in g_i assigned to cluster c,
- $\boldsymbol{\mu}_i$ is the mean spectro-temporal value computed from all the pixels of g_i,
- $\mathbf{W}_i = \frac{1}{n_i} \sum_{c=1}^{C_i} \sum_{k \in c} (\mathbf{x}_{ik} - \boldsymbol{\mu}_{ic})(\mathbf{x}_{ik} - \boldsymbol{\mu}_{ic})^\top = \sum_{c=1}^{C_i} p_{ic} \mathbf{V}_{ic}$ is the within-class covariance matrix,
- $\mathbf{V}_{ic}$ is the empirical covariance matrix of pixels of g_i assigned to cluster c.

Therefore, using Equation (6.4), the MDC associated with g_i can be written as:

$$\text{MDC}_i = \text{trace}(\mathbf{V}_i) = \text{trace}(\mathbf{B}_i) + \text{trace}(\mathbf{W}_i). \tag{6.9}$$

From Equation (6.9), two measures of spectral heterogeneity can be extracted: the between-class variability and the within-class variability. The trace of $\mathbf{B}_i$ quantifies the between-class variability:

$$\text{trace}(\mathbf{B}_i) = \sum_{c=1}^{C_i} p_{ic} \|\boldsymbol{\mu}_{ic} - \boldsymbol{\mu}_i\|^2. \tag{6.10}$$

This measure reflects the inter-classes variance: how the means of clusters in the grassland are different or similar. The more the clusters are different, the higher the between-class variability. If there is only one class in the grassland, then $\text{trace}(\mathbf{B}_i) = 0$.

The within-class variability is quantified by the trace of $\mathbf{W}_i$:

$$\text{trace}(\mathbf{W}_i) = \frac{1}{n_i} \sum_{c=1}^{C_i} \sum_{k \in c} \|\mathbf{x}_{ik} - \boldsymbol{\mu}_{ic}\|^2. \tag{6.11}$$

This measure represents the mean of the clusters variances. The more the grassland has heterogeneous clusters with high variance, the higher the within-class variability. However, if the grassland has many homogeneous clusters, $\text{trace}(\mathbf{W}_i)$ will be low. Contrary to the between-class variability, if there is only one cluster, the within-class variability still provides information on the heterogeneity in the grassland.

6.3.2.2. Entropy

Another measure of spectral heterogeneity that can be derived from the spectral clustering of grasslands is the entropy. The entropy is linked to the proportions of clusters within the grassland g_i and is quantified by:

$$E_i = \sum_{c=1}^{C_i} -p_{ic} \log(p_{ic}). \tag{6.12}$$

The more the dataset has equally-balanced clusters, the higher E_i. The least balanced is the dataset, the closer E_i is to 0. If there is only one cluster in the grassland, $C_i = 1$ and $p_{i1} = 1$, then $E_i = 0$.

The HDDC algorithm provides for each pixel the probability that it belongs to each cluster, which can be understood as a soft assignment with respect to the hard assignment of k-means (Figure 6.6). Therefore, a "finer" measure of entropy can be computed using the probability of assignment of the grassland's pixels to each cluster

c of the global clustering, π_{ic}:

$$\pi_{ic} = \frac{1}{n_i} \sum_{k \in g_i} \pi_{ick} \tag{6.13}$$

with π_{ick} the assignment probability of pixel k from g_i to cluster c provided by the algorithm, $\sum_{c=1}^{C} \pi_{ick} = 1$ (Figure 6.6). Therefore, a finer measure of entropy can be written by replacing p_{ic} by π_{ic} in Equation (6.12) and by summing it to the total number of clusters C:

$$E_{s_i} = \sum_{c=1}^{C} -\pi_{ic} \log(\pi_{ic}). \tag{6.14}$$

This measure of entropy hardly ever reaches null values, unless all the pixels of the grasslands are assigned to the same cluster with a probability of 1.

(**a**) (**b**) (**c**) (**d**)

Figure 6.6.: Grassland clustered with an initial clustering of the landscape into 8 clusters. (**a**) Hard assignment of the pixels. One color corresponds to one cluster (orange, yellow, blue). (**b**–**d**) Soft assignment of the pixels. The grey-scaled color corresponds to the assignment probability π_{ick} to cluster (**b**) orange, (**c**) yellow and (**d**) blue.

The entropy reflects the grassland's clusters evenness: whether it is dominated by one cluster or numerous equally-distributed clusters.

6.3.3. Methodology

To link the proposed SH measures issued from SITS to the Shannon index measured from the species, univariate and multivariate (combining several SH measures), linear regressions are performed. The response variable is the Shannon index, and the explanatory variables are the global variability or MDC (Equation (6.9)), the between-class variability (Equation (6.10)), the within-class variability (Equation (6.11)) and the entropy with soft assignment (Equation (6.14)).

Since the linear regressions assume normality of the distributions, the global variability, the between-class variability and the within-class variability are log-transformed

to Gaussianize them [Neyrinck et al., 2009], as done in [Hall et al., 2012, Möckel et al., 2016]. In the following, the entropy with soft assignment is denoted by E, and the log-transformed global (or MDC), within-class and between-class variabilities are denoted by V, W and B, respectively.

The adjusted coefficient of determination $\bar{R}^2$ is used to measure the goodness of fit of the regressions. It is defined as the proportion of variance explained by the regression model adjusted for the number of explanatory variables.

The proposed methodology including the clustering is synthesized in Figure 6.7. To assess the contribution of temporal variations to the SVH through the use of multitemporal data, we also applied the same methodology using only one acquisition issued from the SITS. We compared the results obtained with the SITS and obtained with a single image by computing a Wilcoxon signed-rank test between the two distributions of predicted values issued from their best models.

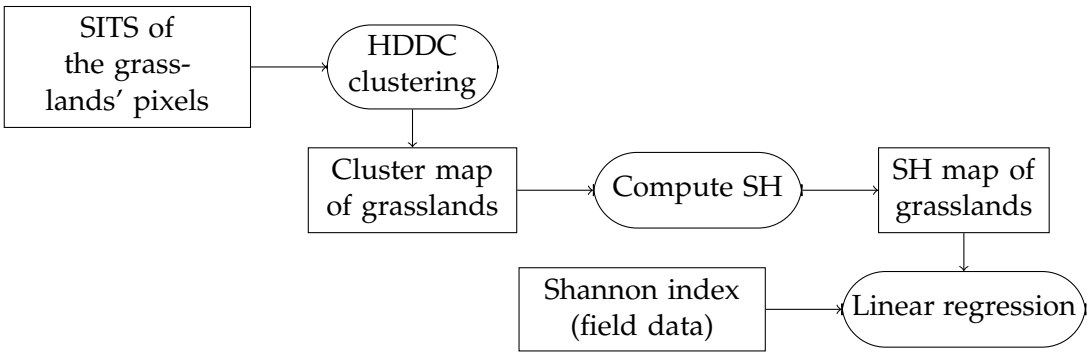

Figure 6.7.: Overview of the method to compare the Spectral Heterogeneity (SH) measures (explanatory variables) to the Shannon index (response variable). Square rectangles correspond to data, and rounded rectangles correspond to a process.

The clustering algorithm, the computation of the SH measures and the statistical analysis were performed in Python through the SciPy (`https://www.scipy.org`), scikit-learn [Pedregosa et al., 2011] and pandas (`http://pandas.pydata.org`) libraries.

The initial number of clusters for the clustering has an influence on the clusters found in each grassland (Figure 6.8). Hence, the correlations are studied for different numbers of initial clusters, from 2–150 clusters (every 2 clusters in the range $[2, 60]$ and every 25 clusters in the range $[75, 150]$). For each number of clusters, 10 runs of the algorithm with different random initializations are performed, and the best result in terms of the Integrated Classification Likelihood (ICL) [Biernacki et al., 2000] is kept.

(**a**) (**b**) (**c**)

Figure 6.8.: (**a**) False color image of a grassland acquired on 30 April 2015. The same grassland clustered using HDDC on multitemporal data with an initial clustering into (**b**) 8 clusters and (**c**) 150 clusters. Each cluster is represented by one color.

6.4. Results

The proposed SH measures were computed using the spectro-temporal data for all the grasslands for different numbers of clusters. Then, the adjusted coefficient of determination of the linear regression between the Shannon index measured in the field (H) and the individual or combined SH measures was calculated (Figure 6.9). The entropy computed with soft assignment (Equation (6.14)) was slightly better correlated with H than the "simple" entropy (Equation (6.12)); therefore, the usual entropy is not shown.

6.4.1. Univariate Correlation with Multitemporal Data

The global variability, or MDC computed at the grassland scale, is significantly correlated with the Shannon index ($\bar{R}^2 = 0.071$, p-value <0.001). Depending on the number of clusters, the entropy and the within-class variability reach higher correlation coefficients than the global variability. For instance, for the entropy, with $C = 8$ and $C = 75$, the adjusted coefficient of determination is $\bar{R}^2 = 0.099$ and $\bar{R}^2 = 0.105$, respectively (p-value <0.001). Its minimum is $\bar{R}^2 = -0.005$ and not significant for $C = 2$. The within-class variability reaches maximum correlation values of $\bar{R}^2 = 0.097$ for $C = 2$ and $\bar{R}^2 = 0.074$ for $C = 6$ (p-value <0.001). Its minimum value is $\bar{R}^2 = 0.034$ for $C = 75$ (p-value <0.05). The between-class variability never reaches as high values as MDC except for $C = 14$ ($\bar{R}^2 = 0.072$, p-value < 0.001). The problem with this measure lies with its null values, which make it not continuous.

The relationships between H and the proposed SH measures for each grassland that reach the highest coefficients of determination are shown in Figure 6.10. The entropy is the SH measure showing the highest coefficient of determination with H. All the

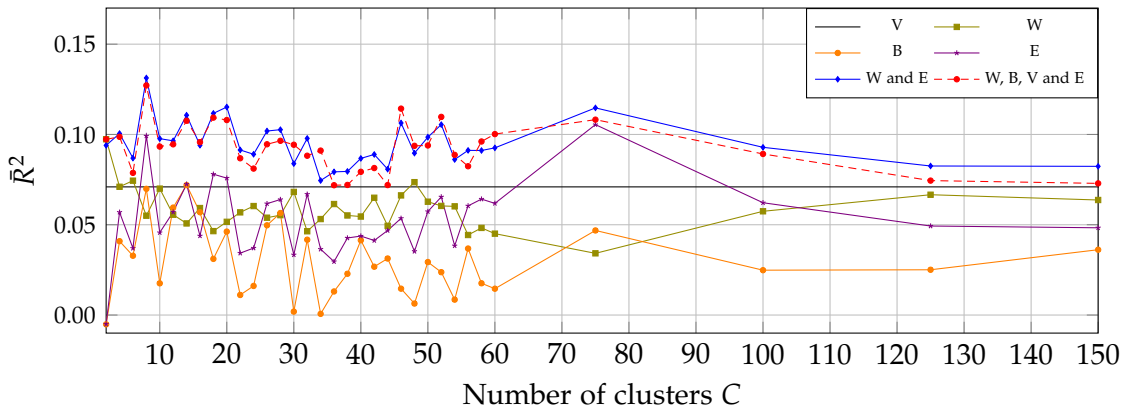

Figure 6.9.: Adjusted coefficient of determination in the multivariate linear regression between different combinations of SH measures (V: log-transformed global variability or MDC, W: log-transformed within-class variability, B: log-transformed between-class variability, E: entropy) computed from multitemporal data and the Shannon index (response variable) depending on the number of clusters.

SH measures tend to increase with the Shannon index suggesting that the spectro-temporal heterogeneity is linked to the species diversity.

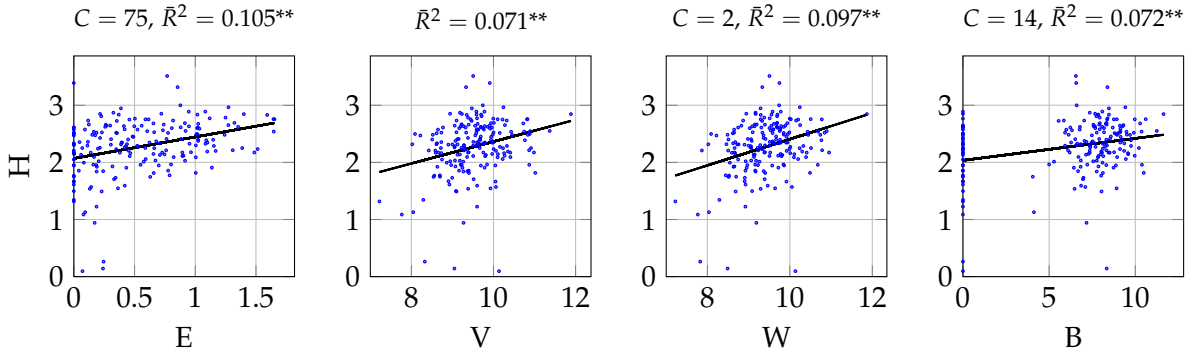

Figure 6.10.: Shannon index (H) best univariate linear correlations with different SH measures (E: entropy, V: log-transformed global variability or MDC, W: log-transformed within-class variability, B: log-transformed between-class variability) computed from multitemporal data. C is the corresponding number of clusters, $\bar{R}^2$ is the adjusted coefficient of determination and ** signifies p-value <0.001. The black line is the linear regression line.

6.4.2. Multivariate Correlation with Multitemporal Data

Multivariate linear regressions were run with different combinations of SH measures to assess which combinations of variables are the most related to H.

The models combining several variables explain better the Shannon index than the univariate models (Figure 6.9, blue and red lines). Indeed, the multivariate model combining the entropy (E) and the within-class variability (W) and the model combining the four proposed SH measures (E, W, B and V) always has higher coefficients of determination than SH measures alone, regardless of the number of clusters. Moreover, for the number of clusters reaching the maximum adjusted coefficient of determination ($C = 8$), the variables contributing the most to explain H are W and E (p-value <0.05), whereas V and B do not contribute much (p-value >0.05, Table 6.2). Therefore, the combination of W and E ($\bar{R}^2 = 0.131$) explains H better than the combination of W, B, V and E ($\bar{R}^2 = 0.127$, Figure 6.9 and Table 6.2). This is the case for most of the numbers of clusters. Additionally, the combination of V and E (data not shown) is worse to explain H than the combination of W and E.

6.4.3. Univariate and Multivariate Correlation with Monotemporal Data

To evaluate the contribution of multitemporal data to the SVH, we compared the above results to results obtained from monotemporal data. We chose two acquisitions dates from the time series: 30 April (near the growth peak, before the occurrence of the management practices such as mowing and grazing) and 29 June (after most of the management practices occurred).

Higher coefficients of correlations are obtained with only one acquisition (Figure 6.11). Using the image of 30 April, the maximum adjusted coefficient of determination is 0.139 (p-value <0.001) with the model combining W and E for $C = 150$ and $\bar{R}^2 = 0.169$ (p-value <0.001) with the model combining W, B, V and E for $C = 150$ (for higher numbers of clusters, $\bar{R}^2$ was lower, data not shown). Using the image of 29 June, $\bar{R}^2 = 0.137$ with the model combining W and E, and $\bar{R}^2 = 0.140$ (p-value <0.001) with the model combining W, B, V and E, both for $C = 20$.

For both images, the combination of the four proposed SH and the combination of W and E are better at explaining the Shannon index than MDC. However, the contributions of each SH measure in the model are not the same as for the model using multitemporal data.

We compared the distributions of the predicted Shannon index values issued from the best models using the three types of data (i.e., multitemporal data: $C = 8$, explanatory variables: W and E; 30 April image: $C = 150$, explanatory variables: W, B, V and E; and 29 June image: $C = 20$, explanatory variables: W, B, V and E) by conducting a Wilcoxon signed-rank test. There were no significant differences between

Table 6.2.: Multivariate linear models for $C = 8$ to explain the Shannon index (H) from the SH measures (V: log-transformed global variability or MDC, W: log-transformed within-class variability, B: log-transformed between-class variability, E: entropy) computed from multitemporal data. Reg. Coeff. is the regression coefficient; Std Err. is the standard error; F stands for the F-value with degrees of freedom in brackets; R^2 is the coefficient of determination; and $\bar{R}^2$ is the adjusted coefficient of determination.

Response Variable	**Explanatory Variables**	**Reg. Coeff.**	**Std Err.**	***p*-Value**
H	W	0.29	0.14	0.04
	B	0.01	0.02	0.61
	V	−0.15	0.14	0.30
	E	0.40	0.13	0.003
	intercept	0.73	0.51	0.16
Model summary: $F_{(4,\ 187)}$ = 8.0, p-value <0.001, R^2 = 0.145, $\bar{R}^2$ = 0.127				
H	W	0.16	0.06	0.005
	E	0.37	0.09	<0.001
	intercept	0.65	0.51	0.20
Model summary: $F_{(2,\ 189)}$ = 15.4, p-value <0.001, R^2 = 0.140, $\bar{R}^2$ = 0.131				

the values predicted by the best models for each data type (p-value >0.05 for each pair of distributions). Therefore, the models are equivalent in terms of predicted H values.

6.5. Discussion

6.5.1. Spectral Heterogeneity Measures

Globally, the variance of the species diversity (represented by the Shannon index) explained by the SH measures derived from the clusterings of grasslands using SITS is weak.

Indeed, low species diversity grasslands are not associated with low SH measures, except for E (Figure 6.10). High species diversity grasslands can be associated with any SH measures: low to medium E values, medium V values, high W values and medium B values. Medium species diversity grasslands, that represent a great percentage of the dataset, can be associated with any SH measures. As a result, the unexplained

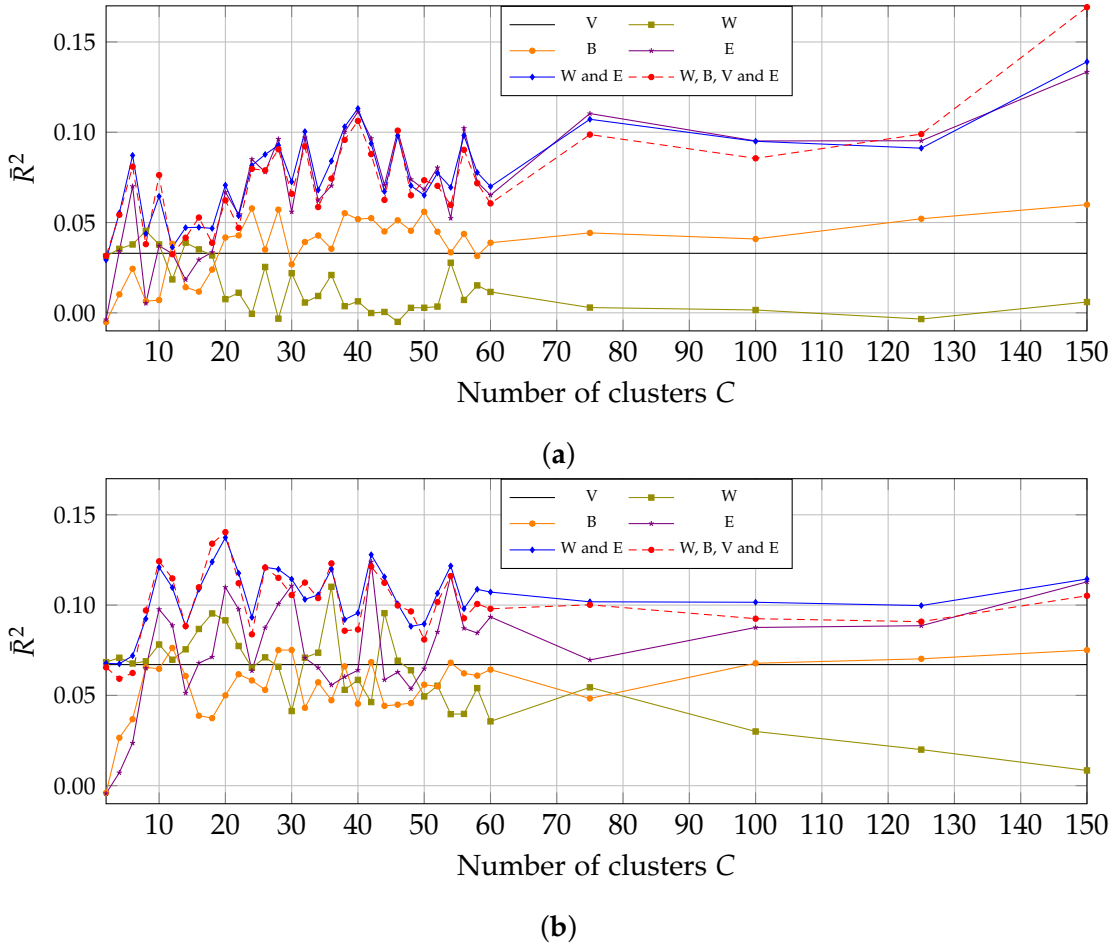

Figure 6.11.: Adjusted coefficient of determination in the multivariate linear regression using one image acquired on (**a**) 30 April and (**b**) 29 June between different combinations of SH measures (V: log-transformed global variability or MDC, W: log-transformed within-class variability, B: log-transformed between-class variability, E: entropy) and the Shannon index (response variable) depending on the number of clusters.

variance of H is very high (87%) with the model combining E and W ($C = 8$). Indeed, it predicts a much smaller range of values than the actual ones (Figure 6.2a): the maximum predicted H is 2.8, while the minimum is 1.8 with a mean of 2.3 and a standard deviation 0.2.

The spatial, but also the spectral resolution of the sensor may have limited the analysis. Indeed, individual grassland's species are particularly small and mixed. A spatial resolution of 10 m is too coarse to detect individual species. In a pixel of 10 m, there

can be a large number of mixed grassland plant species. Moreover, some species are spectrally too similar to be discriminated with low spectral resolution [Price, 1994, Nagendra, 2001]. Consequently, if a grassland has a high level of biodiversity, with a large number of species, and if these species are homogeneously mixed within the grasslands, the pixels will be spectrally similar even if they contain a mix of species. Thus, there would be one cluster in the grassland. This would result in a low spectral entropy, although this grassland has a high Shannon index. This could explain the wide range of SH values associated with grasslands with high species diversity. These SH measures seem to reflect more the variability of homogeneous species assemblages (i.e., the clusters) in the grasslands than the diversity of species, explaining the low, but significant relationship with the ground Shannon index.

Despite the weak relationship with the Shannon index, we proposed SH measures that provide supplementary information on the grassland's heterogeneity with regard to MDC. Indeed, the combination of the entropy and the within-class variability was always more correlated with the species diversity than the MDC alone, regardless of the type of imagery used. These two SH measures contributed the most to explain H.

The within-class variability is an interesting measure since it provides a quantitative information on the grassland's heterogeneity even if there is only one cluster, which cannot be provided by the entropy. Thus, the within-class variability and the entropy are complementary. Their combination was better than the combination of the four proposed SH measures together, or the univariate models, regardless of the number of clusters (Figures 6.9 and 6.11, blue line).

Beyond the relationship with species diversity of the SH measures, the proposed method makes possible the detection of assemblages of species within the grasslands, which share common spectro-temporal properties. These assemblages can indirectly give information about the heterogeneity within the grasslands. The heterogeneity of these groups of species can be quantified with their spectral variability (Figure 6.12). Such a spectral map at the grassland scale would not be possible using MDC.

6.5.2. Clustering

To understand the meaning of the clusters found using multitemporal data ($C = 8$), the mean vectors corresponding to each cluster were extracted, and their NDVI temporal profiles were computed (Figure 6.13). The profiles seem consistent with typical profiles of grasslands. The pixels associated with cluster C7 in Figure 6.13 belong to grasslands varying in species diversity, but all intensively-used. These pixels usually represent the whole grasslands, while grasslands less intensively used can be associated with several other clusters.

Hence, the clusters seem to be more related to phenological profiles linked to man-

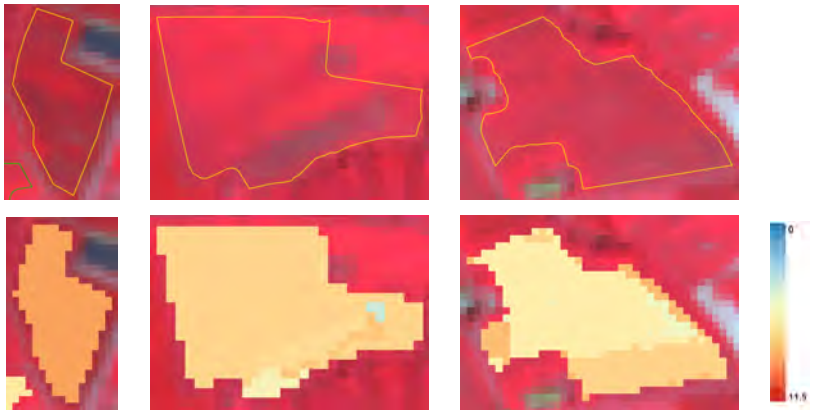

(**a**) (**b**) (**c**)

Figure 6.12.: Maps of spectral heterogeneity inside three grasslands (**a**–**c**). The first row shows the grasslands' polygon limits in yellow on the SPOT5 false color image acquired on 10 May 2015. The second row shows the clusters after an HDDC clustering into eight clusters using multitemporal data. The color scale corresponds to the log-transformed variability of each cluster c in the grassland g_i. (**a**) H = 0.10, E = 0, V = 10.13, W = 10.13, B = 0; (**b**) H = 1.57, E = 0.68, V = 10.06, W = 9.41, B = 9.33; (**c**) H = 2.89, E = 1.06, V = 9.58, W = 9.22, B = 8.42. The floristic record of these three grasslands can be found in the Appendix, Table 6.3.

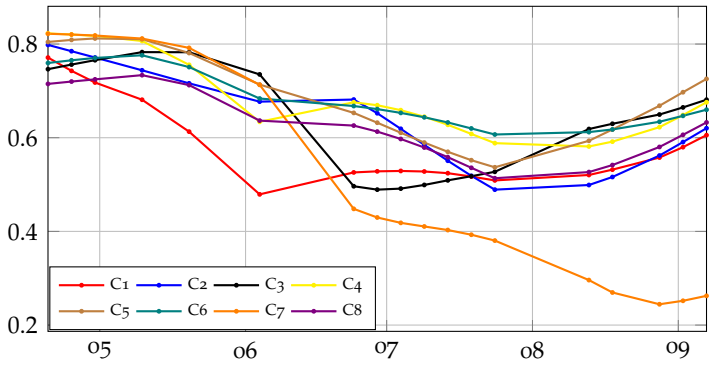

Figure 6.13.: Mean NDVI temporal profiles of each cluster from the clustering into $C = 8$ clusters using multitemporal data. The x-axis is the month of year 2015, and the y-axis is the NDVI.

agement practices than to phenological profiles of species. Indeed, the management practices have an influence on the species distribution and composition [Moog et al., 2002], but they may have a stronger impact on the spatial, temporal and spectral pro-

files of the grasslands because they induce abrupt changes in the grassland (mowing, grazing, fertilizing). In particular, due to the use of acquisitions from April–September, the effect of management practices that usually occur within this period may be very significant.

More precisely, we suspect that clusters are related to the intensity of practices. Indeed, an intensive use with constant defoliation does not allow for the expression of the phenology of species. However, when the grassland is extensively used, species can express different phenologies (during the regrowth after the mowing for instance), and different clusters related to these phenologies can be detected. This could explain the multiple clusters found in extensively-used grasslands (for instance, in Figure 6.12c), while intensively-used grasslands are represented by one cluster, which has a typical signature of intensively-used grassland (Figure 6.12a).

Hence, at a spatial resolution of 10 m, the clusters found using multitemporal data seem to reflect more the intensity of practices in the grasslands than the species composition. This could explain the weak correlations with the Shannon index.

Regarding the number of clusters, the proposed clustering algorithm (HDDC) provides model selection criteria (ICL and BIC) that were not efficient in our experiment. Indeed, the theoretical optimal number of spectral clusters may not correspond to the number of expected clusters of species [Schäfer et al., 2016]. Therefore, our strategy was to test a wide range of numbers of clusters and to keep the one that gives the best $\bar{R}^2$. From an operational viewpoint, this strategy can be time consuming, but it can adapt to any spatial configurations (size and location).

6.5.3. Contribution of Multitemporal Imagery

In this study, we made the assumption that the spectro-temporal variations of a grassland could be related to its species diversity. The results obtained with the monotemporal imagery showed that the multitemporal data do not improve the relationship with the Shannon index. Indeed, higher coefficients of determination were reached with the two dates proposed than with the full SITS. Hence, the SVH with temporal variations, the so-called STVH, is not verified in this work, at a spatial resolution of 10 m.

However, the clusters found in the grasslands using the full SITS create homogeneous patterns within the grasslands, contrary to the clusters found with one image, which are quite "pixelized" and do not seem spatially consistent (Figure 6.14). Considering that the predicted values with models issued from these three datasets were not significantly different, we can also doubt the relationship of the clusters found using one image with the species diversity. However, this would require verification in the field, but this was not possible in the frame of this work.

As previously suggested, the temporal variations measured by the sensor seem to

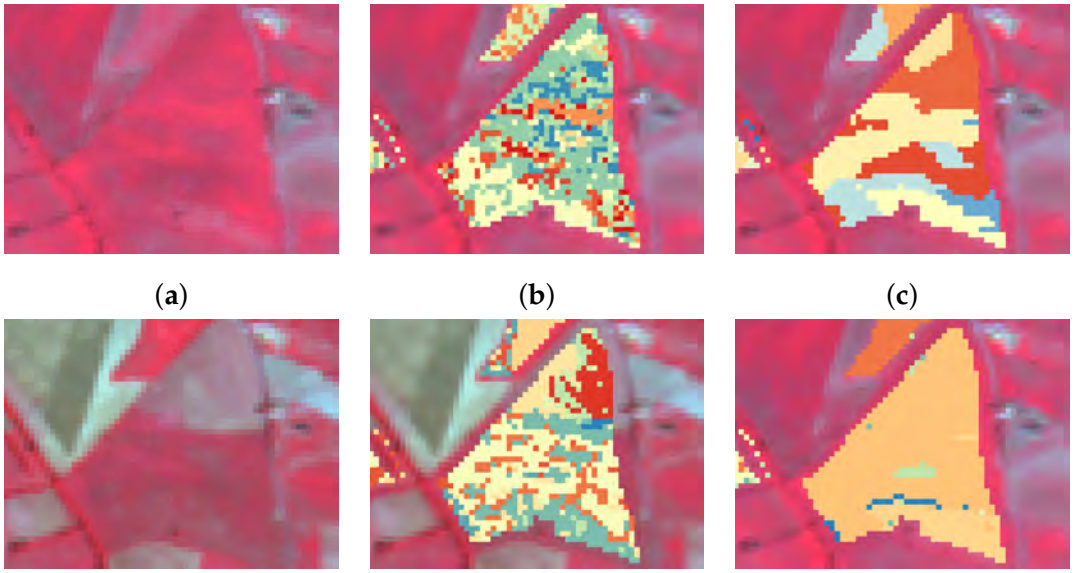

(**a**) (**b**) (**c**)

(**d**) (**e**) (**f**)

Figure 6.14.: Clustering of the same grassland (false color image of (**a**) 30 April and (**d**) 29 June) with an initial clustering into 150 clusters, using (**b**) the image of 30 April and (**c**) the full SITS, and into 20 clusters, using (**e**) the image of 29 June and (**f**) the full SITS.

be more related to the management practices than to the species diversity. Indeed, we used a time series covering the period from mid-April–September. Most of the management practices such as mowing and/or grazing usually occur within this period. To circumvent this effect, the time series could be limited to a period or a combination of periods when there is no management practices, such as the beginning of the growing season, before the growth peak. Moreover, previous studies have shown that the relationships between species diversity and remote sensing metrics can be season-dependent [Maeda et al., 2014]. Therefore, specific care should be considered regarding the dates of the imagery selected.

6.5.4. Limitations

The weak relationships found in this work can be due to the unbalanced H values present in our dataset. Indeed, it was mostly composed of grasslands with a medium level of biodiversity (H between two and 2.5, Figure 6.2a). The H gradient was not very well sampled, with very few grasslands low in species diversity ($H < 1$) and rich in species diversity ($H > 3$). Hence, the regression models were more calibrated on medium level biodiversity and lacked generality. This may be why the models have

an average predicted H value of around 2.3 (Section 6.5.2).

Moreover, we obtained lower coefficients of determination than in other studies that related the species diversity in grasslands with the SH using monotemporal imagery at a very high spatial resolution. For instance, Oldeland et al. [Oldeland et al., 2010] used airborne hyperspectral data at a spatial resolution of 5 m and found significant correlations between the Shannon index of savannah plots and the MDC computed from PCA. They reached significant R^2 ranging from 0.31–0.62 depending on the 20 m $\times$ 50 m plots. Möckel et al. [Möckel et al., 2016] investigated the prediction of grassland species diversity (species richness and inverse Simpson's diversity) in Sweden from airborne hyperspectral data with a spectral response approach and a spectral heterogeneity approach. However, they failed to detect a significant relationship between species diversity and spectral heterogeneity (PCA + MDC) at the plot scale, contrary to the spectral response approach. In the same study area, Hall et al. [Hall et al., 2012] related the species richness (alpha-diversity) and the species turnover (beta-diversity) measured in three plots per grassland with the spectral heterogeneity in the four bands of the QuickBird sensor (2.4 m resolution) and other field variables. The spectral heterogeneity was measured as the mean difference between the mean of each individual 3×3 pixel window (corresponding to each plot) and the mean of all three pixels windows within each grassland site. It can be assimilated to the between-class variability, but with three plots of the same size. They found low, but significant linear correlations between the species richness and the spectral heterogeneity measured with the NIR band ($R^2 = 0.08$) and between the species turnover and the spectral heterogeneity measured in the red band ($R^2 = 0.10$), the NIR band ($R^2 = 0.19$) and the NDVI ($R^2 = 0.14$). Better correlations were found with multivariate models, but only the model predicting the species turnover included the spectral heterogeneity (NIR, $\bar{R}^2 = 0.33$).

However, these studies were conducted at the plot scale, both for the floristic record and the associated spectral information. They used the pixels corresponding only to the sampling unit. Our protocol was different, since the botanical survey was conducted at the grassland scale by a random walk strategy, and only one biodiversity index was computed from it. Yet, grasslands are characterized by patterns of small scale species composition and spatial distribution [Pärtel and Zobel, 1999, Bruun, 2000, Franzén and Eriksson, 2001]. Hence, this estimation of the biodiversity at the grassland level may be difficult to relate to remote sensing data and might have limited our analysis.

Furthermore, the influence of the topography should be considered for future studies because it is known that the topography influences the reflectance.

6.5.5. Outlooks

In terms of methodology, the proposed method could be used to assess the beta-diversity among grasslands. Indeed, in light of the Bray–Curtis dissimilarity [Bray and Curtis, 1957], a spectral dissimilarity could easily be computed from the proportions of clusters in each grassland [Féret and Asner, 2014]. It could be improved by using the probability of belonging to each cluster, similarly to the way done with the entropy. The pairwise spectral Bray–Curtis dissimilarity between grasslands g_i and g_j would be defined as:

$$BC_{ij_{\text{spectral}}} = \frac{\sum_{c=1}^{C} |\pi_{ic} - \pi_{jc}|}{\sum_{c=1}^{C} \pi_{ic} + \pi_{jc}} \tag{6.15}$$

where π_{ic} and π_{jc} are the mean assignment probabilities to cluster c of pixels of grasslands g_i and g_j, respectively, defined in Equation (6.13).

In terms of application, the proposed method is not specific to grasslands, and it could be used to assess the species diversity of other habitats. For instance, it could be used on forest, since the method is not required to work at a specific object scale: it can be applied to a plot of fixed size.

In addition, this work could be extended to the relationship of the spectral heterogeneity with the functional diversity of the habitat. Indeed, some functional traits are related to the way plants reflect light and thus to the signal measured by the sensor [Ustin and Gamon, 2010, Homolová et al., 2013, Skidmore et al., 2015, Jetz et al., 2016] and may be related to the spectral heterogeneity. However to our knowledge, functional diversity has not yet been related to remotely-sensed measures [Jetz et al., 2016, Abelleira Martínez et al., 2016] and has not been discussed in the context of SVH [Rocchini et al., 2010, Rocchini et al., 2016]. The stakes would be to determine which traits and which measures of functional diversity are the most consistent with SVH. Using SITS, we would suggest to select functional traits that are linked to the phenology of the species such as the flowering date, the flowering length and the leaf life span.

6.6. Conclusions

The aim of this work was to attempt to verify the Spectral Variation Hypothesis (SVH) in grasslands under the assumption that the temporal variations could be used in addition to the spectral variations of the habitat as a proxy of its species diversity: the Spectro-Temporal Variation Hypothesis (STVH). To do so, we proposed a method based on an unsupervised clustering of the grasslands using multitemporal and multispectral data, allowing for the derivation of spectro-temporal heterogeneity

measures computed at the grassland level: the within-class variability, the between-class variability and the entropy. We compared them to the commonly-used mean distance to the centroid. The method was applied on 192 grasslands from southwest France using an inter-annual multispectral time series of SPOT5 images. Univariate and multivariate regression models combining several spectro-temporal heterogeneity measures were run with different numbers of clusters to assess their correlation with the Shannon index measured from field data.

The tested spectral heterogeneity measures were found significantly, but weakly correlated with the Shannon index. The combination of the within-class variability and the entropy was found always better correlated with the Shannon index than the mean distance to the centroid, regardless of the number of clusters. The best regression model explained 13.1% of the variance of the ground Shannon index while the mean distance to the centroid explained 7.1% of the variance. Hence, the clustering makes possible the extraction of spectral heterogeneity measures that give supplementary information to the mean distance to the centroid. However, equivalent results were obtained using monotemporal imagery.

Therefore, the spectro-temporal variation hypothesis was not verified using multispectral multitemporal imagery at a spatial resolution of 10 m. The proposed spectro-temporal heterogeneity measures seemed to be more related to the management practices performed in the grasslands than to the species diversity. The use of a whole time series covering the growing season or the season when the management practices occur does not seem to be suitable to detect the diversity in species. A period when no practice occurs should be more appropriate.

More research should be conducted on the extension of the SVH to the functional diversity. The STVH might be more related to functional traits linked to the phenology of species.

Appendix

Table 6.3.: Braun-Blanquet abundance-dominance coefficients associated with each plant species recorded in three grasslands a, b and c having a Shannon index of 0.10, 1.57 and 2.89, respectively. "spp." means that the species from the given genus was not identified.

Species	**a**	**b**	**c**	**Species**	**a**	**b**	**c**
Agrimonia eupatoria			+	*Medicago* spp.	+		
Agrostis capillaris			1	*Muscari comosum*			+
Anthoxanthum odoratum			1	*Orchis purpurea*			+
Arrhenatherum elatius		1		*Plantago lanceolata*			1
Bellis perennis			1	*Poa pratensis*			2
Bromus erectus			1	*Poa trivialis*	+	5	
Carex divulsa			+	*Potentilla reptans*		1	1
Carex flacca			1	*Prunus spinosa*			1
Centaurea nigra			+	*Rafanus* spp.	+		
Cirsium arvense		1		*Ranunculus acris*			1
Cirsium dissectum		1		*Ranunculus bulbosus*			1
Cirsium vulgare		+		*Ranunculus repens*		2	
Convolvulus arvensis		1	1	*Rasica oleacera*	+		
Crepis capillaris			1	*Rhinanthus minor*			+
Crepis spp.		+		*Rubus* spp.			+
Dactylis glomerata		1	3	*Rumex acetosa*			1
Daucus carota			1	*Rumex crispus*		1	+
Festuca arundinacea		2	3	*Senecio jacobaea*			1
Festuca rubra			1	*Sonchus asper*	+		
Galium mollugo			1	*Stachys officinalis*			+
Gaudinia fragilis			1	*Taraxacum officinalis*		1 1	
Holcus lanatus		1		*Tragopogon pratensis*		+	
Hypericum perforatum			+			+	
Hypochaeris radicata		1	1	*Trifolium dubium*			2
Lathyrus pratensis			2	*Trifolium pratense*		1	2
Leucanthemum vulgare			1	*Trifolium repens*			1
Linum usitatissimum			1	*Verbena officinalis*			1
Lolium perenne	5			*Veronica arvensis*			+
Lotus corniculatus			1	*Vicia sativa*	+		1

Acknowledgements

This work was partially supported by the French National Institute for Agricultural Research (INRA) and the French National Institute for Research in Computer Science and Automation (INRIA) Young Scientist Contract (CJS INRA-INRIA) and by the project SEBIOREF ("Promouvoir les Services Ecosystémiques rendus par la Biodiversité à l'agriculture", Région Occitanie, INRA, IRSTEA (French National Institute for Research in Sciences and Technologies for Environment and Agriculture)). The authors would like to thank the botanists who made possible the constitution of the field dataset used in this study: Philippe Caniot, Jérôme Willm, Emilie Andrieu and Gérard Balent. We would also like to thank the people accompanying the botanists: François Calatayud, Romain Carrié, Jean-Philippe Choisis, Donatien Dallery, Bruno Dumora, Camille Gouwy, Wilfried Heintz, Marc Lang and Anne-Sophie Mould. Specials thanks to Clélia Sirami, Romain Carrié, Rémi Duflot and Nicolas Gross for sharing their knowledge about grasslands' species diversity. The authors would like to thank CNES for providing the pre-processed SPOT5 (Take5) data. We thank the anonymous reviewers for their valuable comments that greatly improved the manuscript.

Conclusion of Part III

This part was focused on the definition of continuous ecological indicators of grasslands using satellite image time series. The first chapter assessed the potential of SPOT5 and Sentinel-2 time series to predict the Shannon and the Simpson indices in grasslands through a kernel least-mean square kernel. The second chapter introduced a method to estimate the species diversity of grasslands through their spectro-temporal heterogeneity. We made the assumption that the spectral and the temporal variations could be used as a proxy of species diversity (the Spectro-Temporal Variation Hypothesis). The proposed measures of spectro-temporal heterogeneity derived from the unsupervised clustering of grasslands explained more the Shannon index of grasslands than the commonly used mean distance to centroid. However, the coefficients of determination were low, and there were no significant difference between the Shannon index predicted using monotemporal data and using multitemporal data. Hence, the Spectro-Temporal Variation Hypothesis was not verified with SITS with a high spatial resolution. The results suggested that the clusters found were more related to the intensity of use of grasslands.

Therefore, the results of this part showed that the spatial and spectral resolutions of sensors like Sentinel-2 are too coarse to discriminate the plant species. However, spectro-temporal heterogeneity measures derived from this type of data still give an information of the heterogeneity within the grasslands that can be useful for ecologists. Functional diversity based on functional traits related to the phenology might be a possible outlook of this method.

General Discussion

Summary

The objectives of this thesis were to provide statistical tools suitable for the analysis and the monitoring of semi-natural grasslands from dense satellite image time series (SITS) with a high spatial resolution, to define ecological indicators of grasslands issued from this type of data and to assess the potential of this type of data to monitor grasslands.

To do so, we analyzed the semi-natural grassland's spectro-temporal response by monitoring a set of grasslands from the start to the end of the growing season in the first part of this thesis. Then, in the second part, we developed methods suitable for the supervised classification of semi-natural grasslands using dense satellite image time series with a high spatial resolution. Finally, in the third part, we proposed ecological indicators of grasslands linked to their species diversity issued from SITS.

Analysis of grassland's spectro-temporal response

In the first chapter, we analyzed the spectro-temporal response of semi-natural grasslands according to their natural phenology and to their management practices (one mowing, two mowings, mowing and grazing). Since the Sentinel-2 sensor was not fully operational during this thesis, a field campaign was conducted to collect the spectra during the growing season of a set of grasslands and Sentinel-2 spectral bands were simulated from the hyperspectral data.

The analysis showed differences in the spectro-temporal response depending on the topographic location of the grasslands, their type (annual, semi-natural), the intensity and date of occurrence of the practices. The increase of the variance of the signal appeared to be good indicators of the mowing and the grazing events because they expose the soil. Hence, the analysis led us to build an NDVI evolution model for mown semi-natural grasslands depending on their topographic location (top of a hill or bottom of a valley) and on the period of mowing (before or after the start of senescence) that accounts for the standard deviation of the signal.

We concluded that variance in grasslands should be accounted for, and that hyper-temporal data (less than 15 days) were necessary to monitor grasslands' phenology and management practices, especially during the spring. Sentinel-2, with its temporal resolution of five days, should make possible this continuous monitoring. However, the analysis was conducted with data collected from a field spectroradiometer, and hence, at a very high spatial resolution. The spatial resolution of Sentinel-2 and the atmospheric effects influencing the signal measured by satellite sensors were not accounted for.

Regarding the limits of this study, the analysis was based on a very small sample of grasslands (five grasslands) that were all different, from the annual grassland intensively-used to the semi-natural grassland extensively-used. It was also a very local analysis, specific to the study area (hills and valleys, sub-Atlantic with sub-Mediterranean and mountain influences climate). Hence, the results found might not be very generalizable and further investigations should be conducted on a wider and larger sample. In addition, we did not study much the grazing effect because we were focused on the mowing effect, although grazing is a very common practice in the study area. However, many studies have already investigated the grazing effect on the signal [Turner et al., 1992, Kawamura et al., 2005, Numata et al., 2007, Paudel and Andersen, 2010, Poças et al., 2012, Li et al., 2013, Hilker et al., 2014].

Moreover, we focused the analysis on the widely-used NDVI. Yet, NDVI is not exempt of criticism (it tends to saturate, it is sensitive to canopy background and atmospheric influences [Liu and Huete, 1995]) and we could have tested other indices. However, in our results, NDVI was more sensitive to the mowing than the MSAVI2 and the S2REP, mostly because of the soil exposure after the mowing and its effect on the spectral response. The high standard deviations observed with NDVI led us to conclude that the variance is an important feature in grassland analysis and that representing a grasslands by its mean only seems too limiting.

There were a limited number of temporal acquisitions during this field campaign. Hence, some effects of the phenology or of the management practices might have been missed. Additionally, our analysis was limited by the campaign duration, which started after the start of the season (in February) and ended before the end of the season (in November). Hence, we could not assess the effects of this phenological events on the signal.

The presence of clouds — that was the main reason of the limited number of acquisitions during this field campaign — may also limit the analysis using satellite data. Indeed, in the spring of a temperate climate, there is a high frequency of cloud occurrence that induces noise and missing data in the time series. One can choose to omit the noisy data (reducing the number of observations), or to reconstruct the time series. In this case, an appropriate smoothing algorithm to reconstruct missing data due to clouds is absolutely necessary for this type of application. Indeed, it should not over-smooth/underestimate the local maxima and minima that correspond to phenological events or effect of practices such as the mowing.

Hence, these results led us in the second part of this thesis to develop specific methods for the monitoring of semi-natural grasslands while accounting for heir heterogeneity using dense SITS with a high spatial resolution.

Methodological developments

In Chapter 2, we assessed the efficiency of several smoothing algorithms to reconstruct the time series provided by sensors with high spatial and high temporal resolutions. We chose the Whittaker smoother [Eilers, 2003] because it combines high fidelity to the data and low roughness and it is fast to execute.

Then in Chapters 3 and 4, we developed robust models for the supervised classification of semi-natural grasslands. First, we proposed a representation of the grasslands at the object level, to be consistent with ecological studies and that accounts for their heterogeneity. Moreover, modeling grasslands at the object level reduces the number of samples to process during the statistical analysis, compared to pixel-based analysis. From the behavior of grassland's pixels, we modeled their distribution by a Gaussian distribution, defined by the grassland's empirical mean vector and covariance matrix. We developed new similarity measures suitable for high dimensional data and that can be plugged into the kernel of SVM. We compared these methods to conventional methods that are based on pixel- and object-oriented approaches.

In Chapter 3, we proposed a high dimensional version of the Kullback-Leibler divergence. The efficiency of the proposed High Dimensional Kullback-Leibler divergence was assessed with an inter-annual time series of NDVI to classify the grasslands according to their management practices. It outperformed the Kullback-Leibler divergence. However, it was not significantly different than the conventional methods using RBF kernels (pixel-by-pixel modeling + majority vote, and mean modeling) in terms of classification accuracy.

Hence in Chapter 4 a more general similarity measure based on a flexible mean map kernel was proposed: the α-Gaussian Mean Kernel. The method was tested for two applications: classification of grassland's age using an intra-annual NDVI time series, and classification of grasslands' management practices using intra-annual multispectral (four spectral bands) time series. The α-Gaussian Mean Kernel proved its efficiency by being significantly better than all the other methods in the age application. For the management practices application, it was the best method but not significantly different from the best methods. We concluded that the covariance information must be accounted for in grassland's classification. Hence, a Gaussian modeling makes sense in our context. However, the flexible kernel encompasses both the Gaussian and mean modeling, so it can be used on semi-natural grasslands as well as on more homogeneous grasslands such as artificial grasslands.

These methods were designed to enable the use of all the spectral and the temporal information given by dense SITS, with no dates selection. However, it is still possible to extract only the variables useful for a given application. Indeed, there might be useless information when using all the available bands and dates. For instance, the spectral

information given by all the bands may be redundant because of correlations between certain bands. Moreover, previous works showed that classification overall accuracy using multitemporal data tends to saturate beyond a certain number of acquisitions used in the classification [Schmidt et al., 2014]. Hence, it might be interesting to study which dates and which bands are the most relevant for grassland's analysis.

One of the flaws of this work is that the temporal aspect was not really exploited (except by the smoothing process). Indeed, the order and the link between the variables did not have any importance for the statistical analysis. Yet, this information could help and even improve the differentiation of grasslands based on their phenology. We could use seasonal metrics/statistics (such as the minimum, maximum, mean, standard deviation, maximum derivative) to replace some variables such as done in [Zillmann et al., 2014]. However, in our study area, temporal shifts were very limited. Therefore, seasonal metrics might be more relevant when processing classifications over large spatial extents.

Definition of ecological indicators

The third part was devoted to the definition of ecological indicators of grasslands issued from SITS. In Chapter 5, we assessed the potential of SPOT5 and Sentinel-2 (both 10 meters spatial resolution sensors) to predict two biodiversity indices in grasslands (Shannon and Simpson indices). We used a kernel least-mean square regression, and tested two kernels: RBF kernel with the mean vector, and the empirical mean kernel. The results for both methods were not satisfying (coefficient of determination of around 0.13 for Shannon index and 0.17 for Simpson index in average) and suggested that a high temporal resolution combined with a high spatial resolution and multispectral bands were not sufficient to estimate these biodiversity indices at the grassland scale.

In Chapter 6, we used an indirect approach to estimate the species diversity based on the Spectral Variation Hypothesis. Here, we made the assumption that the temporal variations could be linked to the differences in phenology of the species and hence to the species diversity, so we attempted verifying the SVH using dense multispectral SITS with a high spatial resolution. We proposed to use spectro-temporal heterogeneity measures derived from the unsupervised clustering of grasslands. The clustering algorithm we used was developed for high dimensional data. We proposed several spectral heterogeneity measures (between-class variability, inter-class variability, entropy with soft assignment) derived from this clustering and compared them to the commonly used mean distance to spectral centroid. We assessed their correlation with the Shannon index through linear regression models. We also compared the results obtained using the whole time series with results obtained using one im-

age from the SITS. For the multitemporal analysis, the best models combined the inter-class variability and the entropy and yielded a significant but low coefficient of determination of 0.133 with the Shannon index measured on the field. The Shannon index was always better explained with models combining these two measures than the models based on the mean distance to centroid. However, there were no significant difference between the Shannon index values predicted using multitemporal data and using mono-temporal data.

Hence, we proposed spectral heterogeneity measures derived from the unsupervised clustering of grasslands that explain more the species diversity in grasslands than the mean distance to centroid. However, the SVH was not verified in grasslands using dense SITS with a high spatial resolution. The clusters found using multitemporal data seemed more related to the intensity of management practices conducted in the grasslands than to the species diversity. A time series that do not cover the period when the practices occur might be more appropriate to relate the spectro-temporal heterogeneity to the species diversity.

Globally, the low correlation coefficients found in both chapters can be explained by the gradients of diversity among the grasslands of the dataset that were not very representative (the same dataset was used). There were a lot of grasslands with medium biodiversity level, but not many with low and high biodiversity levels. Furthermore, the continuous biodiversity indicators measured on the field might be too precise to predict them with a high accuracy. Indeed, the small variations seem to be too fine to be detectable with a 10-meter spatial resolution and low spectral resolution sensor that can smooth the spatial heterogeneity [Rocchini et al., 2016]. Therefore, a spatial resolution of 10 meters might be too coarse for such applications for which very high spatial resolution hyperspectral data might be more suitable [Rocchini et al., 2016, Lopatin et al., 2017].

Moreover, we could argue the modeling of the grasslands at the object level to be consistent with ecologists that work at the grassland scale, for instance one biodiversity indicator per grassland. Indeed, because of the presence of small-scale patterns of species composition within grasslands [Pärtel and Zobel, 1999, Bruun, 2000, Franzén and Eriksson, 2001], trying to link the spatio-spectro-temporal response of a grassland to one ecological indicator might be doubtful. Indeed, the floristic composition on which the biodiversity indices are based were recorded following a random walk strategy within the main facies of the grassland. Hence, some pixels of the grasslands may correspond to parts of the grasslands that were not recorded. Thus, there may not be direct relationship between the pixels of the grasslands and the biodiversity index. This might have limited the relationship between the spectral indices and the biodiversity indices in this work.

Conclusions

In this thesis, we proposed tools for the statistical analysis of semi-natural grasslands using dense SITS with a high spatial resolution. Instead of working at the pixel level, we modeled the grasslands at the object level. It reduced the number of samples to process and solved the big data issues encountered when working on a pixel-by-pixel basis. We modeled the distribution of the pixels in a grassland by a Gaussian distribution to account for the grassland's heterogeneity. The methods developed are robust in a high dimensional context. They enable the use of all the spectral and the temporal information provided by the new generation satellites such as Sentinel-2.

We highlighted the spectral but also the temporal variability induced by the phenology, the management practices and the composition of grasslands. Prior to this study, most of the works represented grasslands by their mean only, sometimes adding the standard deviation. By modeling grasslands by a Gaussian distribution, we included the covariance feature in their representation. Given the results, this modeling proved to be more likely to capture the trends and heterogeneity of semi-natural grasslands found in southwest France.

However, we found difficulties to link the spectro-temporal information of grasslands to their species composition. The floristic composition of grasslands was recorded visually in the most representative facies of the grassland. The spatial limits of grasslands were extracted from the French agricultural land use database (Registre Parcellaire Graphique – RPG), and hence, based on the farmers declarations. However, even if the grassland is a homogeneous feature in an agronomic viewpoint (same practices in one parcel), it can present very different facies and gradients of composition, due to the topography and the presence of semi-natural elements such as a stream, hedgerows, trees, shrubs... Hence, the representation of the grassland based on its agronomic boundaries may not make sense in an ecological viewpoint, and in a remote sensing viewpoint as well, because of the presence of these facies. Working at the pixel level would not be a solution, given the large amount of pixels to process with high spatial resolution data. However, we could consider sub-units within the "agronomic parcel" that would make more sense ecologically and spectrally.

Therefore, even if the spatial and spectral properties of Sentinel-2 seem limited to assess the species diversity in grasslands, this sensor should make possible the continuous monitoring of grassland phenology and of factors influencing biodiversity in grasslands. The high temporal resolution and the free data access policy will enable the study of grasslands at different temporal scales, from a local scale to analyze short phenological events to an inter-annual scale to study global phenological events.

Outlooks

The work conducted in this thesis opens up new prospects for research on remote sensing for ecology and natural habitats.

From a thematic viewpoint, the methods presented in this work that were applied for alpha-diversity assessment could easily by extended to beta-diversity. Beta-diversity refers to the differentiation of communities along habitat gradients [Whittaker, 1972]. It is used to compare the diversity of two habitats or the evolution of the species diversity of a habitat. Indeed, the similarity measures could be used as "spectral beta-diversity", and we proposed a spectral dissimilarity measure based on the clusterings of grasslands in Chapter 6.

Moreover, we focused on the species diversity, but the functional diversity is also important for the study of biodiversity and ecosystem services [Tilman et al., 1997, Duru et al., 2005, Cadotte et al., 2011, Jetz et al., 2016]. It might also be more related to the spectral signal, since certain traits are linked to properties that can influence the signal measured by the sensor [Ustin and Gamon, 2010, Homolová et al., 2013, Skidmore et al., 2015, Jetz et al., 2016]. However, the functional traits need to be chosen carefully. We would recommend to use functional traits related to the phenology when using multitemporal data. Moreover, trait databases are not accessible for everyone and are not always complete. Hence, studies relating functional diversity to remotely sensed data are lacking but needed [Jetz et al., 2016, Abelleira Martínez et al., 2016]. We encourage future research in this direction.

The effect of climate change on the grassland's spectro-temporal response was not assessed in this work. Indeed, we were focused on the intra-annual phenology and on the year-by-year state of the grasslands. However, within a few years, decades of remote sensing data at a high spatial resolution will be accessible to anyone and it should facilitate the monitoring of grasslands throughout the years.

In terms of methodology, the effect of the smoothing on the classification accuracy or on the definition of ecological indicators was not assessed. It would be interesting to compare the results with different intensities of smoothing (smoothing parameter for the Whittaker filter) or different smoothing techniques.

From a methodological viewpoint too, several applications of this work showed that the mowing date constitutes a useful information for grassland's analysis. Yet, there are currently very few methods to detect the mowing dates from optical time series in the literature [Courault et al., 2010, Gómez Giménez et al., 2017]. These existing models could not be applied to our grasslands since the phenology of our grasslands was different from the described models. It confirms that grassland's spectro-temporal response is not unique and depends on the type of grassland, the climate, the soil, the topography and the management practices. Hence, further research on the detection of the mowing practice is highly needed. A possible obstacle on this subject might

be the limited availability of hypertemporal data during the mowing period, in the spring. To circumvent this issue, we would suggest to use radar data, such as done in [Schuster et al., 2011, Voormansik et al., 2013].

In this work, we only worked with optical data. However, it would be interesting to evaluate the contribution of radar data for the analysis of grasslands. Indeed, the most important phenological events occur during the spring, which is generally a cloudy/rainy season in a temperate climate. Hence, during this period, optical data is limited by the occurrence of the clouds. Radar data could help by providing information on the vegetation even during cloudy days. The combination of optical and radar data has already been shown to improve the grassland classification accuracy [Dusseux et al., 2014a]. Sentinel-2 could be used jointly with Sentinel-1 data.

Finally, in terms of applications, the methods developed in this work are not limited to grasslands and could be used on other natural or semi-natural habitats that are small and heterogeneous, such as peatlands, heathlands, wetlands, woodlands... Indeed, our methods were designed to account for the heterogeneity of the objects. They are suitable to high dimensional data, meaning that it is possible to study an object with many variables even if this object is composed of a few pixels (in our works, 10 pixels or more). The methods could be extended to other modelings to adapt to any habitat specificities.

Appendix

A. Spectral signatures

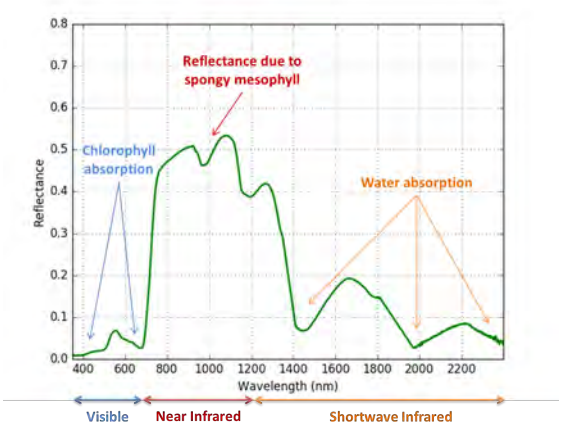

Figure A.1.: Typical spectral reflectance of vegetation.

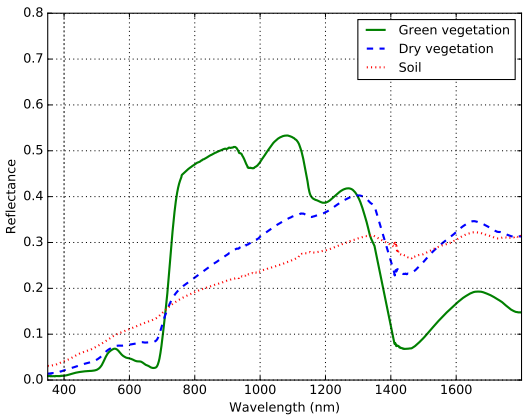

Figure A.2.: Spectral signatures of different vegetation states that can be found in a grassland.

B. Appendix of Chapter 1

Table B.1.: Abundance-dominance covers in percentage associated to each plant species recorded in the grasslands 36, 131, 405, 406 and 500. "spp" means that the species from the given genus was not identified.

Species	36	131	405	406	500
Agrimonia eupatoria	0	0.2	0	0	0
Agrostis spp	0	0	0	0	2.5
Ajuga reptans	0	2.5	0.2	0	2.5
Anthoxanthum odoratum	2.5	15	15	0	2.5
Avenula pubescens	0	2.5	0.2	0	2.5
Bellis perennis	15	0	2.5	0	0
Brachypodium pinnatum	0	0	0	0	15
Briza media	0	0.2	0.2	0	0
Bromus erectus	0	0	37.5	0	2.5
Bromus hordeaceus	2.5	0	0	0	0
Calystegia sepium	0	15	0	0	0
Cardamine pratensis	0	0.2	0	0	2.5
Carex flacca	0	2.5	2.5	0	2.5
Centaurea nigra	0	0	15	0	15
Cerastium fontanum	2.5	0	0.2	0	0
Cynosurus cristatus	0.2	0.2	2.5	0	0
Dactylis glomerata	2.5	2.5	2.5	0	2.5
Daucus carota	0	2.5	2.5	0	2.5

Euphorbia flavicoma	0	0	0	0	15
Festuca arundinacea	2.5	0	0	0	0
Festuca rubra	0	15	0	0	3
Filipendula vulgaris	0	0	2.5	0	15
Galium mollugo	0	0	2.5	0	2.5
Galium verum	0	15	2.5	0	15
Gaudinia fragilis	0.2	0	0	0	0
Geranium dissectum	2.5	0	0	0	0
Hieracium pilosella	0	0	0.2	0	0
Holcus lanatus	0	0	2.5	0	0
Hypochaeris radicata	0.2	2.5	0.2	0	0
Lathyrus pratensis	0	15	2.5	0	15
Leucanthemum vulgare	0	0.2	0	0	0
Linum usitatissimum	2.5	0.2	0	0	2.5
Lolium perenne	0.2	0	0	87.5	0
Lotus corniculatus	0	37.5	37.5	0	2.5
Luzula campestris	0	2.5	0	0	0
Luzula spp	0	0	2.5	0	2.5
Lychnis flos-cuculi	0	0.2	0	0	2.5
Medicago arabica	2.5	0	0	0	0
Medicago lupulina	2.5	0	15	0	0
Medicago spp	0	0	0	0.2	0
Muscari comosum	0	0	2.5	0	0
Oenanthe spp	0	15	0.2	0	0
Plantago lanceolata	15	15	2.5	0	15
Plantago media	0	0	0.2	0	0
Poa pratensis	0	2.5	15	0	3
Poa trivialis	15	0	15	0.2	0

Potentilla reptans	0	2.5	2.5	0	2.5
Rafanus spp	0	0	0	0.2	0
Ranunculus acris	0	37.5	2.5	0	0
Ranunculus bulbosus	2.5	0	2.5	0	15
Rasica oleacera	0	0	0	0.2	0
Rhinanthus minor	0	0	0.2	0	0
Rumex acetosa	0	2.5	0.2	0	2.5
Rumex crispus	0.2	0	0.2	0	0
Sanguisorba minor	0	0	0	0	15
Senecio jacobaea	0.2	0.2	0	0	0.2
Serapias lingua	0	0.2	0	0	0
Serapias spp	0	0	2.5	0	0
Sonchus asper	0	0	0	0.2	0
Sonchus oleraceus	0	0	0.2	0	15
Succisa pratensis	0	2.5	0	0	0
Taraxacum officinale	2.5	0	2.5	0	2.5
Tragopogon pratensis	0	0	2.5	0	0
Trifolium pratense	15	15	15	0	0
Trifolium repens	37.5	0	2.5	0	0
Veronica arvensis	0.2	0	0	0	0
Veronica chamaedrys	0	0.2	0	0	0
Veronica serpyllifolia	0	0.2	0	0	0
Vicia hirsuta	2.5	0	0	0	0
Vicia sativa	0	0	2.5	0.2	0
Vulpia myuros	2.5	0	0	0	0

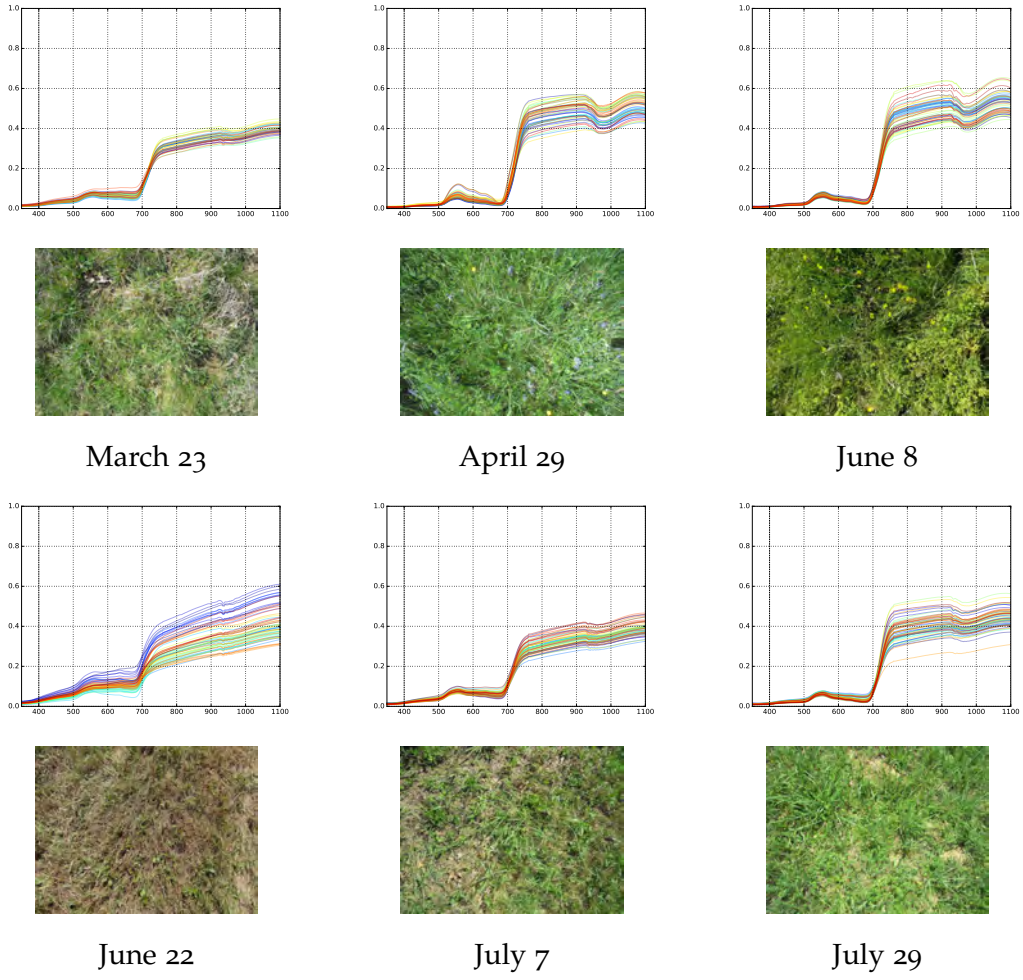

Figure B.1.: Spectral evolution of a semi-natural grassland mown on June 20 (ID 500) and photographs of measurement plots (one randomly chosen per date). The x-axis is the wavelength (nm) and the y-axis is the reflectance value. One color corresponds to one spectrum.

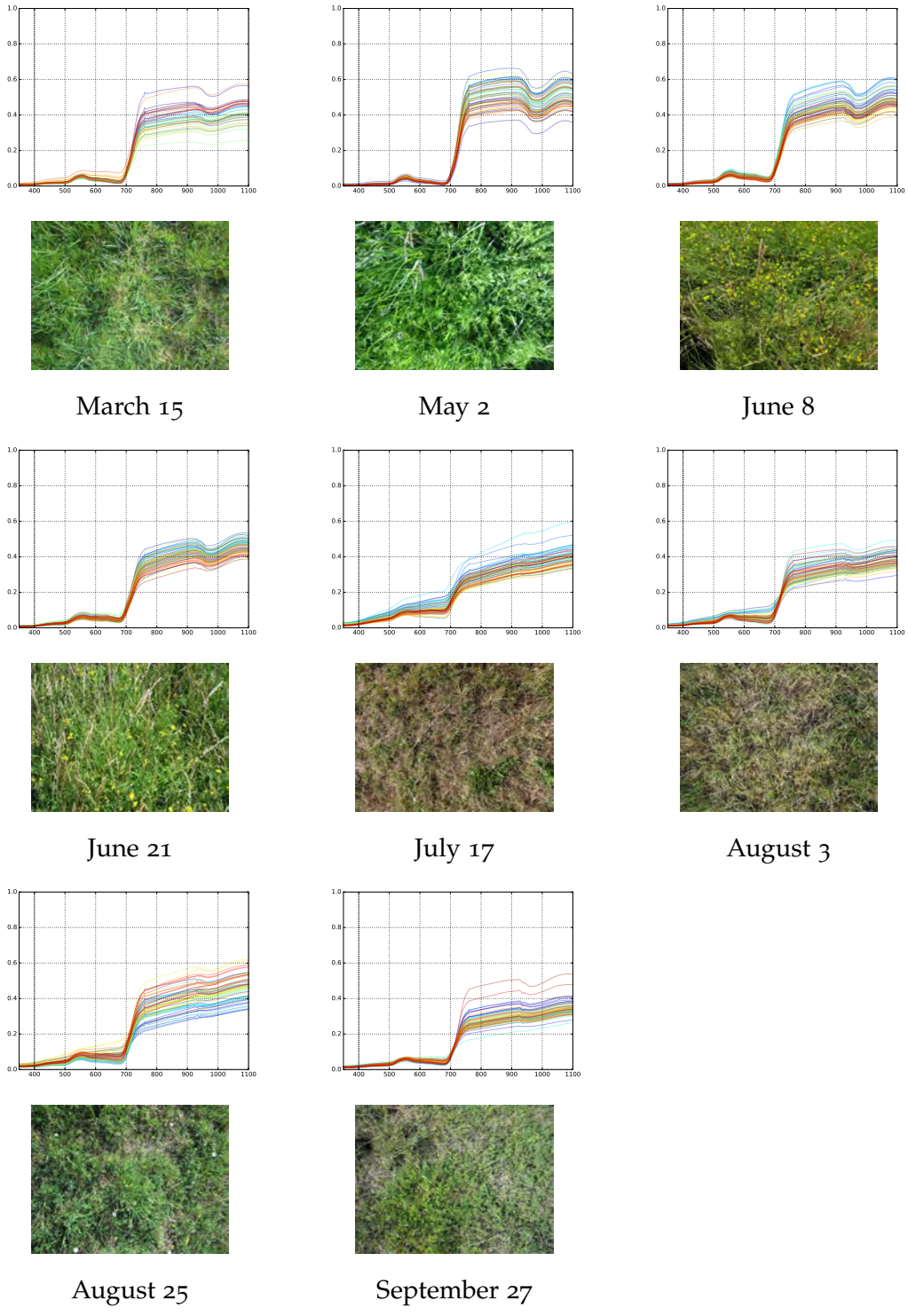

Figure B.2.: Spectral evolution of a semi-natural grassland mown on July 5 (ID 405) and photographs of measurement plots (one randomly chosen per date). The x-axis is the wavelength (nm) and the y-axis is the reflectance value. One color corresponds to one spectrum.

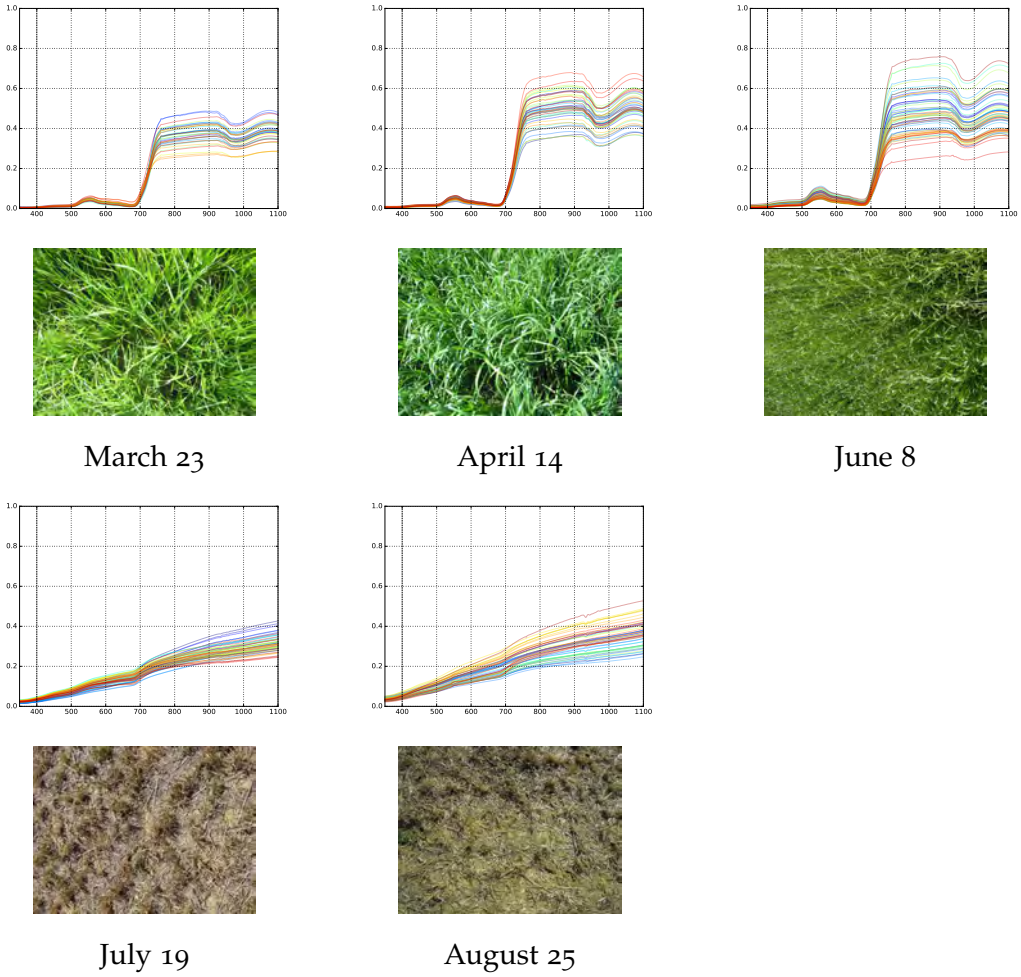

Figure B.3.: Spectral evolution of a sown grassland mown twice: April 29 and June 20 (ID 406) and photographs of measurement plots (one randomly chosen per date). The x-axis is the wavelength (nm) and the y-axis is the reflectance value. One color corresponds to one spectrum.

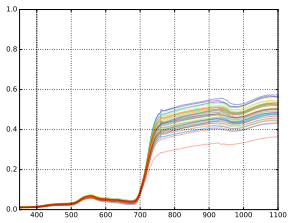


March 23

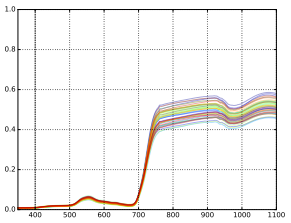


April 12

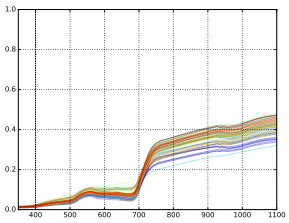


June 21

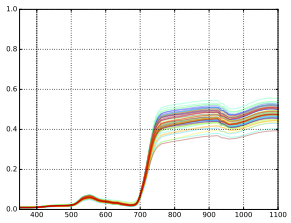


June 19

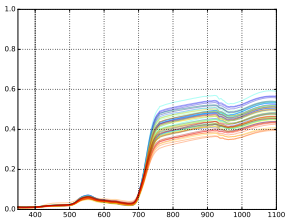


August 3

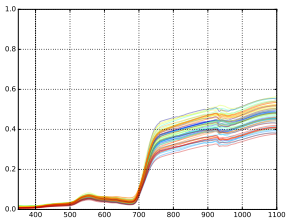


August 25

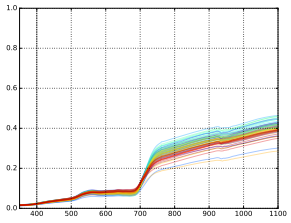


September 27

Figure B.4.: Spectral evolution of a semi-natural grassland mown on June 9 and grazed between September 1-15 (ID 131) and photographs of measurement plots (one randomly chosen per date). The x-axis is the wavelength (nm) and the y-axis is the reflectance value. One color corresponds to one spectrum.

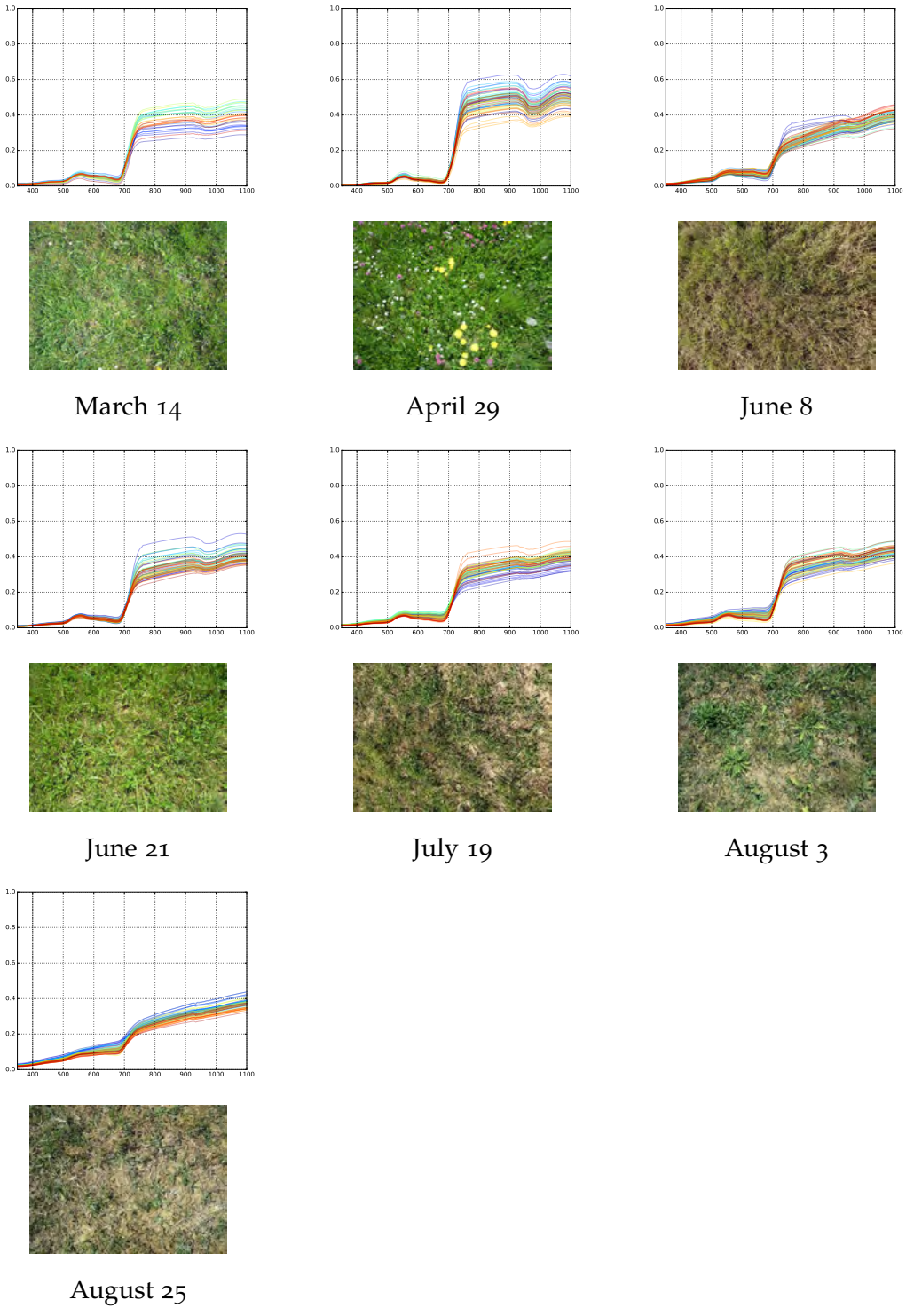

Figure B.5.: Spectral evolution of a grassland mown (on May 27) and grazed between July 6-15 and August 4-15 (ID 36) and photographs of measurement plots (one randomly chosen per date). The x-axis is the wavelength (nm) and the y-axis is the reflectance value. One color corresponds to one spectrum.

C. Supplementary materials of Chapter 4

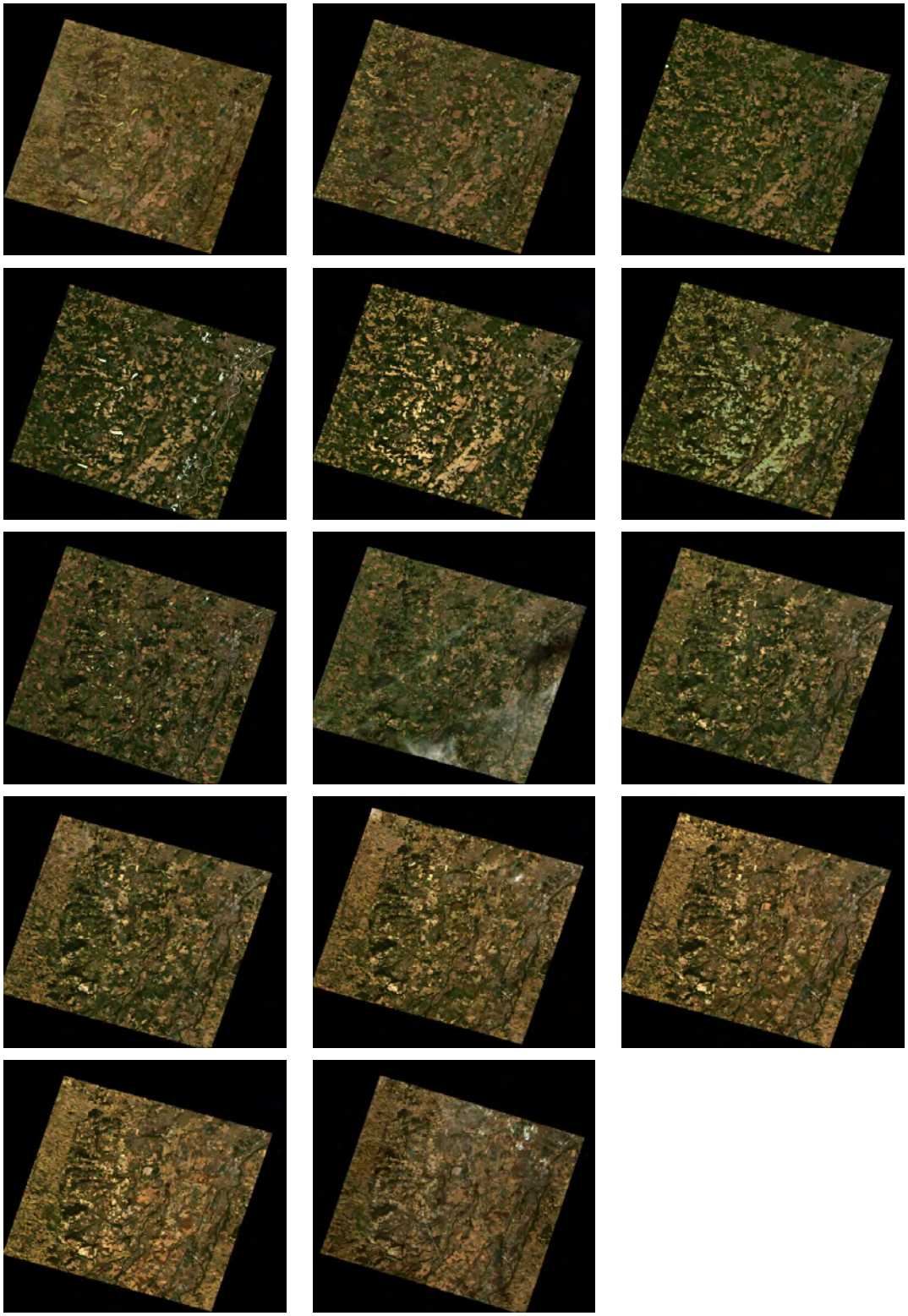

Figure C.1.: True color composite images of the Formosat-2 time series of 2014 (© CNES/Kalideos NSPO - Distribution Airbus DS).

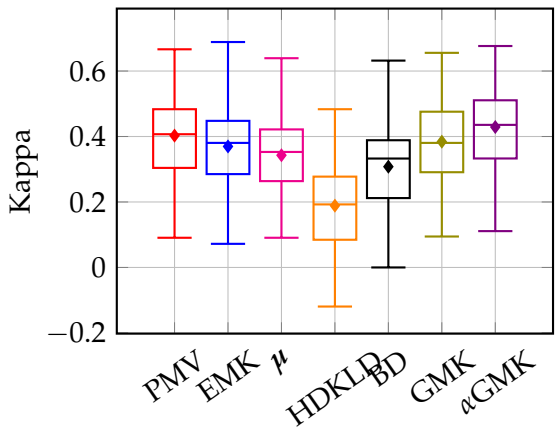

Figure C.2.: Boxplot of Kappa coefficient repartitions for the classification of the old and young grasslands. The line in the box stands for the median whereas the dot stands for the mean.

Table C.1.: Average user accuracy (UA) and producer accuracy (PA) (%) over the 100 repetitions for each class, 1: Old, 2: Young.

	UA1	UA2	PA1	PA2
PMV	85.8	90.9	30.9	99.2
EMK	70.0	90.8	30.9	97.9
μ	60.3	90.8	31.5	96.7
HDKLD	31.8	89.7	27.5	90.8
BD	65.4	90.1	26.3	97.5
GMK	65.5	91.1	34.4	97.0
αGMK	74.7	91.4	36.6	97.9

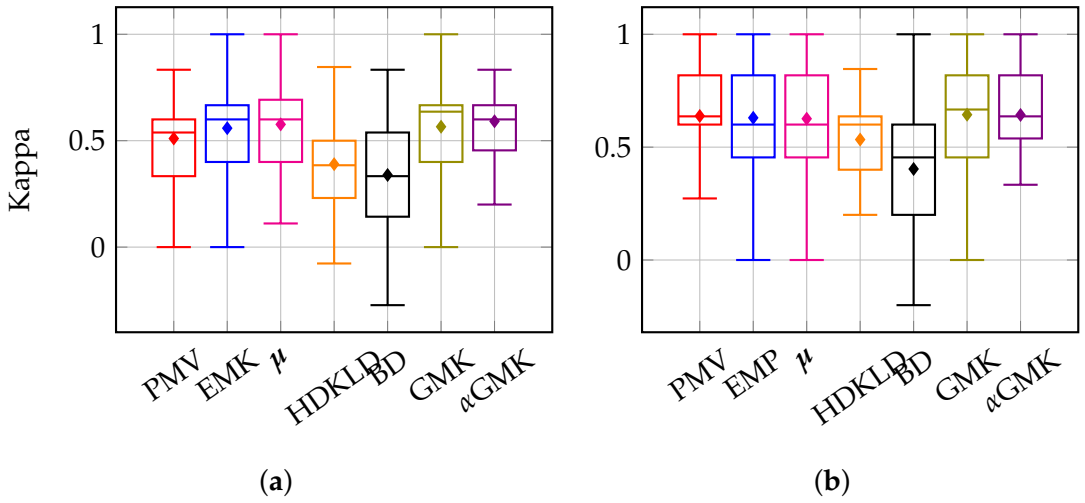

Figure C.3.: Boxplot of Kappa coefficient repartitions for classification of management practices using time series of year (**a**) 2013 and (**b**) 2014. The line in the box stands for the median whereas the dot stands for the mean.

Table C.2.: Average user accuracy (UA) and producer accuracy (PA) (%) over the 100 repetitions for each class, 1: Mowing, 2: Mixed, 3: Grazing.

	UA1	UA2	UA3	PA1	PA2	PA3
			2013			
PMV	80.5	45.5	78.7	95.4	28.5	64.0
EMK	85.5	36.3	75.5	97.5	25.0	70.0
μ	87.1	37.3	69.1	97.9	25.0	71.5
HDKLD	82.7	41.4	41.5	86.3	33.5	46.5
BD	83.5	26.0	34.3	85.3	32.5	33.0
GMK	87.2	34.8	68.8	97.4	26.5	68.5
αGMK	87.1	45.0	69.8	96.9	33.5	68.5
			2014			
PMV	88.8	53.9	81.0	97.5	49.0	63.5
EMK	86.8	51.8	86.4	94.5	41.0	80.0
μ	86.2	52.6	88.2	94.3	41.5	80.0
HDKLD	84.0	69.5	47.2	96.4	58.0	35.5
BD	80.7	56.4	45.0	86.7	50.5	37.5
GMK	87.5	54.2	87.3	94.5	46.5	78.5
αGMK	87.9	52.5	80.3	96.5	39.5	78.5

D. List of scientific productions

Peer-reviewed publications in international journals

Published

M. Lopes, M. Fauvel, A. Ouin, and S. Girard. Spectro-Temporal Heterogeneity Measures from Dense High Spatial Resolution Satellite Image Time Series: Application to Grassland Species Diversity Estimation. *Remote Sensing*, 9(10):993, 2017. Special Issue "Dense Image Time Series Analysis for Ecosystem Monitoring".

M. Lopes, M. Fauvel, S. Girard, and D. Sheeren. Object-Based Classification of Grasslands from High Resolution Satellite Image Time Series Using Gaussian Mean Map Kernels. *Remote Sensing*, 9(7):688, 2017.

D. Sheeren, M. Fauvel, V. Josipović, **M. Lopes**, C. Planque, J. Willm, and J.-F. Dejoux. Tree species classification in temperate forests using Formosat-2 satellite image time series. *Remote Sensing*, 8(9):734, 2016.

Submitted

R. Carrié, **M. Lopes**, A. Ouin, and E. Andrieu. Bee diversity in crop fields is influenced by remotely sensed nesting resources in surrounding permanent grasslands. 2017.

Proceedings of international conferences

M. Lopes, M. Fauvel, A. Ouin, and S. Girard. Potential of Sentinel-2 and SPOT5 (Take5) time series for the estimation of grasslands biodiversity indices, *2017 9th International Workshop on the Analysis of Multitemporal Remote Sensing Images (MultiTemp)*, pp. 1-4, Brugge, Belgium, 2017.

M. Lopes, M. Fauvel, S. Girard, and D. Sheeren. High dimensional Kullback-Leibler divergence for grassland management practices classification from high resolution satellite image time series, *2016 IEEE International Geoscience And Remote Sensing Symposium (IGARSS)*, pp. 3342-3345, Beijing, China, 2016.

Communications

Oral communications

M. Lopes, M. Fauvel, A. Ouin, and S. Girard. Estimation de la diversité en espèces des prairies à partir de leur hétérogénéité spectrale en utilisant des séries temporelles d'images satellite à haute résolution spatiale, *Rencontres d'Ecologie des Paysages 2017*, Toulouse, France, 2017.

M. Fauvel, **M. Lopes**, and S. Girard. Object-based classification of grassland from high resolution satellite image time series with Gaussian mean map kernels, *Journée GDR-ISIS / CCT-TSI Séries d'images multi-temporelles à haute revisite*, Toulouse, France, 2017.

S. Girard, **M. Lopes**, M. Fauvel, and D. Sheeren. Object-based classification of grassland from high resolution satellite image time series with Gaussian mean map kernels, *27th Annual Conference of the International Environmetrics Society*, Bergamo, Italy, 2017.

M. Fauvel, **M. Lopes**, A. Ouin, and S. Girard. Evaluation de la biodiversité des prairies semi-naturelles par télédétection hyperspectrale. *5ème Colloque scientifique du groupe thématique hyperspectral de la Société Française de Photogrammétrie et Télédétection*, Brest, France, 2017.

M. Lopes, S. Girard, and M. Fauvel. Divergence de Kullback-Leibler en grande dimension pour la classification des prairies à partir de séries temporelles d'images satellite à haute résolution. *48èmes Journées de Statistique de la Société Française de Stastique*, Montpellier, France, 2016.

Posters

M. Lopes, M. Fauvel, S. Girard, D. Sheeren, and M. Lang. High Dimensional Kullback-Leibler Divergence for grassland object-oriented classification from high resolution satellite image time series. *2016 European Space Agency Living Planet Symposium*, Prague, Czech Republic, 2016.

M. Lopes, M. Fauvel, S. Girard, D. Sheeren, and M. Lang. High Dimensional Kullback-Leibler Divergence for grassland object-oriented classification from high resolution satellite image time series. *4ème journée thématique du Programme National de Télédétection Spatiale*, CNES, Paris, France, 2016.

Bibliography

[Abelleira Martínez et al., 2016] Abelleira Martínez, O. J., Fremier, A. K., Günter, S., Ramos Bendaña, Z., Vierling, L., Galbraith, S. M., Bosque-Pérez, N. A., and Ordoñez, J. C. (2016). Scaling up functional traits for ecosystem services with remote sensing: concepts and methods. *Ecology and Evolution*, 6(13):4359–4371.

[Abou–moustafa and Ferrie, 2012] Abou–moustafa, K. T. and Ferrie, F. P. (2012). A note on metric properties of some divergence measures: The Gaussian case. In *Proc. of the 4th ACML, JMLR W&CP*, pages 1–15.

[Ali et al., 2016] Ali, I., Cawkwell, F., Dwyer, E., Barrett, B., and Green, S. (2016). Satellite remote sensing of grasslands: from observation to management. *Journal of Plant Ecology*, 9(6):649–671.

[Allan et al., 2015] Allan, E., Manning, P., Alt, F., Binkenstein, J., Blaser, S., Blüthgen, N., Böhm, S., Grassein, F., Hölzel, N., Klaus, V. H., Kleinebecker, T., Morris, E. K., Oelmann, Y., Prati, D., Renner, S. C., Rillig, M. C., Schaefer, M., Schloter, M., Schmitt, B., Schöning, I., Schrumpf, M., Solly, E., Sorkau, E., Steckel, J., Steffen-Dewenter, I., Stempfhuber, B., Tschapka, M., Weiner, C. N., Weisser, W. W., Werner, M., Westphal, C., Wilcke, W., and Fischer, M. (2015). Land use intensification alters ecosystem multifunctionality via loss of biodiversity and changes to functional composition. *Ecology Letters*, 18(8):834–843.

[Ansquer et al., 2009] Ansquer, P., Al Haj Khaled, R., Cruz, P., Theau, J.-P., Therond, O., and Duru, M. (2009). Characterizing and predicting plant phenology in species-rich grasslands. *Grass and Forage Science*, 64(1):57–70.

[Asam et al., 2013] Asam, S., Fabritius, H., Klein, D., Conrad, C., and Dech, S. (2013). Derivation of leaf area index for grassland within alpine upland using multi-temporal RapidEye data. *International Journal of Remote Sensing*, 34(23):8628–8652.

[Asrar et al., 1986] Asrar, G., Weiser, R., Johnson, D., Kanemasu, E., and Killeen, J. (1986). Distinguishing among tallgrass prairie cover types from measurements of multispectral reflectance. *Remote Sensing of Environment*, 19(2):159 – 169.

[Atzberger and Eilers, 2011a] Atzberger, C. and Eilers, P. H. (2011a). A time series for monitoring vegetation activity and phenology at 10-daily time steps covering large parts of south america. *International Journal of Digital Earth*, 4(5):365–386.

[Atzberger and Eilers, 2011b] Atzberger, C. and Eilers, P. H. C. (2011b). Evaluating the effectiveness of smoothing algorithms in the absence of ground reference measurements. *International Journal of Remote Sensing*, 32(13):3689–3709.

[Austrheim and Olsson, 1999] Austrheim, G. and Olsson, E. G. A. (1999). How does continuity in grassland management after ploughing affect plant community patterns? *Plant Ecology*, 145(1):59–74.

[Beck et al., 2006] Beck, P. S., Atzberger, C., Høgda, K. A., Johansen, B., and Skidmore, A. K. (2006). Improved monitoring of vegetation dynamics at very high latitudes: A new method using MODIS NDVI. *Remote Sensing of Environment*, 100(3):321 – 334.

[Biernacki et al., 2000] Biernacki, C., Celeux, G., and Govaert, G. (2000). Assessing a mixture model for clustering with the integrated completed likelihood. *IEEE Trans. Pattern Anal. Mach. Intell.*, 22(7):719–725.

[Blaschke et al., 2014] Blaschke, T., Hay, G. J., Kelly, M., Lang, S., Hofmann, P., Addink, E., Feitosa, R. Q., van der Meer, F., van der Werff, H., van Coillie, F., and Tiede, D. (2014). Geographic object-based image analysis – towards a new paradigm. *ISPRS Journal of Photogrammetry and Remote Sensing*, 87:180 – 191.

[Bock et al., 2005] Bock, M., Xofis, P., Mitchley, J., Rossner, G., and Wissen, M. (2005). Object-oriented methods for habitat mapping at multiple scales – case studies from Northern Germany and Wye Downs, UK. *Journal for Nature Conservation*, 13(2–3):75 – 89.

[Bork and Su, 2007] Bork, E. W. and Su, J. G. (2007). Integrating lidar data and multispectral imagery for enhanced classification of rangeland vegetation: A meta analysis. *Remote Sensing of Environment*, 111(1):11 – 24.

[Bottou and Lin, 2007] Bottou, L. and Lin, C.-J. (2007). Support vector machine solvers. *Large scale kernel machines*, 3(1):301–320.

[Bouveyron et al., 2007a] Bouveyron, C., Girard, S., and Schmid, C. (2007a). High-dimensional data clustering. *Computational Statistics & Data Analysis*, 52(1):502 – 519.

[Bouveyron et al., 2007b] Bouveyron, C., Girard, S., and Schmid, C. (2007b). High-dimensional discriminant analysis. *Communications in Statistics - Theory and Methods*, 36(14):2607–2623.

[Bradley et al., 2007] Bradley, B. A., Jacob, R. W., Hermance, J. F., and Mustard, J. F. (2007). A curve fitting procedure to derive inter-annual phenologies from time series of noisy satellite NDVI data. *Remote Sensing of Environment*, 106(2):137 – 145.

[Braun-Blanquet et al., 1932] Braun-Blanquet, J., Fuller, G., and Conard, H. (1932). *Plant Sociology: The Study of Plant Communities : Authorized English Translation of Pflanzensoziologie*. McGraw-Hill publications in the Botanical Sciences. McGraw-Hill.

[Bray and Curtis, 1957] Bray, J. R. and Curtis, J. T. (1957). An ordination of the upland forest communities of Southern Wisconsin. *Ecological Monographs*, 27(4):325–349.

[Brenner et al., 2012] Brenner, J. C., Christman, Z., and Rogan, J. (2012). Segmentation of Landsat Thematic Mapper imagery improves buffelgrass (pennisetum ciliare) pasture mapping in the sonoran desert of mexico. *Applied Geography*, 34:569 – 575.

[Bruun, 2000] Bruun, H. H. (2000). Patterns of species richness in dry grassland patches in an agricultural landscape. *Ecography*, 23(6):641–650.

[Buades et al., 2011] Buades, A., Coll, B., and Morel, J.-M. (2011). Non-Local Means Denoising. *Image Processing On Line*, 1.

[Buck et al., 2015] Buck, O., Millán, V. E. G., Klink, A., and Pakzad, K. (2015). Using information layers for mapping grassland habitat distribution at local to regional scales. *International Journal of Applied Earth Observation and Geoinformation*, 37:83 – 89. Special Issue on Earth observation for habitat mapping and biodiversity monitoring.

[Butchart et al., 2010] Butchart, S. H. M., Walpole, M., Collen, B., van Strien, A., Scharlemann, J. P. W., Almond, R. E. A., Baillie, J. E. M., Bomhard, B., Brown, C., Bruno, J., Carpenter, K. E., Carr, G. M., Chanson, J., Chenery, A. M., Csirke, J., Davidson, N. C., Dentener, F., Foster, M., Galli, A., Galloway, J. N., Genovesi, P., Gregory, R. D., Hockings, M., Kapos, V., Lamarque, J.-F., Leverington, F., Loh, J., McGeoch, M. A., McRae, L., Minasyan, A., Morcillo, M. H., Oldfield, T. E. E., Pauly, D., Quader, S., Revenga, C., Sauer, J. R., Skolnik, B., Spear, D., Stanwell-Smith, D., Stuart, S. N., Symes, A., Tierney, M., Tyrrell, T. D., Vié, J.-C., and Watson, R. (2010). Global biodiversity: Indicators of recent declines. *Science*, 328(5982):1164–1168.

[Cadotte et al., 2011] Cadotte, M. W., Carscadden, K., and Mirotchnick, N. (2011). Beyond species: functional diversity and the maintenance of ecological processes and services. *Journal of Applied Ecology*, 48(5):1079–1087.

[Cao et al., 2015] Cao, R., Chen, J., Shen, M., and Tang, Y. (2015). An improved logistic method for detecting spring vegetation phenology in grasslands from MODIS EVI time-series data. *Agricultural and Forest Meteorology*, 200:9 – 20.

[CaraDonna et al., 2014] CaraDonna, P. J., Iler, A. M., and Inouye, D. W. (2014). Shifts in flowering phenology reshape a subalpine plant community. *Proceedings of the National Academy of Sciences*, 111(13):4916–4921.

[Carboni et al., 2015] Carboni, M., Dengler, J., Mantilla-Contreras, J., Venn, S., and Török, P. (2015). Conversation value, management and restoration of Europe's semi-natural open landscapes. *Haquetia*, 14(1):5–17.

[Carrié et al., 2017] Carrié, R., Andrieu, E., Cunningham, S. A., Lentini, P. E., Loreau, M., and Ouin, A. (2017). Relationships among ecological traits of wild bee communities along gradients of habitat amount and fragmentation. *Ecography*, 40(1):85–97.

[Carvalho et al., 2013] Carvalho, S., Schlerf, M., van der Putten, W. H., and Skidmore, A. K. (2013). Hyperspectral reflectance of leaves and flowers of an outbreak species discriminates season and successional stage of vegetation. *International Journal of Applied Earth Observation and Geoinformation*, 24:32 – 41.

[Cha, 2007] Cha, S.-H. (2007). Comprehensive survey on distance/similarity measures between probability density functions. *International Journam of Mathematical Models and Methods in Applied Sciences*, 1(4):300–307.

[Chen et al., 2004] Chen, J., Jönsson, P., Tamura, M., Gu, Z., Matsushita, B., and Eklundh, L. (2004). A simple method for reconstructing a high-quality NDVI time-series data set based on the savitzky–golay filter. *Remote Sensing of Environment*, 91(3–4):332 – 344.

[Chen et al., 2009] Chen, J., Shen, M., Zhu, X., and Tang, Y. (2009). Indicator of flower status derived from in situ hyperspectral measurement in an alpine meadow on the tibetan plateau. *Ecological Indicators*, 9(4):818 – 823.

[Chiarucci et al., 1999] Chiarucci, A., Wilson, J. B., Anderson, B. J., and De Dominicis, V. (1999). Cover versus biomass as an estimate of species abundance: does it make a difference to the conclusions? *Journal of Vegetation Science*, 10(1):35–42.

[Cid and Brizuela, 1998] Cid, M. S. and Brizuela, M. A. (1998). Heterogeneity in tall fescue pastures created and sustained by cattle grazing. *Journal of Range Management*, 51(6):644–649.

[Cihlar and Howarth, 1994] Cihlar, J. and Howarth, J. (1994). Detection and removal of cloud contamination from AVHRR images. *IEEE Transactions on Geoscience and Remote Sensing*, 32(3):583–589.

[Cingolani et al., 2004] Cingolani, A. M., Renison, D., Zak, M. R., and Cabido, M. R. (2004). Mapping vegetation in a heterogeneous mountain rangeland using landsat

data: an alternative method to define and classify land-cover units. *Remote Sensing of Environment*, 92(1):84 – 97.

[Cleland et al., 2006] Cleland, E. E., Chiariello, N. R., Loarie, S. R., Mooney, H. A., and Field, C. B. (2006). Diverse responses of phenology to global changes in a grassland ecosystem. *Proceedings of the National Academy of Sciences*, 103(37):13740–13744.

[Clevers et al., 2007] Clevers, J., van der Heijden, G., Verzakov, S., and Schaepman, M. (2007). Estimating grassland biomass using svm band shaving of hyperspectral data. *Photogrammetric Engineering & Remote Sensing*, 73(10):1141–1148.

[Cole et al., 2006] Cole, L., Bradford, M. A., Shaw, P. J., and Bardgett, R. D. (2006). The abundance, richness and functional role of soil meso- and macrofauna in temperate grassland—a case study. *Applied Soil Ecology*, 33(2):186 – 198. Soil Biodiversity in an Upland Grassland.

[Colwell, 1974] Colwell, J. E. (1974). Vegetation canopy reflectance. *Remote Sensing of Environment*, 3(3):175 – 183.

[Corbane et al., 2013] Corbane, C., Alleaume, S., and Deshayes, M. (2013). Mapping natural habitats using remote sensing and sparse partial least square discriminant analysis. *International Journal of Remote Sensing*, 34(21):7625–7647.

[Corbane et al., 2015] Corbane, C., Lang, S., Pipkins, K., Alleaume, S., Deshayes, M., Millán, V. E. G., Strasser, T., Borre, J. V., Toon, S., and Michael, F. (2015). Remote sensing for mapping natural habitats and their conservation status – new opportunities and challenges. *International Journal of Applied Earth Observation and Geoinformation*, 37:7 – 16. Special Issue on Earth observation for habitat mapping and biodiversity monitoring.

[Cord et al., 2017] Cord, A. F., Brauman, K. A., Chaplin-Kramer, R., Huth, A., Ziv, G., and Seppelt, R. (2017). Priorities to advance monitoring of ecosystem services using earth observation. *Trends in Ecology & Evolution*, 32(6):416 – 428.

[Cortes and Vapnik, 1995] Cortes, C. and Vapnik, V. (1995). Support-vector networks. *Machine learning*, 20(3):273–297.

[Courault et al., 2010] Courault, D., Hadria, R., Ruget, F., Olioso, A., Duchemin, B., Hagolle, O., and Dedieu, G. (2010). Combined use of formosat-2 images with a crop model for biomass and water monitoring of permanent grassland in mediterranean region. *Hydrology and Earth System Sciences*, 14(9):1731–1744.

[Cousins and Eriksson, 2002] Cousins, S. A. and Eriksson, O. (2002). The influence of management history and habitat on plant species richness in a rural hemiboreal landscape, sweden. *Landscape Ecology*, 17(6):517–529.

[Critchley et al., 2004] Critchley, C., Burke, M., and Stevens, D. (2004). Conservation of lowland semi-natural grasslands in the UK: a review of botanical monitoring results from agri-environment schemes. *Biological Conservation*, 115(2):263 – 278.

[Dallery, 2016] Dallery, D. (2016). Suivi des prairies par mesures hyperspectrales et séries temporelles d'images satellitaires à haute résolution spatiale : influence des modes de gestion sur le signal spectral. Master's thesis, Université de Rennes 2.

[Darvishzadeh et al., 2008] Darvishzadeh, R., Skidmore, A., Schlerf, M., Atzberger, C., Corsi, F., and Cho, M. (2008). LAI and chlorophyll estimation for a heterogeneous grassland using hyperspectral measurements. *ISPRS Journal of Photogrammetry and Remote Sensing*, 63(4):409 – 426.

[Ding et al., 2014] Ding, Y., Zhao, K., Zheng, X., and Jiang, T. (2014). Temporal dynamics of spatial heterogeneity over cropland quantified by time-series NDVI, near infrared and red reflectance of Landsat 8 OLI imagery. *International Journal of Applied Earth Observation and Geoinformation*, 30:139 – 145.

[Donoho, 2000] Donoho, D. L. (2000). High-dimensional data analysis: The curses and blessings of dimensionality. In *AMS Conference on math challenges of the 21st century*.

[Drusch et al., 2012] Drusch, M., Bello, U. D., Carlier, S., Colin, O., Fernandez, V., Gascon, F., Hoersch, B., Isola, C., Laberinti, P., Martimort, P., Meygret, A., Spoto, F., Sy, O., Marchese, F., and Bargellini, P. (2012). Sentinel-2: ESA's optical high-resolution mission for GMES operational services. *Remote Sensing of Environment*, 120:25 – 36. The Sentinel Missions - New Opportunities for Science.

[Duniway et al., 2012] Duniway, M. C., Karl, J. W., Schrader, S., Baquera, N., and Herrick, J. E. (2012). Rangeland and pasture monitoring: an approach to interpretation of high-resolution imagery focused on observer calibration for repeatability. *Environmental Monitoring and Assessment*, 184(6):3789–3804.

[Duro et al., 2007] Duro, D. C., Coops, N. C., Wulder, M. A., and Han, T. (2007). Development of a large area biodiversity monitoring system driven by remote sensing. *Progress in Physical Geography*, 31(3):235–260.

[Duro et al., 2012] Duro, D. C., Franklin, S. E., and Dubé, M. G. (2012). A comparison of pixel-based and object-based image analysis with selected machine learning algorithms for the classification of agricultural landscapes using SPOT-5 HRG imagery. *Remote Sensing of Environment*, 118:259 – 272.

[Duru et al., 2005] Duru, M., Tallowin, J., and Cruz, P. (2005). Functional diversity in low-input grassland farming systems: characterisation, effect and management. *Agronomy Research*, 3(2):125–138.

[Dusseux et al., 2014a] Dusseux, P., Corpetti, T., Hubert-Moy, L., and Corgne, S. (2014a). Combined use of multi-temporal optical and radar satellite images for grassland monitoring. *Remote Sensing*, 6(7):6163–6182.

[Dusseux et al., 2014b] Dusseux, P., Vertès, F., Corpetti, T., Corgne, S., and Hubert-Moy, L. (2014b). Agricultural practices in grasslands detected by spatial remote sensing. *Environmental Monitoring and Assessment*, 186(12):8249–8265.

[Dusseux et al., 2014c] Dusseux, P., Xing, G., Hubert-Moy, L. L., and Corpetti, T. (2014c). Identification of grassland management practices from leaf area index time series. *Journal of applied remote sensing*, 8(1):083559.

[Eilers, 2003] Eilers, P. H. C. (2003). A perfect smoother. *Analytical Chemistry*, 75(14):3631–3636. PMID: 14570219.

[Eriksson et al., 1995] Eriksson, A., Eriksson, O., and Berglund, H. (1995). Species abundance patterns of plants in Swedish semi-natural pastures. *Ecography*, 18(3):310–317.

[Eriksson et al., 2002] Eriksson, O., Cousins, S. A., and Bruun, H. H. (2002). Land-use history and fragmentation of traditionally managed grasslands in scandinavia. *Journal of Vegetation Science*, 13(5):743–748.

[Esch et al., 2014] Esch, T., Metz, A., Marconcini, M., and Keil, M. (2014). Combined use of multi-seasonal high and medium resolution satellite imagery for parcel-related mapping of cropland and grassland. *International Journal of Applied Earth Observation and Geoinformation*, 28:230 – 237.

[Eurostat, 2010] Eurostat (2010). Agricultural statistics - main results - 2008-09. Technical report, European Commission.

[Evans and Geerken, 2006] Evans, J. and Geerken, R. (2006). Classifying rangeland vegetation type and coverage using a Fourier component based similarity measure. *Remote Sensing of Environment*, 105(1):1 – 8.

[Fahrig et al., 2011] Fahrig, L., Baudry, J., Brotons, L., Burel, F. G., Crist, T. O., Fuller, R. J., Sirami, C., Siriwardena, G. M., and Martin, J.-L. (2011). Functional landscape heterogeneity and animal biodiversity in agricultural landscapes. *Ecology Letters*, 14(2):101–112.

[Fairbanks and McGwire, 2004] Fairbanks, D. H. K. and McGwire, K. C. (2004). Patterns of floristic richness in vegetation communities of California: Regional scale analysis with multi-temporal NDVI. *Global Ecology and Biogeography*, 13(3):221–235.

[Fan and Gijbels, 1996] Fan, J. and Gijbels, I. (1996). *Local Polynomial Modelling and Its Applications: Monographs on Statistics and Applied Probability 66*. Chapman & Hall/CRC Monographs on Statistics & Applied Probability. Taylor & Francis.

[Fauvel et al., 2013] Fauvel, M., Tarabalka, Y., Benediktsson, J. A., Chanussot, J., and Tilton, J. C. (2013). Advances in spectral-spatial classification of hyperspectral images. *Proceedings of the IEEE*, 101(3):652–675.

[Fava et al., 2010] Fava, F., Parolo, G., Colombo, R., Gusmeroli, F., Marianna, G. D., Monteiro, A., and Bocchi, S. (2010). Fine-scale assessment of hay meadow productivity and plant diversity in the European Alps using field spectrometric data. *Agriculture, Ecosystems & Environment*, 137(1–2):151 – 157. Special section Harvested perennial grasslands: Ecological models for farming's perennial future.

[Feilhauer et al., 2016] Feilhauer, H., Doktor, D., Schmidtlein, S., and Skidmore, A. K. (2016). Mapping pollination types with remote sensing. *Journal of Vegetation Science*, 27(5):999–1011.

[Feilhauer et al., 2011] Feilhauer, H., Faude, U., and Schmidtlein, S. (2011). Combining isomap ordination and imaging spectroscopy to map continuous floristic gradients in a heterogeneous landscape. *Remote Sensing of Environment*, 115(10):2513 – 2524.

[Feilhauer et al., 2013] Feilhauer, H., Thonfeld, F., Faude, U., He, K. S., Rocchini, D., and Schmidtlein, S. (2013). Assessing floristic composition with multispectral sensors—a comparison based on monotemporal and multiseasonal field spectra. *International Journal of Applied Earth Observation and Geoinformation*, 21:218 – 229.

[Foerster et al., 2012] Foerster, S., Kaden, K., Foerster, M., and Itzerott, S. (2012). Crop type mapping using spectral–temporal profiles and phenological information. *Computers and Electronics in Agriculture*, 89:30 – 40.

[Fontana et al., 2008] Fontana, F., Rixen, C., Jonas, T., Aberegg, G., and Wunderle, S. (2008). Alpine grassland phenology as seen in AVHRR, VEGETATION, and MODIS NDVI time series - a comparison with in situ measurements. *Sensors*, 8(4):2833–2853.

[Frampton et al., 2013] Frampton, W. J., Dash, J., Watmough, G., and Milton, E. J. (2013). Evaluating the capabilities of Sentinel-2 for quantitative estimation of biophysical variables in vegetation. *ISPRS Journal of Photogrammetry and Remote Sensing*, 82:83 – 92.

[Franke et al., 2012] Franke, J., Keuck, V., and Siegert, F. (2012). Assessment of grassland use intensity by remote sensing to support conservation schemes. *Journal for Nature Conservation*, 20(3):125 – 134.

[Franzén and Eriksson, 2001] Franzén, D. and Eriksson, O. (2001). Small-scale patterns of species richness in Swedish semi-natural grasslands: the effects of community species pools. *Ecography*, 24(5):505–510.

[Friedl et al., 1994] Friedl, M. A., Michaelsen, J., Davis, F. W., Walker, H., and Schimel, D. S. (1994). Estimating grassland biomass and Leaf Area Index using ground and satellite data. *International Journal of Remote Sensing*, 15(7):1401–1420.

[Féret and Asner, 2014] Féret, J.-B. and Asner, G. P. (2014). Mapping tropical forest canopy diversity using high-fidelity imaging spectroscopy. *Ecological Applications*, 24(6):1289–1296.

[Gamon et al., 1993] Gamon, J. A., Field, C. B., Roberts, D. A., Ustin, S. L., and Valentini, R. (1993). Airbone imaging spectrometry functional patterns in an annual grassland during an AVIRIS overflight. *Remote Sensing of Environment*, 44(2):239 – 253.

[Gardi et al., 2002] Gardi, C., Tomaselli, M., Parisi, V., Petraglia, A., and Santini, C. (2002). Soil quality indicators and biodiversity in northern italian permanent grasslands. *European Journal of Soil Biology*, 38(1):103 – 110.

[Girard and Saracco, 2016] Girard, S. and Saracco, J. (2016). Supervised and Unsupervised Classification Using Mixture Models. In *EAS Publications Series*, volume 77 of *EAS Publications Series*, pages 69–90.

[Gitelson and Merzlyak, 1994] Gitelson, A. and Merzlyak, M. N. (1994). Spectral Reflectance Changes Associated with Autumn Senescence of Aesculus hippocastanum L. and Acer platanoides L. Leaves. Spectral Features and Relation to Chlorophyll Estimation. *Journal of Plant Physiology*, 143(3):286 – 292.

[Gomez-Chova et al., 2010] Gomez-Chova, L., Camps-Valls, G., Bruzzone, L., and Calpe-Maravilla, J. (2010). Mean map kernel methods for semisupervised cloud classification. *IEEE Transactions on Geoscience and Remote Sensing*, 48(1):207–220.

[Gould, 2000] Gould, W. (2000). Remote sensing of vegetation, plant species richness, and regional biodiversity hotspots. *Ecological Applications*, 10(6):1861–1870.

[Goward et al., 1991] Goward, S. N., Markham, B., Dye, D. G., Dulaney, W., and Yang, J. (1991). Normalized difference vegetation index measurements from the advanced very high resolution radiometer. *Remote Sensing of Environment*, 35(2):257 – 277.

[Groom et al., 2006] Groom, G., Mücher, C. A., Ihse, M., and Wrbka, T. (2006). Remote sensing in landscape ecology: Experiences and perspectives in a European context. *Landscape Ecology*, 21(3):391–408.

[Grytnes, 2000] Grytnes, J. A. (2000). Fine-scale vascular plant species richness in different alpine vegetation types: relationships with biomass and cover. *Journal of Vegetation Science*, 11(1):87–92.

[Gu and Wylie, 2015] Gu, Y. and Wylie, B. K. (2015). Developing a 30-m grassland productivity estimation map for central Nebraska using 250-m MODIS and 30-m Landsat-8 observations. *Remote Sensing of Environment*, 171:291 – 298.

[Gu et al., 2013] Gu, Y., Wylie, B. K., and Bliss, N. B. (2013). Mapping grassland productivity with 250-m eMODIS NDVI and SSURGO database over the greater platte river basin, USA. *Ecological Indicators*, 24:31 – 36.

[Gómez Giménez et al., 2017] Gómez Giménez, M., de Jong, R., Della Peruta, R., Keller, A., and Schaepman, M. E. (2017). Determination of grassland use intensity based on multi-temporal remote sensing data and ecological indicators. *Remote Sensing of Environment*, 198:126 – 139.

[Haasdonk and Bahlmann, 2004] Haasdonk, B. and Bahlmann, C. (2004). Learning with distance substitution kernels. In Rasmussen, C., Bülthoff, H., Schölkopf, B., and Giese, M., editors, *Pattern Recognition*, volume 3175 of *Lecture Notes in Computer Science*, pages 220–227. Springer Berlin Heidelberg.

[Hagolle et al., 2010] Hagolle, O., Huc, M., Villa Pascual, D., and Dedieu, G. (2010). A multi-temporal method for cloud detection, applied to FORMOSAT-2, VENuS, LANDSAT and SENTINEL-2 images. *Remote Sensing of Environment*, 114(8):1747–1755.

[Halabuk et al., 2015] Halabuk, A., Mojses, M., Halabuk, M., and David, S. (2015). Towards detection of cutting in hay meadows by using of NDVI and EVI time series. *Remote Sensing*, 7(5):6107.

[Hall et al., 2012] Hall, K., Reitalu, T., Sykes, M. T., and Prentice, H. C. (2012). Spectral heterogeneity of QuickBird satellite data is related to fine-scale plant species spatial turnover in semi-natural grasslands. *Applied Vegetation Science*, 15(1):145–157.

[Hansson and Fogelfors, 2000] Hansson, M. and Fogelfors, H. (2000). Management of a semi-natural grassland; results from a 15-year-old experiment in southern Sweden. *Journal of Vegetation Science*, 11(1):31–38.

[Hastie and Tibshirani, 1986] Hastie, T. and Tibshirani, R. (1986). Generalized additive models. *Statistical Science*, 1(3):297–310.

[Hastie et al., 2009] Hastie, T., Tibshirani, R., and Friedman, J. (2009). *The Elements of Statistical Learning*. Springer-Verlag New York.

[He et al., 2009] He, Y., Guo, X., and Wilmshurst, J. F. (2009). Reflectance measures of grassland biophysical structure. *International Journal of Remote Sensing*, 30(10):2509–2521.

[Hermance et al., 2007] Hermance, J. F., Jacob, R. W., Bradley, B. A., and Mustard, J. F. (2007). Extracting phenological signals from multiyear AVHRR NDVI time series: Framework for applying high-order annual splines with roughness damping. *IEEE Transactions on Geoscience and Remote Sensing*, 45(10):3264–3276.

[Hilker et al., 2014] Hilker, T., Natsagdorj, E., Waring, R. H., Lyapustin, A., and Wang, Y. (2014). Satellite observed widespread decline in Mongolian grasslands largely due to overgrazing. *Global Change Biology*, 20(2):418–428.

[Hill, 2013] Hill, M. J. (2013). Vegetation index suites as indicators of vegetation state in grassland and savanna: An analysis with simulated SENTINEL-2 data for a North American transect. *Remote Sensing of Environment*, 137:94 – 111.

[Hird and McDermid, 2009] Hird, J. N. and McDermid, G. J. (2009). Noise reduction of NDVI time series: An empirical comparison of selected techniques. *Remote Sensing of Environment*, 113(1):248 – 258.

[Homolová et al., 2013] Homolová, L., Malenovský, Z., Clevers, J. G., García-Santos, G., and Schaepman, M. E. (2013). Review of optical-based remote sensing for plant trait mapping. *Ecological Complexity*, 15:1 – 16.

[Hönigová et al., 2012] Hönigová, I., Vačkář, D., Lorencová, E., Melichar, J., Götzl, M., Sonderegger, G., Oušková, V., Hošek, M., and Chobot, K. (2012). Survey on grassland ecosystem services. *Report to the EEA–European Topic Centre on Biological Diversity. Prague: Nature Conservation Agency of the Czech Republic*, page 78.

[Hooper, 1998] Hooper, D. U. (1998). The role of complementarity and competition in ecosystem responses to variation in plant diversity. *Ecology*, 79(2):704–719.

[Huete et al., 2002] Huete, A., Didan, K., Miura, T., Rodriguez, E., Gao, X., and Ferreira, L. (2002). Overview of the radiometric and biophysical performance of the modis vegetation indices. *Remote Sensing of Environment*, 83(1):195 – 213. The Moderate Resolution Imaging Spectroradiometer (MODIS): a new generation of Land Surface Monitoring.

[Huete et al., 1985] Huete, A., Jackson, R., and Post, D. (1985). Spectral response of a plant canopy with different soil backgrounds. *Remote Sensing of Environment*, 17(1):37 – 53.

[Huete et al., 1999] Huete, A., Justice, C., and Leeuwen, W. (1999). MODIS vegetation index (MOD 13). Algorithm theoretical basis document ATBD13.

[Inglada et al., 2015] Inglada, J., Arias, M., Tardy, B., Hagolle, O., Valero, S., Morin, D., Dedieu, G., Sepulcre, G., Bontemps, S., Defourny, P., and Koetz, B. (2015). Assessment of an operational system for crop type map production using high temporal and spatial resolution satellite optical imagery. *Remote Sensing*, 7(9):12356–12379.

[Ishii et al., 2009] Ishii, J., Lu, S., Funakoshi, S., Shimizu, Y., Omasa, K., and Washitani, I. (2009). Mapping potential habitats of threatened plant species in a moist tall grassland using hyperspectral imagery. *Biodiversity and Conservation*, 18(9):2521–2535.

[Jackson and Huete, 1991] Jackson, R. D. and Huete, A. R. (1991). Interpreting vegetation indices. *Preventive Veterinary Medicine*, 11(3):185 – 200.

[Jetz et al., 2016] Jetz, W., Cavender-Bares, J., Pavlick, R., Schimel, D., Davis, F. W., Asner, G. P., Guralnick, R., Kattge, J., Latimer, A. M., Moorcroft, P., Schaepman, M. E., Schildhauer, M. P., Schneider, F. D., Schrodt, F., Stahl, U., and Ustin, S. L. (2016). Monitoring plant functional diversity from space. *Nature plants*, 2(3).

[Jönsson and Eklundh, 2004] Jönsson, P. and Eklundh, L. (2004). TIMESAT—a program for analyzing time-series of satellite sensor data. *Computers & Geosciences*, 30(8):833 – 845.

[Kawamura et al., 2005] Kawamura, K., Akiyama, T., omi Yokota, H., Tsutsumi, M., Yasuda, T., Watanabe, O., and Wang, S. (2005). Quantifying grazing intensities using geographic information systems and satellite remote sensing in the Xilingol steppe region, Inner Mongolia, China. *Agriculture, Ecosystems & Environment*, 107(1):83 – 93.

[Kerr and Ostrovsky, 2003] Kerr, J. T. and Ostrovsky, M. (2003). From space to species: ecological applications for remote sensing. *Trends in Ecology & Evolution*, 18(6):299 – 305.

[Klumpp et al., 2011] Klumpp, K., Tallec, T., Guix, N., and Soussana, J.-F. (2011). Long-term impacts of agricultural practices and climatic variability on carbon storage in a permanent pasture. *Global Change Biology*, 17(12):3534–3545.

[Kohler et al., 2006] Kohler, F., Gillet, F., Gobat, J.-M., and Buttler, A. (2006). Effect of cattle activities on gap colonization in mountain pastures. *Folia Geobotanica*, 41(3):289–304.

[Kullback, 1987] Kullback, S. (1987). Letter to the editor: The Kullback-Leibler distance. *The American Statistician*, 41(4):340–341.

[Lagrange et al., 2017] Lagrange, A., Fauvel, M., and Grizonnet, M. (2017). Large-scale feature selection with gaussian mixture models for the classification of high dimensional remote sensing images. *IEEE Transactions on Computational Imaging*, 3(2):230–242.

[Laliberte et al., 2007] Laliberte, A. S., Fredrickson, E. L., and Rango, A. (2007). Combining decision trees with hierarchical object-oriented image analysis for mapping arid rangelands. *Photogrammetric engineering & Remote sensing*, 73(2):197–207.

[Landmann et al., 2015] Landmann, T., Piiroinen, R., Makori, D. M., Abdel-Rahman, E. M., Makau, S., Pellikka, P., and Raina, S. K. (2015). Application of hyperspectral remote sensing for flower mapping in african savannas. *Remote Sensing of Environment*, 166:50 – 60.

[Ledoit and Wolf, 2004] Ledoit, O. and Wolf, M. (2004). A well-conditioned estimator for large-dimensional covariance matrices. *Journal of Multivariate Analysis*, 88(2):365 – 411.

[Li et al., 2013] Li, Z., Huffman, T., McConkey, B., and Townley-Smith, L. (2013). Monitoring and modeling spatial and temporal patterns of grassland dynamics using time-series MODIS NDVI with climate and stocking data. *Remote Sensing of Environment*, 138:232 – 244.

[Liu and Huete, 1995] Liu, H. Q. and Huete, A. (1995). A feedback based modification of the ndvi to minimize canopy background and atmospheric noise. *IEEE Transactions on Geoscience and Remote Sensing*, 33(2):457–465.

[Liu et al., 2008] Liu, W., Pokharel, P. P., and Principe, J. C. (2008). The kernel least-mean-square algorithm. *IEEE Transactions on Signal Processing*, 56(2):543–554.

[Lopatin et al., 2017] Lopatin, J., Fassnacht, F. E., Kattenborn, T., and Schmidtlein, S. (2017). Mapping plant species in mixed grassland communities using close range imaging spectroscopy. *Remote Sensing of Environment*, 201:12 – 23.

[Lopes et al., 2016] Lopes, M., Fauvel, M., Girard, S., and Sheeren, D. (2016). High dimensional Kullback-Leibler divergence for grassland management practices classification from high resolution satellite image time series. In *2016 IEEE International Geoscience and Remote Sensing Symposium (IGARSS)*, pages 3342–3345.

[Losvik, 1991] Losvik, M. H. (1991). A hay meadow in western Norway-changes in the course of a growing season. *Nordic Journal of Botany*, 11(5):577–586.

[Louault et al., 2005] Louault, F., Pillar, V., Aufrère, J., Garnier, E., and Soussana, J.-F. (2005). Plant traits and functional types in response to reduced disturbance in a semi-natural grassland. *Journal of Vegetation Science*, 16(2):151–160.

[Lu, 2006] Lu, D. (2006). The potential and challenge of remote sensing-based biomass estimation. *International Journal of Remote Sensing*, 27(7):1297–1328.

[Lucas et al., 2007] Lucas, R., Rowlands, A., Brown, A., Keyworth, S., and Bunting, P. (2007). Rule-based classification of multi-temporal satellite imagery for habitat and agricultural land cover mapping. *ISPRS Journal of Photogrammetry and Remote Sensing*, 62(3):165 – 185.

[Maeda et al., 2014] Maeda, E. E., Heiskanen, J., Thijs, K. W., and Pellikka, P. K. (2014). Season-dependence of remote sensing indicators of tree species diversity. *Remote Sensing Letters*, 5(5):404–412.

[Magurran, 1988] Magurran, A. (1988). *Ecological Diversity and Its Measurement*. Croom Helm.

[Magurran, 2004] Magurran, A. (2004). *Measuring Biological Diversity*. Wiley.

[Mašková et al., 2008] Mašková, Z., Zemek, F., and Květ, J. (2008). Normalized difference vegetation index (NDVI) in the management of mountain meadows. *Boreal environment research*, 13(5).

[McCoy, 2004] McCoy, R. (2004). *Field Methods in Remote Sensing*. Guilford Publications.

[Mehta and Gray, 2010] Mehta, N. A. and Gray, A. G. (2010). Generative and latent mean map kernels. *CoRR*, abs/1005.0188.

[Melgani, 2006] Melgani, F. (2006). Contextual reconstruction of cloud-contaminated multitemporal multispectral images. *IEEE Transactions on Geoscience and Remote Sensing*, 44(2):442–455.

[Merzlyak et al., 1999] Merzlyak, M. N., Gitelson, A. A., Chivkunova, O. B., and Rakitin, V. Y. (1999). Non-destructive optical detection of pigment changes during leaf senescence and fruit ripening. *Physiologia Plantarum*, 106(1):135–141.

[Millennium Ecosystems Assessment, 2005] Millennium Ecosystems Assessment (2005). *Ecosystems and Human Well-Being*, volume 2005. World Ressource Institute, Washington, DC.

[Mitchell, 1997] Mitchell, T. M. (1997). *Machine Learning*. McGraw-Hill, Inc., New York, NY, USA, 1 edition.

[Moody and Johnson, 2001] Moody, A. and Johnson, D. M. (2001). Land-surface phenologies from AVHRR using the discrete fourier transform. *Remote Sensing of Environment*, 75(3):305 – 323.

[Moog et al., 2002] Moog, D., Poschlod, P., Kahmen, S., and Schreiber, K.-F. (2002). Comparison of species composition between different grassland management treatments after 25 years. *Applied Vegetation Science*, 5(1):99–106.

[Muandet et al., 2012] Muandet, K., Fukumizu, K., Dinuzzo, F., and Schölkopf, B. (2012). Learning from distributions via support measure machines. In *Advances in neural information processing systems*, pages 10–18.

[Muller, 2002] Muller, S. (2002). Appropriate agricultural management practices required to ensure conservation and biodiversity of environmentally sensitive grassland sites designated under Natura 2000. *Agriculture, Ecosystems & Environment*, 89(3):261 – 266.

[Myneni et al., 1995] Myneni, R. B., Hall, F. G., Sellers, P. J., and Marshak, A. L. (1995). The interpretation of spectral vegetation indexes. *IEEE Transactions on Geoscience and Remote Sensing*, 33(2):481–486.

[Möckel et al., 2014] Möckel, T., Dalmayne, J., Prentice, H. C., Eklundh, L., Purschke, O., Schmidtlein, S., and Hall, K. (2014). Classification of grassland successional stages using airborne hyperspectral imagery. *Remote Sensing*, 6(8):7732.

[Möckel et al., 2016] Möckel, T., Dalmayne, J., Schmid, B. C., Prentice, H. C., and Hall, K. (2016). Airborne hyperspectral data predict fine-scale plant species diversity in grazed dry grasslands. *Remote Sensing*, 8(2).

[Müller et al., 2015] Müller, H., Rufin, P., Griffiths, P., Siqueira, A. J. B., and Hostert, P. (2015). Mining dense Landsat time series for separating cropland and pasture in a heterogeneous Brazilian savanna landscape. *Remote Sensing of Environment*, 156:490 – 499.

[Nagendra, 2001] Nagendra, H. (2001). Using remote sensing to assess biodiversity. *International Journal of Remote Sensing*, 22(12):2377–2400.

[Nagendra et al., 2013] Nagendra, H., Lucas, R., Honrado, J. P., Jongman, R. H., Tarantino, C., Adamo, M., and Mairota, P. (2013). Remote sensing for conservation monitoring: Assessing protected areas, habitat extent, habitat condition, species diversity, and threats. *Ecological Indicators*, 33:45 – 59. Biodiversity Monitoring.

[Newton et al., 2009] Newton, A. C., Hill, R. A., Echeverría, C., Golicher, D., Rey Benayas, J. M., Cayuela, L., and Hinsley, S. A. (2009). Remote sensing and the future of landscape ecology. *Progress in Physical Geography*, 33(4):528–546.

[Neyrinck et al., 2009] Neyrinck, M. C., Szapudi, I., and Szalay, A. S. (2009). Rejuvenating the matter power spectrum: Restoring information with a logarithmic density mapping. *The Astrophysical Journal Letters*, 698(2):L90.

[Nitze et al., 2015] Nitze, I., Barrett, B., and Cawkwell, F. (2015). Temporal optimisation of image acquisition for land cover classification with random forest and MODIS time-series. *International Journal of Applied Earth Observation and Geoinformation*, 34:136 – 146.

[Norderhaug et al., 2000] Norderhaug, A., Ihse, M., and Pedersen, O. (2000). Biotope patterns and abundance of meadow plant species in a norwegian rural landscape. *Landscape Ecology*, 15(3):201–218.

[Numata et al., 2007] Numata, I., Roberts, D. A., Chadwick, O. A., Schimel, J., Sampaio, F. R., Leonidas, F. C., and Soares, J. V. (2007). Characterization of pasture biophysical properties and the impact of grazing intensity using remotely sensed data. *Remote Sensing of Environment*, 109(3):314 – 327.

[Odenweller and Johnson, 1984] Odenweller, J. B. and Johnson, K. I. (1984). Crop identification using landsat temporal-spectral profiles. *Remote Sensing of Environment*, 14(1):39 – 54.

[Oindo and Skidmore, 2002] Oindo, B. O. and Skidmore, A. K. (2002). Interannual variability of NDVI and species richness in Kenya. *International Journal of Remote Sensing*, 23(2):285–298.

[Oldeland et al., 2010] Oldeland, J., Wesuls, D., Rocchini, D., Schmidt, M., and Jürgens, N. (2010). Does using species abundance data improve estimates of species diversity from remotely sensed spectral heterogeneity? *Ecological Indicators*, 10(2):390 – 396.

[O'Mara, 2012] O'Mara, F. P. (2012). The role of grasslands in food security and climate change. *Annals of Botany*, 110(6):1263.

[Ovalle et al., 2006] Ovalle, C., Del Pozo, A., Casado, M. A., Acosta, B., and de Miguel, J. M. (2006). Consequences of landscape heterogeneity on grassland diversity and productivity in the Espinal Agroforestry System of Central Chile. *Landscape Ecology*, 21(4):585–594.

[Palmer et al., 2002] Palmer, M. W., Earls, P. G., Hoagland, B. W., White, P. S., and Wohlgemuth, T. (2002). Quantitative tools for perfecting species lists. *Environmetrics*, 13(2):121–137.

[Pan et al., 2015] Pan, Z., Huang, J., Zhou, Q., Wang, L., Cheng, Y., Zhang, H., Blackburn, G. A., Yan, J., and Liu, J. (2015). Mapping crop phenology using NDVI time-series derived from HJ-1 A/B data. *International Journal of Applied Earth Observation and Geoinformation*, 34:188 – 197.

[Parsons et al., 2004] Parsons, L., Haque, E., and Liu, H. (2004). Subspace clustering for high dimensional data: A review. *SIGKDD Explor. Newsl.*, 6(1):90–105.

[Paudel and Andersen, 2010] Paudel, K. P. and Andersen, P. (2010). Assessing rangeland degradation using multi temporal satellite images and grazing pressure surface model in upper mustang, trans himalaya, nepal. *Remote Sensing of Environment*, 114(8):1845 – 1855.

[Pedregosa et al., 2011] Pedregosa, F., Varoquaux, G., Gramfort, A., Michel, V., Thirion, B., Grisel, O., Blondel, M., Prettenhofer, P., Weiss, R., Dubourg, V., Vanderplas, J., Passos, A., Cournapeau, D., Brucher, M., Perrot, M., and Duchesnay, E. (2011). Scikit-learn: Machine learning in Python. *Journal of Machine Learning Research*, 12:2825–2830.

[Peeters, 2009] Peeters, A. (2009). Importance, evolution, environmental impact and future challenges of grasslands and grassland-based systems in Europe. *Grassland Science*, 55(3):113–125.

[Peñuelas and Filella, 1998] Peñuelas, J. and Filella, I. (1998). Visible and near-infrared reflectance techniques for diagnosing plant physiological status. *Trends in Plant Science*, 3(4):151–156.

[Peterson and Aunap, 1998] Peterson, U. and Aunap, R. (1998). Changes in agricultural land use in Estonia in the 1990s detected with multitemporal Landsat MSS imagery. *Landscape and Urban Planning*, 41(3):193 – 201.

[Pettorelli et al., 2014] Pettorelli, N., Laurance, W. F., O'Brien, T. G., Wegmann, M., Nagendra, H., and Turner, W. (2014). Satellite remote sensing for applied ecologists: opportunities and challenges. *Journal of Applied Ecology*, 51(4):839–848.

[Plantureux et al., 2005] Plantureux, S., Peeters, A., and McCracken, D. (2005). Biodiversity in intensive grasslands: Effect of management, improvement and challenges. *Agronomy Research*, 3(2):153–164.

[Poças et al., 2012] Poças, I., Cunha, M., and Pereira, L. S. (2012). Dynamics of mountain semi-natural grassland meadows inferred from SPOT-VEGETATION and field spectroradiometer data. *International Journal of Remote Sensing*, 33(14):4334–4355.

[Price, 1994] Price, J. C. (1994). How unique are spectral signatures? *Remote Sensing of Environment*, 49(3):181 – 186.

[Price et al., 2002] Price, K. P., Guo, X., and Stiles, J. M. (2002). Optimal Landsat TM band combinations and vegetation indices for discrimination of six grassland types in eastern kansas. *International Journal of Remote Sensing*, 23(23):5031–5042.

[Psomas et al., 2011] Psomas, A., Kneubuhler, M., Huber, S., Itten, K., and Zimmermann, N. E. (2011). Hyperspectral remote sensing for estimating aboveground biomassand for exploring species richness patterns of grassland habitats. *International Journal of Remote Sensing*, 32:9007–9031.

[Punalekar et al., 2016] Punalekar, S., Verhoef, A., Tatarenko, I. V., van der Tol, C., Macdonald, D. M. J., Marchant, B., Gerard, F., White, K., and Gowing, D. (2016). Characterization of a highly biodiverse floodplain meadow using hyperspectral remote sensing within a plant functional trait framework. *Remote Sensing*, 8(2):112.

[Pärtel and Zobel, 1999] Pärtel, M. and Zobel, M. (1999). Small-scale plant species richness in calcareous grasslands determined by the species pool, community age and shoot density. *Ecography*, 22(2):153–159.

[Qi et al., 1994] Qi, J., Chehbouni, A., Huete, A., Kerr, Y., and Sorooshian, S. (1994). A modified soil adjusted vegetation index. *Remote Sensing of Environment*, 48(2):119 – 126.

[Reed et al., 1994] Reed, B. C., Brown, J. F., VanderZee, D., Loveland, T. R., Merchant, J. W., and Ohlen, D. O. (1994). Measuring phenological variability from satellite imagery. *Journal of Vegetation Science*, 5(5):703–714.

[Richards and Jia, 1999] Richards, J. A. and Jia, X. (1999). *Remote Sensing Digital Image Analysis: An Introduction*. Springer-Verlag New York, Inc., Secaucus, NJ, USA, 3rd edition.

[Richardson et al., 2013] Richardson, A. D., Keenan, T. F., Migliavacca, M., Ryu, Y., Sonnentag, O., and Toomey, M. (2013). Climate change, phenology, and phenological control of vegetation feedbacks to the climate system. *Agricultural and Forest Meteorology*, 169:156 – 173.

[Robinson and Sutherland, 2002] Robinson, R. A. and Sutherland, W. J. (2002). Post-war changes in arable farming and biodiversity in great britain. *Journal of Applied Ecology*, 39(1):157–176.

[Rocchini, 2007] Rocchini, D. (2007). Effects of spatial and spectral resolution in estimating ecosystem α-diversity by satellite imagery. *Remote Sensing of Environment*, 111(4):423 – 434.

[Rocchini et al., 2010] Rocchini, D., Balkenhol, N., Carter, G. A., Foody, G. M., Gillespie, T. W., He, K. S., Kark, S., Levin, N., Lucas, K., Luoto, M., Nagendra, H., Oldeland, J., Ricotta, C., Southworth, J., and Neteler, M. (2010). Remotely sensed spectral heterogeneity as a proxy of species diversity: Recent advances and open challenges. *Ecological Informatics*, 5(5):318 – 329. Special Issue on Advances of Ecological Remote Sensing Under Global Change.

[Rocchini et al., 2016] Rocchini, D., Boyd, D. S., Féret, J.-B., Foody, G. M., He, K. S., Lausch, A., Nagendra, H., Wegmann, M., and Pettorelli, N. (2016). Satellite remote sensing to monitor species diversity: potential and pitfalls. *Remote Sensing in Ecology and Conservation*, 2(1):25–36.

[Rouse et al., 1973] Rouse, J. W., Haas, R. H., Schell, J. A., and Deering, D. W. (1973). Monitoring vegetation systems in the Great Plains with ERTS. In *Proceedings of the Third ERTS Symposium*, volume 1, pages 309–317. NASA.

[Ryschawy et al., 2012] Ryschawy, J., Choisis, N., Choisis, J. P., Joannon, A., and Gibon, A. (2012). Mixed crop-livestock systems: an economic and environmental-friendly way of farming? *Animal*, 6(10):1722–1730.

[Sakai, 2001] Sakai, S. (2001). Phenological diversity in tropical forests. *Population Ecology*, 43(1):77–86.

[Sakamoto et al., 2005] Sakamoto, T., Yokozawa, M., Toritani, H., Shibayama, M., Ishitsuka, N., and Ohno, H. (2005). A crop phenology detection method using time-series MODIS data. *Remote Sensing of Environment*, 96(3–4):366 – 374.

[Sala and Paruelo, 1997] Sala, O. E. and Paruelo, J. M. (1997). Ecosystem services in grasslands. *Nature's services: Societal dependence on natural ecosystems*, pages 237–251.

[Schimel et al., 1991] Schimel, D. S., Kittel, T. G. F., Knapp, A. K., Seastedt, T. R., Parton, W. J., and Brown, V. B. (1991). Physiological interactions along resource gradients in a tallgrass prairie. *Ecology*, 72(2):672–684.

[Schmidt et al., 2014] Schmidt, T., Schuster, C., Kleinschmit, B., and Forster, M. (2014). Evaluating an intra-annual time series for grassland classification - how many acquisitions and what seasonal origin are optimal? *Selected Topics in Applied Earth Observations and Remote Sensing, IEEE Journal of*, 7(8):3428–3439.

[Schmidtlein and Sassin, 2004] Schmidtlein, S. and Sassin, J. (2004). Mapping of continuous floristic gradients in grasslands using hyperspectral imagery. *Remote Sensing of Environment*, 92(1):126 – 138.

[Schuster et al., 2011] Schuster, C., Ali, I., Lohmann, P., Frick, A., Förster, M., and Kleinschmit, B. (2011). Towards detecting swath events in TerraSAR-X time series to establish NATURA 2000 grassland habitat swath management as monitoring parameter. *Remote Sensing*, 3(7):1308–1322.

[Schuster et al., 2015] Schuster, C., Schmidt, T., Conrad, C., Kleinschmit, B., and Förster, M. (2015). Grassland habitat mapping by intra-annual time series analysis – comparison of RapidEye and TerraSAR-X satellite data. *International Journal of Applied Earth Observation and Geoinformation*, 34:25 – 34.

[Schäfer et al., 2016] Schäfer, E., Heiskanen, J., Heikinheimo, V., and Pellikka, P. (2016). Mapping tree species diversity of a tropical montane forest by unsupervised clustering of airborne imaging spectroscopy data. *Ecological Indicators*, 64:49 – 58.

[Sha et al., 2016] Sha, Z., Zhong, J., Bai, Y., Tan, X., and Li, J. (2016). Spatio-temporal patterns of satellite-derived grassland vegetation phenology from 1998 to 2012 in inner mongolia, china. *Journal of Arid Land*, 8(3):462–477.

[Shannon, 1948] Shannon, C. E. (1948). A mathematical theory of communication. *Bell System Technical Journal*, 27(3):379–423.

[Shao et al., 2016] Shao, Y., Lunetta, R. S., Wheeler, B., Iiames, J. S., and Campbell, J. B. (2016). An evaluation of time-series smoothing algorithms for land-cover classifications using MODIS-NDVI multi-temporal data. *Remote Sensing of Environment*, 174:258 – 265.

[Sheeren et al., 2016] Sheeren, D., Fauvel, M., Josipović, V., Lopes, M., Planque, C., Willm, J., and Dejoux, J.-F. (2016). Tree species classification in temperate forests using Formosat-2 satellite image time series. *Remote Sensing*, 8(9):734.

[Shen et al., 2015] Shen, H., Li, X., Cheng, Q., Zeng, C., Yang, G., Li, H., and Zhang, L. (2015). Missing information reconstruction of remote sensing data: A technical review. *IEEE Geoscience and Remote Sensing Magazine*, 3(3):61–85.

[Shen et al., 2010] Shen, M., Chen, J., Zhu, X., Tang, Y., and Chen, X. (2010). Do flowers affect biomass estimate accuracy from NDVI and EVI? *International Journal of Remote Sensing*, 31(8):2139–2149.

[Simpson, 1949] Simpson, E. H. (1949). Measurement of diversity. *Nature*.

[Sims and Gamon, 2002] Sims, D. A. and Gamon, J. A. (2002). Relationships between leaf pigment content and spectral reflectance across a wide range of species, leaf structures and developmental stages. *Remote Sensing of Environment*, 81(2):337 – 354.

[Skidmore et al., 2015] Skidmore, A. K., Pettorelli, N., Coops, N. C., Geller, G. N., Hansen, M., Lucas, R., Mücher, C. A., O'Connor, B., Paganini, M., Pereira, H. M., Schaepman, M. E., Turner, W., Wang, T., and Wegmann, M. (2015). Environmental science: Agree on biodiversity metrics to track from space. *Nature*, 523(7561):403.

[Socher et al., 2012] Socher, S. A., Prati, D., Boch, S., Müller, J., Klaus, V. H., Hölzel, N., and Fischer, M. (2012). Direct and productivity-mediated indirect effects of fertilization, mowing and grazing on grassland species richness. *Journal of Ecology*, 100(6):1391–1399.

[Stenzel et al., 2017] Stenzel, S., Fassnacht, F. E., Mack, B., and Schmidtlein, S. (2017). Identification of high nature value grassland with remote sensing and minimal field data. *Ecological Indicators*, 74:28 – 38.

[Sullivan et al., 2010] Sullivan, C. A., Skeffington, M. S., Gormally, M. J., and Finn, J. A. (2010). The ecological status of grasslands on lowland farmlands in western ireland and implications for grassland classification and nature value assessment. *Biological Conservation*, 143(6):1529 – 1539.

[Suttie et al., 2005] Suttie, J., Reynolds, S., Batello, C., Food, and of the United Nations, A. O. (2005). *Grasslands of the World*. FAO plant production and protection series. Food and Agricultural Organization of the United Nations.

[Tarantola, 2005] Tarantola, A. (2005). *Inverse Problem Theory and Methods for Model Parameter Estimation*. Society for Industrial and Applied Mathematics, Philadelphia, PA, USA.

[Tews et al., 2004] Tews, J., Brose, U., Grimm, V., Tielbörger, K., Wichmann, M. C., Schwager, M., and Jeltsch, F. (2004). Animal species diversity driven by habitat heterogeneity/diversity: the importance of keystone structures. *Journal of Biogeography*, 31(1):79–92.

[Tilman, 1999] Tilman, D. (1999). Global environmental impacts of agricultural expansion: The need for sustainable and efficient practices. *Proceedings of the National Academy of Sciences*, 96(11):5995–6000.

[Tilman et al., 2001] Tilman, D., Fargione, J., Wolff, B., D'Antonio, C., Dobson, A., Howarth, R., Schindler, D., Schlesinger, W. H., Simberloff, D., and Swackhamer, D. (2001). Forecasting agriculturally driven global environmental change. *Science*, 292(5515):281–284.

[Tilman et al., 1997] Tilman, D., Knops, J., Wedin, D., Reich, P., Ritchie, M., and Siemann, E. (1997). The influence of functional diversity and composition on ecosystem processes. *Science*, 277(5330):1300–1302.

[Toivonen and Luoto, 2003] Toivonen, T. and Luoto, M. (2003). Landsat TM images in mapping of semi-natural grasslands and analysing of habitat pattern in an agricultural landscape in south-west Finland. *Fennia - International Journal of Geography*, 181(1):49 – 67.

[Tscharntke et al., 2005] Tscharntke, T., Klein, A. M., Kruess, A., Steffan-Dewenter, I., and Thies, C. (2005). Landscape perspectives on agricultural intensification and biodiversity – ecosystem service management. *Ecology Letters*, 8(8):857–874.

[Tucker, 1979] Tucker, C. J. (1979). Red and photographic infrared linear combinations for monitoring vegetation. *Remote Sensing of Environment*, 8(2):127 – 150.

[Turner et al., 1992] Turner, C. L., Seastedt, T. R., Dyer, M. I., Kittel, T. G. F., and Schimel, D. S. (1992). Effects of management and topography on the radiometric response of a tallgrass prairie. *Journal of Geophysical Research: Atmospheres*, 97(D17):18855–18866.

[Turner et al., 2003] Turner, W., Spector, S., Gardiner, N., Fladeland, M., Sterling, E., and Steininger, M. (2003). Remote sensing for biodiversity science and conservation. *Trends in Ecology & Evolution*, 18(6):306 – 314.

[Ullah et al., 2012] Ullah, S., Si, Y., Schlerf, M., Skidmore, A. K., Shafique, M., and Iqbal, I. A. (2012). Estimation of grassland biomass and nitrogen using meris data. *International Journal of Applied Earth Observation and Geoinformation*, 19:196 – 204.

[Ustin and Gamon, 2010] Ustin, S. L. and Gamon, J. A. (2010). Remote sensing of plant functional types. *New Phytologist*, 186(4):795–816.

[Verbesselt et al., 2010] Verbesselt, J., Hyndman, R., Zeileis, A., and Culvenor, D. (2010). Phenological change detection while accounting for abrupt and gradual trends in satellite image time series. *Remote Sensing of Environment*, 114(12):2970 – 2980.

[Voormansik et al., 2013] Voormansik, K., Jagdhuber, T., Olesk, A., Hajnsek, I., and Papathanassiou, K. P. (2013). Towards a detection of grassland cutting practices with dual polarimetric TerraSAR-X data. *International Journal of Remote Sensing*, 34(22):8081–8103.

[Waldhardt and Otte, 2003] Waldhardt, R. and Otte, A. (2003). Indicators of plant species and community diversity in grasslands. *Agriculture, Ecosystems & Environment*, 98(1–3):339 – 351. Biotic Indicators for Biodiversity and Sustainable Agriculture.

[WallisDeVries et al., 2002] WallisDeVries, M. F., Poschlod, P., and Willems, J. H. (2002). Challenges for the conservation of calcareous grasslands in northwestern Europe: integrating the requirements of flora and fauna. *Biological Conservation*, 104(3):265 – 273.

[Wang et al., 2010] Wang, K., Franklin, S. E., Guo, X., and Cattet, M. (2010). Remote sensing of ecology, biodiversity and conservation: A review from the perspective of remote sensing specialists. *Sensors*, 10(11):9647–9667.

[Werling et al., 2014] Werling, B. P., Dickson, T. L., Isaacs, R., Gaines, H., Gratton, C., Gross, K. L., Liere, H., Malmstrom, C. M., Meehan, T. D., Ruan, L., Robertson, B. A., Robertson, G. P., Schmidt, T. M., Schrotenboer, A. C., Teal, T. K., Wilson, J. K., and Landis, D. A. (2014). Perennial grasslands enhance biodiversity and multiple ecosystem services in bioenergy landscapes. *Proceedings of the National Academy of Sciences*, 111(4):1652–1657.

[White et al., 2009] White, M. A., De Beurs, K. M., Didan, K., Inouye, D. W., Richardson, A. D., Jensen, O. P., O'keefe, J., Zhang, G., Nemani, R. R., Van Leeuwen, W. J. D., Brown, J. F., De Wit, A., Schaepman, M., Lin, X., Dettinger, M., Bailey, A. S., Kimball, J., Schwartz, M. D., Baldocchi, D. D., Lee, J. T., and Lauenroth, W. K. (2009). Intercomparison, interpretation, and assessment of spring phenology in North America estimated from remote sensing for 1982–2006. *Global Change Biology*, 15(10):2335–2359.

[White et al., 2000] White, R. P., Murray, S., Rohweder, M., Prince, S., Thompson, K., et al. (2000). *Pilot Analysis of Global Ecosystems - Grassland ecosystems*. World Resources Institute Washington, DC.

[Whittaker, 1972] Whittaker, R. H. (1972). Evolution and measurement of species diversity. *Taxon*, 21(2/3):213–251.

[Whittington et al., 2015] Whittington, H. R., Tilman, D., Wragg, P. D., and Powers, J. S. (2015). Phenological responses of prairie plants vary among species and year in a three-year experimental warming study. *Ecosphere*, 6(10):1–15. art208.

[Wilcox and Murphy, 1985] Wilcox, B. A. and Murphy, D. D. (1985). Conservation strategy: The effects of fragmentation on extinction. *The American Naturalist*, 125(6):879–887.

[Wilcoxon, 1945] Wilcoxon, F. (1945). Individual comparisons by ranking methods. *Biometrics Bulletin*, 1(6):80–83.

[Wilson et al., 2002] Wilson, J., Fuller, S. J., and Mather, P. B. (2002). Formation and maintenance of discrete wild rabbit (Oryctolagus cuniculus) population systems

in arid Australia: Habitat heterogeneity and management implications. *Austral Ecology*, 27(2):183–191.

[Wulder et al., 2004] Wulder, M. A., Hall, R. J., Coops, N. C., and Franklin, S. E. (2004). High spatial resolution remotely sensed data for ecosystem characterization. *BioScience*, 54(6):511–521.

[Wylie et al., 2002] Wylie, B., Meyer, D., Tieszen, L., and Mannel, S. (2002). Satellite mapping of surface biophysical parameters at the biome scale over the North American grasslands: A case study. *Remote Sensing of Environment*, 79(2–3):266 – 278. Recent Advances in Remote Sensing of Biophysical Variables.

[Zechmeister et al., 2003] Zechmeister, H., Schmitzberger, I., Steurer, B., Peterseil, J., and Wrbka, T. (2003). The influence of land-use practices and economics on plant species richness in meadows. *Biological Conservation*, 114(2):165 – 177.

[Zillmann et al., 2014] Zillmann, E., Gonzalez, A., Herrero, E. J. M., van Wolvelaer, J., Esch, T., Keil, M., Weichelt, H., and Garzón, A. M. (2014). Pan-european grassland mapping using seasonal statistics from multisensor image time series. *IEEE Journal of Selected Topics in Applied Earth Observations and Remote Sensing*, 7(8):3461–3472.

[Öster et al., 2007] Öster, M., Cousins, S. A., and Eriksson, O. (2007). Size and heterogeneity rather than landscape context determine plant species richness in seminatural grasslands. *Journal of Vegetation Science*, 18(6):859–868.

Abstract

Long résumé en français

La biodiversité est en déclin depuis les dernières décennies et l'intensitification de l'agriculture est une des principales causes de ce déclin. Les prairies sont d'une importance capitale pour la biodiversité car ce sont des habitats riches en espèces et elles représentent l'un des plus grands écosystèmes de la planète. Cependant, la surface globale des prairies diminue constamment et les prairies sont dégradées à cause de l'intensification de l'agriculture, de l'abandon et de l'urbanisation. Il est donc très important pour les écologues de surveiller les prairies semi-naturelles ayant un fort potentiel en biodiversité.

La télédétection constitue un outil unique pour le suivi des prairies sur de grandes étendues spatiales et au cours des années. Jusqu'à récemment, l'analyse des prairies dans des paysages fragmentés était limitée par la résolution des capteurs satellite. Les satellites de nouvelle génération tels que Sentinel-2 offrent de nouvelles opportunités pour le suivi des prairies, grâce à leurs hautes résolutions spatiale et temporelle combinées. Cependant, le nouveau type de données fourni par ces capteurs implique des problèmes liés au big data et à la grande dimension en raison du grand nombre de pixels à traiter et du nombre élevé de variables spectro-temporelles. Les méthodes statistiques conventionnelles utilisées en télédétection ne sont pas optimales avec ce type de données, et les modèles appropriés manquent.

Les objectifs de cette thèse sont de :

1. Fournir des outils adaptés à l'analyse et au suivi des prairies semi-naturelles en utilisant des séries temporelles d'images satellite avec une haute résolution spatiale et temporelle.
2. Définir des variables écologiques issues de ce type de données, qui caractérisent les prairies et qui peuvent être utilisées en variables d'entrée de modèles écologiques.
3. Evaluer le potentiel de Sentinel-2 pour la caractérisation et le suivi des prairies semi-naturelles dans des paysages fragmentés.

Le cadre de cette thèse concerne les prairies semi-naturelles ou les "prairies permanentes" utilisées de façon extensive, avec un grand potentiel en biodiversité, et qui fournissent des services écosystémiques liés à la pollinisation et à la régulation des ravageurs. Ainsi, contrairement à la plupart des études, nous ne sommes pas focalisés sur la production de biomasse ou la couverture végétale des prairies, mais sur leur potentiel pour la biodiversité. Nous nous intéressons à la caractérisation des facteurs qui influent sur la biodiversité dans les prairies : la diversité spécifique, l'hétérogénéité, l'âge, le type et l'intensité des pratiques agricoles.

Pour cela, nous avons analysé la réponse spectro-temporelle des prairies semi-naturelles en suivant un échantillon de prairies du début à la fin de la saison de croissance dans la première partie de cette thèse. Ensuite, dans la seconde partie, nous avons développé des méthodes adaptées à la classification supervisée des prairies semi-naturelles à partir de séries temporelles denses d'images satellite (STIS) avec une haute résolution spatiale. Enfin, dans la troisième partie, nous avons proposé des indicateurs écologiques des prairies liés à leur diversité en espèces et issus de STIS.

Analyse de la réponse spectro-temporelle des prairies

Dans le premier chapitre, nous avons analysé la réponse spectro-temporelle des prairies semi-naturelles en fonction de leur phénologie naturelle et de leur mode de gestion (une fauche, deux fauches, fauche et pâture). Puisque Sentinel-2 n'était pas entièrement opérationnel durant cette thèse, une campagne terrain a été menée pour collecter des spectres durant la saison de croissance d'un échantillon de prairies et les bandes spectrales de Sentinel-2 ont été simulées à partir des données hyperspectrales.

L'analyse a montré des différences dans la réponse spectro-temporelle en fonction de la situation topographique des prairies, de leur type (annuelle à semi-naturelle), de l'intensité et de la date des pratiques. Nous avons remarqué que l'indice de végétation par différence normalisé (NDVI) commence à diminuer avant la fauche pour les prairies fauchées tard dans la saison, en raison de la sénéscence naturelle de la végétation. Cependant, la fauche implique toujours une diminution abrupte du NDVI, ainsi qu'une augmentation de son écart-type, à cause de l'exposition du sol après la fauche. L'écart-type de toutes les bandes spectrales (du visible au proche infra-rouge) augmente après la fauche. Puis, le NDVI ré-augmente durant la repousse, la vitesse de croissance dépendant de la période et du type de prairies, mais toujours avec un écart-type plus élevé qu'avant la fauche, car la repousse est hétérogène au sein des prairies. Une telle étude avec des prairies gerées de manière extensive et qui peuvent être fauchées tard n'avait jamais été réalisée avant à notre connaissance. Ainsi, cette analyse nous a conduit à proposer un modèle d'évolution du NDVI pour les prairies semi-naturelles fauchées, en fonction de leur situation topographique (haut de coteau ou fond de vallée) et de la période de fauche (avant ou après le début de sénéscence).

Nous avons conclu que la variance dans les prairies devrait être prise en compte et que des données hypertemporelles (moins de 15 jours) étaient nécessaires pour le suivi de la phénologie et des pratiques de gestion des prairies, particulièrement durant le printemps. Sentinel-2, avec sa résolution temporelle de cinq jours, devrait permettre ce suivi continu. Cependant, l'analyse a été conduite avec des données acquises par un spectroradiomètre de terrain, et donc à une très haute résolution spatiale. La résolution spatiale de Sentinel-2 et les effets atmosphériques influençant le signal mesuré par les capteurs satellite n'ont pas été pris en compte.

La présence de nuages dans les STIS peut limiter l'analyse des prairies. En effet, au printemps dans un climat tempéré, il y a une forte fréquence d'apparition des nuages, qui cause du bruit et des données manquantes dans la série temporelle. On peut choisir d'omettre les données bruitées (réduisant le nombre d'observations), ou de reconstruire la série temporelle. Dans ce cas, un algorithme de lissage approprié pour reconstruire les données manquantes dues aux nuages est absolument nécessaire pour ce type d'application. En effet, il ne doit pas surlisser/sous-estimer les maxima et minima locaux qui correspondent à des évènements phénologiques ou des effets des pratiques telles que la fauche.

Ainsi, ces résultats nous ont conduit dans la seconde partie de cette thèse à développer des méthodes spécifiques pour le suivi des prairies semi-naturelles en prenant en compte leur hétérogénéité et en utilisant des STIS denses avec une haute résolution spatiale.

Développements méthodologiques

Les développements méthologiques de la deuxième partie ont été appliqués sur des séries temporelles Formosat-2.

Dans le Chapitre 2, nous avons évalué l'efficacité de plusieurs algorithmes de lissage pour reconstruire les séries temporelles issues de capteurs à haute résolution spatiale et temporelle. Nous avons choisi le filtre de Whittaker car il combine grande fidélité aux données et faible rugosité, et il est rapide à exécuter, permettant de traiter un millier de pixels en quelques secondes.

Puis dans les Chapitres 3 et 4, nous avons développé des modèles robustes pour la classification supervisée des prairies semi-naturelles adaptés à la grande dimension des données. Tout d'abord, nous avons proposé une représentation des prairies à l'échelle de l'objet, pour être cohérent avec les études écologiques, et qui prend en compte leur hétérogénéité. De plus, modéliser les prairies à l'échelle de l'objet réduit le nombre d'échantillons à traiter durant les analyses statistiques, comparé à des analyses basées sur les pixels. A partir du comportement observé des pixels de prairies, nous avons modélisé leur distribution par une loi gaussienne, définie par le vecteur moyen et la matrice de covariance empiriques de la prairie.

Pour des raisons de classification, des mesures de similarité sont requises entre chaque paire de prairies, *i.e.*, chaque paire de lois gaussiennes. La plupart des mesures de similarités entre les distributions requièrent l'inversion de matrices de covariance et la calcul de leur déterminant. Cependant, les prairies sont des petits éléments qui représentent en moyenne une centaine de pixels de 10 mètres de résolution spatiale. Avec des STIS denses, le nombre de variables spectro-temporelles acquises durant une année est généralement du même ordre de grandeur. Les matrices de covariance sont souvent non-inversibles ou mal conditionnées, rendant instable le calcul de leur inverse et de leur déterminant. Pour pallier ce problème, nous avons développé des nouvelles mesures de similarité adaptées aux données de grande dimension et qui peuvent être insérées dans le noyau des machines à vecteurs de support (SVM). Nous avons comparé ces méthodes à des méthodes conventionnelles qui sont basées sur des approches orientées pixel et objet.

Dans le Chapitre 3, nous avons proposé une version haute dimensionelle de la divergence de Kullback-Leibler. Nous avons utilisé un modèle qui suppose que les plus petites valeurs propres de la matrice de covariance sont égales. En suivant ce modèle, l'inverse de la matrice de covariance peut être calculé explicitement. L'efficacité de la divergence de Kullback-Leibler haute dimensionnelle proposée (*i.e.*, *High Dimensional Kullback-Leibler Divergence*) a été évaluée avec une série temporelle de NDVI intra-annuelle pour classifier les prairies en fonction de leur mode de gestion. Elle a été plus performante que la divergence de Kullback-Leibler. Cependant, elle n'a pas été significativement différente des méthodes conventionnelles utilisant des noyaux RBF (modélisation pixel par pixel + vote majoritaire, et modélisation par la moyenne) en termes de précision de classification.

Ainsi dans le Chapitre 4, une mesure de similarité plus générale basée sur un noyau "mean map" flexible a été proposée : α-*Gaussian Mean Kernel*. Il s'agit d'une généralisation du *Gaussian Mean Kernel* qui inclut déja un terme de régularisation *ridge* dans le calcul de l'inverse et du déterminant de la matrice de covariance. De plus, le paramètre α permet de pondérer l'influence de la matrice de covariance dans le cas de très petites prairies (quand le nombre de pixels est plus petit que le nombre de variables). La méthode a été testée pour deux

applications : classification de l'âge des prairies en utilisant une série temporelle de NDVI inter-annuelle, et classification des pratiques des prairies en utilisant une série temporelle multispectrale (quatre bandes spectrales) intra-annuelle. L'*α-Gaussian Mean Kernel* a prouvé son efficacité en étant significativement meilleur que les autres méthodes dans la classification en fonction de l'âge. Concernant les pratiques, il s'agit de la meilleure méthode mais elle n'a pas été significativement différente des autres méthodes, car le jeu de données était petit.

Nous avons conclu que l'information de covariance doit être prise en compte dans la classification des prairies. Ainsi, la modélisation gaussienne s'avère sensée dans notre contexte. Cependant, le noyau flexible inclut la modélisation gaussienne et la modélisation par la moyenne. Il peut ainsi être utilisé sur des prairies semi-naturelles mais aussi sur des prairies plus homogènes.

Définition d'incateurs écologiques issus de séries temporelles d'images satellite à haute résolution spatiale et temporelle

La troisième partie est dédiée à la définition d'indicateurs écologiques des prairies issus des STIS. Elle est centrée sur l'évaluation de la diversité spécifique dans les prairies à travers des indices de biodiversité.

Dans le Chapitre 5, nous avons évalué le potentiel de séries temporelles issues de SPOT5 et Sentinel-2 (tous les deux à 10 mètres de résolution spatiale) pour prédire deux indices de biodiversité dans les prairies (les indices de Shannon et de Simpson). Nous avons utilisé une régression à noyau à moindres carrés et testé deux noyaux : le noyau RBF avec un vecteur moyen, et le noyau moyen empirique avec une modélisation basée sur les pixels. Les résultats pour les deux méthodes n'ont pas été satisfaisants (coefficient de détermination d'environ 0.13 pour l'indice de Shannon et de 0.17 pour l'indice de Simpson en moyenne) et ont suggéré qu'une haute résolution temporelle combinée à une haute résolution spatiale et des bandes multispectrales semblent limitées pour prédire de tel indices précis.

Dans le Chapitre 6, nous avons utilisé une approche indirecte pour estimer la diversité spécifique basée sur l'Hypothèse de Variation Spectrale (SVH). Cette hypothèse suppose que la variabilité spectrale est liée à la variabilité de l'habitat et qu'elle peut donc être utilisée comme proxy pour sa diversité spécifique. Cette hypothèse a été vérifiée dans différents habitats en utilisant des données hyperspectrales avec une très haute résolution spatiale. Ici, nous avons supposé que les variations temporelles pouvaient être liées aux différences de phénologie des espèces et donc à la diversité spécifique. Nous avons donc tenté de vérifier la SVH en utilisant des STIS denses multispectrales avec une haute résolution spatiale. Nous avons proposé d'utiliser des mesures d'hétérogénéité spectro-temporelle dérivées du clustering non supervisé des prairies. L'algorithme de clustering que nous avons utilisé a été développé pour des données de grande dimension. Nous avons proposé plusieurs mesures d'hétérogénéité spectro-temporelle (la variabilité intra-classe, la variabilité inter-classe et l'entropie) dérivées du clustering et nous les avons comparées à la distance moyenne au centroïde spectral communément utilisée. Nous avons évalué leur corrélation avec l'indice de Shannon à partir de modèles de régression linéaire univariée et multivariée. Nous avons aussi comparé les résultats obtenus en utilisant une série temporelle entière avec ceux obtenus en utilisant une seule image de la série temporelle. Pour l'analyse multitemporelle, les meilleurs modèles combinaient

la variabilité inter-classe et l'entropie et ont atteint un coefficient de détermination significatif mais bas de 0.133 avec l'indice de Shannon mesuré sur le terrain. L'indice de Shannon était toujours mieux expliqué par les modèles combinant ces deux mesures que les modèles basés sur la distance moyenne au centroïde. Cependant, il n'y a pas eu de différences significatives entre les valeurs prédites de l'indice de Shannon en utilisant des données multitemporelles et en utilisant des données monotemporelles.

Ainsi, nous avons proposé des mesure d'hétérogénéité spectrale dérivées du clustering non supervisé des prairies qui expliquent plus la diversité spécifique dans les prairies que la distance moyenne au centroïde. Cependant, l'hypothèse de SVH n'a pas été vérifiée dans les prairies en utilisant des STIS denses avec une haute résolution spatiale. En effet, les clusters trouvés à partir des données multitemporelles semblent être plus liés à l'intensité des pratiques agricoles conduites dans les prairies qu'à leur diversité spécifique. Une série temporelle qui ne couvre pas la période où les pratiques ont lieu semble être plus appropriée pour relier l'hétérogénéité spectro-temporelle à la diversité spécifique.

Conclusion

Les résolutions spatiale et spectrale de Sentinel-2 paraissent être limitées pour estimer la diversité en espèces des prairies. En revanche, les propriétés spectrales, spatiales et temporelles ce capteur semblent être un bon compromis pour assurer le suivi des facteurs influençant la biodiversité dans les prairies.

Au cours de cette thèse, nous avons développé des outils capables de gérer la grande dimension des données, permettant d'utiliser toute l'information temporelle et spectrale fournie par les satellites de nouvelle génération. Nous avons mis en évidence l'importance de la variabilité spectrale et temporelle induite par la phénologie, les pratiques agricoles et la composition des prairies. La modélisation Gaussienne de la distribution des pixels dans une prairie semble être appropriée étant donné les résultats obtenus.

Par la suite, l'approche fonctionnelle devrait être envisagée puisque certaines traits fonctionnels sont liés à des propriétés qui influencent le signal mesuré par le capteur.

Les méthodes développées au cours de cette thèse ne sont pas limitées aux prairies, et elles pourraient être utilisées sur d'autres habitats naturels ou semi-naturels hétérogènes, tels que les zones humides, les tourbières, les landes, les bois...

English abstract

Grasslands are a significant source of biodiversity in farmed landscapes that is important to monitor. New generation satellites such as Sentinel-2 offer new opportunities for grassland's monitoring thanks to their combined high spatial and temporal resolutions. Conversely, the new type of data provided by these sensors involves big data and high dimensional issues because of the increasing number of pixels to process and the large number of spectro-temporal variables. This thesis explores the potential of the new generation satellites to monitor biodiversity and factors that influence biodiversity in semi-natural grasslands. Tools suitable for the statistical analysis of grasslands using dense satellite image time series (SITS) with high spatial resolution are provided. First, we show that the spectro-temporal response of grasslands is characterized by its variability within and among the grasslands. Then, for the statistical analysis, grasslands are modeled at the object level to be consistent with ecological models that represent grasslands at the field scale. We propose to model the distribution of pixels in a grassland by a Gaussian distribution. Following this modeling, similarity measures between two Gaussian distributions robust to the high dimension are developed for the classification of grasslands using dense SITS: the High-Dimensional Kullback-Leibler Divergence and the α-Gaussian Mean Kernel. The latter outperforms conventional methods used with Support Vector Machines for the classification of grasslands according to their management practices and to their age. Finally, indicators of grassland biodiversity issued from dense SITS are proposed through spectro-temporal heterogeneity measures derived from the unsupervised clustering of grasslands. Their correlation with the Shannon index is significant but low. The results suggest that the spectro-temporal variations measured from SITS at a spatial resolution of 10 meters covering the period when the practices occur are more related to the intensity of management practices than to the species diversity. Therefore, although the spatial and spectral properties of Sentinel-2 seem limited to assess the species diversity in grasslands directly, this satellite should make possible the continuous monitoring of factors influencing biodiversity in grasslands. In this thesis, we provided methods that account for the heterogeneity within grasslands and enable the use of all the spectral and temporal information provided by new generation satellites.

Key words: Remote sensing, satellite image time series, high dimension, grassland, landscape ecology, biodiversity.

Résumé en français

Les prairies représentent une source importante de biodiversité dans les paysages agricoles qu'il est important de surveiller. Les satellites de nouvelle génération tels que Sentinel-2 offrent de nouvelles opportunités pour le suivi des prairies grâce à leurs hautes résolutions spatiale et temporelle combinées. Cependant, le nouveau type de données fourni par ces satellites implique des problèmes liés au big data et à la grande dimension des données en raison du nombre croissant de pixels à traiter et du nombre élevé de variables spectro-temporelles. Cette thèse explore le potentiel des satellites de nouvelle génération pour le suivi de la biodiversité et des facteurs qui influencent la biodiversité dans les prairies semi-naturelles. Des outils adaptés à l'analyse statistique des prairies à partir de séries temporelles d'images satellites (STIS) denses à haute résolution spatiale sont proposés. Tout d'abord, nous montrons que la réponse spectro-temporelle des prairies est caractérisée par sa variabilité au sein des prairies et parmi les prairies. Puis, pour les analyses statistiques, les prairies sont modélisées à l'échelle de l'objet pour être cohérent avec les modèles écologiques qui représentent les prairies à l'échelle de la parcelle. Nous proposons de modéliser la distribution des pixels dans une prairie par une loi gaussienne. A partir de cette modélisation, des mesures de similarité entre deux lois gaussiennes robustes à la grande dimension sont développées pour la classification des prairies en utilisant des STIS denses: *High-Dimensional Kullback-Leibler Divergence* et *α-Gaussian Mean Kernel*. Cette dernière est plus performante que les méthodes conventionnelles utilisées avec les machines à vecteur de support (SVM) pour la classification du mode de gestion et de l'âge des prairies. Enfin, des indicateurs de biodiversité des prairies issus de STIS denses sont proposés à travers des mesures d'hétérogénéité spectro-temporelle dérivées du clustering non supervisé des prairies. Leur corrélation avec l'indice de Shannon est significative mais faible. Les résultats suggèrent que les variations spectro-temporelles mesurées à partir de STIS à 10 mètres de résolution spatiale et qui couvrent la période où ont lieu les pratiques agricoles sont plus liées à l'intensité des pratiques qu'à la diversité en espèces. Ainsi, bien que les propriétés spatiales et temporelles de Sentinel-2 semblent limitées pour estimer directement la diversité en espèces des prairies, ce satellite devrait permettre le suivi continu des facteurs influençant la biodiversité dans les prairies. Dans cette thèse, nous avons proposé des méthodes qui prennent en compte l'hétérogénéité au sein des prairies et qui permettent l'utilisation de toute l'information spectrale et temporelle fournie par les satellites de nouvelle génération.

Mots clés : Télédétection, séries temporelles d'images satellite, grande dimension, prairie, écologie du paysage, biodiversité.